THERMODYNAMIC AND KINETIC STUDIES
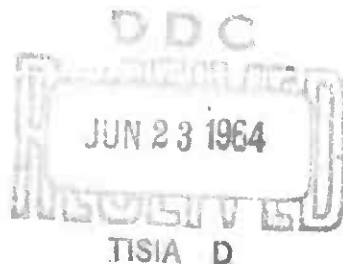# FOR A REFRACTORY MATERIALS PROGRAM

TECHNICAL DOCUMENTARY REPORT NO. ASD - TDR - 62 - 204, PART III

APRIL 1964

Air Force Materials Laboratory
Research and Technology Division
Air Force Systems Command
Wright - Patterson Air Force Base, Ohio

Project No. 7350, Task No. 735001

FOREWORD

This report was prepared hy Arthur D. Little, Inc., under USAF Contract No. AF 33(616)-7472. This contract was initiated under Project No. ⁻ i50, "Refractory Inorganic Nonmetallic Materials," Task No. 735001, "Non-C aphitic." The work was administered under the direction of the Metals and C ramics Laboratory, Directorate of Materials and Processes, Aeronautical Systems Division, with Mr. Fred W. Vahldiek acting as project engineer.

This report covers work conducted from January 1, 1963 through February 29, 1964.

Portions of the work reported herein were carried out under suh-contracts with Arthur D. Little, Inc., as acknowledged in the text.

ABSTRACT

Work during 1963 is reported and the work from mid-1960 reviewed on a comprehensive program of thermodynamic and kinetic studies necessary to the theoretical consideration to temperatures of 3000K of the reactions of the zirconium and hafnium carbides and borides with oxygen- or halogen-containing atmospheres.

Work presented includes: preparation of borides and carbides; low temperature heat capacity measurements on HfB_2, HfC and hafnium metal; estimation of entropies at 298K for refractory diborides, nitrides, carbides, and oxides from high temperature heat content data; current status of heats of formation of the borides and carbides from oxygen and fluorine bomb calorimetry; and studies proving the feasibility of the "matrix isolation technique" for spectroscopy of high temperature molecules through studies on the Lithium halides. Status of electron diffraction, equilibria, and heat of solution studies of the hafnium and zirconium halides is presented.

Kinetic studies completed on the oxidation and fluorination of the hafnium and zirconium carbides and diborides are presented in detail. From ac and dc electrical conductivity studies on tetragonal ZrO_2, a model of the defect structure is devised and oxygen diffusion in ZrO_2 is calculated.

This technical documentary report has been reviewed and is approved.

W.G. RAMKE
Chief, Ceramics and Graphite Branch
Metals and Ceramics Division
Air Force Materials Laboratory

iii

TABLE OF CONTENTS

LIST OF TABLES

LIST OF FIGURES

LIST OF FIGURES (Continued)

LIST OF FIGURES (Continued)

I. INTRODUCTION

The zirconium and hafnium carbides and diborides are among those
materials being considered for structural uses in our current high temperature
technology. They can be more readily evaluated for specific engineering appli-
cations if we have the thermodynamic and kinetic knowledge which permits
predictions of their chemical behavior.

A theoretical evaluation of the chemical behavior of a material at high
temperatures and under corrosive atmospheric conditions requires information
from several diverse studies. To calculate the chemical equilibrium condition
for a given system requires the ability to predict the products which will form,
in addition to having available the thermochemical data for both the products and
the reactants. Knowledge may also be required of the vaporization process, vapor
pressures, activities as a function of composition, heats of vaporization, and heats
of formation. Furthermore, to fully evaluate the usefulness of a material, one
must have information on the kinetics of the chemical interactions involved in order
to determine whether equilibrium conditions will be attained. A very detailed under-
standing of the mechanisms of the overall kinetic process may be required, since
impurities in low concentration can strongly modify the solid state chemistry of
materials.

The same basic thermodynamic, and kinetic knowledge necessary for
predictions of chemical behavior can also guide future materials development
programs. For example, during the interaction of solids with gaseous atmospheres,
surface coatings sometimes form which inhibit the reaction. As our understanding
of the kinetic mechanism is improved, it is conceivable that we can modify materials
to favor the formation of surface coatings which will provide increased protection in
high temperature applications.

We undertook in mid-1960 a comprehensive program of thermodynamic
and kinetic studies. the purpose of which was to provide data necessary for theo-
retical considerations on the use of the zirconium and hafnium carbides and borides
at temperatures to 3000K and in atmospheres of oxygen, oxygen plus water, chlorine,
hydrogen fluoride, and fluorine.

The program as planned included materials preparation, calorimetry,
mass spectrometry, vaporization, spectroscopy, electron diffraction, equilibria,
chemical rate, and mass transport studies. Thermodynamic data were sought on
both the solid carbides and borides and on gaseous molecules which can be important
products in the reactions of the carbides and borides with oxygen- or halogen-
containing atmospheres.

The total program breaks readily into three categories. First, the preparation and characterization of the carbide, boride, and oxide samples required for the experimental studies; second, studies which provide thermodynamic data on the carbides and borides and on selected gaseous molecules; and third, studies related to the mechanism and kinetics of oxidation or fluorination. These categories have accounted for one-sixth, one-third, and one-half, respectively, of the experimental effort.

This program was carried out by a combination of in-house and subcontracted studies. Almost without exception, the individual studies will be submitted for publication in the open literature by the principal investigators concerned. Several papers resulting from these studies have already been published.

This is the final report under this contract. Therefore, we present a review of the three and one-half year program in addition to reporting on accomplishments of the different studies during the period January 1, 1963, to February 29, 1964.

Work during the period July 1, 1960, to December 31, 1961, was presented in Technical Documentary Report ASD-TDR-62-204, Part I, published in April of 1962, and work from January 1 to December 31, 1962, was presented in ASD-TDR-62-204, Part II, published in May 1963.

II. PROGRAM REVIEW

A. MATERIALS PREPARATION

The basic value of thermodynamic and kinetic studies is closely related to the information known and reported about the sample material. Thermodynamic and kinetic studies are affected by one or more of the material properties such as purity, stoichiometry, crystallite size, and porosity. Since no commercial materials were available meeting the requirements for this program, we undertook to prepare suitable materials in our laboratories under the direction of George Feick. Accomplishments during this report period are presented and the total program is reviewed in detail in Section III of this report.

Using zone-melting facilities supplied by ADL, a technique was developed for producing high purity, non-porous, macrocrystalline samples of zirconium and hafnium carbides and borides by an induction heated, vertical, floating-zone melting method. The advantages and limitations of this technique for preparing samples of high melting refractories are compared.

The floating-zone melting method was used to produce the large samples (about 200 grams each) of ZrC, ZrB_2 and HfB_2 required for this program. In addition small batches (about 50 grams) of these materials, as well as HfC, were prepared in special purity or stoichiometry.

An arc melting technique was used to produce the large quantity of HfC required by the program. The difficulties in zone-melting HfC are discussed and means outlined to overcome them.

Boules of high purity ZrO_2 were produced utilizing an arc imaging furnace. Efforts were made to procure high purity hafnium metal for low temperature heat capacity measurements under this program. Material of the required purity was finally obtained through a loan to Professor Westrum from the Oak Ridge National Laboratory.

Difficulties were experienced in this work in obtaining reproducible free carbon analyses on carbides. Improvements were made in the analytical technique so that more reliable free carbon analyses can be obtained.

Subsequent to the development of the floating-zone melting method for the production of crystal bars of carbides and borides required by this program, the method has been successfully applied under other programs to the production of samples of transition metal nitrides, silicides, carbides and borides. At the present time, samples of rare earth hexaborides are being made by this technique.

3

B. THERMODYNAMIC DATA FOR SOLID ZIRCONIUM AND HAFNIUM CARBIDES AND BORIDES

1. Low Temperature Heat Capacity

Low temperature heat capacity measurements were completed on HfC, HfB_2, ZrC, ZrB_2 and hafnium metal by Dr. E. F. Westrum, Jr. at the University of Michigan. Results on ZrB_2 and ZrC were reported previously in Parts I and II respectively of this report and were recently published.[9][19] Results on HfB_2, HfC, and hafnium metal are presented in Appendix III of this report. For each material thermodynamic functions (C_p, S^O, $H^O-H_0^O$, and $-(G^O-H_0^O)/T$) are calculated and tabulated at selected temperatures from 5 to 298.15°K.

2. High Temperature Heat Content

Dr. John L. Margrave now at Rice University (formerly at University of Wisconsin) undertook to determine heat contents of the zirconium and hafnium carbides and diborides to about 2200K. The results and status of this effort are presented in Appendix II of this report. Heat contents of ZrB_2 prepared under this program were determined from 410 to 1125°K. A computer program was developed for selecting combinations of Debye and/or Einstein functions to fit the experimental points and permit more reliable extrapolations to high temperatures. Tabulations and extrapolations to 2000K of smooth thermodynamic functions for ZrB_2 are presented in Table 47.

On moving his laboratory from Wisconsin to Rice, the calorimeter used in the heat content studies was disassembled and is now in the process of reassembly and modification so that heat content studies may be completed to 2000K. The samples are all on hand and Dr. Margrave anticipates that results will be available by early 1965.

Prior to the availability of samples prepared under this program, powdered samples of ZrC and HfB_2 from Carborundum Company were studied to about 1200K. Results and a selected set of thermodynamic functions for ZrC in the range 0-2000K were presented previously in Part II of this report. Calculated thermodynamic functions for HfB_2 were presented in Part I of this report.

Professor Margrave utilized available high temperature heat content data and a computer program to estimate entropies at 298K for refractory diborides, nitrides, carbides and oxides. This effort is also presented in Appendix II.

4

High temperature heat capacity data for ZrB_2 reported in the literature are compared in Table 48, comprising part of the report of Professor Margrave. The result for the material prepared under this program is, at 1000C, the lowest of four experimental values. One reviewer has recently attributed the large differences between different workers to experimental error. We wish to emphasize that the differences reported are apparently real and due to differences in sample rather than errors in calorimetry. Professor Margrave reported previously[166] on an exchange between his laboratory and that of Southern Research Institute of samples studied by Barnes et al.,[132] and SRI.[131] They were able to duplicate each other's results quite well. This does not prove that all calorimetry is accurate, but it does show that very appreciable differences in heat content can be obtained for different samples. We believe that the differences must be due to differences in sample stoichiometry and purity.

As an indication of the magnitude of the effects of sample stoichiometry and purity we have estimated the heat capacity of the powdered ZrB_2 material which we obtained from Carborundum Corporation as a starting material for preparation of the high purity crystal bars by the zone melting technique. This powder from Carborundum was of much higher purity than other commercial samples we examined. Nevertheless, on the basis of its carbon, oxygen, and excess boron content we estimate that its heat capacity at 1000C would have measured 17.97 rather than the 17.07 cal-deg^{-1}-mole^{-1} found for the crystal bar material.

3. Heats of Combustion

Heats of formation may be calculated from heat of combustion studies. We supplied samples of the carbides prepared under this program to Dr. K. K. Kelley at the Berkeley Thermodynamics Laboratory of the U. S. Bureau of Mines and samples of the diborides to Dr. Ward Hubbard at Argonne National Laboratory. Both groups had interest in these materials within their own programs. Dr. Kelley informs us[53] that Mrs. Mah has completed the combustion calorimetry of samples of HfC, ZrC, and $ZrC_{.67}$ supplied by us. The heats of formation calculated from the combustion studies are for HfC, $\Delta H_{f298.15} = -52.3 \pm 0.4$ kcal/mole and for ZrC, $\Delta H_{f298.15} = -47.0 \pm 0.4$ kcal/mole. This latter value is higher than the much earlier value of $\Delta H_{f298.15} = -44.1 \pm 1.5$ kcal/mole reported by Mah and Boyle[164] on a sample of lower purity. The heat of formation for the $ZrC_{.67}$ sample is $\Delta H_{f298.15} = -46.6 \pm 1.2$ kcal/mole of carbon. This corresponds to -31.2 kcal/mole for the composition $ZrC_{.67}$.

Dr. Ward N. Hubbard, Dr. Elliott Greenberg, and co-workers at Argonne National Laboratory have completed heat of fluorination studies on ZrB_2 and HfB_2. They report[165] that large uncertainties must be assigned to the heats of formation due primarily to an uncertainty of ± 0.02 in the boron to zirconium ratio as determined by present chemical analytical techniques. A paper is currently being prepared for submission to the Journal of Physical Chemistry in which available results from their own and other work are compared and evaluated. They propose that the current "best" value for $\Delta H_{f298.15}$ is -76 ± 3 kcal/mole. Only a preliminary calculation has been completed for hafnium diboride, giving for the composition $HfB_{2.02}$ a value of -76.6 (a very tentative value). We must emphasize that the studies mentioned here will be published by these workers in papers in the open literature. The values given should be considered tentative and subject to revision prior to publication.

4. Vaporization

Knowledge of vaporization processes, vapor pressures as a function of composition and heats of vaporization of refractories are essential in order to apply thermodynamic techniques to prediction of their high temperature behavior. Our program in this area has included studies by mass spectrometry and a continuous recording microbalance technique.

Dr. Alfred Buchler utilizing mass spectrometry studied the vaporization of $ZrB_{2.05}$ and $ZrB_{1.96}$. This work was reported in Part I of this report. Zirconium and Boron atoms were found to be the only vapor species present. These studies, as well as other data in the literature, provided convincing evidence that the borides and carbides vaporize to their elements. Therefore, since the vapor species were recognized, it was more efficient to utilize a conventional microbalance technique for vapor pressure studies.

Dr. Paul Blackburn presents in Section VI of this report the results of his vapor pressure studies, using a microbalance technique, on $Zr\bar{B}_{1.99}$, Hafnium, $HfB_{2.03}$, $HfB_{1.75}$, $HfC_{.97}$, $ZrC_{.97}$, $ZrC_{.65}$, and $HfC +$ excess C. Heats of vaporization and formation for the carbides and borides are calculated. In all but one case, the calculated heat of formation of the compound was within experimental error (± 3 kcal) of the calorimetric value. Contrary to previously reported measurements in tungsten Knudsen cells, where evaporization coefficients between 0.025 and 0.1 for ZrB_2 and 0.1 for HfB_2 were reported, the study reported here indicates that the evaporation coefficient for each of these compounds is close to unity. The vapor pressure data reported here taken together with available information in the literature provide knowledge of activity variation across the range of homogeneity for zirconium carbide and hafnium diboride.

C. THERMODYNAMIC DATA FOR GASEOUS MOLECULES

1. Spectroscopy

When the electronic, vibrational, and rotational spectra of gaseous species are known, accurate data on entropy and heat capacity of the species can be obtained through statistical thermodynamic calculations. However, spectroscopy of gaseous molecules at high temperatures is extremely difficult. A potentially rewarding method for the spectral study of high temperature gaseous species is that of trapping individual gaseous molecules in a matrix of inert material.

Professor Otto Schnepp, Israel Institute of Technology, undertook to prove the feasibility of the technique and to apply it to gaseous hafnium and zirconium species such as ZrO and HfO. In Appendix I he reports on studies of the lithium halides by this technique. These molecules were investigated first since their vapor spectra were already well known. Definite conclusions are reached concerning the validity and applicability of the technique. It was concluded that all molecular species present in the vapor in equilibrium with the salt can be trapped in inert solids at liquid hydrogen temperatures. Yet to be determined is the question of whether the relative concentrations of species in the vapor are accurately reflected by the ratio found trapped in the matrix. One of the important problems in connection with use of the technique is the frequency shift of the spectra which varies for different matrices. It was not possible to calculate this shift theoretically, but an empirical relationship was observed in the frequency differences between argon and nitrogen matrices and between the argon matrix and the free molecule.

Work was initiated on the vapors over ZrO_2 and HfO_2. Difficulties, now resolved, in the electron beam bombardment furnace required for this study have delayed completion of the work. Dr. Schnepp reports that this project will be completed during the next few months.

2. Electron Diffraction Studies

Rotational fine structure data necessary for statistical thermodynamic calculations are generally not obtainable from infrared spectra. Spectral studies in the microwave region are required. However, the rotational contributions to the partition functions for gaseous species can be computed when the molecular dimensions are known. Electron diffraction studies of gases can provide such data.

Dr. S. H. Bauer at Cornell University has been pioneering in the application of electron diffraction techniques to high temperature gaseous species. As a

part of this program he undertook to include the study of several hafnium and zirconium tetrahalides in his research program. A preliminary report on the results of studies on $ZrCl_4$, $HfCl_4$, $HfBr_4$ and HfI_4 is presented in Appendix V. In addition to providing the structure and molecular dimensions of the specific compounds studied, the work will also make the estimation of these properties for other related hafnium and zirconium halides more certain.

3. Equilibria and Heats of Solution

A program to determine chemical thermodynamic data for the subhalides of hafnium and zirconium was undertaken by Dr. Robert Freeman at Oklahoma State University. His program includes studies of the disproportionation equilibria of the subhalides, as well as determination of the heats of formation by solution calorimetry.

He summarizes the status of his work in Appendix IV of this report. Necessary facilities for the equilibria and calorimetry measurements have been developed. A technique under study for preparing high purity samples of the subhalides is discussed. These studies will be continuing in Dr. Freeman's laboratories.

D. KINETIC DATA

1. Oxidation

Under the direction of Professor John L. Margrave at Rice University (formerly at University of Wisconsin) kinetic studies were made, utilizing a weight gain technique, of the oxidation of ZrB_2 at 945-125$5$C and ZrC at 554-652C. The results were presented in Part II of this report. It was found that the ZrB_2-O_2 reaction is parabolic throughout the temperature range studied, whereas the ZrC-O_2 reaction is linear. In the former case, a molten layer of boron oxide is formed which protects against further direct attack of oxygen on the ZrB_2, while in the latter, a rather porous film of zirconium oxide is formed which is not protective.

In Section IV of this report Dr. Joan Berkowitz-Mattuck presents a complete report of her work on the oxidation of zirconium and hafnium borides and carbides. Studies ranged from 1100 to 2100K and 1 to 700 Torr using a flow system with inductively heated samples and a thermal conductivity bridge to measure the net oxygen consumption during the oxidation.

Parabolic rate behavior was observed for ZrB_2 and HfB_2. The work on ZrB_2 overlapped the studies of Margrave mentioned above and good agreement between the two workers is reported. Above 1400K an activation energy of 77 ± 5 kcal/mole was calculated for the oxidation of ZrB_2. Below 1400K the activation energy is much lower and the mechanism is clearly different. For HfB_2 an activation energy of 46 ± 6 kcal/mole is observed in the range 1480-1870K. Around 1970K, the transition temperature for the monoclinic to tetragonal phase change in HfO_2, there is an abrupt increase in the rate of oxidation. The results for ZrB_2 and HfB_2 are compared on an alloy consumption basis and possible mechanisms of oxidation are discussed.

Linear rates of oxidation were observed for ZrC and HfC. Oxidation occurs preferentially along grain boundaries and gradually extends into the interior of crystallites.

One intriguing question is the markedly different behavior of the ZrO_2 coatings formed on oxidation of ZrC and ZrB_2. On ZrC the coating is porous and loosely adherent while on ZrB_2 a dense, adherent coating which apparently acts as an oxygen barrier is formed. Understanding this behavior is important not only to clarify and explain the observed oxidation behavior but also for the insight such understanding may offer to the problem of adherence for protective coatings in general.

In the oxidation process we can imagine that both zirconium and carbon or zirconium and boron atoms are competing for available oxygen under a ZrO_2 coating. We estimate that at 2000K the partial pressures of both carbon monoxide and boron monoxide in equilibrium with elemental carbon or boron and with oxygen deficient ZrO_2 would be well below atmospheric pressure. Thus, these gaseous species should not be expected to rupture the oxide coating. Rather, we might expect their formation to be inhibited because of the lack of opportunity for gaseous oxides to escape. We can expect some solubility of boron and carbon in zirconium oxide. This would help insure that the activities of these elements are much less than the free elements and would decrease the tendency for gaseous oxide formation below that already estimated. In addition, this solubility would provide a mechanism for transport by diffusion of carbon and boron through the oxide layer in order that volatilization may occur at the atmosphere side of the coating. We would also expect that the presence of carbon may stabilize a ZrO phase which is not known in the pure zirconium-oxygen system.

In our opinion it may be the formation of a thin layer of ZrO stabilized by carbon which accounts for the different behavior of the ZrO_2 coatings on oxidation of ZrC compared with ZrB_2. One would expect a gradient of carbon concentration through a stabilized ZrO coating on ZrC. Below a certain concentration of carbon the ZrO phase would become unstable with respect to ZrO_2 + Zr and recrystallization would occur. This recrystallization process may account for the porous, nonadherent oxide coating formed on ZrC. The ZrO phase could be thin and difficult to

9

distinguish from ZrC. Under steady state conditions, a constant thickness of the ZrO phase could exist and a linear rate might be observed. If these thoughts have any validity, kinetic behavior should be quite different at very low oxygen pressures. At low enough pressures a parabolic rate behavior may be observed.

Dr. Joan Berkowitz-Mattuck completed a run on HfC at 1mm O_2 pressure subsequent to completing the write-ups presented in Section IV. This pressure is far higher than we were thinking about in the preceding paragraph. Nevertheless she did observe parabolic rate behavior in this run as opposed to the linear rate behavior at higher oxygen pressures. If nothing else, this result does indicate that more can be learned concerning the kinetics of oxidation of the carbides if the studies are extended to much lower oxygen pressures.

2. Fluorination

Studies on the fluorination of the zirconium and hafnium carbides and diborides, graphite, silicon and boron were carried out at the University of Wisconsin and Rice University by Dr. A. K. Kuriakose and Dr. John L. Margrave. Their report is presented in Appendix II and studies on ZrC and ZrB_2 have been published[81] recently. They find that the borides are more resistant to fluorine than the carbides. While the carbides begin to react at about 300C under low fluorine partial pressures, the borides are only attacked above the volatilization points of the metallic fluorides. The rates for these materials are gas diffusion controlled above 600C. In terms of moles, the rates of fluorination of the hafnium compounds are found to be four to five times faster than those for the zirconium compounds.

In conjunction with kinetic studies of carbides and borides it is desirable to understand the mechanism of fluorination of carbon and boron. Reports from Drs. Kuriakose and Margrave covering work on these materials as well as silicon, are included in Appendix II.

3. Mass Transport

As reported above, the oxidation of zirconium and hafnium diborides are found to exhibit parabolic rate behavior which is probably indicative of diffusion through the oxide coating as the rate controlling step. In such instances the complete interpretation of the oxidation mechanism and any possible future control of the oxidation rate require knowledge of the defect structure and transport properties of the oxide. In Section V of this report, Drs. L. A. McClaine and C. P. Coppel report on electrical conductivity studies on ZrO_2 carried out with the objective of obtaining insight into the defect structure and transport mechanisms in this oxide.

10

Experimental data are presented for ac and dc electrical resistance in tetragonal ZrO_2 over the range of 1100 to 1500C and 1 to 10^{-12} atmospheres oxygen. From these data are derived the electronic and ionic conduction behavior as a function of temperature and oxygen pressure, and a defect structure model is devised which appears to fit the conduction behavior. Diffusion data for oxygen in ZrO_2 are calculated from ionic conduction data, and on the basis of the defect structure model the energy of formation of the defects is derived from the activation energy for n-type electronic conduction. This energy for defect formation when combined with the energy for defect motion known from studies on lime stabilized zirconia can be used to calculate an activation energy of about 60 kcal/mole for intrinsic diffusion of anion vacancies in ZrO_2.

4. Oxidation of Molybdenum

In Part II of this report we presented the results of a mass spectrometry study on the oxidation kinetics of molybdenum. This study represented a continuation of work initiated under contract AF 33(616)-6154, which contract studies were incorporated within this program in 1962.

Oxidation studies were carried out in the temperature range 1400 to 2000K at oxygen pressures of 10^{-5} to 10^{-6} atmospheres. The results proved that a solid oxide film does not form on the molybdenum surface during oxidation, although solid MoO_2 is stable at these temperatures and pressures. A reaction mechanism was postulated in which the rate of formation of an adsorbed MoO molecule is rate determining. This study was of special significance in that it provides an understanding of initial steps in the overall oxidation reaction.

E. RECOMMENDATIONS FOR FUTURE WORK

1. Materials Preparation

We strongly believe that the effects of sample state and purity on the results of thermodynamic and kinetic studies must always be carefully considered. The allocation of funds and time for proper preparation and/or characterization of sample material is essential. In several instances in the course of this program we have attempted to compare our results with those of previous work reported in the literature only to find little or no information on the sample material studied. In such cases, no real basis for comparison exists. It is true that samples selected for study will almost always represent a compromise between our desires and what is available commercially. However, one should not be too easily satisfied and when a sample is selected for study it should be carefully characterized so that the results of the study can provide a firm basis for further developments in the field.

2. Thermodynamic Studies

Many opportunities exist in the materials field for further thermodynamic studies such as reported here for solids and gases. Such efforts on well characterized materials need continued support.

3. Kinetic Studies

Impurity content can also exert a marked effect on the kinetics of reaction. Major advances in the field of refractory materials may well come from a greater understanding of the solid state chemistry involved in the overall kinetic processes and the influence of impurities on this chemistry. This is an area of investigation that, in our opinion, merits much more intensive study.

The studies on the kinetics of oxidation of the zirconium and hafnium carbides should be extended to much lower pressures for the information that may be gained on the detailed mechanism of oxidation. Studies of ion transport presented in this report on pure ZrO_2 should be extended to impurity content ZrO_2 and the total study repeated on HfO_2. The much greater oxidation resistance of HfB_2 compared to ZrB_2 must be related to differences in the transport properties of HfO_2 as compared to ZrO_2.

In the past, pure hafnium compounds have seldom been examined because of the difficulty of obtaining them and the expectation that their chemical properties would be the same as those observed for the zirconium compound. In view of the results observed in this work, one should now examine more carefully the kinetic behavior of pure hafnium compounds.

III. PREPARATION OF SAMPLES*

During the present report period, experimental work has been confined to ZrC, Hf, HfB_2 and HfC. The results of this work are discussed in Section B below.

For the purposes of this final report, we have included in Section A below a critique of the induction floating-zone melting method based on experience gained under this contract. In Section B below, we have given, in addition to a discussion of current work, a brief summary of results with each of the compounds studied and in a few cases a comparison of analytical results obtained by different laboratories.

A. CRITIQUE OF THE INDUCTION FLOATING-ZONE MELTING METHOD

The majority of the samples prepared for this project were made by zone-melting in an inert atmosphere using an induction-heated, vertical, floating-zone apparatus. The rods needed for zone-refining were prepared by sintering commercial powders under moderate pressure in graphite or boron nitride molds. Details of the apparatus and procedures are given in Part I of this report.

A summary of the advantages and limitations of this method based on our experience is given below.

1. Advantages

a. The induction heating method is in many cases the only known way of melting highly refractory substances such as ZrB_2 and ZrC out of contact with possible sources of contamination and of causing their solidification in the orderly manner needed for producing dense, crack-free crystals.

In contrast, the electron-beam heating method requires a high-vacuum for operation, which results in undue evaporation of the melt at the very high temperatures involved. The arc-melting method also produces undue vaporization of the melt and, as usually carried out, results in rapid solidification, severe thermal shock, and cracking of the product.

b. The zone-refined product is a dense, single or polycrystalline bar of low surface area. This is especially desirable for low-temperature work in order to minimize the undesirable adsorption of the helium used in the calorimeter.

---

*Prepared by George Feick, Arthur D. Little, Inc.

c. The bars produced by this melt process are highly homogeneous. This is indicated by the narrowness of the X-ray diffraction peaks as contrasted to the broader peaks obtained with sintered preparations which have never been molten.

d. The zoned bars permit examination for extraneous phases by standard metallographic techniques, and by electron beam microprobe methods. These methods are more sensitive indicators of unwanted phases than the usual analytical procedures and form a valuable extension of X-ray diffraction, chemical, and spectroscopic analytical methods.

e. A considerable purification of the sample is produced by the melting process. The concentration of most of the volatile metallic impurities is reduced by a factor of 10 or more. The levels of oxygen and carbon in the borides can be reduced to very low values by the formation of CO which is lost during melting. The oxygen content of the carbides is very low for the same reason.

f. The composition of the starting powder can be adjusted by suitable additions before sintering to compensate for lack of stoichiometry or for preferential volatilization of an element during melting.

2. Limitations

a. The induction-heating method is well adapted only to metallic materials or to semiconductors which become highly conductive on heating.

b. It is limited to materials which melt congruently or to those which can be grown peritectically from a melt of different composition.

c. Materials which undergo phase changes or decomposition on cooling to room temperature cannot usually be prepared, for example Z_1B and ZrB_{12}.

d. Substances having one or more components highly volatile at the melting point cannot be readily prepared by this method. If the volatility is moderate, however, the composition can be adjusted by adding an excess of the volatile component (for example boron to the borides and carbon to the carbides).

e. We have found that substances of extremely high melting point, such as HfC, are difficult to zone refine by this method because of poor control of the molten zone. We have produced a few short sections of zone-refined HfC, however, and believe the process could be improved by using denser starting bars.

14

B. DISCUSSION OF INDIVIDUAL COMPOUNDS

1. Zirconium Diboride

The preparation and characterization of zirconium diboride are dis-
cussed in Parts I and II of this report. The analytical data are summarized in
Table 1. Metallographic examination of this material disclosed the presence of
a few percent of a second phase which was identified as ZrB by X-ray diffraction
methods. This result is in agreement with the slight boron deficiency shown by
the chemical analysis.

Since our last report, we have received additional analytical data on
this lot of ZrB_2 from Dr. T. F. Lyon of the General Electric Company and from
Dr. Elliott Greenberg of Argonne National Laboratory. The boron and zirconium
analyses obtained by the various laboratories are summarized in Table 2 which
shows atom ratios of boron to zirconium varying from 1.96 to 2.01.

Metallographic examination of this ZrB_2 showed the presence of a lamel-
lar structure consisting of thin layers of a second phase alternating with much
thicker layers of the major phase. (See Part I of this report, p. 22, Figure 5.)
X-ray diffraction analysis showed this second phase to have the structure of ZrB.
Because of the simple geometry, it was possible to estimate that the second phase
was present to the extent of about 1.53% by volume corresponding to 1.67% by
weight of ZrB. If the sample is considered to consist only of Zr and B, this cor-
responds to a boron content of 19.1% or a B/Zr ratio of 1.99. This is about in the
middle of the range shown in Table 2 except for the General Electric Co. data
which are significantly lower. Considering all the data, the best value of B/Zr
for this lot of material appears to be about 1.99.

Dr. Greenberg reports the following results for trace impuritie 352
and 1363 PPM carbon, 231 and 290 PPM oxygen, 6 and 8 PPM hydrogen, 36 and 37
PPM nitrogen, .04 and .05% Fe, .04 and .05% Hf, .001 to .02% Ti, .01% V, .001
to .01% Cr, .001 to .002% Mg, .0001 to .001% Mn, .001 to .01% Si, and .001 to
.01% Mo.

Dr. Lyon reports 1060 PPM of carbon, 14 PPM oxygen, 37 PPM nitrogen,
21 PPM hydrogen.

These results may be compared with Table 1 and indicate approximate
agreement in most cases.

15

TABLE 1

SUMMARY OF ZrB_2 ANALYSES

Element	As Received	Zone Refined
Zr	77.25%	79.82, 80.57%
B	19.58%	18.80, 19.04%
O	0.2%	52 ppm
C	0.57%	215 ppm
N	-----	134 ppm
H	-----	1.52 ppm
Ag	-----	.001%
Al	.01 to .05%	.001 to .01%
Ca	.01 to .05%	ND*
Cr	.01 to .05%	.001%
Cu	.005 to .01%	.001%
Fe	.01 to .05%	.01%
Hf	.001 to .005%	.01%
Mg	-----	.001 to .01%
Mn	.05 to .1%	.001%
Ni	.01 to .05%	ND
Si	.01 to .05%	.01 to .1%
Ti	.005 to .01%	.001%
V	-----	.001%

*ND = not detected.

TABLE 2

BORON AND ZIRCONIUM ANALYSES ON ZrB_2

BAR NUMBER	83-4 (a)	87-4B (a)	94-1A (b)	79 (b)	83 (c)	85 (c)
Boron-%	18.70 18.90	18.98 19.09	18.31	18.32	18.99 18.95	18.89 18.87
Average	18.80	19.04			18.97	18.88
Range-%	±0.53	±0.26			±0.11	±.05
Zirconium-%	80.05 79.60	80.74 80.40	81.16	81.13	80.27 80.43	80.21 80.56
Average	79.82	80.57			80.35	80.38
Range-%	±0.27%	±0.21%			±.09%	±.21%
Zr + B - %	98.62 ± .32	99.61 ± .22	99.47	99.45	99.32 ± .10	99.26 ± .19
B/Zr	1.96 ± .016	1.99 ± .009	1.90	1.90	2.01 ± .004	1.97 ± .005

(a) From Part I of this report.

(b) Data of Dr. T. F. Lyon - General Electric Co.

(c) Data of Dr. Elliott Greenberg - Argonne National Laboratory.

2. Zirconium Carbide

Zirconium carbide is characterized by a wide range of homogeneity extending from a composition of about $ZrC_{0.65}$ to $ZrC_{1.0}$. The preparation of nearly stoichiometric ZrC has been described in Parts I and II of this report. A summary of the analytical data on this material is given in Table 3.

During the present report period we have made a number of zirconium carbide bars whose composition falls near the lower end of the homogeneity range. Samples of this material have been distributed to Dr. Blackburn for vapor pressure measurements; to Dr. Berkowitz-Mattuck and to Dr. Margrave for kinetic studies; and to Dr. Kelley for heat-of-combustion measurements.

This sample was made by adding pure ZrO_2 to ZrC powder before sintering into rods for zone-refining. The amount of ZrO_2 added was calculated to bring the carbon content to about 8% assuming all the oxygen to be removed as CO during melting. No particular difficulty was encountered in zone refining this material except that the evolution of CO caused a few small droplets of carbide to be thrown off from the molten zone.

The following additional analytical data were obtained on the product:

Carbon: 7.80%, 7.97%; average 7.88%

Oxygen: 0.178%, 0.21 %, 0.302%, 0.247%; average 0.236%

Nitrogen: 0.217%

As shown in Table 3 the major metallic impurities are 0.12% Ti and 0.07% B with no other metallic impurity present in excess of 100 PPM.

A single analysis for free carbon gave a value of 0.031%. However, no free graphite or other second phase could be detected metallographically, and we have obtained evidence that the usual method of free carbon analysis gives high results. For these reasons, we believe that no appreciable free carbon is present in this sample. A detailed discussion of the problem of free carbon analysis and a modified procedure are given below under hafnium carbide.

3. Zirconium Oxide

Attempts to zone-melt zirconium oxide using induction heating at 450 KC or 5 MC were unsuccessful because insufficient energy was absorbed by the rod even when it was strongly preheated. We were able to grow polycrystalline boules of pure ZrO_2, however, by means of the ADL-Strong arc-imaging crystal

18

TABLE 3

ANALYSIS OF ZIRCONIUM CARBIDE

Element	As Received	Zone Refined
Zr	88.16%	89.27%
C	11.45%	11.22%
B	.05 to .1%	.07%
O	.05%	.005%
N	0.15%	.067%
Ag	.0002%	ND*
Al	.001 to .005%	.01%
Ca	.001 to .005%	.001%
Co	.001 to .005%	ND
Cu	.05 to .1%	.001%
Fe	0.12%	.07%
Hf	-----	.001%
Mg	.005 to .01%	.001 to .01%
Mn	.05 to .1%	.001%
Mo	.001 to .005%	.001%
Ni	.05 to .1%	ND
Pb	.005 to .01%	.001%
Sb	.01 to .05%	ND
Si	.01 to .05%	.001%
Sn	.005 to .01%	.01%
Ti	.01 to .05%**	.12%

*ND = not detected.

**Suppliers analysis.

19

growing furnace. Details of this preparation are given in Part II of this report. Analytical data on the two samples of ZrO_2 used are given in Table 4.

4. Hafnium Metal

Hafnium metal was obtained in the form of arc-melted ingot from the Wah Chang Corp. The major impurity in this sample was 0.226% of oxygen (weighted average value for the two ingots, which contained 0.217% and 0.231%) which caused the sample to be somewhat brittle. Metallographic examination revealed the presence of many microscopic cracks (due apparently to severe thermal stresses during melting) and a possible very slight trace of a second phase.

Other detected impurities were 0.0306% N, 0.027% Zr, 0.021% C, 0.015% Nb, 0.005% Si, 0.002% Al.

Assuming the oxygen, carbon, and nitrogen to be present as HfO, HfC, and HfN, respectively, the proximate analysis of the sample is: 2.75% HfO, 0.33% HfC, and 0.42% HfN. By difference, the metallic hafnium content is 96.53%.

Two attempts were made to reduce the oxygen content of this sample by electron-beam melting. The first product contained 0.180% of oxygen but the second contained only 0.0468%. Samples of this latter material were furnished to Dr. Freeman for preparation of high purity halides and to Dr. Blackburn for evaporation studies.

For purposes of low-temperature heat capacity measurements, however, a sample of "iodide" hafnium was loaned to Prof. Westrum by Dr. J. O. Betterton of Oak Ridge National Laboratory. This is the same sample used by Kneip et al.,[1] for their low-temperature specific heat measurements. The following analysis is reported by these authors: 500 PPM Zr; 65 PPM Si; 200 PPM Fe; 7 PPM Ni; 3 PPM Cu; 43 PPM Mo; 1 PPM W; 18 PPM O_2; 130 PPM C; <1 PPM H_2; and <5 PPM N_2.

5. Hafnium Diboride

The preparation and characterization of HfB_2 is described in detail in Part II of this report. The first lot of material was found to contain 1.31% of major metallic impurities and was rejected as unfit for use in this program.

A second lot of HfB_2 was therefore made using a purer starting powder. The analytical data for this lot are summarized in Tables 5 and 6. Table 6 gives an indication of the uncertainty of the analyses and presents also some data recently received from Dr. T. F. Lyon of the General Electric Co. The B/Hf ratios are in

20

reasonable agreement despite the large uncertainty indicated by the analysis of Bar No. 439. The agreement between the two laboratories is better than in the case of ZrB_2. Metallographic examination disclosed the presence of two minor extraneous phases which were identified by X-ray diffraction and electron microprobe methods as free boron and the hitherto-unknown HfB_{12}. These results are in agreement with the slight excess of free boron shown by the chemical analysis.

Dr. Lyon also reports for this sample: 1750 PPM carbon, 16 PPM oxygen. 1 PPM nitrogen and less than 1 PPM hydrogen. Except for the nitrogen analysis, these results are in reasonable agreement with Table 5.

The second sample of HfB_2 was used in all studies except the fluorine-bomb calorimetry work at Argonne Laboratory for which the 1600 PPM of carbon was considered unacceptably high. We therefore made a third preparation with the aim of producing a low-carbon material. The raw material was made by Wah Chang Corp. and was generously made available to us by Dr. Larry Kaufman of Manlabs, Inc. We have no detailed analysis of this raw material but its purity, except for the lower carbon content, was generally similar to that used in lot 2 above.

Analysis of lot 3 after zone-refining gave 89.33% of hafnium and 10.73% of boron (both average of 3 determinations) or a mole ratio of 1.98 boron to hafnium.

Duplicate carbon analyses gave 254 PPM and 429 PPM or an average of 342 PPM. Further analyses showed 111 PPM of oxygen and 120 PPM of nitrogen. Spectrographic analysis showed 10 PPM each of Ag, Al, Na and Ti and less than 1 PPM each of Cu, Fe and Mg. Metallographic examination showed small traces of a second phase in some sections of the bar and none in others - in agreement with the elemental analysis above.

6. Hafnium Carbide

Because of its extremely high melting point, the preparation of high-quality samples of hafnium carbide has presented more difficulty than any of the other materials of interest to this program. In Part II of this report we have discussed the problems involved both in zone-refining and in arc-melting this material. During the present report period, we have prepared samples of HfC both by zone-refining and by arc-melting.

The availability of a new zone-refining apparatus made it appear worthwhile to renew our attempts to zone-refine this material. Because of a change in the high-frequency power supply, the new equipment is less susceptible to arcing than that previously used and is thus more suitable for use with high-melting materials and close coil clearance.

21

TABLE 4

ZrO$_2$ ANALYSES

Impurity	Wah Chang ZrO$_2$	ZrO$_2$ from Metal
Al	125 ppm	.01 to 1.0%
B	0.2	.001
Cd	0.3	ND
Co	<5	ND
Cr	<10	.001 to .01
Cu	<25	.001 to .01
Fe	790	.01 to 1.0
Hf	<40	.001 to .01
Mg	30	.001 to .1
Mn	10	.001 to .01
Mo	<10	ND
Ni	<5	ND
Pb	<5	.001 to .01
Si	40	.01 to .1
Sn	<10	.001
Ti	52	ND
V	<5	ND
W	<25	.001 to .01
Zn	<50	ND
Ge	-	.001 to .01
Sr	-	.001 to .01
Ba	-	.001 to .1
Na	-	.001 to .01
Bi	-	.0001

Note: < = less than.
       ND = not detected.

22

TABLE 5

SUMMARY OF HfB$_2$ ANALYSES (FOR LOT 2)

Element	As Received	Zone Refined
Hf	-	88.98% (average)
B	10.6%	10.97% (average)
C	0.26%	0.16%
N	0.01%	42 ppm
O	0.14%	26 ppm
Al	<100 ppm	ND*
Cb	<100 ppm	ND
Cd	<100 ppm	ND
Co	<100 ppm	ND
Cr	<100 ppm	.001%
Cu	<100 ppm	.001%
Fe	0.05%	30 ppm
Mg	<100 ppm	.001%
Mn	<100 ppm	ND
Mo	<100 ppm	ND
Ni	<100 ppm	ND
Pb	<100 ppm	ND
Si	0.05%	10 ppm
Sn	<100 ppm	ND
Ta	<100 ppm	ND
Ti	<100 ppm	30 ppm
V	<100 ppm	ND
W	<100 ppm	ND
Zn	<100 ppm	ND
Zr	450 ppm	0.01 to 0.1%

*ND = not detected.

23

TABLE 6

BORON AND HAFNIUM ANALYSES ON SECOND LOT OF HfB_2

BAR NUMBER	452-3 (a)	457-4 (a)	439 (a)	450-3 (b)
Boron-%	10.98	10.98	10.78 11.11	10.88
Average			10.945	
Range-%			±1.5	
Hafnium-%	89.11	89.10	88.59 88.90	89.64
Average			88.745	
Range-%			±0.18	
Hf + B	100.09	100.08	99.69 ± .31	100.52
B/Hf	2.034	2.035	2.036 ± .34	2.01

(a) From Part II of this report.

(b) Data of Dr. T. F. Lyon - General Electric Co.

24

In order to reduce the radiation loss from the heated zone, the diameter of the sintered bar was reduced from 3/8" to 5/16" or 1/4".

In order to reduce the temperature of the molten zone, a large excess of carbon (15 to 30 atomic percent) was added to the material before sintering in the hope that the melt would approach the HfC-C eutectic.

Somewhat over thirty bars were made, the density of which was varied from about 50% to 65% of theoretical by varying the particle size of the starting power. Although considerable difficulty was experienced with irregular melting, we succeeded in producing a few small zoned pieces from this lot of material. Within the above-mentioned range, changes of density did not appear to have a major effect on melting behavior.

The above experiments show that it is in fact possible to melt hafnium carbide by induction heating, but we have yet to demonstrate adequate control of the molten zone. We now believe that such control can be obtained by using sintered bars of high density (80% or higher) which will limit migration of liquid within the sintered rod. Preliminary experiments and quotations from outside sources indicated that it would not be feasible to produce the needed high-density bars within the scope of the present contract.

Analysis of several of these zoned pieces showed carbon content ranging from about 5.6% to 6.1% total carbon. This is considerably below the theoretical value of 6.3% although a large excess of carbon was used in the sintered bars. This result indicates a considerable vaporization of carbon at the melting temperature and may indicate that the highest-melting composition in the system contains less than the theoretical amount of carbon.

Because of the low yield of zone-melted HfC obtained with the presently available sintered bars and because the range of carbon content is about the same as can be produced by arc-melting, it was decided to produce the large sample needed for low-temperature heat capacity measurements by the latter method.

About 300 grams of HfC were made by arc-melting sintered bars on a water-cooled copper hearth using a water-cooled tungsten electrode. In order to minimize loss of carbon during melting, the operation was conducted in an atmosphere of argon containing 3.14% of ethylene and 11.4% of hydrogen.

Two analyses for total carbon on composite samples gave 6.08% and 6.18% or an average of 6.13%. Since the carbon content of the original powder was 6.25%, some loss of carbon took place despite the use of a carburizing atmosphere. Spot analyses of several preliminary melts indicated that the local carbon content may deviate a few tenths percent from the average value because of preferential carbon loss from areas directly acted on by the arc.

25

Considerable difficulty was encountered in obtaining a reliable free-carbon analysis of this material. Five separate analyses gave values of 2000, 550, 540, 700 and 156 PPM respectively. Metallographic examination, however, showed no free graphite in the sample although portions of the surface were slightly blackened with soot from the arc-melting. We therefore considered that the lower values of free carbon were more nearly correct and that the erratic and high values were due to incomplete oxidation of the combined carbon during acid treatment. To substantiate this conjecture, the following experiments were performed:

A sample of the arc-melted HfC was crushed and screened to -100 mesh and treated with HNO_3 and HF as recommended by Kriege.[2] The white residue of basic salts was then dissolved in excess KHF_2 and the few remaining dark particles filtered off. When these particles were examined under the microscope, they appeared translucent and dark red in color. They were almost completely soluble in 10% NaOH solution.

This behavior is in contrast to that of commercial HfC powder, which leaves an opaque, black residue. This black residue is insoluble in NaOH and undoubtedly represents true uncombined carbon.

The red residue from the arc-melted carbide appears to represent combined carbon which is incompletely oxidized during acid treatment. The amount of such residue probably depends on the particle size of the carbide and on the details of the acid treatment. This would account for the earlier variable results of the combined carbon analysis.

Chemically, this red residue probably consists of polymeric carboxylic acids related to mellitic acid. This constitution would account for its solubility in NaOH and is in agreement with the results of Pauson et al.,[3] who find similar residues from the acid leaching of thorium and uranium carbides.

A sixth sample of HfC was therefore analyzed for free carbon by the following procedure:* A 3g portion of the sample is weighed into a Pt dish. Add 20 ml HF and then add HNO_3 dropwise until reaction ceases. Heat on a steam bath, then allow to evaporate to a volume of 2 ml. Dilute with 20 ml HF and 2 ml HNO_3 and again evaporate to 2 ml. Dilute to 80 ml with hot H_2O, warm on a steam bath for 10 minutes. Filter the solution through an asbestos gooch which has previously been thoroughly washed with dilute HCl and ignited. Wash the residue as follows; 5 times with hot H_2O, 5 times with hot 10% NaOH, 5 times with hot water, 5 times with 10% HCl and finally 10 times with hot water. Dry gooch for 1/2 hour at 105°C.

Transfer the asbestos and the free carbon to a Leco combustion cuplet. Add 1 gram of electrolytic iron powder and 1 low carbon copper ring (Leco product). Ignite the sample in the Leco Conductometric Carbon Analyzer and measure the resulting CO_2 by recording the change in potential between the weak $Ba(OH)_2$ solutions with the conventional oscilloscope attachment.

Correct for a blank which has been taken through the entire procedure along with the sample portion.

Standardize by running an appropriate Bureau of Standards steel sample.

Duplicate analyses by this procedure gave 120 and 145 PPM free carbon or an average of 137 PPM, which we believe to be the best value for free carbon in this arc-melted material. This value probably represents mainly the soot deposited on the surface of the sample during arc-melting.

Subtracting this value of free carbon from the value of 6.13% previously for the total carbon obtained, we find a combined carbon content of 6.12% for this sample, corresponding to a formula of $HfC_{.968}$.

Chemical and spectrographic analyses gave the following results for the arc-melted product: 0.035% Zr; 0.031% N; 0.005% Fe; 0.003% O; 0.002% each Ti and Si; 0.001% each of H, Cu, Mn, and Mg. No tungsten from the electrode could be detected.

A preliminary investigation was carried out with the aim of preparing a sample of carbon-deficient HfC near the lower end of its homogeneity range. No accurate data exist regarding the composition of the carbide at this point but Sara and Dolloff[4] report that the lower limit of homogeneity of ZrC occurs at a composition of $ZrC_{.63}$.

We therefore arc-melted (in helium) a mixture of Hf metal with HfC, calculated to give a product containing 4.3% of carbon and corresponding to a composition of $HfC_{.66}$. This preparation was turned, mixed and remelted several times in order to ensure a homogeneous product. This product was found by analysis to contain 4.24% of carbon, indicating a slight carbon loss during melting. Its X-ray diffraction pattern showed the presence of between 5% and 10% of free hafnium.

A portion of this melt was powdered to -100 mesh and leached with HF until only about 1/4 of the material remained undissolved. This residue gave an X-ray diffraction pattern of pure HfC with no detectable free hafnium. Its carbon content was found to be 4.52%, corresponding to a composition of $HfC_{.705}$ for the lower limit of homogeneity of HfC. The homogeneous range of HfC therefore appears to be somewhat narrower than that of ZrC.

This conclusion is subject to the reservation, however, that the leached residue may have contained free carbonaceous material released from the dissolved carbide by the action of the HF. If this is the case, the observed carbon content is too high. A more reliable value for the lower homogeneity limit should be obtained from preparation of further arc-melted samples. On the other hand if we assume that the original arc-melted sample consists of $HfC_{.705}$ and carbon-free hafnium metal, then its free metal content is calculated to be 6.2%. This is in the range indicated by the X-ray analysis.

IV. OXIDATION OF ZIRCONIUM AND HAFNIUM BORIDES AND CARBIDES*

A manuscript describing the thermal conductivity apparatus used in this laboratory to study the oxidation of metals and alloys at temperatures above 900°C has been submitted for publication to the Journal of the Electrochemical Society under the title "High Temperature Oxidation. I. Copper." A final draft of the second paper of the series "High Temperature Oxidation. II. Molybdenum Silicides" has been prepared and will be submitted to the same journal. This report comprises results which will be presented as papers III. and IV. of the series on the oxidation of the borides and carbides respectively of Hf and Zr.

A. ZIRCONIUM AND HAFNIUM DIBORIDE

1. Background

The oxidation of ZrB_2 was studied by F. H. Brown, Jr. in 1955 in the temperature range 649-1315°C in pure oxygen, and moist dry air.[5] Since Brown worked with porous compacts of the diboride, his initial surface areas are unknown, and undoubtedly changed due to sintering during the course of exposure at high temperatures. He was able to conclude qualitatively that ZrB_2 is oxidized more rapidly in oxygen than in dry air in the range 650-1100°C, and much more rapidly in moist air than in dry at 650°C.

Samsonov[6] oxidized ZrB_2 in air at 1000°C, and measured a depth of corrosion of 0.45 mm after 150 hours. For material of theoretical density, this would correspond to stoichiometric oxidation of 0.274 g/cm^2 of the alloy, or to a total oxygen consumption of 0.0873 g/cm^2. The net weight change cannot be computed since an unknown portion of the $B_2O_3(\ell)$ must certainly have evaporated during the experiment. From metallographic examination of the oxide scale, Samsonov postulated the existence of $ZrO(s)$ immediately adjacent to the alloy, and a molten layer of B_2O_3 at the surface of the oxidized specimen. He assumed that with increasing time of exposure, oxygen would diffuse through the $B_2O_3(\ell)$ to the alloy and react with $ZrO(s)$ to form $ZrO_2(s)$, while at the same time B_2O_3 would gradually vaporize.

More recently, the oxidation of ZrB_2 was studied by Kuriakose and Margrave,[7] who measured net weight change of fully dense samples with time, at temperatures of 1218-1529°K and oxygen pressures between 100 and 760 torr.

---

*Prepared by Dr. Joan Berkowitz-Mattuck, Arthur D. Little, Inc.

They were able to fit their data to a parabolic rate law, with an activation energy for net weight gain of 19.8 ± 1.0 kcal/mole. The oxidation rate was independent of carrier gas flow rate, and directly proportional to the oxygen partial pressure in helium.

No quantitative data has been reported in the literature for the oxidation of HfB_2. Hafnium is expensive and difficult to separate from zirconium. The two metals are so similar in chemical properties, that the oxidation characteristics of their respective diborides would normally be assumed to be identical. Samsonov exposed HfB_2 in air in a series of screening experiments, and reported intensive oxidation above 600-700°C, and disintegrative oxidation at 1000-1200°C.[8]

The present work was undertaken to obtain quantitative data on the oxidation of ZrB_2 over a wider temperature and pressure range than that covered in previous studies, and to compare the oxidation of ZrB_2 and HfB_2 experimentally. In addition, in order to evaluate the effect of B_2O_3 volatility in the oxidation of ZrB_2, several measurements of total oxygen consumption were made under conditions for which Kuriakose and Margrave [7] had obtained net weight change data.

2. Experimental Method

Samples of ZrB_2 were synthesized by the zone melting technique described by Westrum and Feick.[9][*] Hafnium diboride was prepared [*] by the same technique with a high-purity powdered starting material supplied by Wah Chang Corp. The resultant zone refined bars contained less than 0.1% of zirconium.

The experimental procedure has been described in detail in earlier publications.[10][11] The only essential change necessitated in the work with borides was the substitution of platinum or rhodium support rods for the Al_2O_3 or ThO_2 fingers used previously. The B_2O_3 formed in the oxidation of diborides reacts with refractory oxides. Platinum was suitable for pellet temperatures up to 1600°C; rhodium was required for higher temperature runs. Samples in the form of pellets, 0.3 cm long and 0.7 cm in diameter, were polished through diamond dust, cleaned, and degassed in helium prior to oxidation. A thermal conductivity apparatus was used to measure the net oxygen consumed during the oxidation of inductively heated samples in a stream of helium and oxygen at a total pressure of one atmosphere.

---

*Also see Chapter III of this report.

3. Results for Zirconium Diboride

a. Experimental data. The experimental data for ZrB_2 are summarized in Table 7. The initial weights listed are weights taken after degassing the samples in pure helium at about 1870°K until the signal from the thermal conductivity bridge dropped to zero (approximately 30 minutes). Weight changes during this period were in every case less than 2×10^{-4} g. The sample surface areas (A) were calculated from the gross physical dimensions of the specimens. It will be shown below that this may introduce considerable uncertainty in the calculated absolute rates, since oxidation along the length of cracks seems to proceed just as it does on the outer sample surface. The densities are simply initial sample weights divided by geometric sample volumes. The range in densities, computed in this crude way, is from 5.56 to 6.04, with an average value of 5.86 ± 0.11 g/cc. The average is to be compared to a theoretical X-ray density for ZrB_2 of 6.09 g/cc. The temperatures are measured pyrometer temperatures read during the oxidation runs, corrected for sample emissivity (assumed equal to 0.6) and the measured transmission characteristics of the optical system. Temperatures can usually be held to $\pm$ 5°C during the course of heating. The oxygen pressures are partial pressures in helium. The carrier gas flow rate of 95 ml/min corresponds to a linear flow velocity in the neighborhood of the sample pellet of about 3.1 cm/sec. The exposure times indicate the duration of each oxidation experiment from the time the induction unit is turned on until it is turned off. The weight changes are simply the differences in weight of each pellet before and after oxidation, divided by initial geometric surface area. The total oxygen consumed is computed from the area under the thermal conductivity curve as described below and represents the amount of oxygen in all of the product oxides formed during the oxidation experiment.

b. Analysis of the data. In the experiments described, a helium-oxygen stream is passed through the reference cell of a thermal conductivity bridge, and over an inductively heated sample pellet which removes some of the oxygen by reaction. The gas stream, depleted in oxygen, is passed through the sampling cell of the thermal conductivity bridge. The reference and sampling cells form two arms of a Wheatstone bridge, whose output is continuously recorded. The signal obtained is proportional to the difference in oxygen partial pressure or gas density in the two cells. Since the measurements are carried out in an open flow system, the total pressure is everywhere close to one atmosphere. Thus, when an experiment is run in pure oxygen, a zero signal is obtained, in spite of the fact that oxygen is consumed, because the pressure of oxygen is always one atmosphere in both the reference and sampling cells.

31

TABLE 7

SUMMARY OF EXPERIMENTAL DATA ON ZrB_2

Pellet	Initial Weight (g)	Area (cm²)	Density (g/cc)	Temp. (°K)	Oxygen Pressure (Torr)	Flow (cc/min)	Exposure Time (min)	Weight Change (g/cm²)	Total O₂ Consumed (g/cm²)	K_p (g²/cm⁴-min) x 10⁹
XVII-6	0.5696	1.2794		1202	37.5	95		0.0006	0.0008	5.81
XII-40	0.8089	1.673	5.82	1217	37.5	119	112	--	0.000895	5.6
XII-48	0.6663	1.418	5.99	1260	37.5	59.5	131	0.0002	0.0006	3.10
XII-45	0.6604	1.419	5.89	1260	37.5	119	120			3.26
				1314	37.5	119	114			8.08
				1372	37.5	119	119			18.70
XVII-10	0.6568	1.4361		1202	694	95	50	0.0014	0.0019	75.7
				1829	694	95	80	0.0363	0.1415	129,800
XIV-5	0.6880	1.4355	5.875	1540	16.5	95	121	0.0023	0.00976	1,020
XIV-18	0.6804	1.529	5.56	1556	38.75	95	120	0.00439	0.01654	2,620
XIV-20	0.7240	1.602	5.57	1556	27.0	95	120	0.00424	0.01552	2,550
XIV-1	0.7068	1.5155		1560	11.3	95	130	0.00324	0.01698	2,590
XIII-47	0.7586	1.6097	5.82	1550	19.9	95	117	0.00267	0.01342	2,300
XIII-49	0.7715	1.6368	5.78	1562	8.5	95	133	0.0030	0.01518	2,720
XIII-45	0.8033	1.6452	5.98	1604	19.9	95	135	0.00546	0.0296	10,570
XI-48	0.6627	1.453	5.80	1633	9.9	95	130	0.0095	0.0509	28,900
XIII-2	0.7403	1.5536	5.91	1654	8.25	95	118	0.00572	0.0362	21,300
XIII-6	0.7080	1.5172	5.84	1656	10.1	95	120	0.00686	0.0350	17,400
XIII-16	0.6963	1.5038	5.82	1687	7.0	95	128	0.00671	0.0302	15,300
XIII-42	0.7623	1.5864	5.94	1711	19.9	95	120	0.0204	0.0403	19,120
XIII-4	0.7597	1.5782	5.96	1729	8.0	95	144	0.00984	0.0519	40,000
XIII-8	0.7578	1.5738	5.97	1759	13.2	95	120	0.01282	0.0709	73,400
XIII-40	0.7688	1.5994	5.93	1805	19.9	95	114	0.01452	0.0798	78,300
XIV-12	0.8293	1.674	6.04	1550	19.9	95		--	--	4,070
				1657						12,600
				1701						20,400
XIV-8	0.6761	1.454	5.88	1557	27.0	95		--	--	1,870
					16.5					

32

The output from the bridge, S, in millivolts is proportional to the difference in oxygen density in g/cc, $(\rho_1 - \rho_2)$ in the reference and sampling cells, respectively.

$$S = k(\rho_1 - \rho_2) \tag{1}$$

Since the total pressure is essentially the same in the two cells, the flow rates must be different. If v_1 (cc/min) is the flow rate through the reference cell and v_2 is the flow rate through the sampling cell, then the desired rate of oxygen consumption by the sample under investigation, dm/dt (g/cm^2-min) is given by

$$dm/dt = (\rho_1 v_1 - \rho_2 v_2) \tag{2}$$

where m is total oxygen consumption in grams and t is time in min. The flow of helium must be constant throughout the system. Hence

$$\rho_{1,He} v_1 = \rho_{2,He} v_2 \tag{3}$$

where $\rho_{1,He}$ and $\rho_{2,He}$ are the densities of helium in the reference and sampling cells, respectively. Solving (3) for v_2, and substituting in (2), one derives with the aid of (1) and the perfect gas laws an expression for the rate of oxygen consumption, dm/dt, in terms of measured quantities:

$$dm/dt = v_1(S/k)/ \{1 - p_1 + RT(S/k)/M\} \tag{4}$$

where M is the molecular weight of oxygen, T is the temperature at which the flow rate v_1 is measured (298°K), R is the gas constant, and p_1 is the oxygen partial pressure in the initial gas stream in atmospheres. Since $\rho_2 \geq 0$, it follows that in (4) $RT(S/k)/M \leq p_1$. Therefore, if p_1 is a small fraction of an atmosphere, the rate of oxygen consumption, dm/dt, is directly proportional to the observed signal, apart from the previously discussed[10] effects introduced by the separation of reaction and detection sites. At high oxygen partial pressures, equation (4) must be used to interpret the results. In practice, the denominator in (4) is very nearly constant throughout any given experiment.

A typical parabolic plot of m^2 vs t, constructed from the corrected area under the experimental thermal conductivity curve according to equation (4) is shown in Figure 1. Under all conditions investigated in this study, the oxygen consumption vs time data for ZrB_2 could be fitted to a parabolic rate equation after an initial period of about 40 minutes. The parabolic rate constants given in the last column of Table 7 were computed from the final slopes of plots similar to that shown in Figure 1.
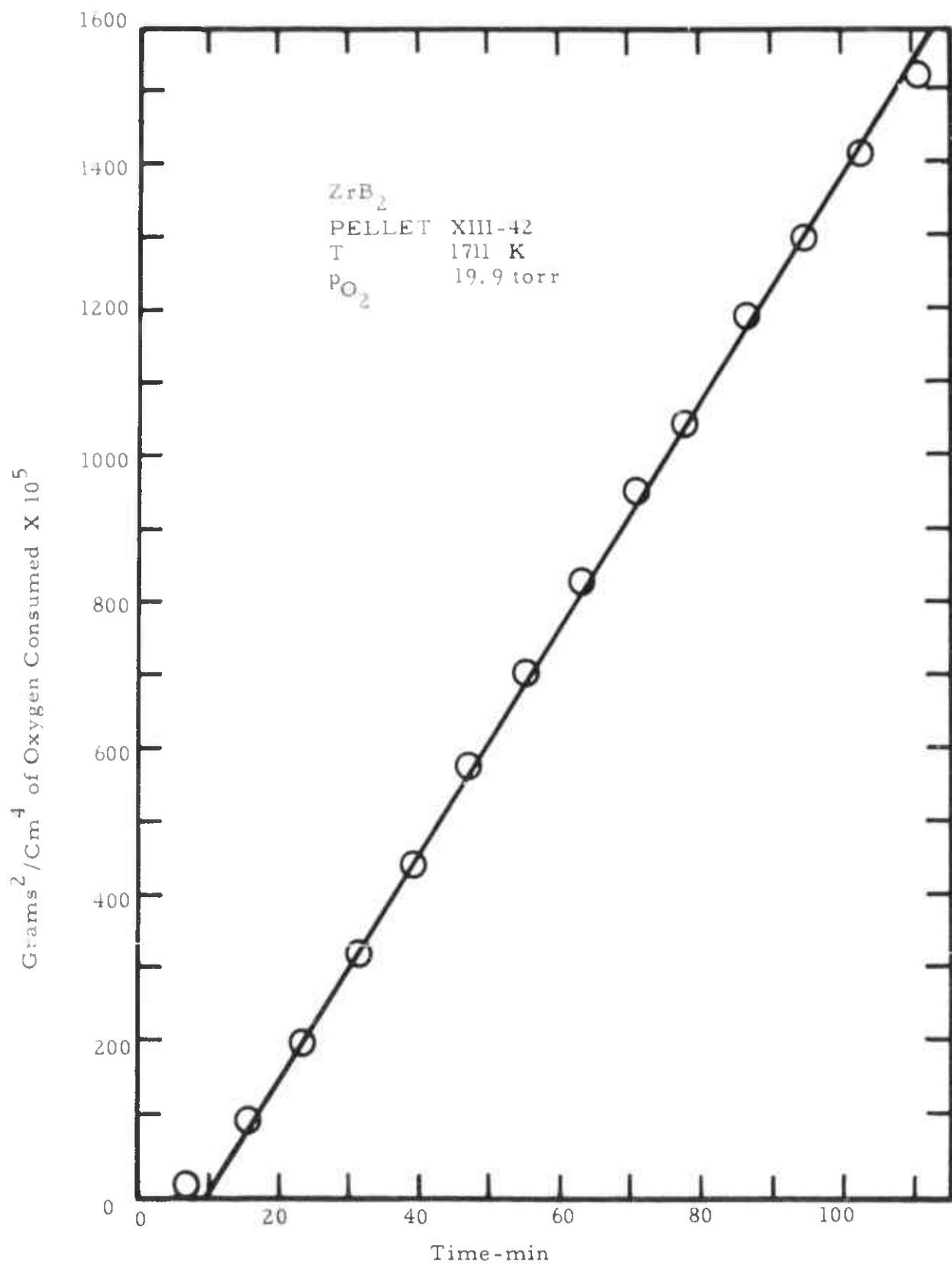
Figure 1   Typical Parabolic Plot of Zirconium Diboride Oxidation Data

c. Temperature dependence of the oxidation rate. The temperature dependence of the parabolic rate constants for total oxygen consumption is shown on a log k_p vs $1/T$ plot in Figure 2. Above 1400°K an activation energy of 77 ± 5 kcal/mole was calculated for the over-all oxidation process by the method of least squares. Below 1400°K, the activation energy is clearly much lower, and will be discussed below in conjunction with the work of Kuriakose and Margrave.[7]

The wide scatter of points about the least squares straight line in the high temperature range is due to the high absolute value of the activation energy, and to the presence of cracks in the as-prepared samples. Since the activation energy is high small errors in temperature measurement or small fluctuations in temperature during a run will result in large uncertainties in measured oxidation rates. For example, at 1500°K, an error or fluctuation of 10° in experimental temperature will be reflected in more than a 15% error in k_p. The presence of cracks, introduced in the zone-refining process, results in a difference between real and geometric surface areas. It will be shown below, that the surface of a crack that extends into the bulk specimen is oxidized just as if it were external surface. Since the number of cracks is certainly not constant from one sample to another, the area used in computing k_p should really be the sum of gross geometric surface area and surface areas of cracks. The use of the former alone can introduce the observed scatter in the data.

d. Pressure dependence of the oxidation rate. Measurements of the pressure dependence of the oxidation rate were hampered by temperature fluctuations within a single run. At 1560°K, the results given in Table 7 for pellets XIV-18, XIV-20, XIV-1, and XIII-49 show no trend with oxygen partial pressure over the range 8.5 - 39 torr. In order to check direct pressure dependence found by Kuriakose and Margrave at 1329°K over the range 100 - 760 torr, measurements were extended to 694 torr. The data on pellets XVII-10 and XVII-6 at 1200°K show an increase in parabolic rate constant from 5.8 to 75.7×10^{-9} with an increase in pressure from 37.5 to 694 torr. At 1830°K, the parabolic rate constant at 20 torr, found by extrapolation of the data in Figure 2, is 1.1×10^{-4} which is essentially the same as a measured value of 1.3×10^{-4} at 694 torr. Thus, there appears to be a fundamental difference in the mechanism of oxidation of ZrB_2 at intermediate and high temperature. Below 1330°K, the oxidation proceeds with an activation energy of about 20 kcal/mole, at 1330°K the rate is directly proportional to the oxygen partial pressure. Above 1550°K, the activation energy is greater than 70 kcal/mole; and at 1830°K, the rate is nearly independent of oxygen partial pressure.

e. Metallographic examination of the oxide films. Pellet XIII-40 was mounted and polished for metallographic examination, after it had been oxidized for 114 minutes at a temperature of 1805°K and an oxygen partial pressure of
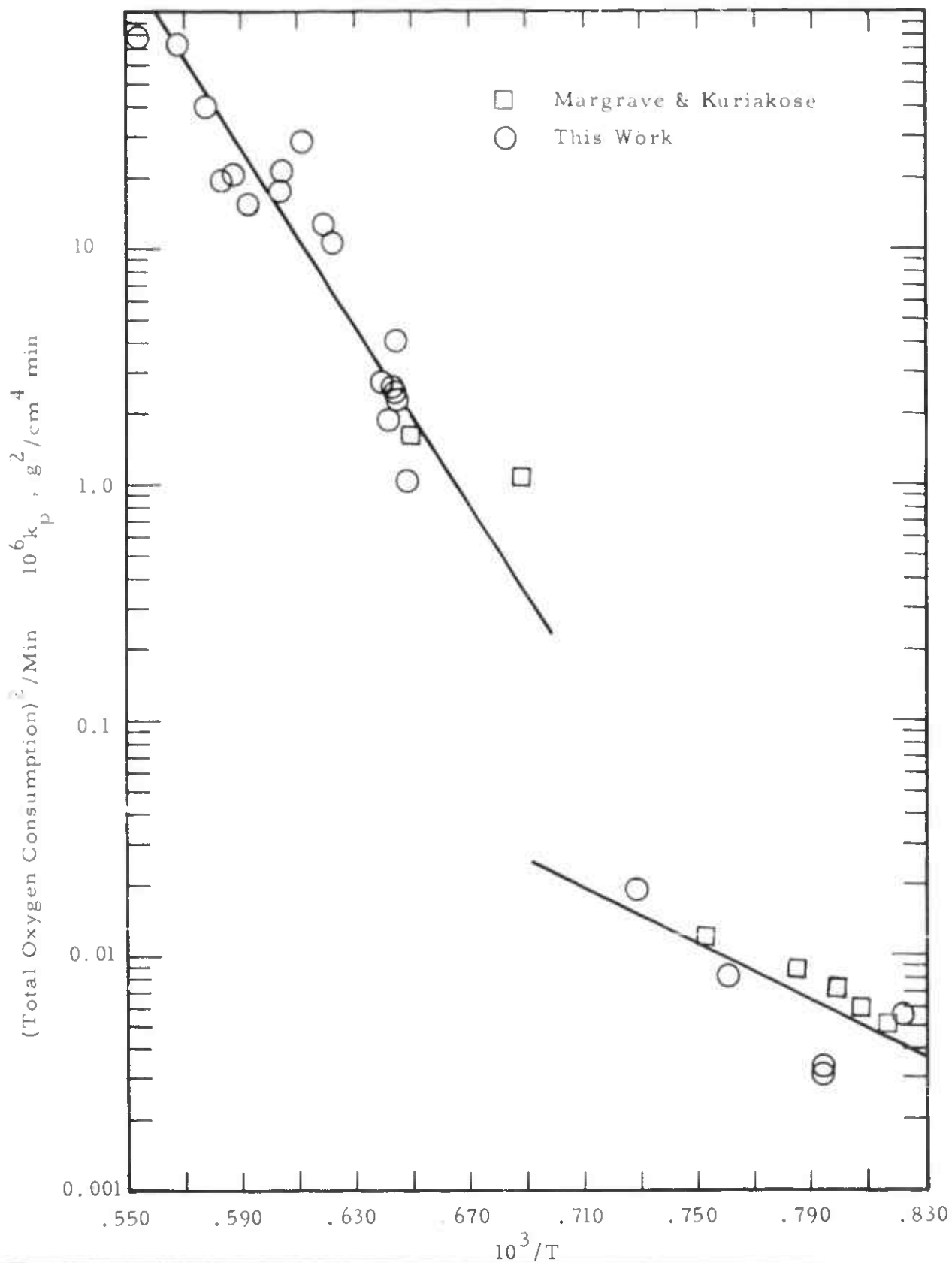
Figure 2   Temperature Dependence of the Rate of Total Oxygen Consumption
for Zirconium Diboride - Arrhenius Plot of Parabolic Rate Constants

19.9 torr. Figure 3a taken at a magnification of about 90X, shows clearly both the grain structure of the bulk material and the dense columnar oxide which forms on the surface during oxidation. Figure 3b is similar, but shows a region with an extensive crack running parallel to the ZrB_2 surface. Figure 3c at a magnification of about 450X focusses on the oxide within such a crack. The product is very similar to that on the surface of the refractory, and appears to grow into the bulk material at certain preferred growth sites. Figures 3d, e, f and g show the surface oxide once more at higher magnifications than Figure 3a. The oxide is seen to be crystalline in nature, with the grains running for the most part perpendicular to the ZrB_2 surface. The oxide-metal interface is clearly not smooth, but the points of maximum growth rate do not seem to be related in an obvious way to the structure of the substrate. The interesting photomicrograph in Figure 3h at a magnification of 30X (and the same area at 90X magnification in Figure 3i) shows the oxidation behavior of ZrB_2 in the neighborhood of a crack that inter - sects the surface. The surface of the crack as seen in these pictures is almost certainly the surface of the original alloy. Therefore, the oxide must grow by inward diffusion of oxygen. The columns of oxide are seen to run perpendicular to the outer surface of ZrB_2, and in like manner, are seen to run perpendicular to the surface of the crack (parallel to the sample surface). A crack then effectively increases the surface area of the alloy above that of the outer surface area. Furthermore, the oxide on ZrB_2 does not have the "self healing" character, which is desirable for all high temperature protective coatings. The oxide on $MoSi_2$ would bridge over a crack, partially fill it in. The oxide on ZrB_2 simply grows from the surface of the crack into the bulk alloy.

X-ray analysis of the oxidized surfaces of all of the ZrB_2 samples showed lines for monoclinic ZrO_2, and no extraneous lines. Analysis was of course performed on quenched samples and therefore does not necessarily reflect accurately the structure of the high temperature oxide. Evidence was not found in either the photomicrographs or in X-ray for the existence of a lower oxide adjacent to alloy substrate.

f. Comparison between net weight change and total oxygen consumption data. The oxidation of ZrB_2 is expected to yield the oxides ZrO_2 and B_2O_3. The latter has an appreciable vapor pressure, ranging from 2.3×10^{-6} atm at 1400°K to 5.4×10^{-2} atm at 2000°K.[12] Thus the total oxygen consumption measurements reported above represent the sum of the amounts of oxygen in each of the product oxides. The net weight change measurements of Kurlakose and Margrave[7] represent the sum of a weight gain due to formation of condensed oxides, and a weight loss due to vaporization of boron as $B_2O_3(g)$. In order to compare the results, it is necessary to evaluate the importance of oxide volatility in the overall oxidation process.

3a   90X
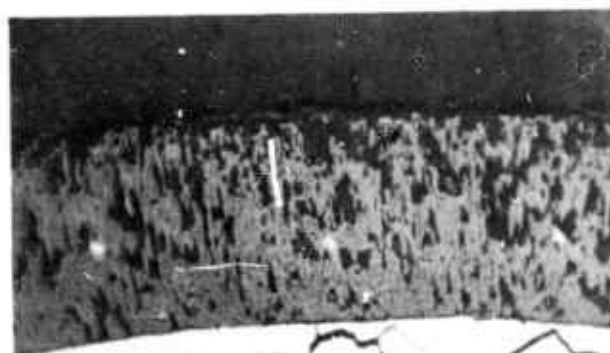
3b   90X

3c   450X

3d   170X

Figure 3   a-d

Photomicrographs of oxidized ZrB_2 (Pellet XIII-40).

$T = 1805K$, $P_{O_2} = 19.9$ Torr

38
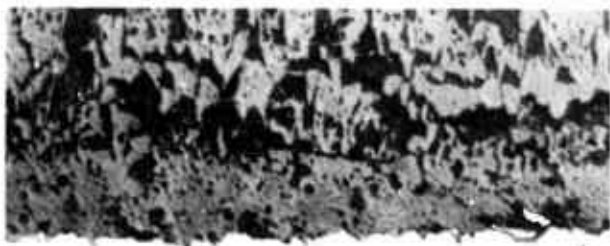
3e   240X   3f   240X
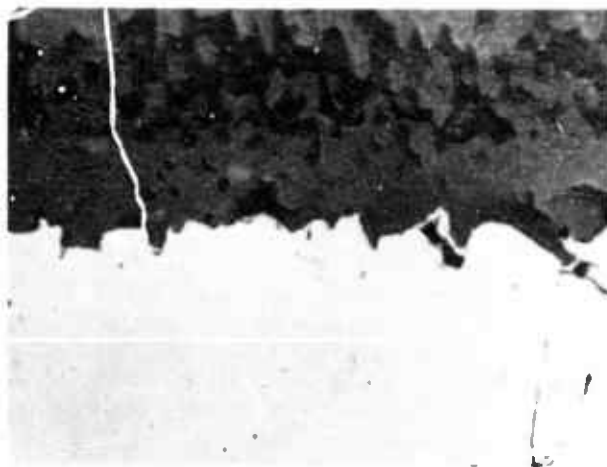
3g   450X

Figure 3 e-g

Photomicrographs of oxidized ZrB_2 (Pellet XIII-40).
$T = 1805K$, $P_{O_2} = 19.9$ Torr

3h   30X   3i   90X
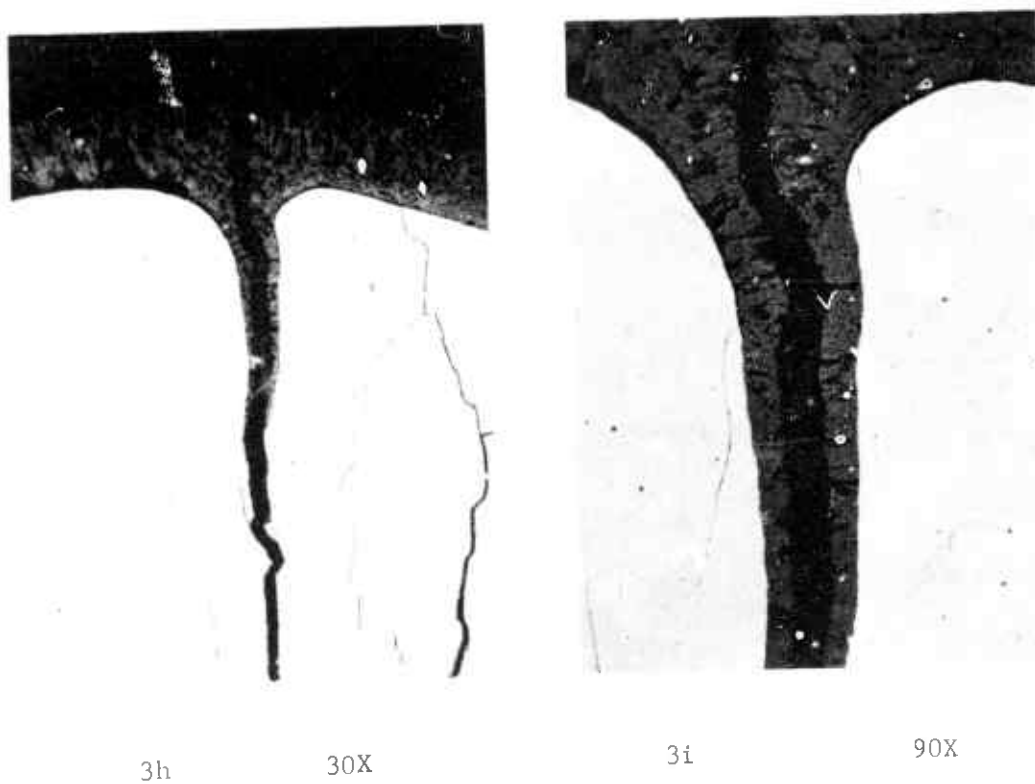
Figure 3 h and i

Photomicrographs of oxidized ZrB_2 (Pellet XIII-40).
$T = 1805K$, $P_{O_2} = 19.9$ Torr

If it is assumed that the composition of the boride is not changed dur-
ing oxidation, then the oxidation reaction may be considered in terms of two non-
elementary steps as follows:

$$ZrB_2(c) + (5/2)\ O_2(g) \longrightarrow ZrO_2(c) + B_2O_3(\ell) \tag{5}$$

$$B_2O_3(\ell) \longrightarrow B_2O_3(g) \tag{6}$$
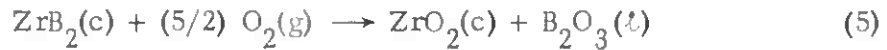
The total oxygen consumed, m, up to some time t, may be written as

$$m = \frac{2\ \lceil O \rceil}{\lceil ZrO_2 \rceil} \cdot w_{ZrO_2(c)} + \frac{3[O]}{[B_2O_3]} \cdot w_{B_2O_3(\ell)} \tag{7}$$

where w_X is the number of grams of product X formed per unit boride surface
area up to time t, and the symbols in brackets are molecular weights. Since
the oxidation is supposed to be non-preferential, the number of moles of $ZrO_2(c)$
formed must be equal to the number of moles of B_2O_3 (ℓ) formed in the same
time period. The total oxygen consumed m and the net weight change w_{net} differ
by the amount of B_2O_3 vaporized:

$$w_{net} = m - w_{B_2O_3(g)} \tag{8}$$

If the amount of B_2O_3 that vaporizes is negligible, then:

$$w_{net} = m \tag{9}$$

If B_2O_3 vaporizes as rapidly as it forms, then $w_{B_2O_3(g)} = w_{B_2O_3(\ell)}$, and

$$w_{net} = \left\{ \frac{2}{5} - \frac{2[B]}{5[O]} \right\} m \tag{10}$$

The equilibrium rate of vaporization of B_2O_3 in vacuum is known. At
a total pressure of one atmosphere, the rate of vaporization is expected to be a
factor of 10 to 1000 times less than the equilibrium rate.[13] For the purposes
of this discussion, it will be assumed that during the oxidation of ZrB_2, B_2O_3
vaporizes linearly at one one-hundredth of the equilibrium rate G as long as
liquid B_2O_3 is present. If the rate of formation of B_2O_3 (ℓ) is smaller than
0.01G, the liquid will vaporize as rapidly as it forms.

41

Since the total oxygen consumption was found to follow a parabolic rate law, it follows from (7) and from the assumption of stoichiometric oxidation that the condensed oxides ZrO_2 (c) and B_2O_3 (l) must also grow parabolically. Hence, at any temperature, there will be some time t_o after which the rate of vaporization of B_2O_3 (g) will exactly balance the rate of formation of B_2O_3 (l). At t_o:

$$\frac{dw_{B_2O_3(g)}}{dt} = \frac{dw_{B_2O_3(l)}}{dt} \tag{11}$$

On the basis of the preceding discussion:

$$\frac{dw_{B_2O_3(g)}}{dt} = 0.01G \tag{12}$$

and

$$\frac{dw_{B_2O_3(l)}}{dt} = \frac{(k_p)^{\frac{1}{2}}\left[B_2O_3\right]}{(2)t^{\frac{1}{2}}(5)[O]} \tag{13}$$

where k_p is the parabolic rate constant for total oxygen consumption. Equating (12) and (13), one can solve for the time t_o:

$$t_o = \frac{0.1894 \times 10^4 k_p}{G^2} \tag{14}$$

where k values can be taken from Figure 2 and G values from the literature.

At 1330°K, t_o = 570 min, and the loss of B_2O_3 (g) over the two-hour period of the present oxidation experiments is negligible. Therefore, to an excellent approximation, at all temperatures below 1330°K, weight gain and total oxygen consumption should be identical. At 1440°K and above, $t_o \leq 5$ min. Hence above 1440°K B_2O_3 should vaporize as rapidly as it forms, and the relationship between weight gain and total oxygen consumption should be given by equation (10).

For purposes of comparison in Figure 2, the weight change data of Margrave and Kuriakose, [7] obtained at an oxygen pressure of one atmosphere, were converted to total oxygen consumption values at an oxygen pressure of 37.5 torr by means of equation (9) below 1330°K and equation (10) above 1440°K, with the assumption of linear pressure dependence. On this basis, agreement between the two laboratories is good.

4. Results for Hafnium Diboride

a. Experimental data. The experimental data for HfB_2 are summarized in Table 8. For all of the conditions investigated, the data could be fitted to a parabolic rate equation. Results of the experiments on pellets XV-5, XV-1, and XII-36, in which the temperature was varied during the run, are plotted parabolically in Figures 4, 5, and 6 respectively.

b. Temperature dependence of the oxidation rate. The parabolic rate constants listed in Table 8 are plotted in the form $\log k_p$ vs $1/T$ in Figure 7. The activation energy for total oxygen consumption is 46 ± 6 kcal/mole in the range 1480-1870°K. Around 1970°K, the transition temperature for the monoclinic to tetragonal phase change in HfO_2, there is a remarkably abrupt increase in the rate of oxidation. Following the analysis presented earlier for ZrB_2 it is found at temperatures above 1488°K, the lowest temperature investigated, that the rate of vaporization of B_2O_3 should be equal to its rate of formation, and HfO_2 (c) should be the only condensed oxide on the surface of HfB_2. Therefore, the change in slope of the Arrhenius curve is not due to a change in the relative rates of formation of $B_2O_3(\ell)$ and $B_2O_3(g)$ as it might be in the ZrB_2 case, and it can be correlated directly with a phase change in the metal oxide.

c. Pressure dependence of the oxidation rate. The data taken at 1760°K for oxygen partial pressures between 1.4 and 694 torr are plotted as a function of oxygen partial pressure on a log-log plot in Figure 8. A least squares analysis of the data yields a pressure coefficient for total oxygen consumption of 0.4 ± 0.1; i.e.:

$$k_p \propto p^{0.4 \pm 0.1}$$

At 1735°K (pellet XV-40) no pressure dependence of rate was observed within experimental error over the range 8.5 to 27 torr. At 1630°K (pellet XV-16) over the same pressure range, a pressure coefficient of 0.5 was determined from the data plotted in Figure 8.

43
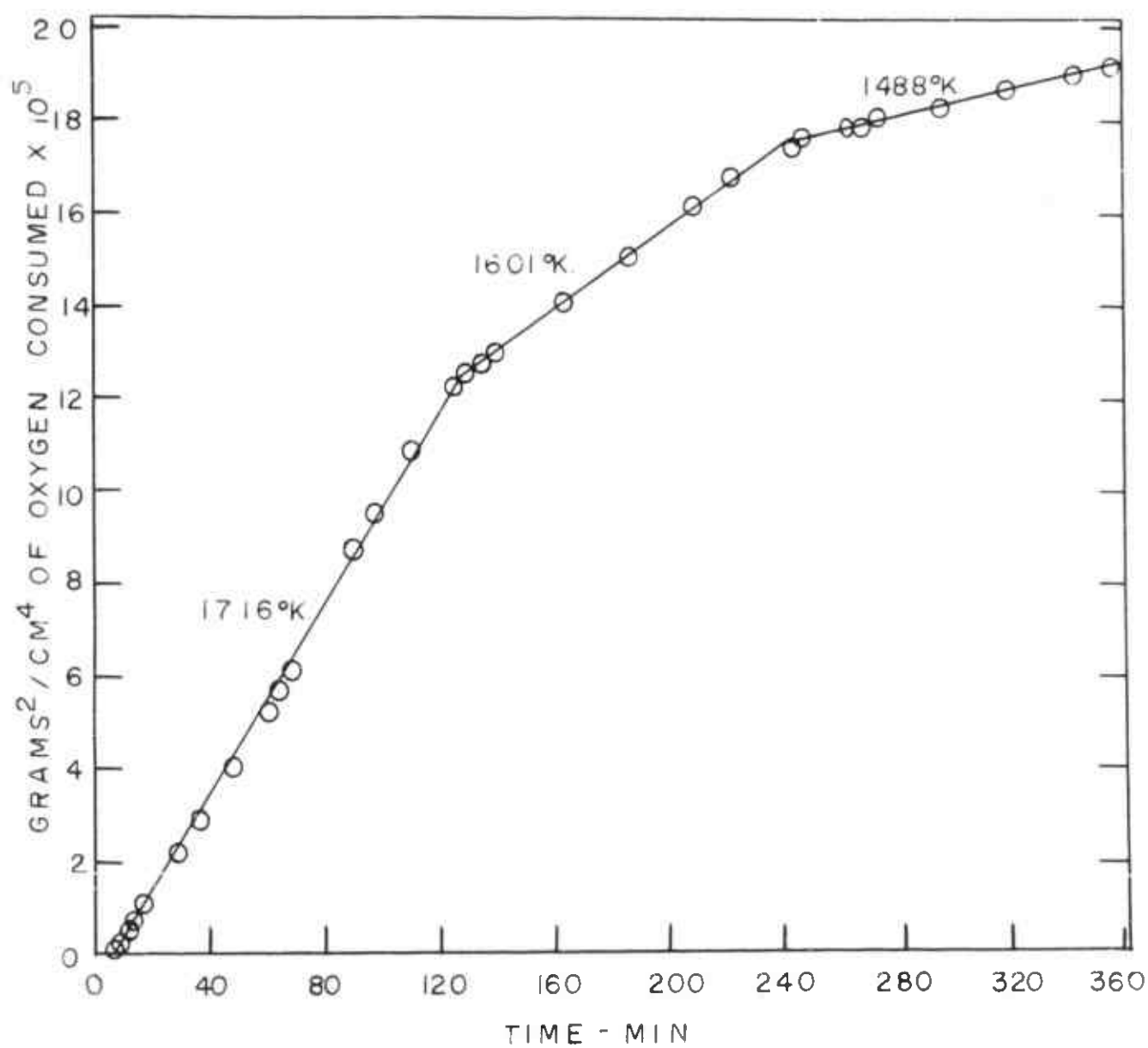
Figure 4   Parabolic plots of HfB$_2$ oxidation data (pellet XV-5)
                Temperature 1720, 1600 and 1490°K, p$_{O_2}$ 19.9 Torr

44
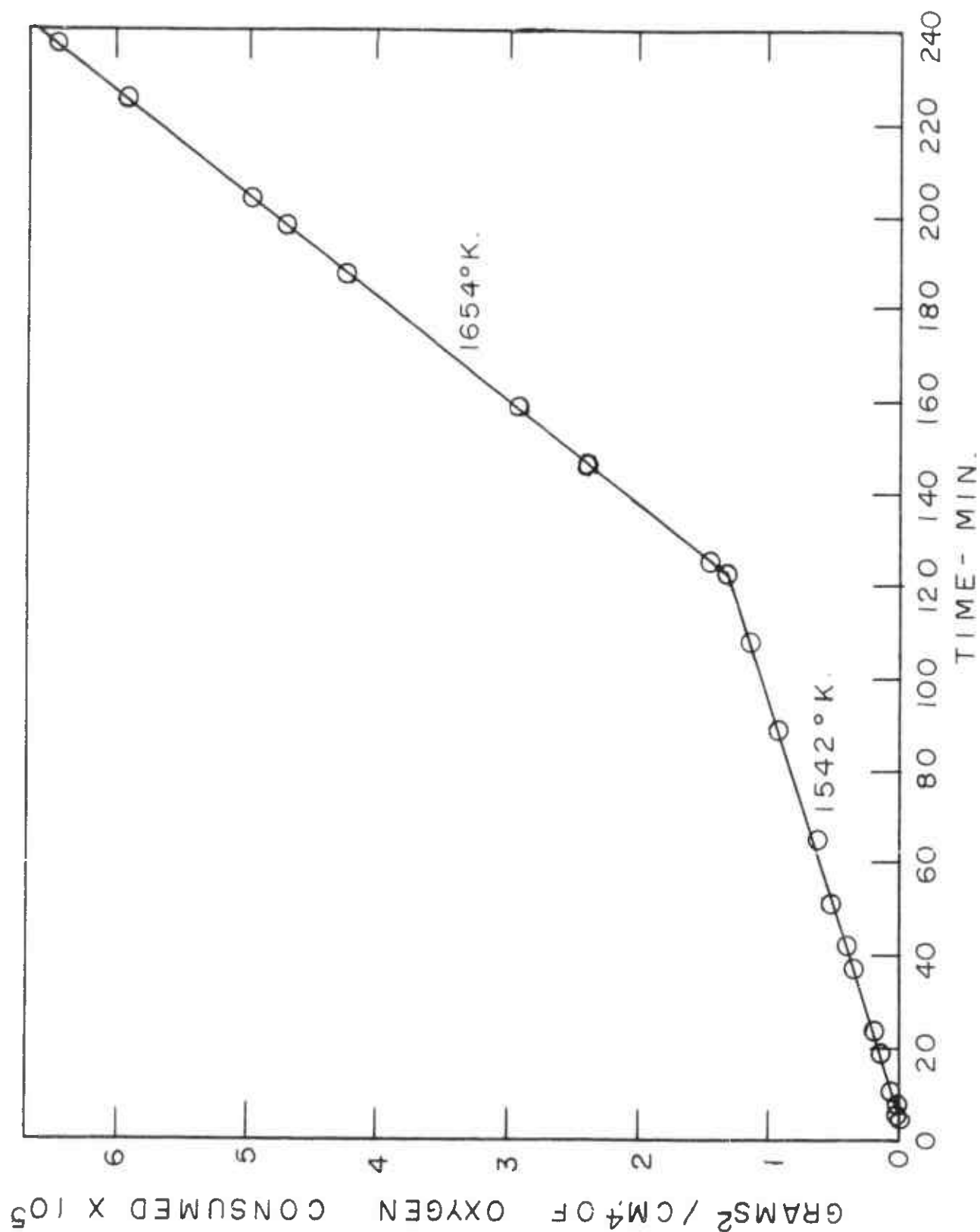
Figure 5   Parabolic plots of HfB$_2$ oxidation data (pellet XV-1)
Temperature 1650 and 1542°K, P$_{O_2}$ 19.9 Torr
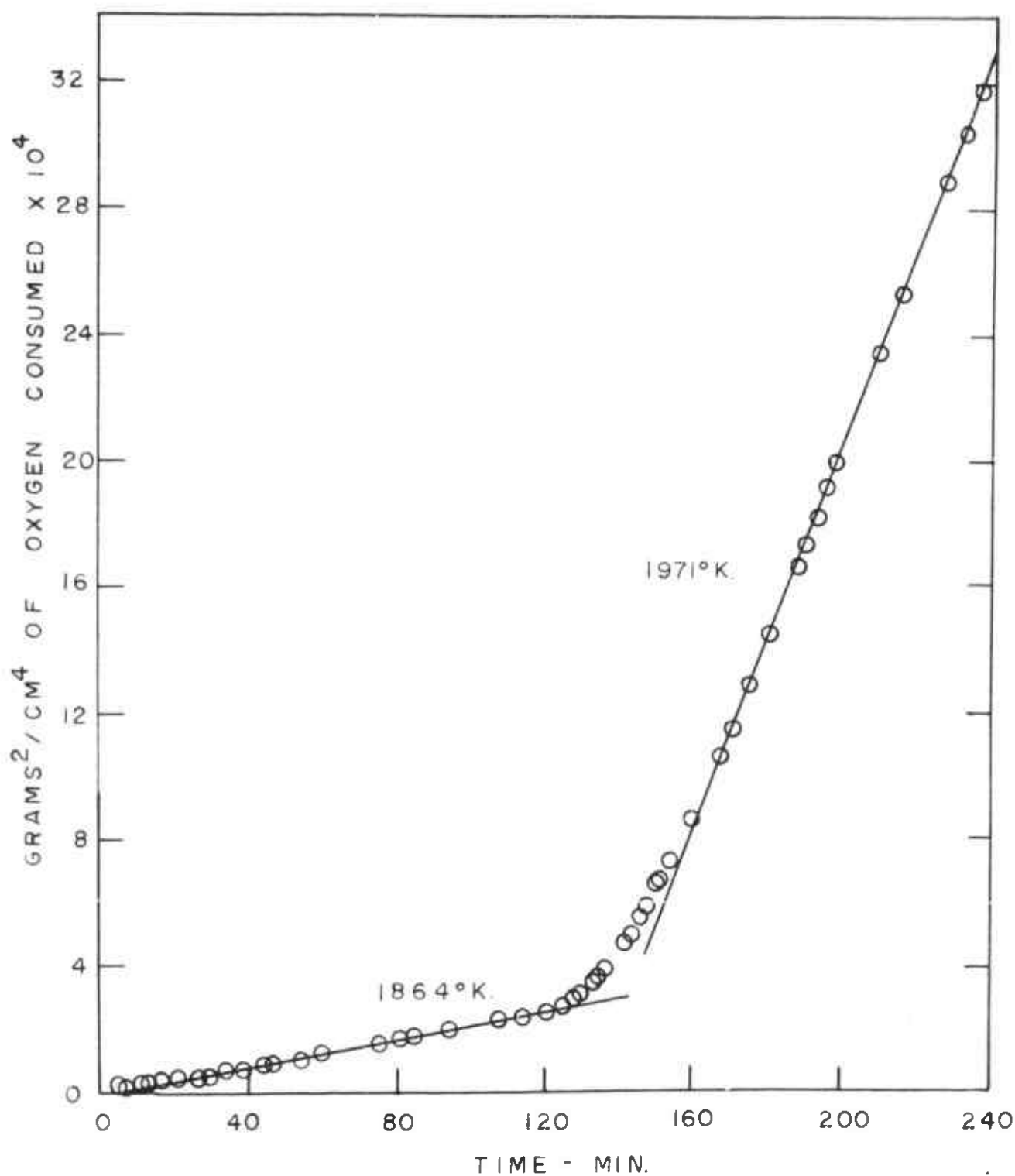
Figure 6   Parabolic plots of HfB$_2$ oxidation data (pellet XII-36)
            Temperature 1860 and 1970°K, p$_{O_2}$ 18.5 Torr

TABLE 8

SUMMARY OF EXPERIMENTAL DATA ON HfB$_2$

Pellet	Initial Weight (g)	Area (cm²)	Density (g/cc)	Temp. (°K)	Oxygen Pressure (Torr)	Flow (cc/min)	Exposure Time (min)	Weight Change (g/cm²)	Total O$_2$ Consumed (g/cm²)	Kp (g²/cm⁴-min) x 10⁹
XV-5	0.8720	1.157	10.22	1716	19.9	95	122			0.103
				1601			119			0.045
				1488			116	0.0011	0.0135	0.0148
XV-1*	0.8652	1.190	9.9	1654	19.9	95	114			0.045
				1542			123	0.0007	0.0081	0.0112
XV-40	0.8352	1.102	10.3	1733	8.5	95	120			0.117
				1739	16.5		120			0.118
				1735	19.9		120			0.106
				1735	27.0		120	0.0017	0.0017	0.115
XII-36*	0.9208	1.156	10.8	1864	18.5	119	125	0.0068	0.0584	0.225
				1971			120			3.03
XVI-1	1.0041	1.250	10.6	1999	18.5	119	118	0.0153	0.1389	25.9
XV-16	0.7977	1.088	10.2	1628	8.5	95	121			0.0304
				1629	16.5		124			0.0428
				1629	27.0		119	0.0006	0.0060	0.0558
XVII-12	0.9907	1.2645		1760	7.5	95		0.0003		0.1178
XVII-14	1.1323	1.3923		1760	16.5	95				0.1328
XVII-16	0.9280	1.1652		1760	19.3	95				0.1542
XVII-18*	0.7996	1.0542		1760	26.8	95				0.1084
XVII-36	0.8353	1.1258		1760	40.7	95				0.1147
XVII-32	1.0350	1.3432		1760	40.7	95				0.1462
XVII-1	0.9345	1.2403		1760	26.8	95				0.188
					19.3					0.158
					16.5					0.147
					7.5					0.138
XVII-48	0.8087	1.120		1760	694	95				0.825
XVIII-8	0.8066	1.0768		1760	1.4	95				0.033

*Polished and examined metallographically after oxidation.

47
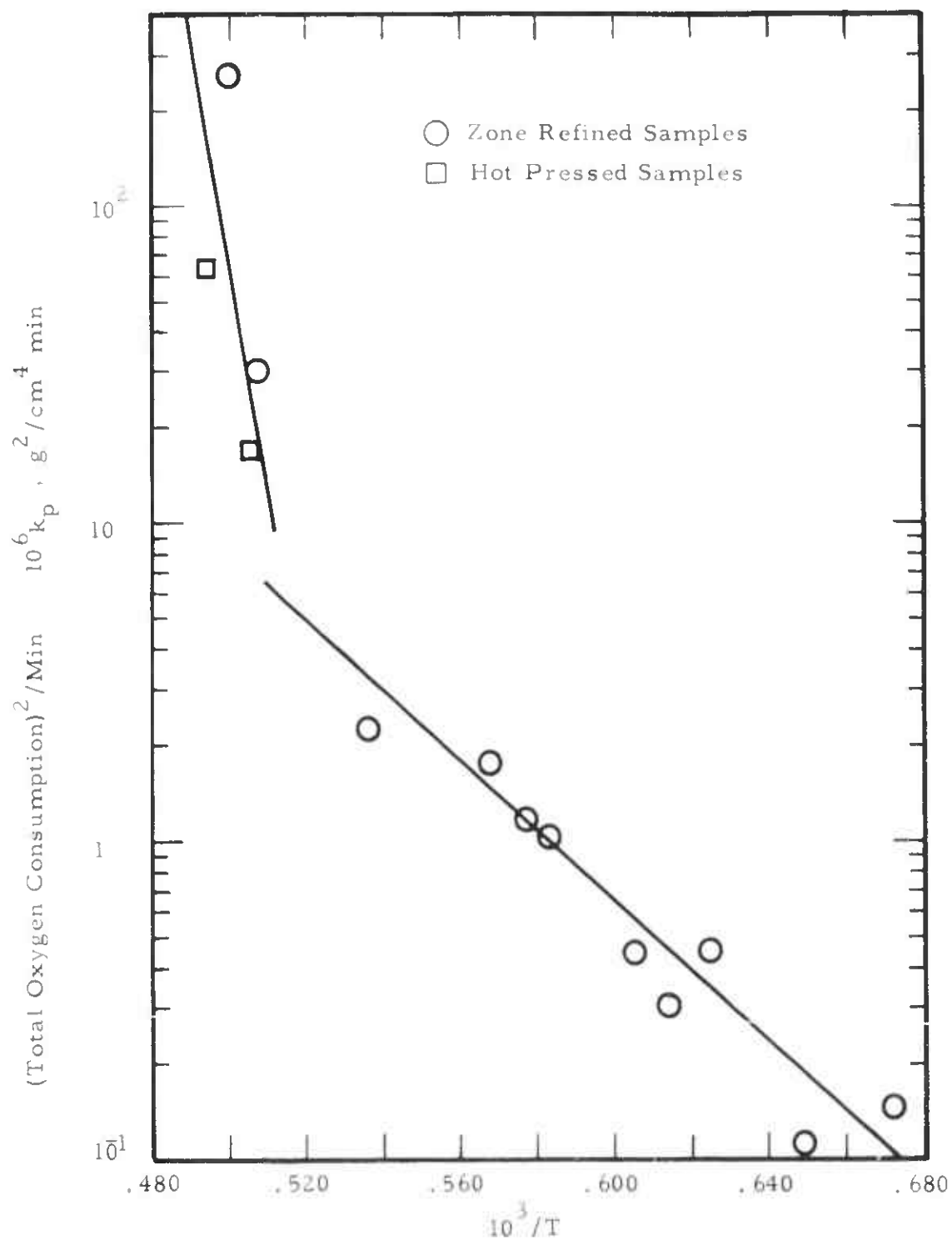
Figure 7   Temperature Dependence of the Rate of Total Oxygen Consumption
            for Hafnium Diboride - Arrhenius Plot of Parabolic Rate Constants

48
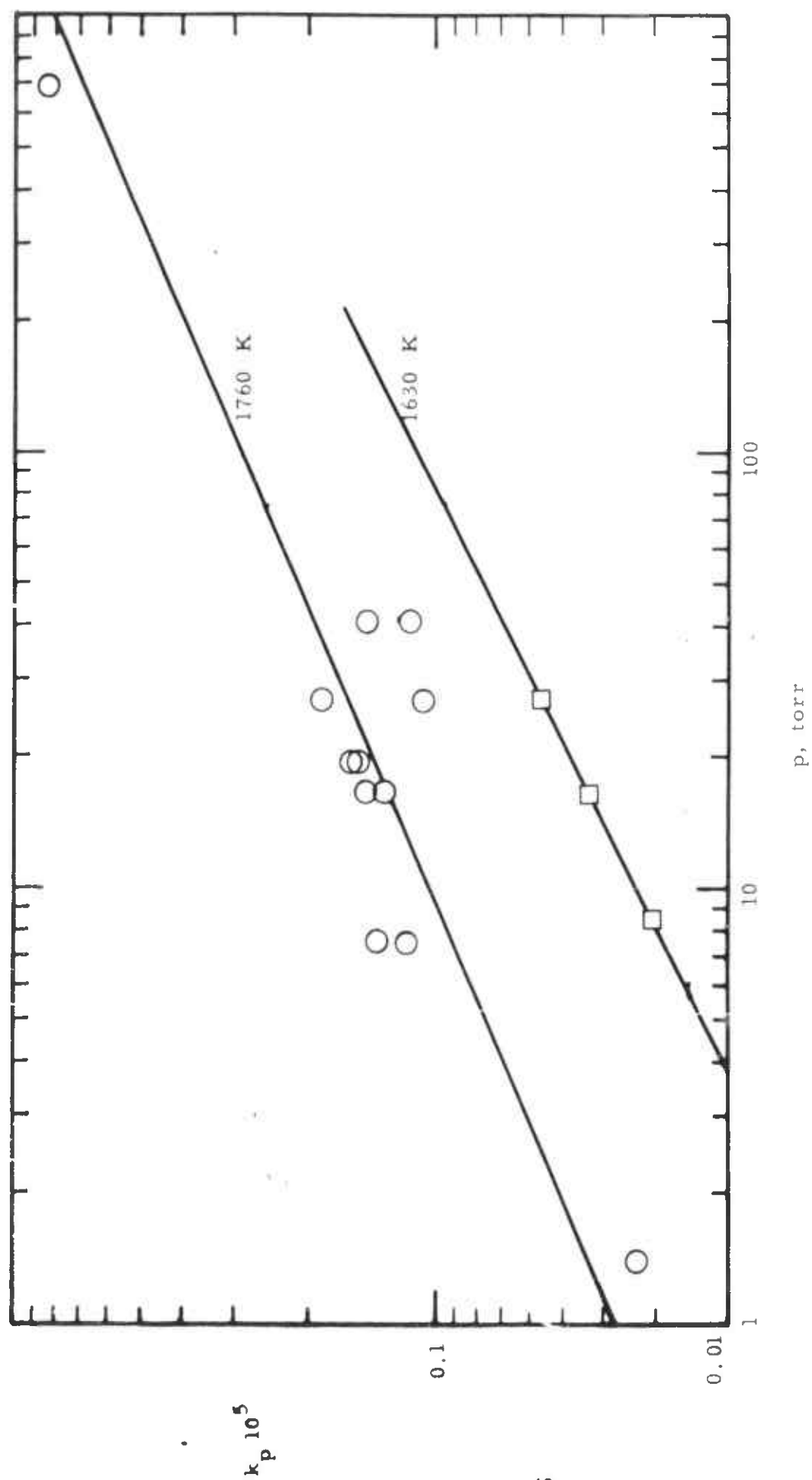
Figure 8   Pressure Dependence of the Oxidation of Hafnium Diboride at 1760 and 1630 K

d. Metallographic examination of the oxide films. Pellets XVII-18, XII-36, and XV-1 were mounted and polished for metallographic examination after oxidation. Oxide was polished off one circular part, revealing the alloy beneath and leaving the oxide at the outer rim. A photomicrograph of pellet XVII-18, that had been oxidized for two hours at 1760°K and 26.8 torr, is shown in Figure 9. The structure of the oxide is quite different from that shown in Figure 3 on zirconium diboride. Two layers are clearly visible, a thin outer region and a thicker inner one. The patches of oxide at the left, apparently unconnected with the oxide at the outer rim, are probably areas of the surface which were oxidized more rapidly than the bulk alloy, and hence were not polished away during preparation of the sample. The oxidation rate may be a function of the crystalline orientation of the diboride. The crack in the right hand quarter of the figure may be filled with oxide, suggesting that the oxide grows in part by outward diffusion of hafnium.

Photomicrographs of the surface of pellet XII-36, that had been oxidized for two hours at 1864°K and for two hours at 1971°K at an oxygen partial pressure of 18.5 torr are shown in Figure 10. The thicker outer layer of oxide was probably formed at the higher temperature, the narrower inner layer at the lower, again suggesting motion of hafnium. In Figure 11 a photomicrograph of pellet XV-1, that had been oxidized for two hours at 1654°K and for two hours at 1542°K at an oxygen pressure of 19.9 torr, is shown. The oxide is very similar to that shown in Figure 9. A layered structure, due to the change in temperature in the middle of the run could not be positively identified.

X-ray analysis of the oxidized surfaces of all of the HfB_2 samples showed lines for monoclinic HfO_2, and no others.

e. Effect of water vapor in the oxidation of HfB_2. At 1760°K and an oxygen partial pressure of 19.3 torr, in the presence of 4.6 torr of water vapor, a parabolic rate constant for oxidation of 1.4×10^{-6} g^2/cm^4 - min was obtained. In the absence of water vapor, under the same conditions, a value of 1.5×10^{-6} g^2/cm^4 - min was obtained. Thus, the effect of water vapor under these conditions appears to be negligible. It might be anticipated that water vapor would accelerate the rate of vaporization of B_2O_3, but at 1760°K, boron oxide is already evaporating as rapidly as it forms. Water vapor might therefore influence the oxidation kinetics at lower temperatures.
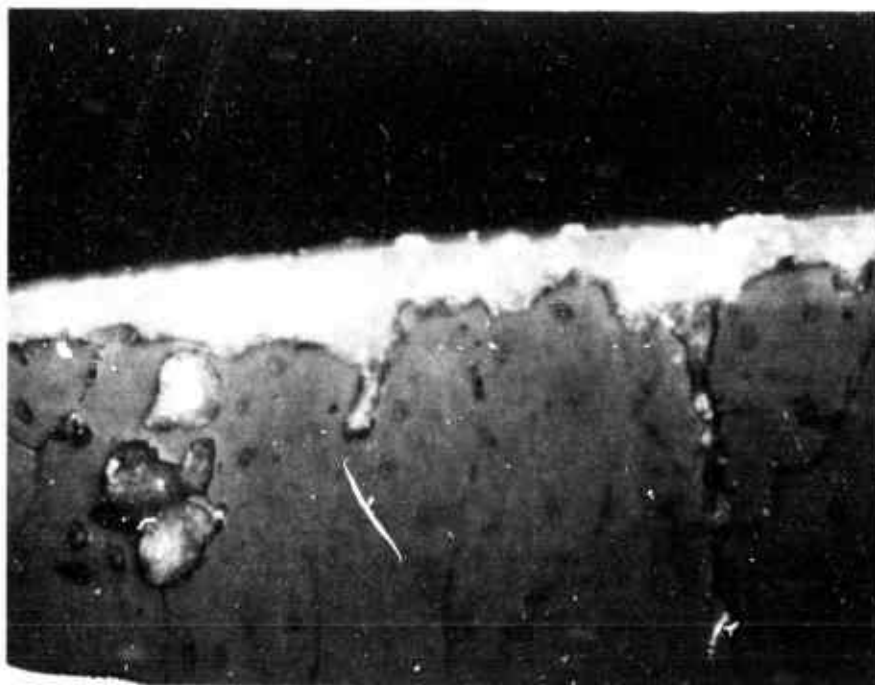
260X

Figure 9   Photomicrograph of Oxidized Hafnium Diboride
                Pellet XVII-18, Temperature 1760°K, P_{O_2} 26.8 Torr
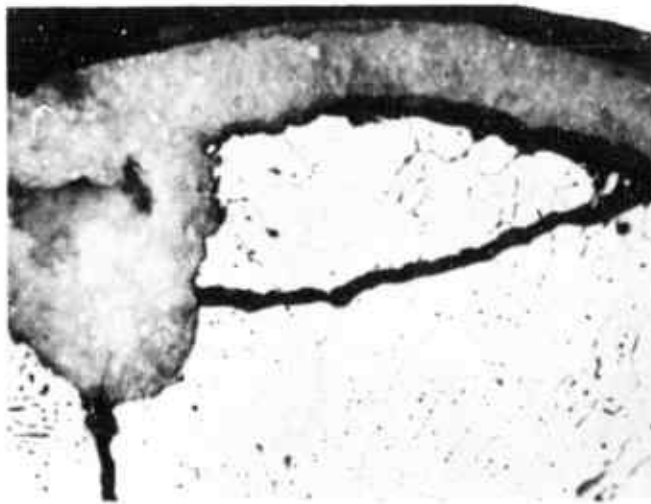
65X
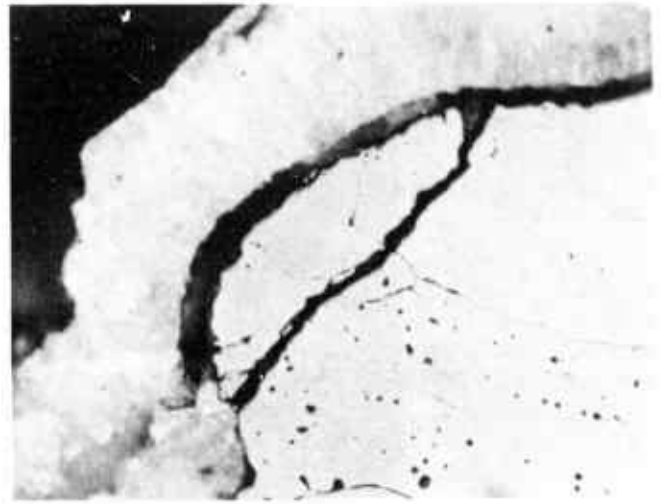
130X
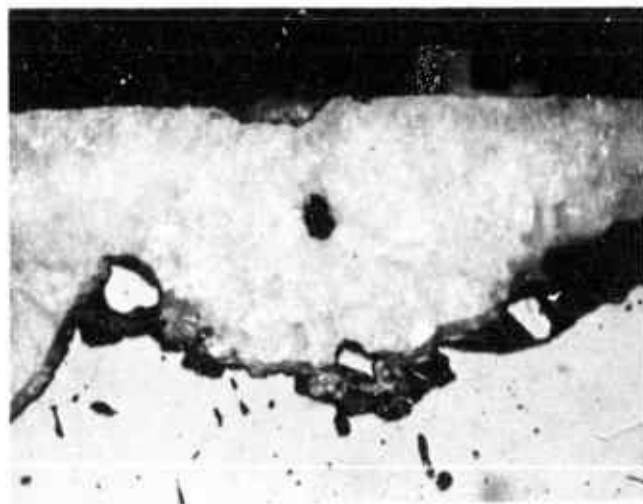
130X

Figure 10   Photomicrographs of Oxidized Hafnium Diboride
                 Pellet XI1-36,   Temperature $1970^{\circ}K$, p_{O_2} 18.5 Torr
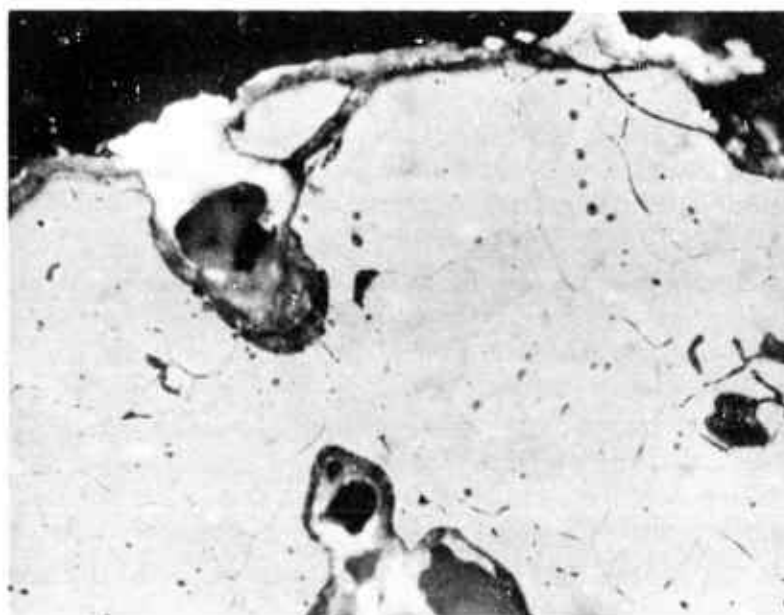
130X

Figure 11   Photomicrograph of Oxidized Hafnium Diboride
Pellet XV-1, Temperature 1650 and $1540^{\circ}K$, p_{O_2} 19.9 Torr

5. Discussion

In order to compare the zirconium diboride and hafnium diboride results in the 1400-1900°K range, the parabolic rate constants in Tables 7 and 8 were converted to an alloy consumption basis for the densities listed, on the assumption of non-preferential oxidation of the alloys to B_2O_3 (g) and metal dioxide. The results are compared in an Arrhenius plot in Figure 12. In this temperature range, the parabolic rate constants for oxidation of HfB_2 are almost an order of magnitude less than the corresponding constants for ZrB_2. In Figures 2 and 7, it is seen that the rate of oxidation of zirconium diboride increases sharply near 1400°K, while the rate of oxidation of hafnium diboride shows a similar increase around 1970°K. In the case of hafnium diboride, the jump in oxidation rate is clearly due to the monoclinic to tetragonal transition in the oxide. In the case of zirconium diboride, the phase transition in ZrO_2 does occur around 1400°K, but the increase in oxidation rate might also be due to the fact that B_2O_3 (ℓ) is present on the surface of the alloy in the low temperature range, but vaporized as rapidly as it is formed at higher temperatures. In any case, for both ZrB_2 and HfB_2 the monoclinic oxide appears to impart greater oxidation resistance than the tetragonal modification.

Although the experimental data for both zirconium diboride and hafnium were fitted to a parabolic rate equation, the mechanism of oxidation is not clear. ZrO_2 and HfO_2 are normally considered to be anion deficit semiconductors, and one might expect the oxidation of HfB_2 and ZrB_2 to be controlled by diffusion of oxygen ions via vacancies in the respective metal oxides. If this mechanism were valid, however, the activation energy for diffusion should be equal to the activation energy for oxidation, and the rate of oxidation should be independent of oxygen partial pressure.[14] The linear pressure dependence for oxidation of ZrB_2 found by Margrave and Kuriakose at 1329°K over the range 100-760 torr, and confirmed by us at 1200°K, precludes a simple diffusion mechanism via anion vacancies in this temperature range. Above the phase transition temperature for ZrO_2, diffusion data is not available. However, the activation energy of 77 ± 5 kcal/mole found for oxidation is not an unreasonable energy for diffusion[15] and furthermore at 1830°K the parabolic rate constant for total oxygen consumption was found to be independent of oxygen pressure.

The oxidation of HfB_2 to monoclinic HfO_2 (c) and gaseous B_2O_3(g) was found to depend upon the 0.4 ± 0.1 power of the oxygen pressure, which again is too high to be consistent with a diffusion mechanism via oxygen anion vacancies. In fact, the oxidation behavior in the neighborhood of a crack, and the layered structure observed when the temperature was raised or lowered in the middle of a run, suggested that hafnium is the major diffusing species during the oxidation of HfB_2.
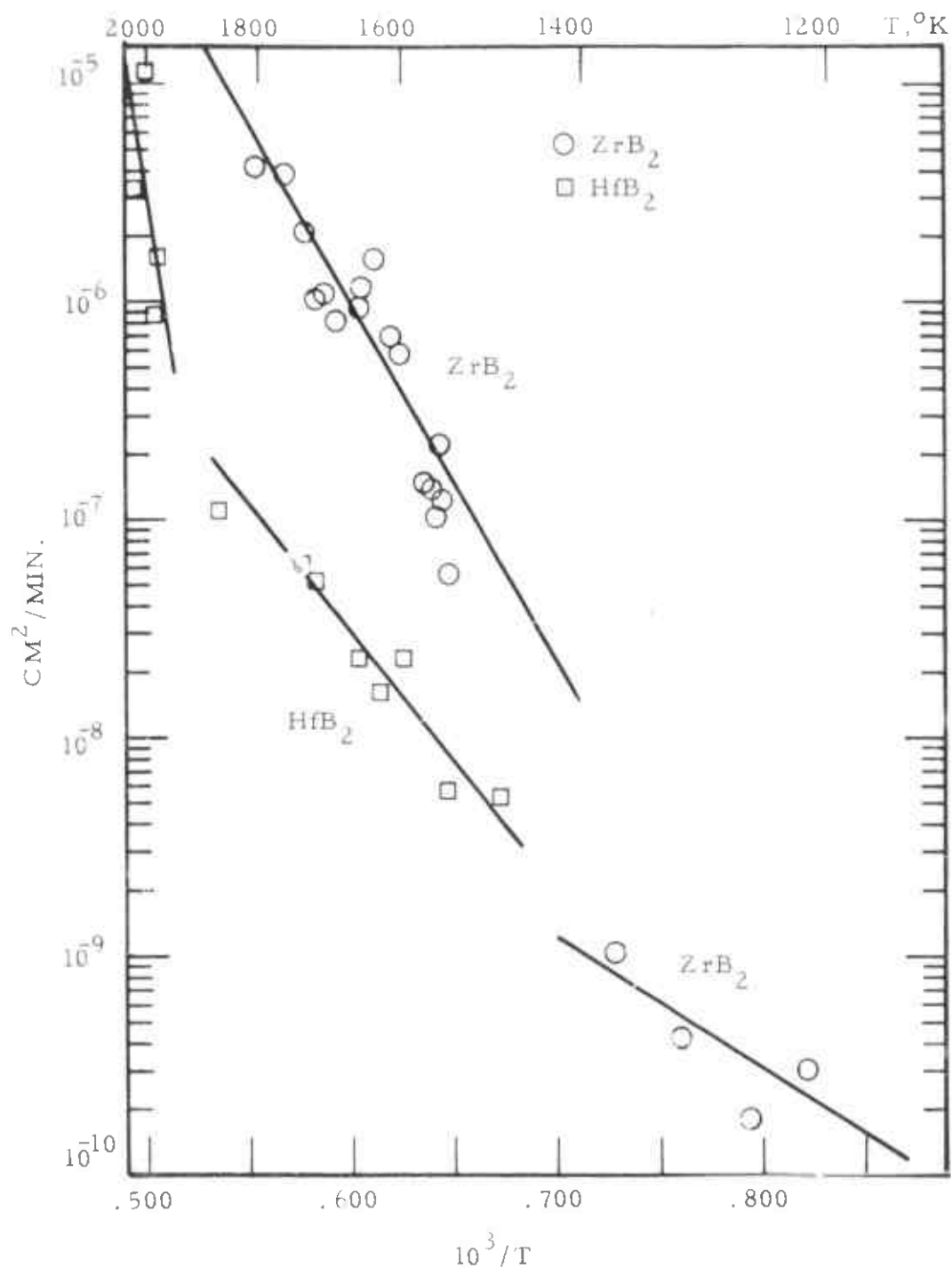
Figure 12   Comparison of parabolic rate constants for oxidation of Hafnium Diboride and Zirconium Diboride as a function of temperature

According to the Wagner theory, the parabolic rate constant for oxidation should be proportional to the product $(\tau_a + \tau_c) \tau_e \varkappa_0$ when τ_a, τ_c, τ_e are the transference numbers of anions, cations, and electrons in the oxide film, and $\varkappa_0$ is the total conductivity of the oxidant at oxygen pressure of one atmosphere. Thus, in order to calculate a rate constant for the oxidation of ZrB_2 and HfB_2, on the basis of the Wagner mechanism, it is necessary to know both τ and $\varkappa_0$ values for the growing oxide film. If ZrO_2 and HfO_2 were anion deficit semiconductors, with diffusion occurring mainly via anion vacancies, then $\tau_c \approx 0$, $\tau_a << 1$, and of course $\tau_e \approx 1$. The situation, in fact, appears to be more complicated, and the recent work of Kofstad and Ruzicka[16] on the defect structure of ZrO_2 and HfO_2 shows that either n- or p- type conductivity is possible in these oxides. The oxidation of ZrB_2 and HfB_2 will be a function of the detailed defect structure.

B. ZIRCONIUM AND HAFNIUM CARBIDE

1. Background

The oxidation of zirconium carbide has been studied by Margrave and Kuriakose[7] at temperatures of 550-650°C in oxygen at one atmosphere. The oxidation was found to be linear, with an activation energy of 16.7 ± 1.7 kcal/mole.

Bartlett,[17] as part of a doctoral dissertation measured the rate of weight gain of sized powders of ZrC in air, oxygen, and oxygen-helium mixtures at temperatures of 450-580°C, and oxygen pressures of 60μ - 6.8 atm. Semi-quantitative data were obtained at temperatures up to 900°C, at oxygen pressures below 4 mm. Net weight changes were monitored with a spring balance and results were interpreted on the basis of stoichiometric non-preferential oxidation of ZrC to ZrO_2 and CO_2. No attempt was made to analyze the gaseous products separately, or to check that the solid phase composition does remain constant during oxidation. In the 450-580°C range the weight gain vs time curves showed an initially curved part, where oxidation was very rapid, followed by a straight line section for the remainder of the reaction. Runs lasted from 50-900 minutes, with the longer runs being made at lower temperatures. The oxidation product was found to be cubic ZrO_2 in every case, a phase normally thought to be unstable, but which might be stabilized by small amounts of carbon. At oxygen pressures between 0.1 and 1 atm., the reaction rates appeared to be independent of pressure. Between 1 and 6.8 atm., the rate decreased slightly with increasing pressure. Below 4 torr, oxidation rates were linear from zero time (i.e., the weight gain curves failed to show an initially curved portion), and were directly proportional to oxygen pressure. The activation energy for oxidation in the 450-580°C range computed from the final linear portions of the weight

gain curves was found to be 45.7 kcal/mole. In the 580-900°C range, at pressures below 4 mm, the oxidation rate was found to be proportional to oxygen pressure, but virtually independent of temperature. The reason for this may be that under the experimental conditions, the reaction was controlled by the rate of arrival of oxygen at the refractory surface. While some monoclinic ZrO_2 was detected in the product oxide at the higher temperatures, cubic ZrO_2 still seemed to be the major product.

Watt, Cockett, and Hall[18] made a single weight change measurement of 49.8 mg/cm^2 in a solid sample of ZrC of density 6.20 g/cc and 4.8% porosity, exposed to a stream of dry air flowing at 5.3 cm/sec, for 30 minutes at 800°C.

The present study was undertaken to elucidate the mechanism of oxidation of ZrC and the chemically related HfC at temperatures above 900°C, where information is not available from previous investigations.

2. Experimental Method

Cylindrical pellets of ZrC were cut from zone refined bars prepared as described by Westrum and Feick.[19](*) Hafnium carbide powder was prepared by the Carborundum Company from high purity HfO_2 supplied by Wah Chang Corporation. The HfC powder was sintered into bars and arc-melted on a water-cooled copper hearth using a water-cooled tungsten electrode. In order to minimize loss of carbon during melting, the operation was conducted in an atmosphere of argon containing 3.14 o/o of ethylene and 11.4 o/o of hydrogen. The resulting material was slightly carbon deficient, corresponding to a composition $HfC_{0.952}$.[20](*)

The permanent gases, CO(g) and CO_2(g), in addition to the refractory metal oxides, are anticipated products of the oxidation of ZrC and HfC. Therefore, the thermal conductivity method described in previous publications[10][11] cannot be used without modification to study the oxidation. For the carbide work, a known mixture of helium and oxygen was passed through the reference side of a thermal conductivity cell[10] and over an inductively heated carbide pellet, supported on ThO_2 fingers by three point contact. A portion of the oxygen reacted with the pellet to produce oxides of the metal and carbon.

---

*Also see Chapter III of this report.

3. Results for Zirconium Carbide

a. Experimental data. The experimental data for ZrC are summar-
ized in Table 9. The first column identifies each sample pellet. The second
column gives the weight of each pellet after it had degassed at 2200 K in pure
helium until the signal from the thermal conductivity cell indicated that no per-
manent gases were being evolved. The third column gives geometric surface
areas, calculated from micrometer measurements of the height and diameter of
the cylindrical pellets. The fourth column records sample densities, computed
from weights after degassing and pellet dimensions. Columns 5, 6, and 7 record
the pellet temperature, assuming an emissivity of 0.7, oxygen partial pressure,
and carrier gas flow rate, respectively, for each oxidation run. The duration of
the experiment is given in column 11, and the net weight change, total $CO(g)$
produced, and total $CO_2(g)$ produced in this time are given in columns 8, 9, and
10 respectively.

From the measured quantities in columns 8-10, the total carbon con-
sumed and total zirconium consumed, in columns 12-14 can be computed. From
the observed weight changes in the Ascarite bulbs, it is known that both $CO(g)$
and $CO_2(g)$ form during oxidation. In addition, a white nonadherent oxide, with
the X-ray pattern of $ZrO_2(s)$, is visible on the surface of the sample pellets
after reaction. If it is assumed that the only oxidation products are $CO_2(g)$,
$CO(g)$, and $ZrO_2(s)$, then the total carbon consumed, c, is calculated from the
measured weights w_{CO_2} and w_{CO} of $CO_2(g)$ and $CO(g)$,

$$c = \frac{[C]}{[CO_2]} \cdot w_{CO_2} + \frac{[C]}{[CO]} \cdot w_{CO} \qquad (15)$$

where the symbols in brackets, $[\ ]$, represent molecular weights. The total
weight of zirconium, z, that has been converted to oxide is calculated from the
measured weight change, w_0, and the derived carbon consumption:

$$z = \frac{[Zr]}{2[O]} (w_0 + c) \qquad (16)$$

The ratio of the number of grams of zirconium consumed to the number of grams
of carbon consumed during oxidation is given in the column 14 of Table 9. The
ratio is seen to have an approximately constant value of 7.5 ± 0.2. Since the
corresponding ratio in the ZrC starting material is 7.6, it would appear that
the oxidation of ZrC is stoichiometric. That is, for each zirconium atom con-
verted to oxide, a single carbon atom is also converted to oxide. The rate of
oxidation in the last column is shown to be highest for pellet XII-1. In all of the

58

TABLE 9

SUMMARY OF EXPERIMENTAL DATA ON ZrC

Pellet	Initial Weight (g)	Area (cm²)	Density (g/cc)	Temp. (°K)	Oxygen Pressure (Torr)	Flow (cc/min)	Weight Change (g)	CO Formed (g)	CO₂ Formed (g)	Time (min)	C Consumed (g)	Zr Consumed (g)	Zr/C	Weight Change Rate (g/cm²·min) x 10⁻⁴
XII-8	0.4446	1.1031	5.72	1126	22.9	58.6	-	0.0001	0.0611	51	-	-	-	-
XII-5	0.5645	1.3942	5.29	1259	20.4	-	-	-	0.0709	128	-	-	-	-
XII-3	0.6963	1.4926	5.89	1559	21.2	-	-	0.0289	0.0399	62	-	-	-	-
X-31	0.5864	1.310	5.89	1857	9.1	-	0.0402	0.0438	0.0220	129	0.0248	0.1852	7.47	2.38
X-29	0.7073	1.450	6.19	1944	8.1		0.0366	0.0405	0.0145	120	0.0214	0.1652	7.72	2.10
XII-1	0.7051	1.500	5.05	1969	25.9		0.0851	0.0968	0.0356	112	0.0510	0.388	7.60	5.06
X-27	0.6361	1.252	6.71	2066	8.5		0.0389	0.0464	0.0175	124	0.0236	0.1780	7.55	2.50
X-16	0.6840	1.388	6.33	2066	8.5		0.0402	0.0540	0.0073	119	0.0252	0.1862	7.39	2.44
VII-8	0.6643	1.528	5.41	2098	3.0	51.5	0.0207	0.0242	0.0079	180	0.0126	0.0949	7.54	0.754
X-25	0.6812	1.371	6.40	2165	8.9	58.6	0.0356	0.0523	0.0072	120	0.0244	0.1710	7.01	2.16

runs where weight data is given, more than 90% of the oxygen passed over the refractory pellet reacted with it, and the reaction was probably controlled, therefore, by the rate of arrival of oxygen gas at the sample surface. For XII-1, the supply of oxygen was sufficient to permit a significant determination of oxidation rate.

Weight change data is not given for pellets XII-8, XII-5, and XII-3 because at these relatively low temperatures the pellets were broken apart by the oxidation process. At the end of each experiment, the grain boundaries of the ZrC were seen to be outlined by a white material, probably ZrO_2. The growth of the oxide in pre-existing cracks and grain boundaries of ZrC undoubtedly creates enough stress to fracture the carbide.

b. Metallographic analysis of the oxide films. Pellet XII-1 which had been exposed for two hours at a temperature of 1969°K and oxygen partial pressure of 25.9 torr in helium, was mounted and polished for metallographic examination.

Figure 13a shows the prepared oxidized specimen, at a magnification of 7X. The gray outer rim is the oxide, and the inner bright circular area is the surface of carbide. To the naked eye, the outer oxide coating looks white and chalky, and the inner surface from which the oxide coating was polished off, looks bright and metallic. A mottled rim is clearly visible along the oxide-alloy interface; the remaining photomicrographs focus on portions of this interface. In Figure 13b, at a magnification of 60X, the oxide fills the entire upper half of the photograph, and the alloy the lower. The oxide is obviously growing down grain boundaries in the carbide, and enveloping individual alloy crystallites. The structure of the bulk oxide is very different from that on ZrB_2 (Fig. 3) although both show only the X-ray lines for monoclinic ZrO_2. On ZrB_2, the oxide was seen to grow in a columnar structure; on ZrC, the ZrO_2 assumes a grain structure very similar to that of the original alloy. Figures 13c and 13d show the oxide alloy interface at a still higher magnification, 390X, and one sees even more clearly the preferential oxidation of grain boundaries, and the lateral finger like growth of oxide from the boundaries into the crystallite bulk. This would appear to be the mechanism of oxide growth on ZrC at high temperatures--rapid attack at grain boundaries, and slow oxidation of the alloy from the grain boundary surface inward. Figure 13e, at a magnification of 690X, shows portions of the alloy completely enveloped by oxide. Finally, Figure 13f is a view of the alloy surface at a magnification of 690X. This surface had been covered with a dense oxide prior to polishing, and one sees here the penetration of the oxide into grain boundaries of the alloy. Between 1126 and 1559°K, the grain boundary attack results in intergranular fracture of the alloy. Above 1580°K, there is apparently enough plasticity in either alloy, oxide or both, so that the sample remains intact during oxidation.
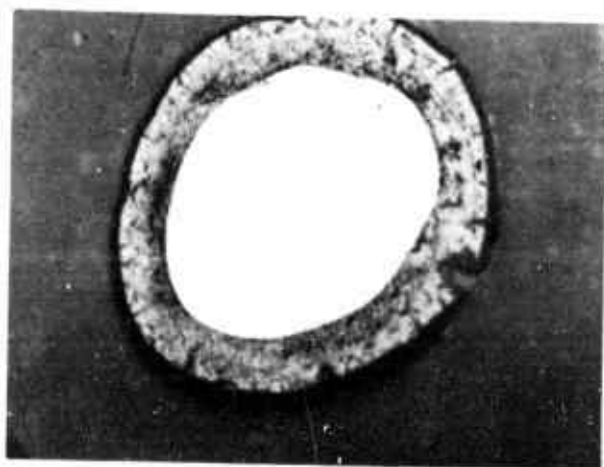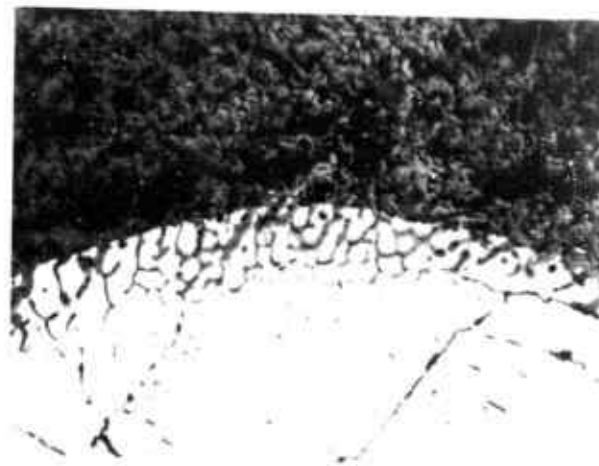
13a   7X   13b   60X
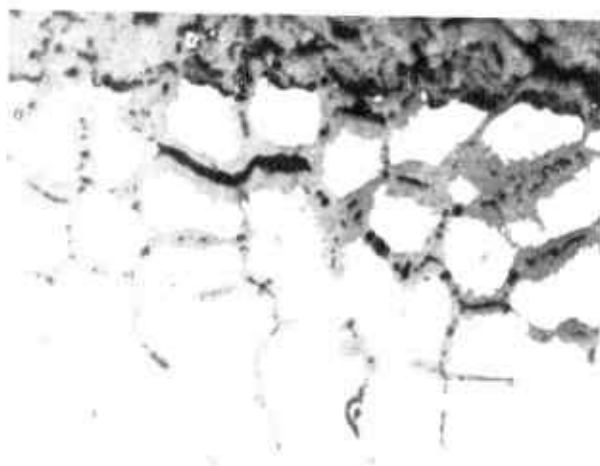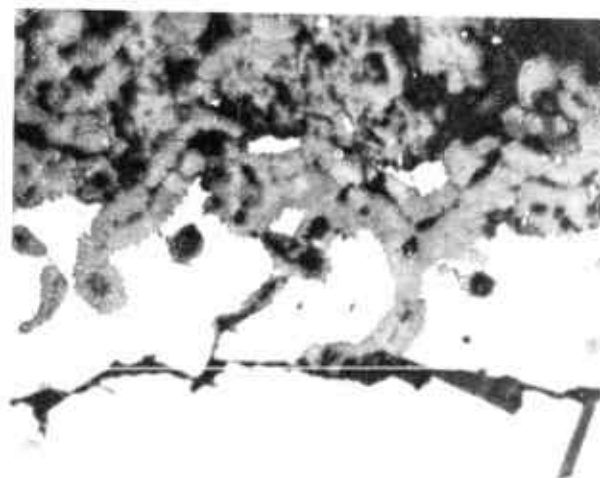
13c   390X   13d   390X

Figure 13 a-d

Photomicrographs of oxidized ZrC (Pellet XII-1).
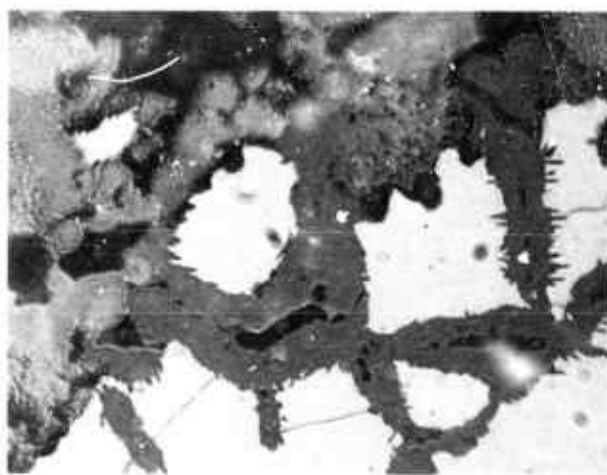
$T = 1969K$, $P_{O_2} = 25.9$ Torr

13e   690X   13f   690X

Figure 13 e and f

Photomicrographs of oxidized ZrC (Pellet XII-1).

$T = 1969K, \quad P_{O_2} = 25.9$ Torr

4. Results for Hafnium Carbide

a. Experimental data. The experimental data for HfC are summarized in Table 10. Since the arc-melted samples were highly irregular in shape, the geometrically calculated surface areas and densities are only approximate. The surface oxide tended to flake and spall upon removal of the sample from the apparatus, and hence, the measured weight gains are maximum values. From the measured maximum net weight gains, and the weights of CO(g) in the product gas stream, the maximum ratio of hafnium to carbon oxidized can be calculated, as described above for the oxidation of ZrC. The experimental values of the ratio are given in Table 10 as 14.1, 10.1, and 15.9, to be compared to a Hf:C ratio in the original alloy of 15.6. Since the experimental ratios are maximum values, it appears that Hf may be oxidized preferentially. Linear oxidation was observed in every case for which a rate law could be determined. For pellet XVI-19, the temperature dropped continuously from 2000 to 1600°K, during the run, resulting in a corresponding drop in the signal from the thermal conductivity bridge.

At 1280°K in pure oxygen at one atmosphere, a hafnium carbide specimen disintegrated into several pieces within three minutes, in a manner very similar to that described above for zirconium carbide. X-ray analysis of the oxide films revealed lines for HfO_2 (c) and no others.

b. Metallographic analysis of the oxide films. Pellet XVI-19 was imbedded in plastic and polished for microscopic observation. In the photomicrographs shown in Figure 14 preferential oxidation is seen to occur along grain boundaries. The oxide is also observed to contain considerable porosity. The photomicrographs in Figure 15 are for a hafnium carbide pellet that had been exposed to a N_2-He mixture for an hour and a quarter at temperatures of 1960°K. The N_2 apparently contained a small quantity of oxygen, and white HfO_2 (c) was identified on the surface of the sample by X-ray diffraction analysis. The net weight change of the sample was $0.0024 g/cm^2$, an order of magnitude less than that observed at an oxygen partial pressure of 11.5 torr in the same temperature range. The oxidation rate was seen to decrease slightly with time, and although grain boundary oxidation is apparent in Figure 15, the oxide seems less porous than that shown in Figure 14, for oxidation at a higher pressure.

TABLE 10

SUMMARY OF EXPERIMENTAL DATA ON HfC

Pellet	Initial Weight (g)	Area (cm²)	Density (g/cc)	Temp. (°K)	Oxygen Pressure (Torr)	Flow (cc/min)	Weight Change (g)	CO Formed (g)	CO_2 Formed (g)	Time (min)	C Consumed (g)	Hf Consumed (g)	Hf/C (max.)	Weight Change Rate (Max.) (g/min)
XVII-4	0.5374	1.076		1791	11.5	119	0.021	0.0160	0.0254	85	0.0138	0.195	14.1	2.5×10^{-4}
XVI-38	0.6544	1.241		1893	11.5	119	0.016	0.0232	0.0355	69	0.0196	0.199	10.1	2.3×10^{-4}
XVI-36	0.7511	1.032	10.23	2005	11.5	119	0.022		0.0191	43				5.1×10^{-4}
XVI-19	0.6057	1.256	11.00		7.5	119	0.038	0.0340	0.0225	120	0.0207	0.328	15.9	
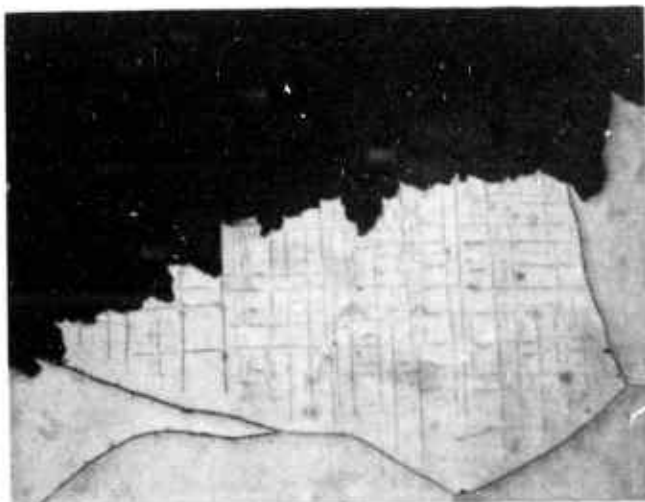
260X
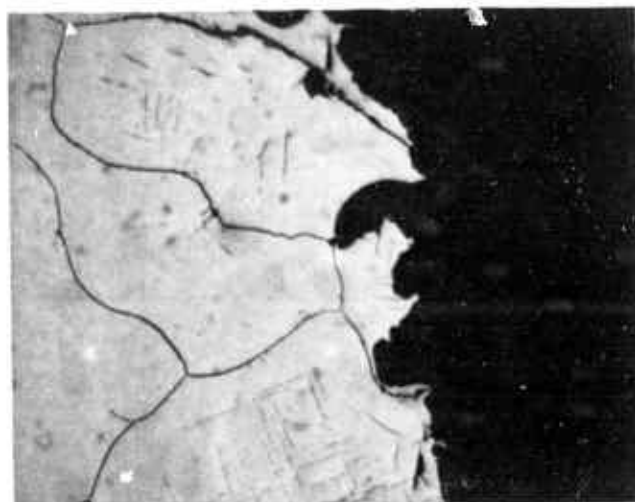
260X
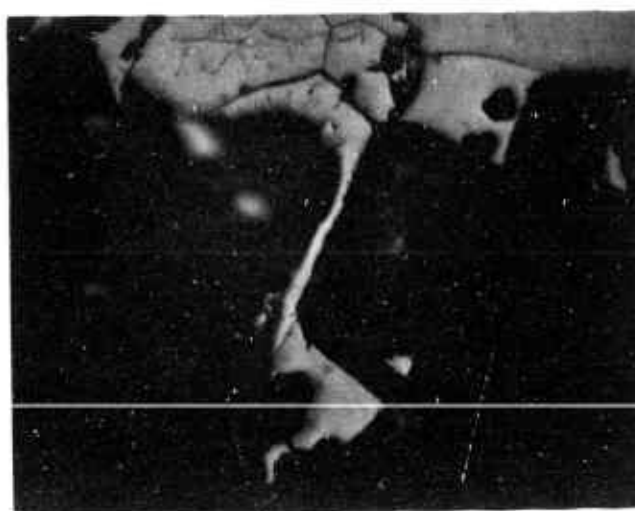
260X

Figure 14   Photomicrographs of Oxidized Hafnium Carbide
Pellet XVI-19, Temperature 1600-2000°K, P_{O_2} 11.5 Torr

65X

260X
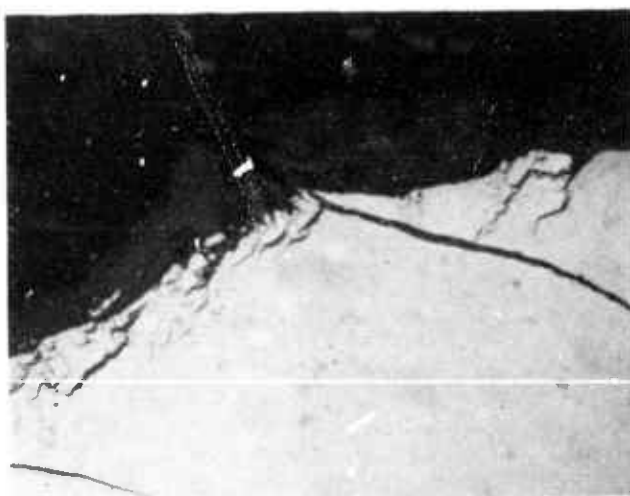
260X

260X

Figure 15   Photomicrographs of Oxidized Hafnium Carbide
Pellet XVI-22, Temperature 1960°K, low oxygen pressure

66

5. Summary

At temperatures of 1130-2160°K and oxygen partial pressures of 3-26 torr the oxidation of ZrC is linear and non-preferential, i.e., zirconium is oxidized at the same rate as carbon. Oxide grows most rapidly along grain boundaries and gradually extends into the interior of crystallites. Between 1130 and 1560°K, the grain boundary oxidation results in fracture of the specimens. The oxidation of HfC, at temperatures of 1790-2000°K and oxygen pressures of around 10 torr, is also linear and occurs preferentially along grain boundaries.

V. MASS TRANSPORT STUDIES*

A. INTRODUCTION

In the oxidation of the carbides and borides oxide coatings will form. Providing that these are adherent and non-porous, the rate of oxidation may be limited by the rate of diffusion through these oxide coatings.

The rates of diffusion through oxides are determined by the defect structure of the materials. The defect structure may also be a factor in whether an adherent and non-porous coating is formed. Thus, a knowledge of transport processes and defect structure in zirconium oxide and the degree to which it can be controlled can be important in understanding observed kinetic behavior and in "engineering" ceramic bodies for specific applications.

We have undertaken the study of mass transport and defect structure in zirconium dioxide. The proposed program of electrical conductivity, ion transport and isotopic tracer studies was discussed in detail in an earlier report, ASD-TDR-62-204, Part 1.[21] Early experimental techniques and the results of ac electrical conductivity measurements and their interpretation were presented in last year's report ASD-TDR-62-204, Part II.[15]

Since the electrical conduction process is related to the motion of charges in the material it is appropriate to investigate electrical conductivity as a means of providing information on both oxygen transport and defect structure. Conductivity (σ) in solids is often found to obey the empirical relationship

$$\sigma = Ke^{-E/kT}$$

and thus a plot of $\ln \sigma$ vs $1/T$ will yield activation energy (E) for the conduction process.

If more than one conduction path exists (i.e. electronic as well as ionic), it will be necessary to separate the various conduction paths. This can be done by a polarization technique in which all ionic transport is blocked by a polarizing electrode.

We present here the results obtained during this report period and attempt to interpret the defect structure of ZrO_2 from the available data. The report will discuss ac electrical conductivity results using a new electrode arrangement and dc polarization measurements, both as a function of oxygen atmosphere and temperature.

---

*Prepared by Dr's L.A. McClaine and C. P. Coppel, Arthur D. Little, Inc.

68

The results are discussed in terms of a separation of the ac and dc measurements into ionic and electronic contributions to the conduction process.

B. EXPERIMENTAL DETAILS

Sample material was prepared by fusing powdered ZrO_2 in an ADL-Strong arc-imaging furnace into boules about one cm diameter and three to five cm's long. Two sources of powder were used in preparation of the boules. One was a spectrographic grade ZrO_2 powder from Wah Chang Corporation and the second was a powder which we prepared by oxidation of pure zirconium sponge obtained from Wah Chang Corporation. The details of preparation and analysis of these materials were presented in an earlier report[15] (see also Section III of this report). Density measurements indicate that material prepared in this manner is at least 99% of theoretical density. A semi-quantitative spectrographic analysis of a wafer cut from a fused boule, when compared to an analysis of the powder, indicated no significant change in composition arising from the fusion operation.

Initial electrical conductivity measurements were made with samples having constant pressure electrical contacts. This sample holder and electrode arrangement were discussed in our previous report.[15] Although good reproducibility in the rate of change of resistance with temperature was obtained, the absolute resistances varied from run to run, and were easily affected by mechanical disturbances of the holder system. Near the end of the last report period a technique was developed for attaching electrical leads directly to the sample faces. This was first accomplished by vapor plating platinum onto the sample, then sintering a platinum lead wire by using a platinum black paint and firing the assembly. Without the platinum vapor coating the platinum black paint apparently did not wet the surface and left a very unsatisfactory bond. Later it was discovered that electrical leads could also be applied directly by first coating the sample with a "liquid platinum" and then sintering on an electrical lead with a platinum black paint. This technique works best if several thin coats of "liquid platinum" are applied and fired before attempting to sinter the lead. This technique eliminates the need for vapor coating platinum on the surface. Samples used in the work reported here had electrodes directly attached by this technique.

The sample was suspended in the furnace by either two or four leads in the holder shown in Figure 16. The leads were protected and insulated by alumina tubes and the tubes were mounted in a rigid structure by cementing alumina disks appropriately. The cemented disks were designed to minimize conduction paths through the alumina in the hot zone of the furnace. A heat shield and support disk (for hanging the sample holder in the furnace) were cemented to the sample holder. This arrangement has worked satisfactorily for the work reported here.

Support Disk

Morganite Recrystallized
99.7% Alumina

Lead Insulating Tubes

Norton RA 1139 High Purity
Alundum Cement

Radiation Shields

Morganite Recrystallized
99.7% Alumina

Electrical Leads or
Thermocouple Leads
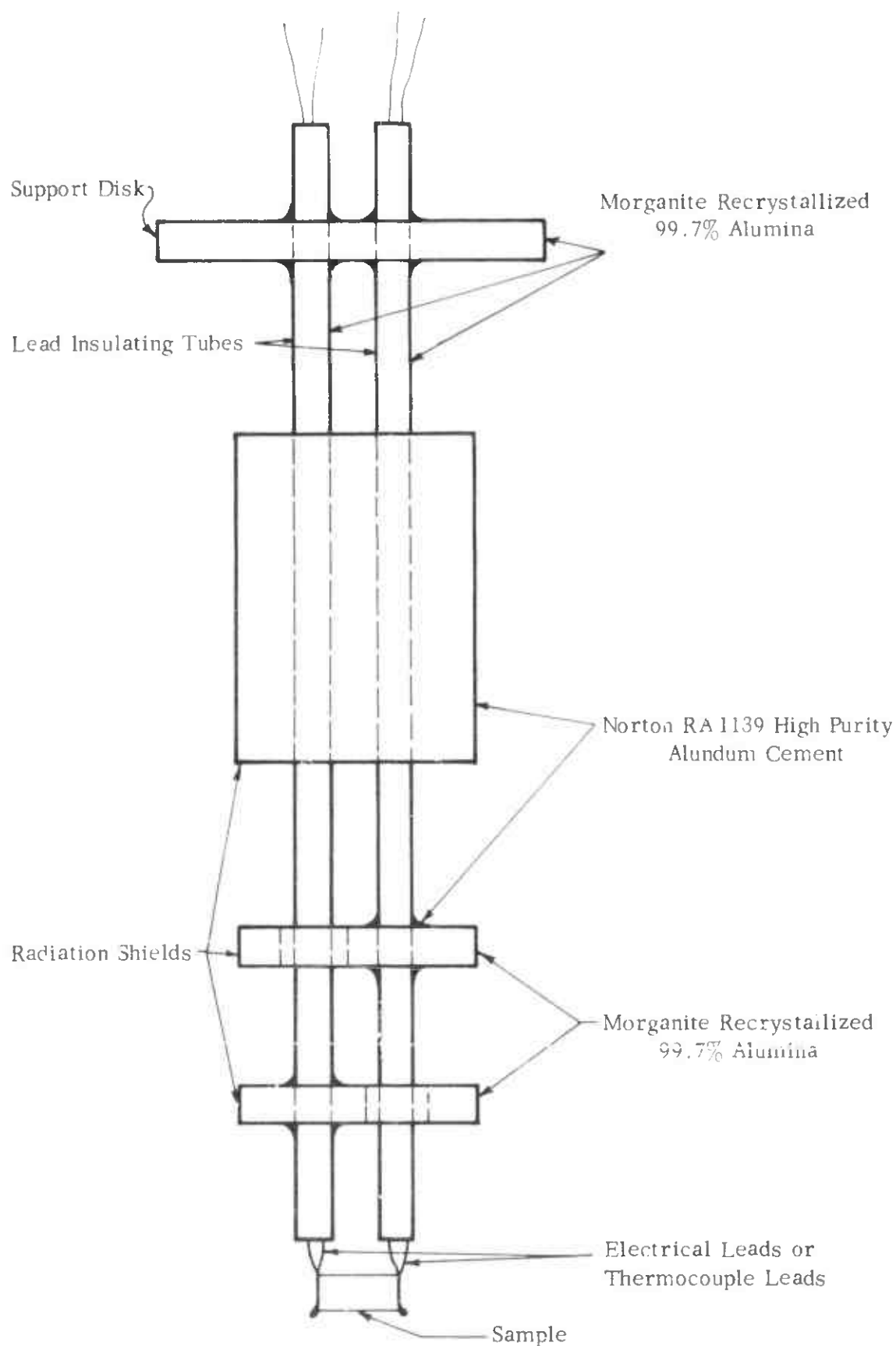
Sample

FIGURE 16   SAMPLE HOLDER FOR ELECTRICAL CONDUCTIVITY
MEASUREMENTS

In early ac resistance work with this holder two platinum leads were attached to the sample. At that time temperature of the sample was determined by either an optical pyrometer sighting into the furnace or a Pt-(Pt-10% Rh) thermocouple placed near the sample. In later work when both ac and dc measurements were required Pt-(Pt-10% Rh) thermocouples were connected directly to the ends of the sample. In this way more accurate sample temperatures could be obtained, temperature gradient across the sample could be measured, and current and potential leads were made available for dc measurements.

For most of our studies two types of electrical measurements were made. An ac resistance was measured at one kc with a General Radio Type 1650-A impedance bridge. A dc measurement was made under conditions favoring polarization by passing a known dc current through the sample and measuring the emf across the sample. The power source was initially an Electro Model D-612t filtered dc power supply but to reduce circuit noise most of the measurements reported here were made using 6 volt dry cells. The emf was measured with a Leeds & Northrup Type K Potentiometer No. 7552 and a Minneapolis Honeywell Doelcam Null Detector. The current leads were the Pt lead of one thermocouple and the Pt-10% Rh lead of the other thermocouple. The potential leads were the pair of either Pt or Pt-10% Rh leads to the two thermocouples. It was not desirable with our sample-thermocouple-electrode arrangement to completely separate current and potential leads, but since the lead resistance was at all times less than 1% of the sample resistance, current flowing in the potential measuring lead did not seriously affect the measured emf. Measurements were made on occasion with current flow through the sample reversed in order to detect any error introduced by the Thompson effect. Only at temperatures above 1430C was a significant difference observed in the potential measurements and in this region curves were drawn to average the resistances calculated for forward and reverse current flow.

Current-voltage measurements were made to determine the polarization curve in order to insure that dc measurements would be carried out in a voltage region below any possible decomposition potential. For pure ZrO_2 we found a straight line I to E relationship below potentials of 0.1V. The curves began to break as potentials were increased beyond this point. The straight line portion of the I-E curve corresponded to currents of up to about 100 μ amps for our sample geometry. Almost all dc measurements reported in this report were made at currents of about 10 - 20 μ amps.

The furnace used in this work consisted of an alumina tube wound with platinum - 10% rhodium wire placed in an insulated container. It was wound to give a fairly large hot zone in the center of the furnace. The arrangement has allowed us to reach temperatures of 1600C which is near the maximum temperature allowed by the construction materials. The temperature is controlled by means of a variac on the output of a constant voltage transformer supplying power

to the furnace. This arrangement gave temperatures constant to $\pm 2°C$. Temperatures were measured with both a pyrometer and Pt-(Pt-10% Rh) thermocouples for measurements carried out in air. For controlled oxygen atmosphere measurements the thermocouples were used alone in order to eliminate the gas leakage path through the pyrometer sight hole. Measurements were made either at constant temperature with the variac at a single setting or under heating or cooling conditions with the variac being mechanically driven. Under heating and cooling conditions temperature changes were on the order of 1-2 degrees per minute.

For controlled atmosphere measurements, two pyrex tubes with side arms were epoxied directly to the ends of the alumina furnace tu·. The epoxy seals were cooled by copper coils with circulating water. The side arms served as gas inlet and outlet and the open ends of the tubes served as inlets for the thermocouple and sample holder. Seals were made through rubber stoppers. This arrangement has been used with furnace temperatures up to $1600°C$.

A gas purifying and mixing system provided known mixtures of oxygen and helium, carbon monoxide and carbon dioxide, or hydrogen, helium and water vapor. The gases were purified, passed through flow meters, then through a mixing tube, through the furnace, and finally out through another flow meter.

The system is by no means vacuum tight and undoubtedly small leaks are present. However these should not seriously affect the validity of the calculated oxygen pressure since this was determined by either; (a) the presence of a substantial amount of O_2 flowing in the system (1 atm to $10^{-2.5}$ atm) or (b) the presence of large amounts of reducing and oxidizing species which would tend to preserve the equilibrium oxygen pressure by reacting with small amounts of leaked gases.

Flow rates were kept at a rate fast enough to avoid thermal diffusion and slow enough to avoid cooling the sample. These ranged from 260 cc/min to 60 cc/min.

C. RESULTS

Our initial measurements were made in air with the ends of the furnace tube open. Figure 17 shows some ac measurement results in the tetragonal region (1050-1650C). Curves 1, 2, 3 were obtained by continuously changing the temperature of the furnace at rates of about $1 - 2°C$ per minute. The furnace temperature was varied by means of a mechanically driven variac. Curve 1 represents 3 cooling and 2 heating cycles, Curve 2 represents 2 cooling and 2 heating cycles. Curve 3 is a single cooling cycle. Each of these curves is
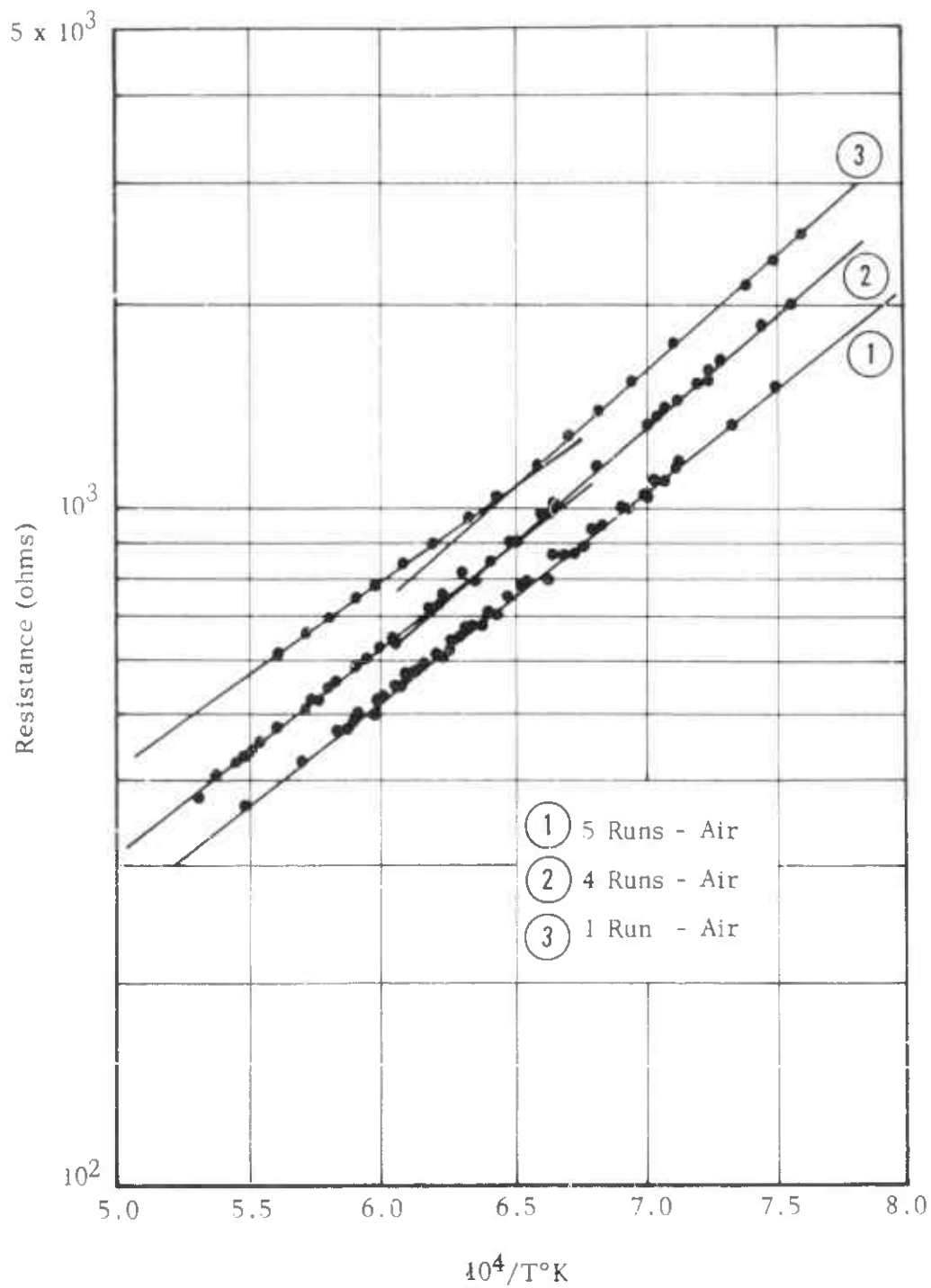
FIGURE 17   ELECTRICAL RESISTANCE VS RECIPROCAL
TEMPERATURE FOR ZrO$_2$ IN THE TETRAGONAL
PHASE REGION

73

a set of measurements taken while in the tetragonal region. Also, each successive set was taken after at least one cycle through the monoclinic-tetragonal transition zone. The successive increases in resistance for the three sets of data may be indicative of cracking in the sample or changes in the sample electrode contact due to sample expansion and contraction on passing through the transition zone. The first series of measurements (Curve 1) gave results which fall generally on a straight line, while the next two series (Curves 2 and 3) indicate either a small curvature or possibly a break from one straight line to another. This work shows the reproducibility of results while remaining within the tetragonal region. It does indicate some change may occur on cycling through the monoclinic-tetragonal transition region. We now believe that the breaks observed were the result of a crack in the sample. The following table summarizes these results and gives activation energies taken from these curves.

TABLE 11

SUMMARY OF EXPERIMENTAL DATA PRESENTED IN FIGURE 17

Curve	Atmosphere	Temperature Conditions	Temperature Range (°C)	Activation Energy (ev)
(1)	Air	Heating and Cooling Cycles	1060-1560	0.605
(2)	Air	Heating and Cooling Cycles	1050-1290	0.653
	Air	Heating and Cooling Cycles	1290-1620	0.595
(3)	Air	Cooling Cycle	1040-1270	0.661
	Air	Cooling Cycle	1270-1510	0.540

Figure 18 shows ac measurement results in the monoclinic region (780-1060C). Again the three curves represent three series of measurements, between which there was at least one pass through the transition zone. The data in all cases approximate a straight line and in general show increasing resistance from run to run. The activation energies taken from these curves are: (1) 1.10 ev, (2) 1.19 ev, and (3) 1.12 ev. These results were all taken in air during either a heating or cooling cycle.

74
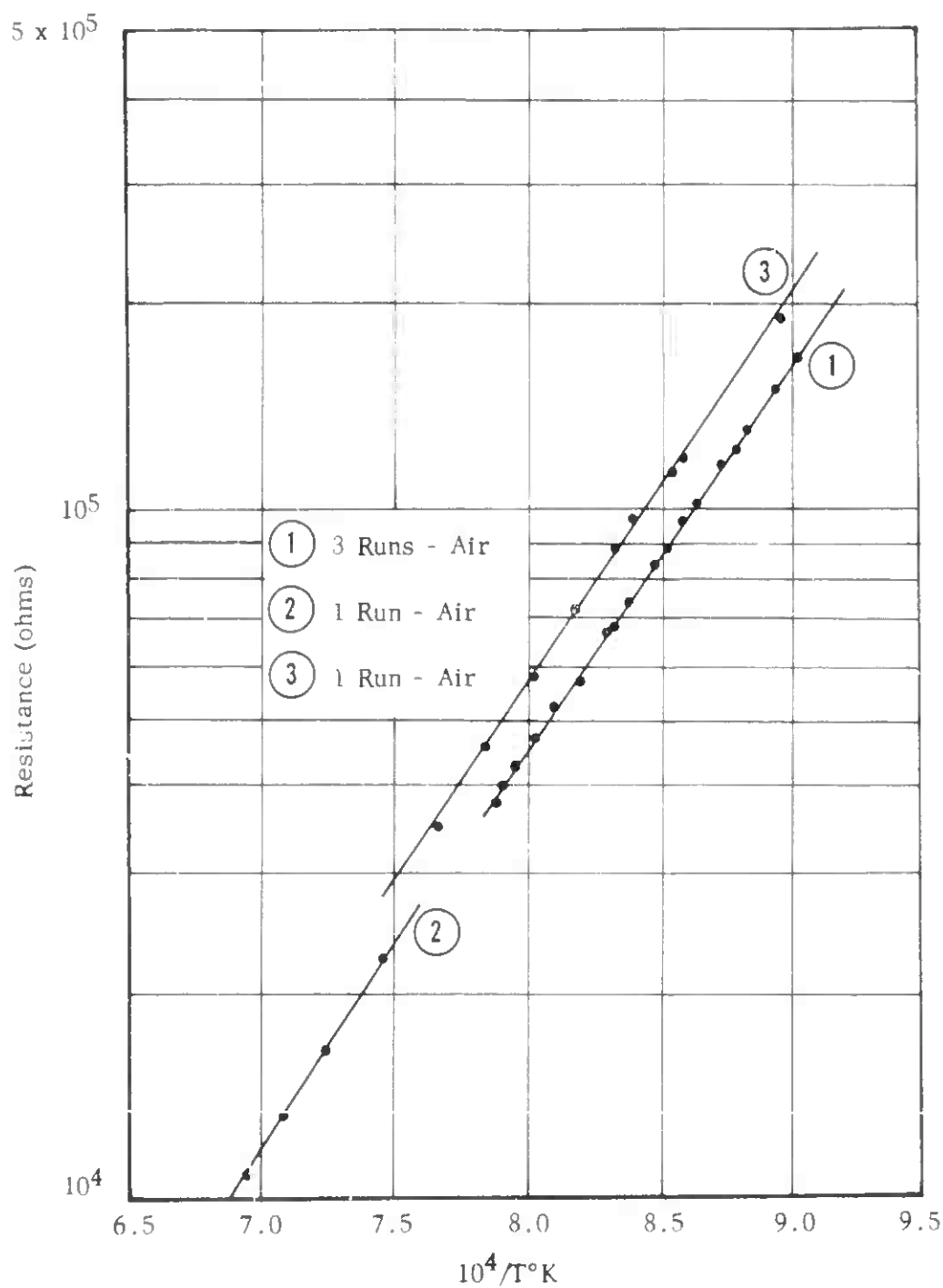
FIGURE 18   ELECTRICAL RESISTANCE VS RECIPROCAL TEMPERATURE FOR ZrO_2 IN THE MONO-CLINIC PHASE REGION

The activation energies obtained from these ac measurements on a sample in both the tetragonal and monoclinic phase are in good agreement with those reported last year in the study using the pressure contact electrode sample holder.

At this point we wanted to start making measurements as a function of oxygen pressure and at the same time carry out a series of measurements aimed at separating ionic and electronic conduction. However when we attempted dc measurements in air we found no difference in resistance from our ac measurements. Subsequent work indicates that we were working at too high a potential, but at the time we thought that platinum might be acting as a reversible oxygen electrode and decided to try other materials as a blocking electrode. The first attempt was made using aluminum oxide as a blocking electrode. Aluminum oxide has heen shown to be essentially an electronic conductor.[22] By placing a layer of aluminum oxide at one end of the zirconia sample, passing a known dc current through the alumina and zirconia in series and measuring the potential drop across part of the zirconia sample we hoped to be able to measure only the electronic conductivity of the zirconia. Total conductivity would be ohtained by either our present technique or an ac measurement on the alumina zirconia sample.

The blocking electrode experiments were attempted in air with thin disks of Linde sapphire and with thin vapor deposited films of aluminum anodized to aluminum oxide but we were not successful in obtaining any meaningful measurements. Subsequent experiments on lime stablized zirconia in air and inert atmospheres which indicated that polarization does not occur in air under the voltage and current conditions at which we were working may imply that the aluminum oxide blocking technique might work under different experimental conditions.

At this point we attempted a series of measurements using platinum electrodes on a known ionic conductor, lime stablized zirconia. The material was obtained from Norton Co. and contained about 9% calcium oxide. The following table lists some typical results on this sample obtained in a N_2 atmosphere.

Temp (°C)	I (μamps)	E (volts)	R_{dc} (ohms)	R_{ac} (ohms)	T_1 $\left(\dfrac{R_{dc}-R_{ac}}{R_{dc}}\right)$	R_i $\left(\dfrac{R_{dc}\,R_{ac}}{R_{dc}-R_{ac}}\right)$
1270	1340	0.453	338	28.0	0.92	30.5
	785	0.289	368		0.92	30 3
	490	0.200	408		0.93	30.1
	270	0.126	466		0.94	29.8
	138	0.0678	491		0.94	29.7

In this table T_i is the ionic transport number, R_1 the ionic resistance, R_{ac} the ac resistance, R_{dc} the dc resistance, I the current flowing in the sample and E the emf across the sample. The sample dimensions were 0.136 x 0.169 x 0.189", the latter being the distance between electrodes. For the measurement at 0.0678 volts and using the equation

$$\sigma = L/AR$$

for conductivity (σ), where L is the length of the sample, A the cross sectional area, and R the resistance; one obtains a value of $\sigma_1 = 0.109$ (ohm^{-1} cm^{-1}) which is in excellent agreement with the value given by Kingery et al.[23]

This experiment indicated that in a nitrogen atmosphere the platinum electrodes do act as blocking electrodes to ionic oxygen conduction and that decomposion potentials are in the 0.2 volt region or higher. The same experiment in air gave identical dc and ac resistances indicating either no polarization or no ionic conduction. Since this material has been shown to be an ionic conductor at oxygen pressures up to one atmosphere[23] it must he concluded that polarization is not taking place in the air atmosphere for the same E and I conditions which were studied in nitrogen.

With this indication of satisfactory polarization behavior with platinum electrodes, at least in low oxygen atmospheres, we attempted further measurements on pure zirconium dioxide samples. We have determined polarization curves for the several different atmospheres used in our studies. At high oxygen pressures the difference between ac and dc measurements was very small but it was real. Earlier difficulties were in part due to the small magnitude of the change and noise in our measuring circuit.

In the course of our experimentation a series of rate of atmosphere equilibration runs were made. These runs were made at a constant current of 14 microamps by switching from inert atmosphere (nitrogen or helium) to air and vice versa. The results are shown in Figure 19. They are of interest for three reasons: (1) They give an indication of times required for equilibration. (2) The shape of the curves implies that the electronic conduction is the result of at least two opposing factors which reach equilibrium at different rates. (3) The presence of a nitrogen atmosphere gives a higher ionic conductance than a helium atmosphere, implying nitrogen interaction with the matrix creating more defects for ionic conduction. All future experiments used helium as the inert gas component.

The major experimental phase of this study consisted of an extensive series of ac and dc measurements on zirconium dioxide samples as a function of oxygen pressure and temperature. The first measurements in the series were made at constant temperature, varying the oxygen pressure. It soon became

77
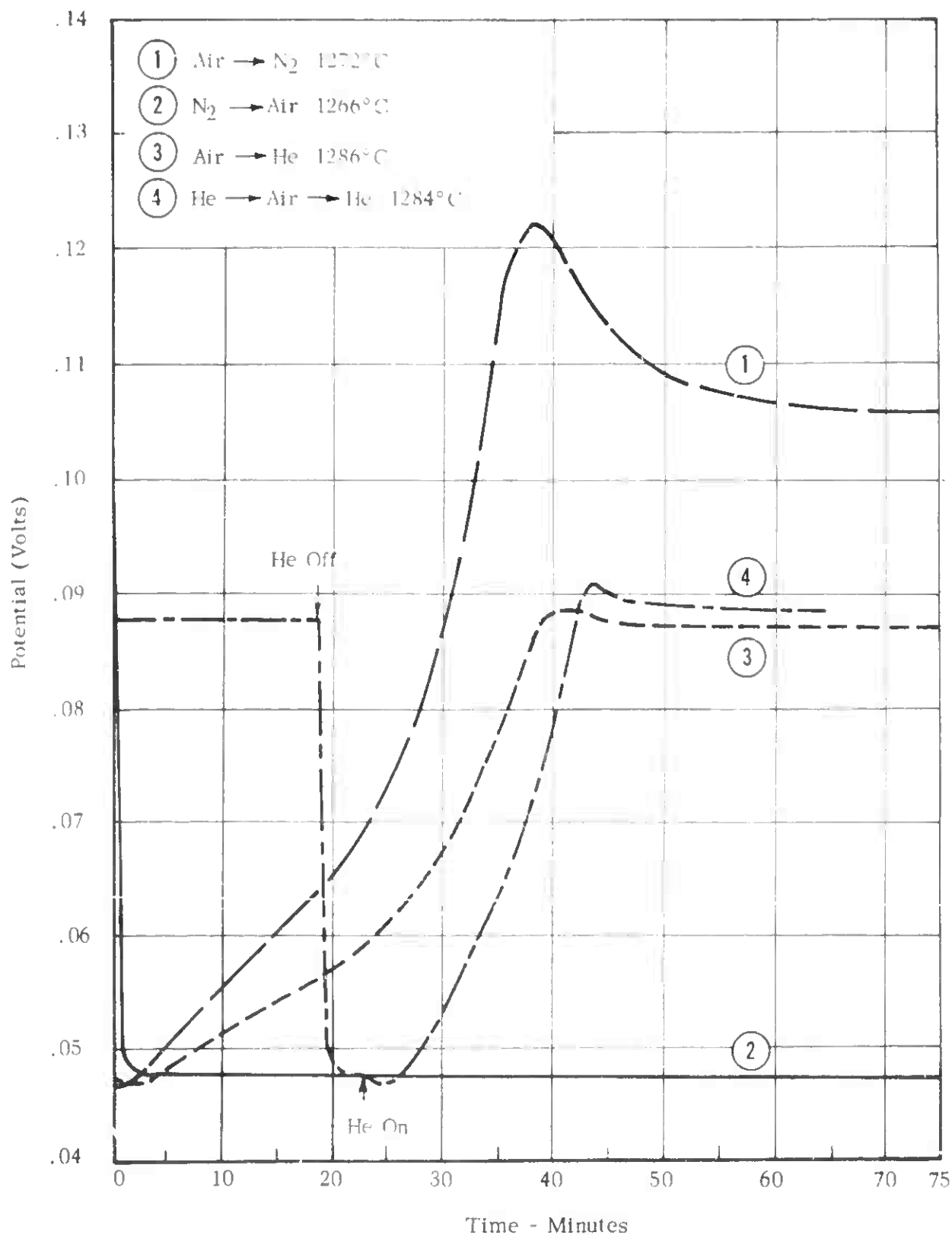
FIGURE 19   RATE OF POLARIZATION AND DEPOLARIZATION
(ZrO$_2$ Sample No. 9 - i = 14 microamps)

apparent that data could be obtained more efficiently by holding oxygen pressure fixed and varying temperature since this technique reduced the waiting periods required for equilibration.

Figures 20 through 24 are representative of the results obtained. Data in Figure 20 were obtained in a pure oxygen atmosphere and data in Figure 21 were obtained in an oxygen helium mixture. In these two graphs oxygen pressure is constant for all temperatures. The other three Figures, 22-24, represent results obtained in carbon dioxide - carbon monoxide mixtures, and hydrogen-helium-water vapor mixtures. In these graphs oxygen pressure varies with temperature as the equilibrium between the various gases shifts with temperature. A few oxygen pressures are given at the top of each graph. Figures 20 and 22 represent more than one temperature cycle and the points for the individual runs indicate the relative reproducibility of the measurements.

Figure 22 gives the results obtained in a high CO_2/CO ratio ($\sim$ 20) atmosphere and two curves for the ac and dc results are plotted. The two sets are identified as I and II in the figure.

The first set of data (I) was taken on the sample after it had been exposed only to oxygen, helium, hydrogen, and water vapor. The second set (II) was taken much later in the samples history after considerable exposure to carbon dioxide - carbon monoxide atmospheres. This behavior is believed to indicate a tendency for carbonaceous atmospheres to change the sample properties. A series of measurements were carried out to evaluate this possibility, these are outlined in Table 12.

Set A of Table 12 shows that a sample in equilibrium with a CO_2 rich CO_2-CO mixture quickly returns to its previous O_2 equilibrium value on exposure to oxygen, and set B shows that the reverse process going back to the CO_2 rich mixture is also essentially reversible (in terms of R_{DC}). The criterion for reversibility being used here in most instances is ionic transport number (t_i). Set C indicates that once the sample has been exposed to a CO rich mixture it does not return to its previous equilibrium in the CO_2 rich system and long exposures to oxygen (Set D) do not return it to its original condition. Set E shows the change in values of the sample after being exposed to oxygen and then returned to first the CO_2 rich mixture followed by the CO rich mixture. Although the values measured are still different from original measurements there is indication for the CO_2 rich mixture that exposure to oxygen has brought values closer to original. Set F is an attempt to force sample into its original condition by long exposure to oxygen and by heating in an oxygen atmosphere. Some reversal in sample properties was achieved, however the sample never returned completely to its original condition.

79
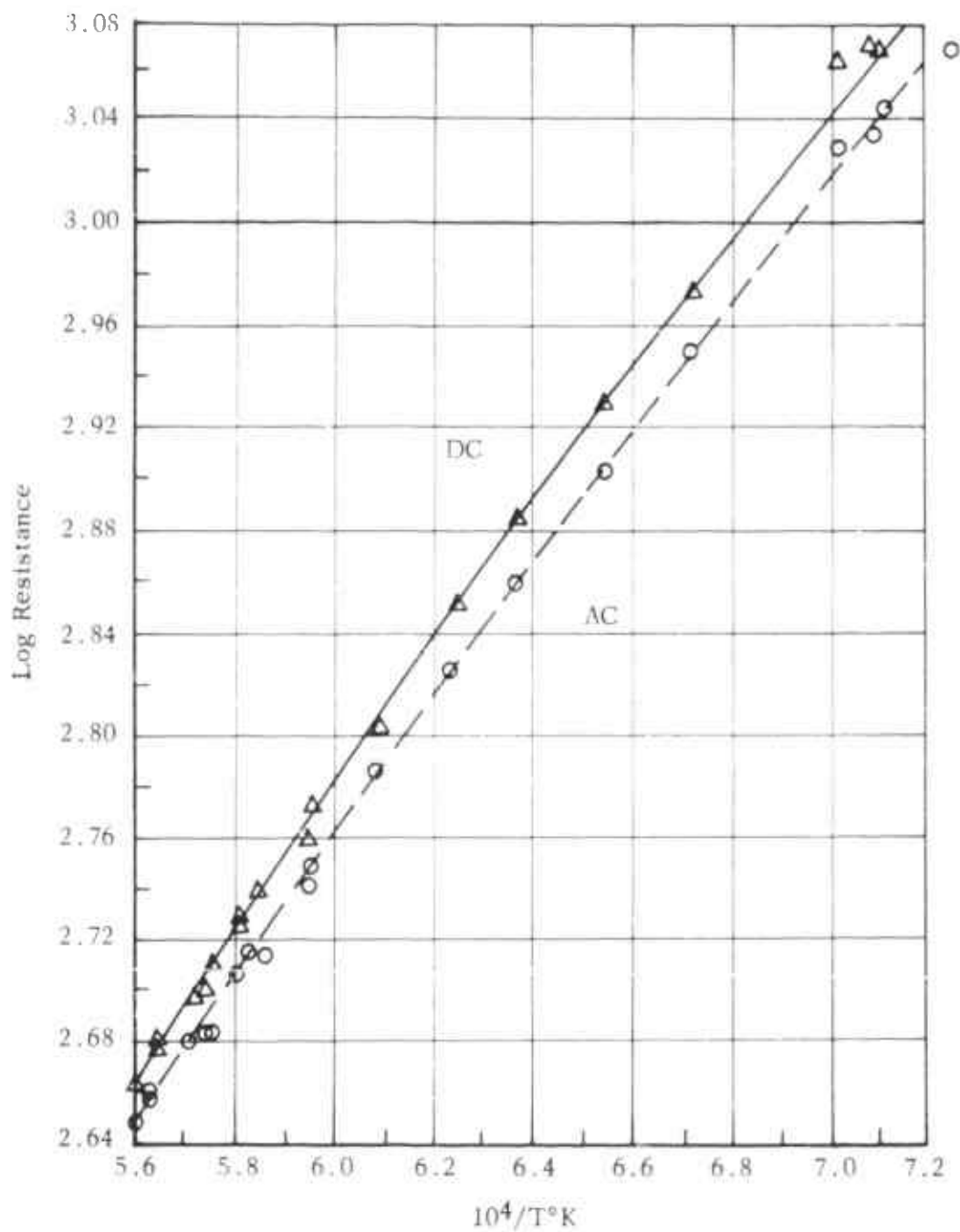
FIGURE 20   ELECTRICAL RESISTANCE VS RECIPROCAL
TEMPERATURE (Oxygen - log P_{O_2} = 0)

80
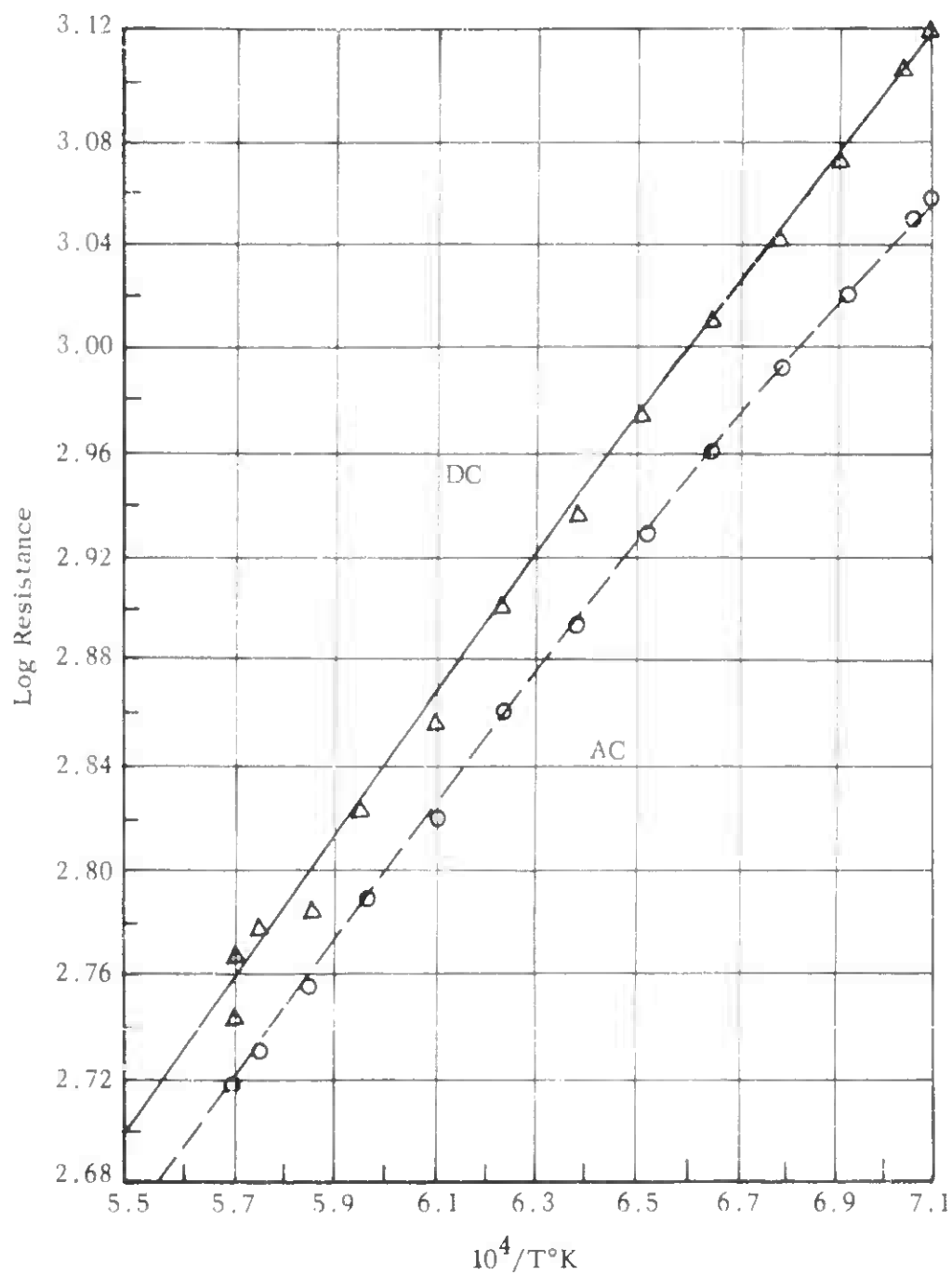
FIGURE 21   ELECTRICAL RESISTANCE VS RECIPROCAL
             TEMPERATURE (Oxygen + Helium - $\log P_{O_2}$ =
             -2.49)

81
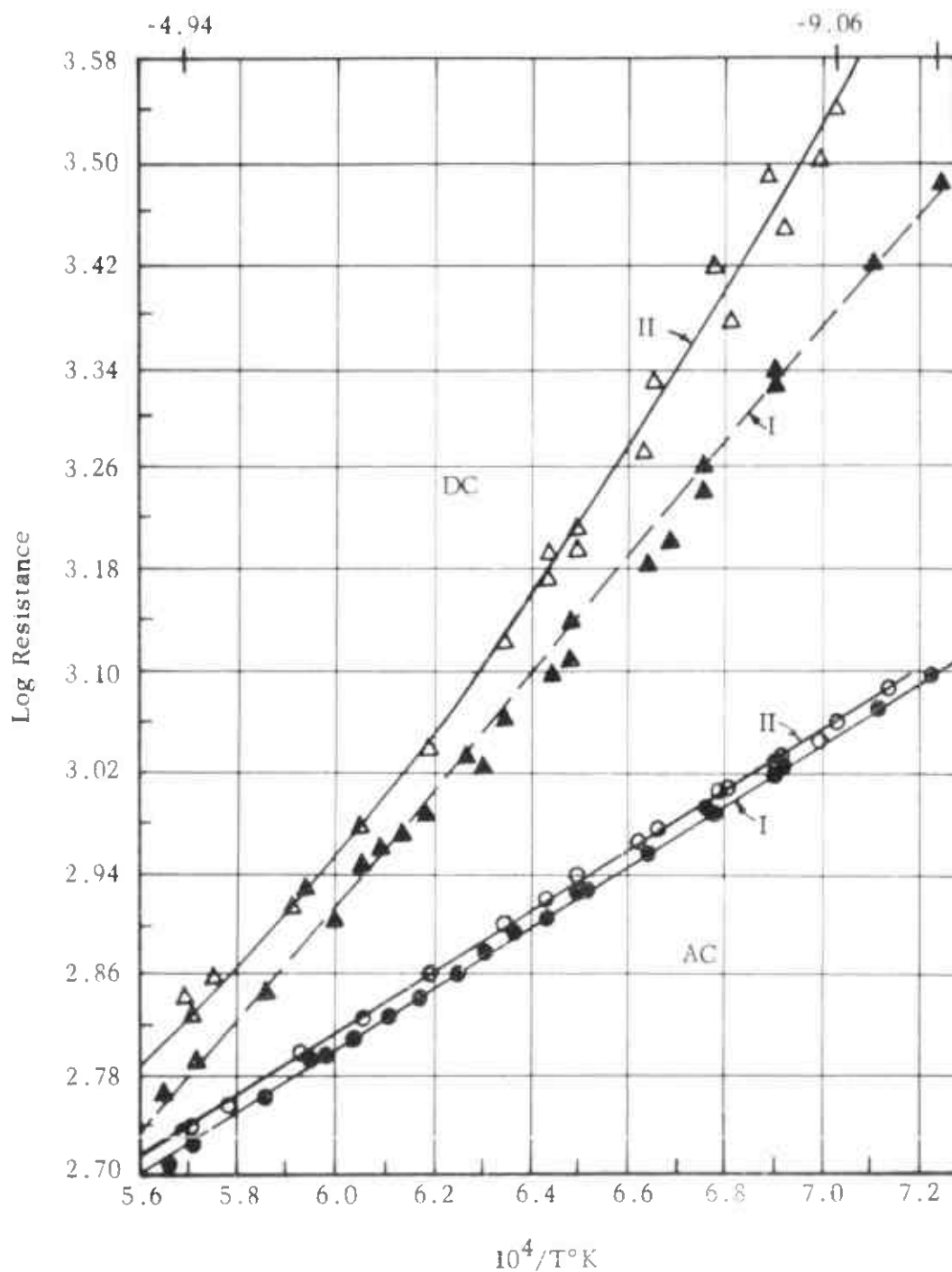
FIGURE 22   ELECTRICAL RESISTANCE 'S RECIPROCAL
TEMPERATURE (Carbon Dioxide + Carbon Mon-
oxide - log P_{O_2} = -9.60 to -4.94)
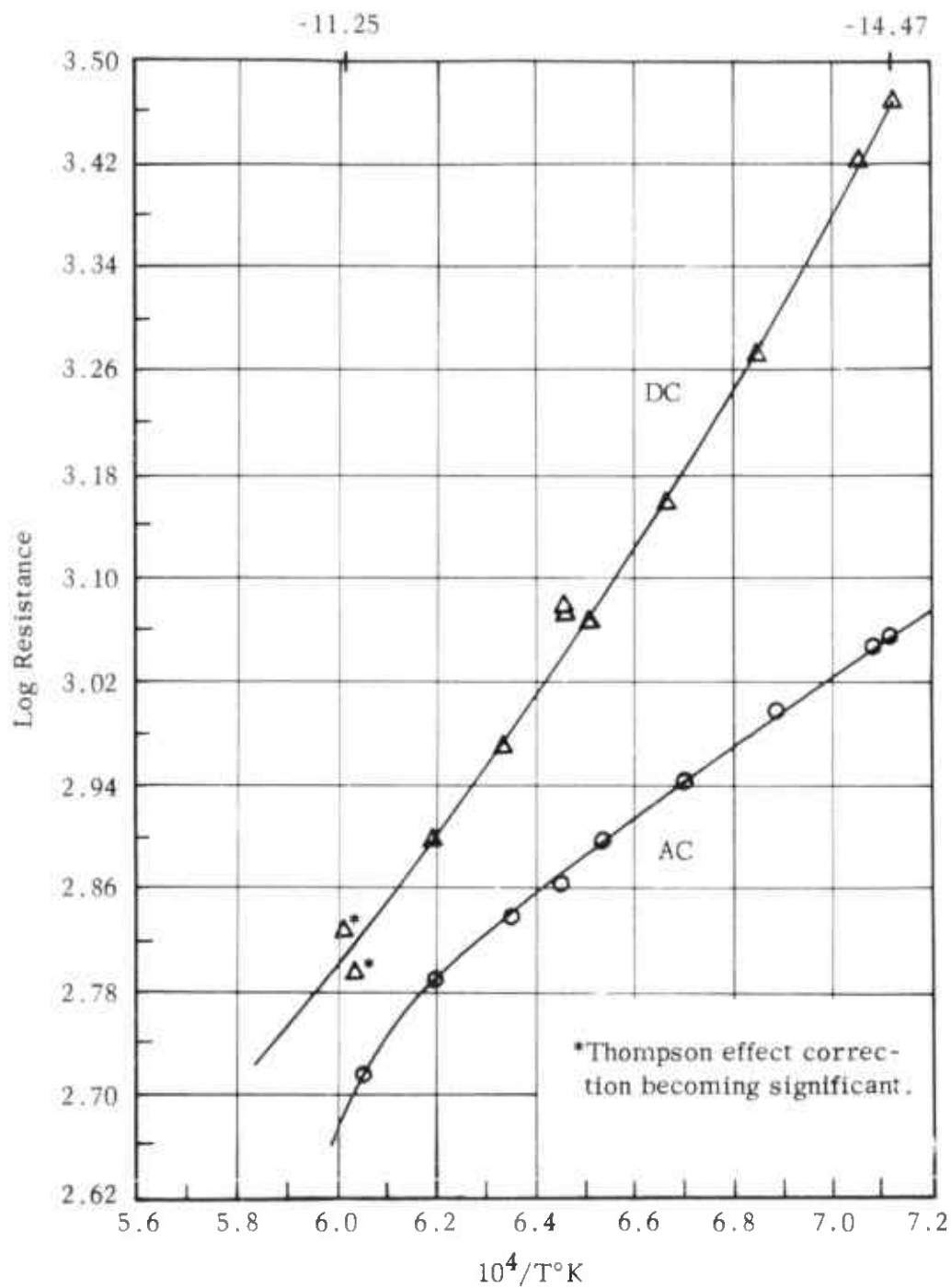
FIGURE 23   ELECTRICAL RESISTANCE VS RECIPROCAL
              TEMPERATURE (Carbon Monoxide + Carbon
              Dioxide $-\log P_{0_2}$ = -14.47 to -11.25)

83
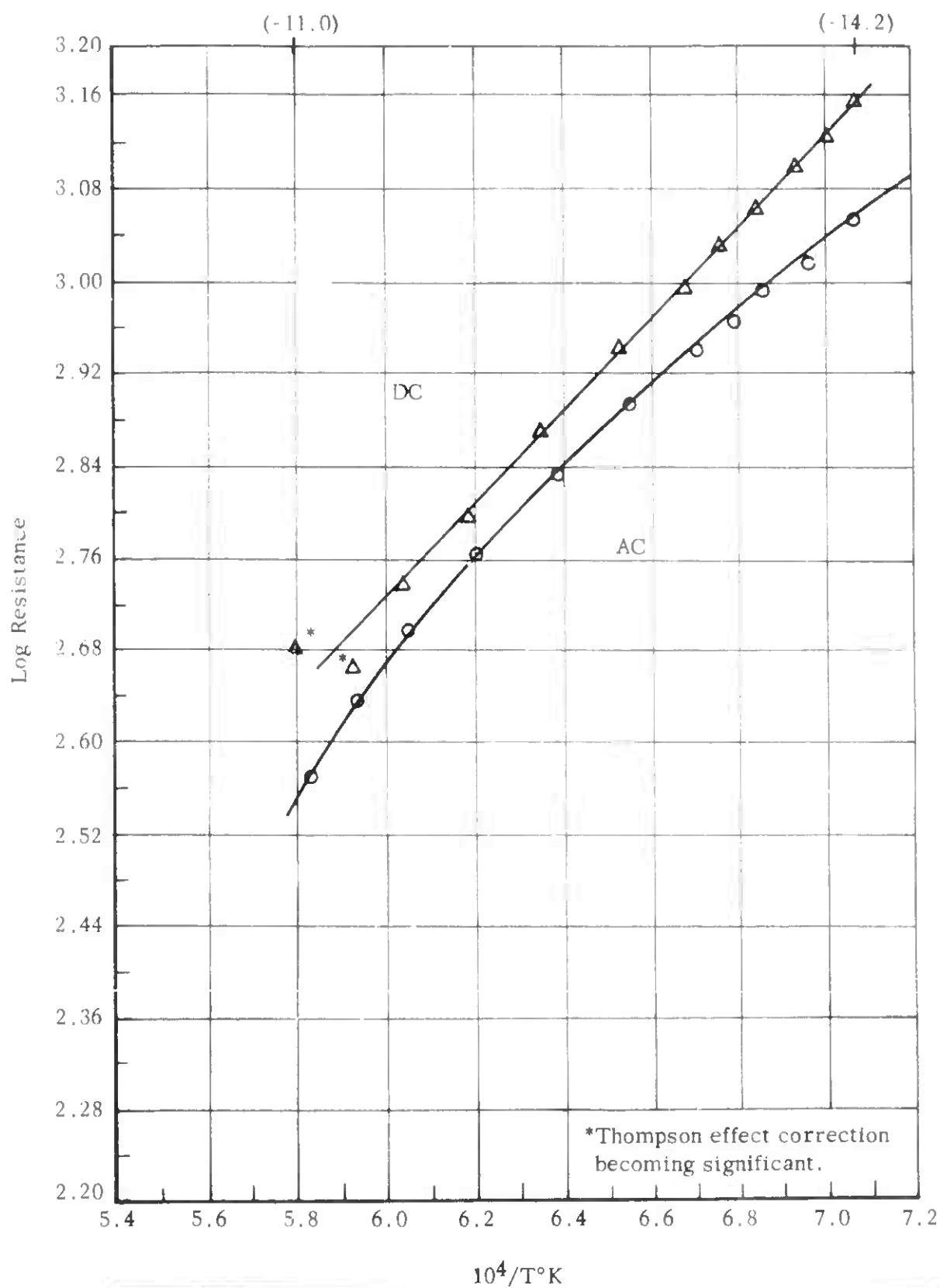
FIGURE 24   ELECTRICAL RESISTANCE VS RECIPROCAL
              TEMPERATURE (Hydrogen + Helium + Water
              Vapor - log P_{O_2} = -14.2 to -11.0)

84

TABLE 12

EFFECT OF CARBONACEOUS ATMOSPHERE
$(1273°C)$

Test	Time (min)	R_{dc} (ohms)	R_{ac} (ohms)	CO_2/CO	$\log P_{O_2}$	t_1	Comments
		819	789	--	0	0.0366	New Sample
		813	769	--	0	0.054	Exposed to $CO_2/CO=20$
A.	0	1546	822	20	- 7.32	0.455	
	4	1561		--	0		
	16	823		--	0		
	48	823	788	--	0	0.055	
B.	4	829		20	- 7.35		
	12	1452		20	- 7.35		
	45	1500		20	- 7.35		
C.	0	1186	730	0.05	-12.6	0.385	
	12	2200		20	- 7.35		
	40	2120		20	- 7.35		
	60	2105	836	20	- 7.35	0.602	
D.	20	859		--	0		
	236	854		--	0		
	1200	855	790	--	0	0.076	
E.	83	2005	850	20	- 7.35	0.575	
	80	1062	747	0.05	-12.6	0.296	
F.	--	873	791	--	0	0.094	Following Tests A-E
	3840	886	828	--	0	0.066	O_2 over week-end
	1440	863	806	--	0	0.066	O_2 overnight + heat to $1470°C$

85

Although there is no direct evidence, we believe this behavior is indicative of carbon interaction with the sample. Calculations indicated that carbon activity in the CO rich mixture which we used might be as high as 10^{-2} and as high as 10^{-6} in the CO_2 rich mixture. Assuming concentration in the ZrO_2 approximately equal to activities this would lead to a significant number of sample defects due to the presence of carbon. In view of this behavior we have favored the earliest data obtained in the CO_2 rich system, i.e. Figure 22 data I, in calculation of ionic and electronic conductivities as a function of oxygen pressure.

Figure 24 presents the results obtained in a hydrogen-helium-water vapor atmosphere. These results were somewhat surprising due to the much smaller difference between dc resistance and ac resistance than was observed for the CO rich system. (Figure 23.) These two sets of experiments covered almost identical oxygen pressure ranges, yet the hydrogen-helium-water vapor system gave much lower dc resistance values. This behavior indicating increased electronic conductivity in the H_2-H_2O mixture is somewhat analogous to that observed by Mollwo[24] and Thomas and Lander[25] for a zinc oxide-hydrogen system. These authors found an increase in conductivity of ZnO when in an atmosphere of hydrogen. This was attributed to hydrogen entering the matrix as an interstitial positive ion with the associated ionization of an electron. Such an interaction would explain our observations. In view of this possible interaction the hydrogen-helium-water vapor results were not used in final calculations of ionic and electronic conductivities as a function of oxygen pressure.

Figures 25 and 26 show the calculated values of electronic and ionic conductivity as a function of oxygen pressure at several temperatures. The electronic and ionic conductivities were calculated from the set of curves of ac and dc resistance given in Figures 20 through 24. The following equations were used for each set of temperature and pressure conditions.

$$R_e = R_{dc}$$

$$R_i = \frac{R_{ac} R_{dc}}{R_{dc} - R_{ac}}$$

$$\sigma = \frac{L}{AR}$$

Most of the results in these two figures are from measurements made on a single sample (No. 12 prepared from Wah Chang sponge). The dashed curve in Figure 25 was obtained in another set of measurements on a different sample
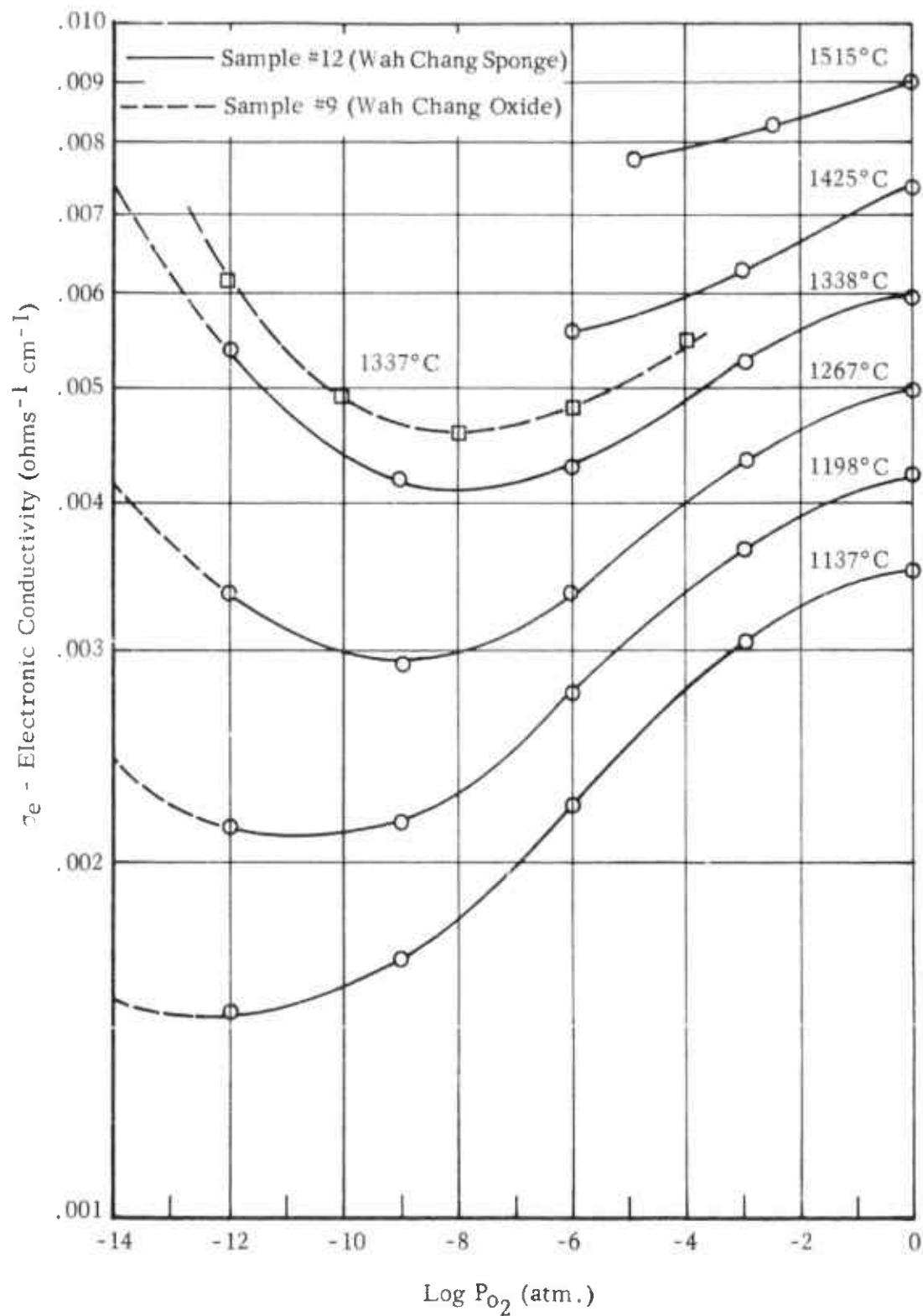
FIGURE 25   ELECTRONIC CONDUCTIVITY VS OXYGEN
              PRESSURE
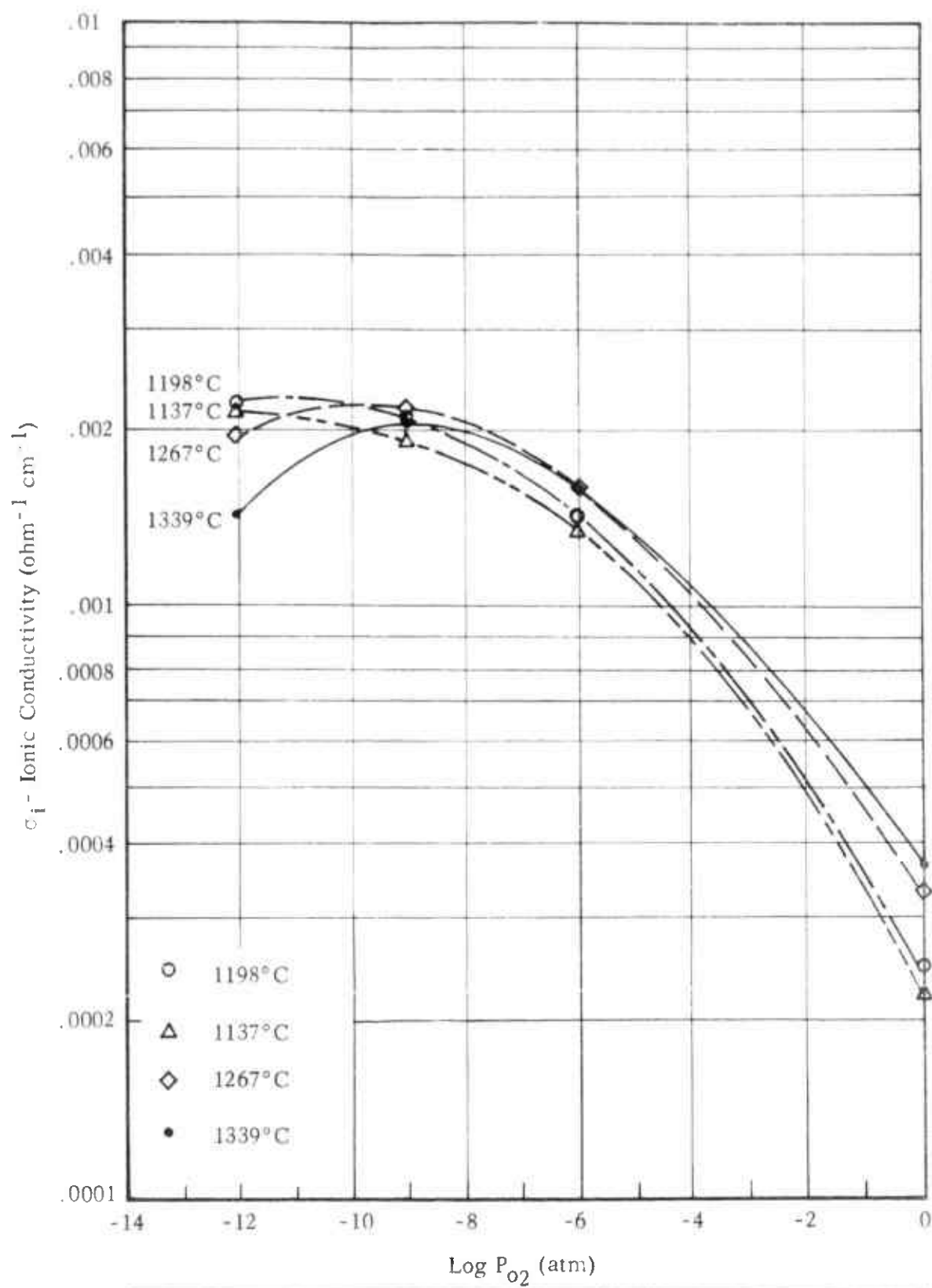
FIGURE 26   IONIC CONDUCTIVITY VS OXYGEN PRESSURE

(No. 9 prepared from Wah Chang oxide). The agreement in both curvature and absolute magnitude between these two sets of measurements is quite good.

Figure 27 shows the calculated ionic transference number as a function of oxygen pressure for several temperatures. The transference numbers were calculated by the equation;

$$t_i = \frac{R_{dc} - R_{ac}}{R_{dc}}$$

D. DISCUSSION

1. A "Defect Structure" Model

The information gained from the electrical conductivity studies are summarized in terms of electronic and ionic conductivity in Figures 25 and 26 respectively. Such data can be utilized to develop a model of the defect structure of the oxide. We will attempt to develop a model that is in accord with this and other known data on the behavior of ZrO_2.

As shown in Figure 25 the electronic conductivity decreases as pressure is reduced from one atmosphere. Such behavior is indicative of p type (hole) conduction. As pressure is further decreased the conductivity reaches a minimum and begins to increase again. The region of increasing conductivity with decreasing pressure is indicative of n type (electron) conduction. In Figure 28 we have plotted curves of electronic conductivity at one atmosphere and 10^{-12} atmosphere vs reciprocal temperature. The slopes of these curves give activation energies of 11,700 and 30,800 cals/mole for the p type and n type conduction respectively.

As shown in Figure 26 ionic conductivity increases as pressure is reduced from one atmosphere indicative of an increasing number of ionic carriers. However the ionic conductivity within the range of our study reaches a maximum and shows a slight decrease for the highest temperature curves. For one atmosphere pressure the ionic conductivity is plotted vs reciprocal temperature in Figure 28 and an activation energy of 12,800 cal/mole is obtained which is quite close to that obtained for electronic conduction at the same pressure.

The presence of either cation vacancies (V_{Zr}) or anion interstitials (O_i) can account for the observed p type electronic conduction at high pressure. We have postulated several different defect models including one or the other of these defects and examined the atomic and electronic disorder relationships. The equations relating the defects were solved by a graphical method discussed

89
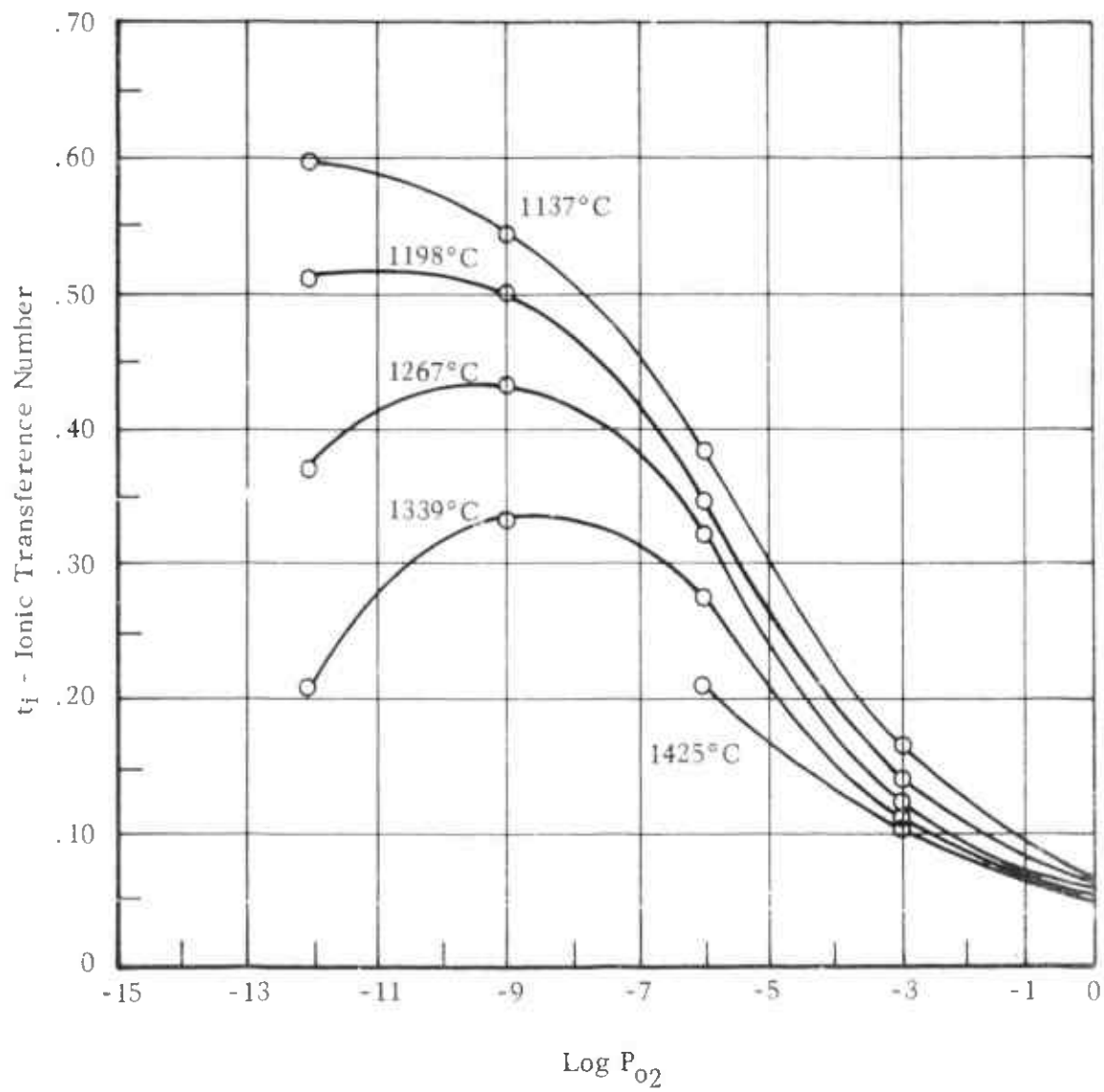
FIGURE 27   IONIC TRANSFERENCE NUMBER VS OXYGEN PRESSURE

90
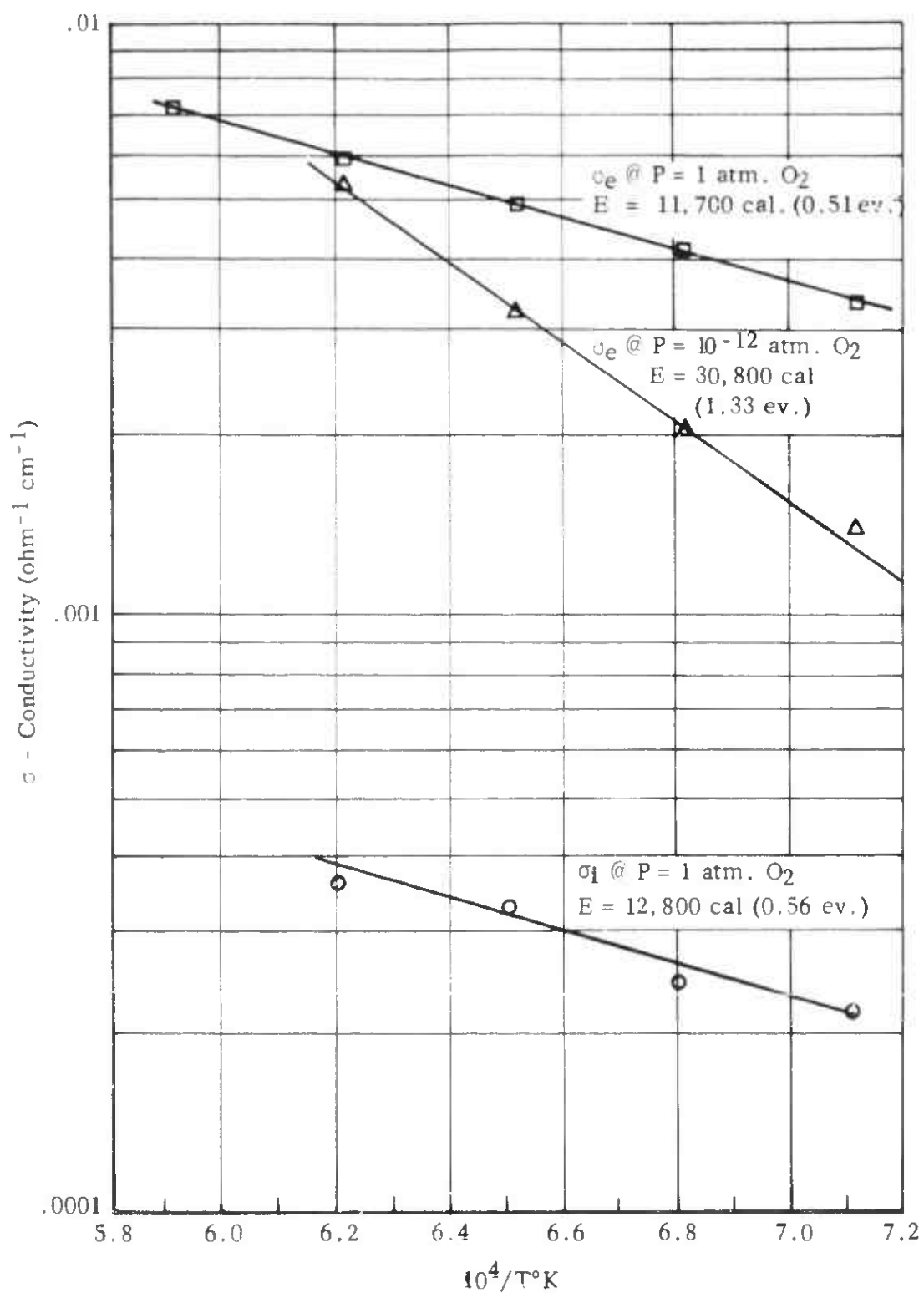
FIGURE 28   CONDUCTIVITY VS RECIPROCAL TEMPERATURE

The figure shows σ – Conductivity (ohm^{-1} cm^{-1}) plotted against $10^4/T°K$.

Labels within the figure:

σ_e @ P = 1 atm. O$_2$
E = 11,700 cal. (0.51 ev.)

σ_e @ P = 10^{-12} atm. O$_2$
E = 30,800 cal
(1.33 ev.)

σ_i @ P = 1 atm. O$_2$
E = 12,800 cal (0.56 ev.)

91

by Kroger and Vink[26] and credited by them to G. Brouwer.[27] One model was found which appears to fit the observed conduction behavior as well as other data known about ZrO_2.

In this model we postulate a Frenkel type disorder in which an oxygen atom leaves a lattice position to form an oxygen vacancy and an oxygen interstitial.

$$O_o = V_o + O_i \qquad\qquad K_F = [V_o][O_i] \qquad (1)$$

The effect of atmospheres on defect structure is accounted for by an equation relating interstitial oxygen with atmospheric oxygen.

$$O_i = \frac{1}{2} O_2 (g) \qquad\qquad K_{ox} = \frac{P_{O_2}^{1/2}}{[O_i]} \qquad (2)$$

The vacancy and interstitial defects can ionize according to the following equations where n and p are electron and hole respectively:

$$O_i = O_i^- + p \qquad\qquad K_3 = \frac{[O_i^-]}{[O_i]} p \qquad (3)$$

$$O_i^- = O_i^{-2} + p \qquad\qquad K_4 = \frac{[O_i^{-2}]}{[O_i^-]} p \qquad (4)$$

$$V_o = V_o^+ + n \qquad\qquad K_5 = \frac{[V_o^+]}{[V_o]} n \qquad (5)$$

Also we have an equation and equilibrium expression for intrinsic ionization of ZrO_2.

$$np = n + p \quad K_i = np \qquad (6)$$

In addition to the above six equilibrium expressions relating the electronic and atomic disorder and the atmospheric oxygen we have one more equation representing the net charge neutrality of the system.

$$[O_i^-] + 2[O_i^{-2}] + n = p + [V_o^+]$$

The graphical solution for these seven equations for four limiting neutrality conditions is presented in Figure 29. As previously mentioned the technique is fully discussed in an article by Kroger and Vink.[26] Figure 29 is a plot of log of defect concentration vs log of atmospheric oxygen pressure. It presents on one figure the way in which the concentration of each of the different defects varies with oxygen pressure under each of the limiting neutrality conditions and permits one readily to compare the relative changes for each defect species in any given region of the plot. The widths of each region and thus the absolute relationship of each defect to others are dependent on the values of the equilibrium constants. We have not attempted for this discussion to fit and select numerical values of equilibrium constants so as to obtain a quantitative solution. It should also be noted that while solutions of the equations can be obtained for the several limiting neutrality conditions the corresponding regions may not always be attainable experimentally. We believe that Regions I and II correspond to the conductivity behavior observed in our studies and under discussion here.

In Region II is the point at which $n = p$ and thus approximately the point at which a minimum will be observed in electronic conductivity. To the right with increasing oxygen pressures $p \gg n$ and p type conduction will prevail. To the left with decreasing oxygen pressure $n \gg p$ and n type conduction will prevail. Holes might be produced by either reaction 3 or 4, but the presence of the doubly ionized interstitial oxygen is necessary to explain observed ionic conductivity effects. Thus we must believe that O_i^- and O_i^{-2} are the major interstitial species present and that with increasing temperature additional holes are produced by reaction 4.

The data of Figure 29 indicate that in region II three ionic species can contribute to ionic conduction. Two of these, O_i^{-2} and V_o^+, will increase in concentration as pressure decreases; one, O_i^-, will decrease with decreasing pressure. Each species will contribute to the total conductivity dependent on the product of its charge, quantity, and mobility. On the basis of the relative charges and concentrations of the ionic defects the total conductivity should increase with decreasing pressure in accordance with experimental observation.

When region I is entered the concentration of O_i^{-2} becomes constant and V_o^+ continues to increase and O_i^- to decrease with decreasing pressure. The product of O_i^- and V_o^+ is a constant. This can be shown by substituting for O_i and V_o in equation (1) from equations (3) and (5) and using equation (6) to eliminate n and p. In order that the model interpret the experimental observations for ionic conduction one must postulate that mobility of the interstitials is much greater than vacanies (a likely situation). Consequently at the high pressure edge of this region the total ionic conductivity will decrease with decreasing pressure in accord with our experience at the low pressure limit of our studies. However the model indicates that as one proceeds further into the region the ionic conduction

93
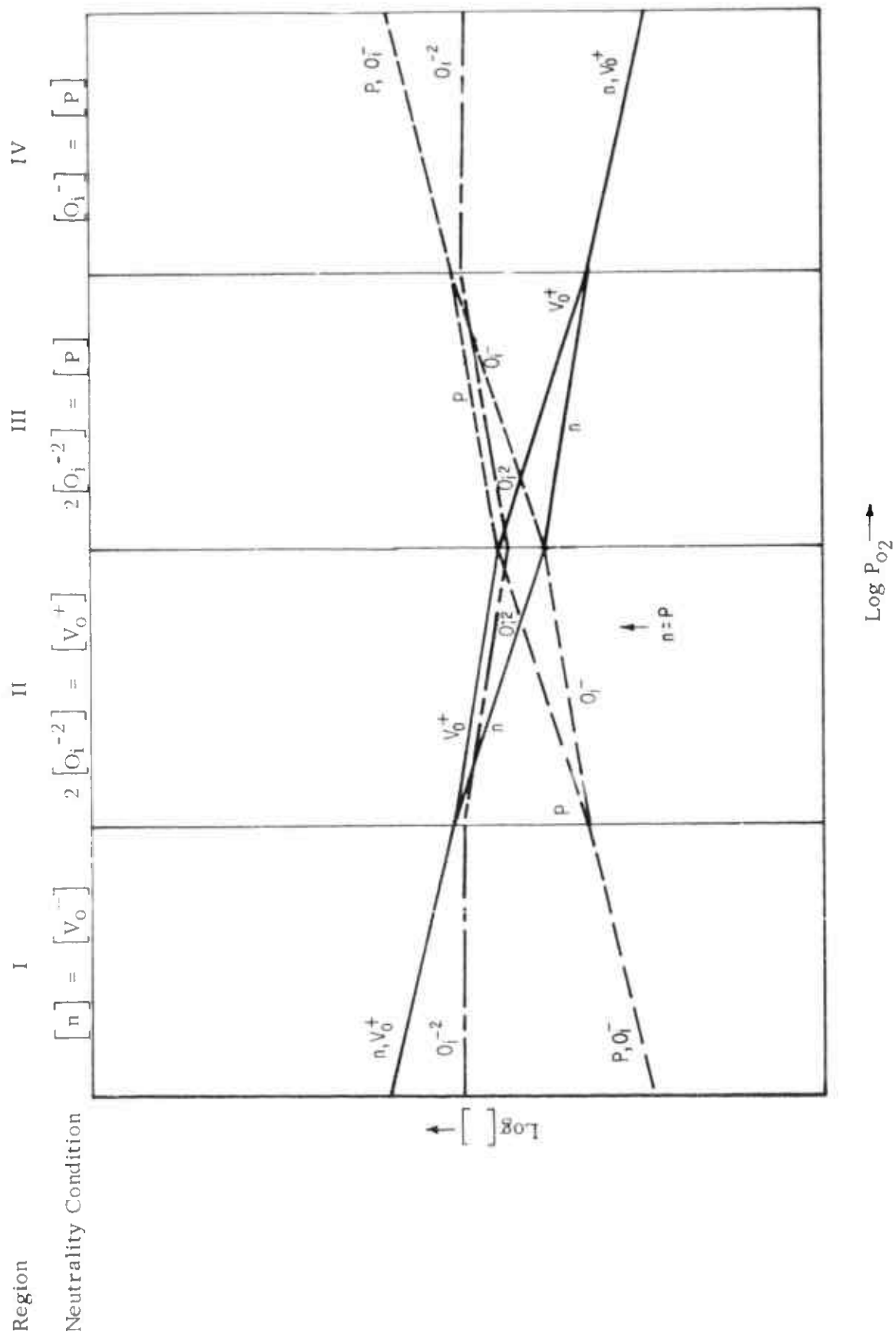
FIGURE 29   GRAPHICAL SOLUTION OF ATOMIC AND ELECTRONIC DISORDER EQUATIONS

94

contribution of V_O^+ will far outweigh the contributions of O_i^- and O_i^{-2} and then the ionic conduction behavior will be that of V_O^+ and will increase again with decreasing pressure. The experimental data are not sufficient to confirm or deny this behavior.

In summary, to explain our experimental results requires a model with (a) Frenkel type defect of oxygen interstitials and vacancies, (b) greater mobility for interstitials than for vacancies and (c) the defects primarily present as V_O^+, O_i^- and O_i^{-2}. We started seeking a model with a prejudice against an oxygen interstitial, especially a highly ionized one, because of the size factor. But we have found no other combination of defects with which to account for the observed behavior. Kofstad[16] had previously proposed an oxygen vacancy and interstitial defect combination. He indicated that the defects must interact in the conduction process to increase the charge transport over that to be expected from the sum of the processes. We have found no need to make this postulate in our model.

2. Diffusion Calculations

One of our main interests in conductivity studies on ZrO_2 was to obtain knowledge and understanding relating to mass transport in this material. From the experimental conductivity data and the defect structure model presented here it is possible to make some calculations relating to diffusion of oxygen in ZrO_2.

The experimental results for ionic conductivity are summarized in Figure 26 for the temperature and pressure range studied. As discussed in an earlier report[21] diffusion coefficients may be calculated from ionic conductivity by utilizing the Nernst-Einstein relationship. For one atmosphere pressure at 1137C and 1339C we calculate $D = 7.5 \times 10^{-10}$ and 1.4×10^{-9} cm^2/sec respectively. Our model as well as the behavior of the data indicate that the observed ionic conduction is due to more than one species of charge carrier. In making the estimates for D we have assumed a -2 charge for all carriers. This will indicate a minimum D. If the charged carriers were all -1 rather than -2 the calculated D would be 4 x greater. If uncharged defects are present, D could be much greater yet. We believe from study of the model developed that the average effective charge would be close to 2 and that the majority of the defects are ionized. With decrease in pressure the ionic conduction increases and for 10^{-12} atmospheres oxygen and 1137C we calculate $D = 7.4 \times 10^{-9}$ cm^2/sec. On the basis of weight losses of ZrO_2 in H_2-H_2O mixtures observed by Aronson[28] we estimated the vacancy content for a ZrO_2 sample under this set of pressure and temperature conditions. On the basis of vacancy contents we find a reasonable relationship between our calculated D and the extrapolations of the studies of Kingery[23] and Douglas.[29]

Based on the model developed we are able to calculate the energy of formation of Frenkel defects from the activation energy observed for n type electronic conduction. For the limiting neutrality condition in Region I we can solve the disorder equations in terms of n and V_o^+ and find

$$n = V_o^+ = p_{O_2}^{-\frac{1}{4}} (K_5 K_F)^{\frac{1}{2}}$$

Thus at constant pressure and with increasing temperature

$$\sigma_e \; \alpha \; n \; \alpha \; (K_5 K_F)^{\frac{1}{2}}$$

The constants $K_5 K_F$ represent the equilibrium constant for the reaction

$$O_o = O_i + V_o^+ + n$$

From the observed activation energy for n type electronic conduction of 1.33 ev as shown on Figure 28 the energy associated with this reaction for the formation of Frenkel defects must be 2.66 ev (61,400 cal). Belle et al.[30] have reported an energy of 71,000 cal/mole for formation of a Frenkel defect in UO_2.

Now we know from the conduction and diffusion studies of Kingery[23] on lime stabilized zirconia in which the defect concentration is temperature independent that the activation energy associated with mobility of vacancies is about 1.26 ev. The activation energy associated with intrinsic conduction or diffusion should be the sum of one half the energy associated with Frenkel defect formation plus that associated with movement of the defects, 1.33 + 1.26 ev, a total of 2.59 ev or 60 kcal/mole. It is interesting to note that Dr. Berkowitz-Mattuck observes in her studies on oxidation of ZrB_2 behavior characteristic of diffusion control with an activation energy of 77 ± 5 kcal/mole.

3. Effects of Impurities

In the course of our experimental work we have observed effects which we attribute to C and H_2 impurity content in ZrO_2. In CO-CO_2 atmospheres carbon apparently builds into the ZrO_2 structure. This can be partially removed in an oxygen atmosphere as shown and discussed with respect to Table 12. We also found as shown in Figure 24 evidence for H_2 entering the ZrO_2 lattice and markedly affecting the electronic conduction when samples were held in H_2-H_2O atmospheres. Aronson[28] has also reported behavior which can be interpreted in the same manner. He found that samples of $ZrO_{1.975}$ when exposed to pure hydrogen-water vapor atmospheres were closer to stoichiometric ZrO_2 (based

on a weight change) than samples exposed to a hydrogen-inert gas-water vapor atmosphere of the same oxygen pressure. He suggests that these erroneous results indicated the presence of an impurity although he was not able to identify the impurity by chemical and spectrographic analysis.

The results we have observed indicate that problems are associated with using $CO-CO_2$ or H_2-H_2' atmospheres to control oxygen pressure over ZrO_2. The use of an ultra high vacuum system with a controlled oxygen leak is indicated.

The conductivity studies presented here should be extended to ZrO_2 samples containing selected impurities. Such studies can help to substantiate or disprove the defect structure model developed from the data now available. In addition they can provide quantitative information on our ability to control mass transport in ZrO_2 by introduction of selected impurities.

VI. VAPOR PRESSURES OVER ZIRCONIUM CARBIDE, ZIRCONIUM DIBORIDE, HAFNIUM CARBIDE, AND HAFNIUM DIBORIDE*

A. INTRODUCTION

In order to predict the reaction between a given compound and the materials with which it comes in contact, it is necessary to have certain thermodynamic data. Most of the data now available is limited to compounds with specific compositions, usually the stoichiometric composition. In many cases these values are misleading since a compound with a range of homogeneity may have quite different properties at opposite ends of the range.

This research was initiated to study the activities of the elements in the compounds zirconium carbide, zirconium diboride, hafnium carbide and hafnium diboride at or near their composition limits.

To determine the activities of the elements in these compounds, the partial pressures of each element will be measured by one of two methods, Langmuir (evaporation from a surface) or Knudsen (effusion from an orifice).

In either case vapor from the sample is condensed on a target which is continuously weighed by an automatic-recording vacuum balance. The fraction of vapor from the Knudsen cell or Langmuir sample striking the target may be calculated from the geometry of the system, and the effusion or evaporation rate may be calculated from the rate at which the target gains weight. The pressure, p , may be calculated from Langmuir's equation,[31]

$$p = \frac{m}{tA} \qquad \frac{2\pi RT}{M} \qquad (1)$$

where m is the weight loss in time t from an orifice or surface of area A, R is the gas constant, T is the absolute temperature and M is the molecular weight of the effusing or vaporizing species.

The reasons for using Knudsen cells to measure the pressure are, first, to eliminate diffusion controlled evaporation. This may occur when the evaporation rate is limited by the rate of migration of one of the elements to the surface. Second, Knudsen cells are used to avoid uncertainties concerning the evaporation coefficient, α_e, which may be defined as

$$\alpha_e = \frac{p_m}{p_{eq}} \qquad (2)$$

where p_m is the measured pressure in a Langmuir experiment and p_{eq} is the equilibrium pressure.

98

A number of investigators have used Knudsen cells for these reasons, but in so doing have encountered other problems: reaction between cell material and sample material, diffusion through the cell wall, and creep from the orifice. In the first instance, the pressure measured may be those in equilibrium with the ternary condensed system: cell material-metal-carbon or cell material-metal-boron. On encountering the latter two difficulties, a high apparent pressure is measured.

In order to avoid these problems in the present study, Langmuir samples or Knudsen cells constructed from sample material are used.

This report describes the apparatus and procedure used for measuring the partial pressures over zirconium carbide, zirconium diboride, hafnium carbide and hafnium diboride, and the results of measurements obtained on these compounds and on pure hafnium. A review of some of the past work on these elements and compounds is given in the following section.

B. LITERATURE REVIEW

1. Zirconium Diboride

Of the four studies on zirconium diboride, the earliest experiments were carried out by Leitnaker, Bowman and Gilles;[32] the later experiments were done by Goldstein and Trulson,[33] by Lyon,[34] and by Wolf and Alcock.[35]

Leitnaker, et al. studied the vapor over metal rich congruently vaporizing ZrB_2 of a composition originally reported as $ZrB_{1.906}$. It was later determined that the composition was closer to $ZrB_{1.97}$.[36] Their experiments were carried out using a tungsten Knudsen cell and a tungsten susceptor. However there is evidence, as suggested by Trulson and Goldstein, that ZrB_2 will react with tungsten. Diffusion data for zirconium in tungsten[37] raises the possibility that the apparently low evaporation coefficient found by Leitnaker on reducing the orifice area was due to zirconium diffusion through the lid.

Trulson and Goldstein studied the effusion of Zr and B over ZrB_2 and of Zr and B from a ZrC cell using a mass spectrometer. Since these data are described very briefly in ARPA Progress Reports it is not possible to completely evaluate their work.

In a brief discussion with Trulson[38] it was established that this work was done in a carbon rich cell and that the vapor from the cell was well collimated so that a surface area of only about four times that of the orifice was exposed to the ionizing chamber. Thus possible diffusion through the walls was minimized as far as the pressure measurements were concerned. These authors feel that their heat

of formation value for ZrB_2 of -71.6 kcal/mole is more reliable than the individual pressures over Zr and B. The reason for this is that ionization cross sections, multiplier efficiencies and other factors in the mass spectrometer are canceled when the partial pressures are compared to those over the elements.

Lyon[34] also measured the pressure over ZrB_2 using a tungsten Knudsen cell. He found an evaporation coefficient of 0.1 by varying the orifice dimensions. It is entirely possible that the apparently low evaporation coefficient is the result of zirconium diffusion through the lid, as discussed above in Leitnaker's work.

Wolf and Alcock[35] measured the evaporation rate of ZrB_2 by the Langmuir method, and found very good agreement with Leitnaker's Knudsen cell work. Wolf and Alcock, therefore believe that the evaporation coefficient of this compound is unity rather than the low value found by Leitnaker.

2. Zirconium

There have been two studies of the vapor pressure of zirconium, and heats of vaporization have been calculated from these measurements. Skinner, Edwards and Johnston[39] measured the pressure by the Langmuir method, using weight loss of the sample and weight of condensed zirconium to calculate the pressure and the ΔH°_{298} = 145.4 kcal/g-atom. Trulson and Goldstein,[40] using a zirconium carbide Knudsen cell and a mass spectrometer determined a heat of vaporization for zirconium of ΔH°_{298} = 140.8 kcal/g-atom. In both cases we cite the heat values calculated by Schick et al.[41] from the original data.

In view of the uncertainty surrounding both the effects of ZrC and C on the pressure of Zr, and the possible diffusion of Zr through the walls of the cell used by Trulson, it would appear that more reliance might be placed on the Skinner, Edwards and Johnston study.

3. Boron

There have been a number of Knudsen effusion studies of the vapor pressure of boron both by weight loss and by mass spectrometry. These experiments yield heats of vaporization which range from 128 to 139 kcal/mole. Various materials were used for the Knudsen cells, few of which are stable in the presence of boron or can act as a barrier to boron diffusion. Only one study has been carried out by the Langmuir method, where container problems are absent. This study by Paule and Margrave[42] gives a ΔH°_{298} of 136.9 kcal/mole. In this study it was assumed that all of the boron vapor reacted with the Ta susceptor.

4. Carbon

Hoch, Blackburn, Dingledy and Johnston[43] studied the vaporization of carbon, WC and TaC, establishing that the heat of formation of carbon to C_1 was the closest to the spectroscopic value of 171 kcal/mole. At the same time Chupka and Inghram[44] demonstrated with high temperature mass spectrometry that carbon vaporizes to a number of polymers. So far it has been found that all the polymers up to and beyond C_{10} exist in the vapor. The most recent data indicated that the common species in the temperature range between 2000 and 3000°K are C_3, C_1 and C_2.[12] Winslow and Thorn[45] have measured evaporation coefficients for each of these three species, find the following: C_3, 0.08; C_1, 0.37; and C_2, 0.34. The earlier study by Hoch et al.[43] and a recent investigation by Blackburn[46] on TaC suggests that the C_1 is the principal species over this compound and that its vaporization coefficient is close to unity.

5. Hafnium

There have been three determinations of the vapor pressure of hafnium where the heat of vaporization ΔH°_{298} was computed. Panish and Reif[47] using the Langmuir method, obtained $\Delta H^\circ_{298} = 143.7$ kcal/mole. Lyon,[48] using the Langmuir method and a target suspended from a vacuum balance, found 146.2 kcal/mole. Trulson and Goldstein[49] using a mass spectrometer and a hafnium carbide Knudsen cell found 147.7 kcal. All of these heat values were calculated by Schick.

6. Hafnium Diboride

Two studies have been made on this compound. The first, by Krupka[50] followed Leitnaker's[32] work on the zirconium compound; the second by Trulson and Goldstein[49] was done with a mass spectrometer. As in Leitnaker's work on ZrB_2, the possible detrimental effect of tungsten is also common to Krupka's study. The use of tungsten both as a Knudsen cell and as a non-reactive hot collimator channeling the vapor to the water cooled target may lead to error. Although no values have been found for diffusion of hafnium in tungsten, there is no reason to believe it should differ substantially from diffusion of zirconium in tungsten.

Krupka was concerned about the diffusion problem and attempted to determine its effects at 2500°K. By varying the orifice dimensions and plotting orifice area against vaporization rate, he shows that the rate drops to zero at zero orifice area. It might be argued that a more convincing test would have been to use a cell without any orifice at all. It is unfortunate that Krupka chose his highest temperature to make this test. The greatest effect, if present, would occur at the lowest temperature, due to the relation of the heat of vaporization to the heat of diffusion,

approximately 150 kcal and 80 kcal respectively. For example, if 50% of the hafnium flux were due to diffusion and 50% to effusion at 2200°K, 87% would be due to effusion and only 13% to diffusion at 2500°K.

Trulson and Goldstein[49] have used a hafnium carbide cell to measure Hf, B and HfB_2 with a mass spectrometer. Their heat of formation for HfB_2 (61.3 kcal) appears to be low, partly because they had no data for the heat capacity of HfB_2 and assumed $\Delta C_p = 0$.

7. Hafnium Carbide

Schick[41] reviewed the data on this compound and found that no calorimetric values had been obtained for the heat of formation. Equilibrium data on the system Hf-C-0 give a value of -49.3 kcal/mole and vaporization of HfC yields a value of -62.8 kcal/mole. A heat of formation for HfC was measured recently by A. D. Mah[53] using material prepared under this program. Her value is -52.3 kcal/mole.

8. Zirconium Carbide

The status of vapor pressure work on this material was reviewed in Part II of this report.[15] It was concluded that both the General Electric Langmuir[51] studies and those by Pollack[52] involved $ZrC_{.9}$. These studies both give $\Delta H^{\circ}_{f298} = 45.6$ kcal/mole for ZrC. Vidale's resonance line adsorption measurements yield a ΔH°_{f298} of -42.0 kcal/mole and Mah's[53] recent calorimetric value on material prepared under this program is -47.0 ± 0.4. The above heat of formation values were calculated by us using Skinner's data for zirconium and Schick's free energy functions.

C. APPARATUS

The equipment used in this research consists of a high vacuum induction furnace, automatic recording vacuum balance and associated control instruments. These are shown in Figures 30, 31 and 32.

1. Vacuum System and Induction Furnace

The vacuum system parts, constructed of 304 stainless steel, are joined with copper or gold gaskets to permit bakeout at 300 to 500°C for high vacuums. The system is pumped with a 720 liter/sec Consolidated ultra high vacuum oil diffusion pump. Use of Dow 705 fluid with a room temperature vapor pressure of
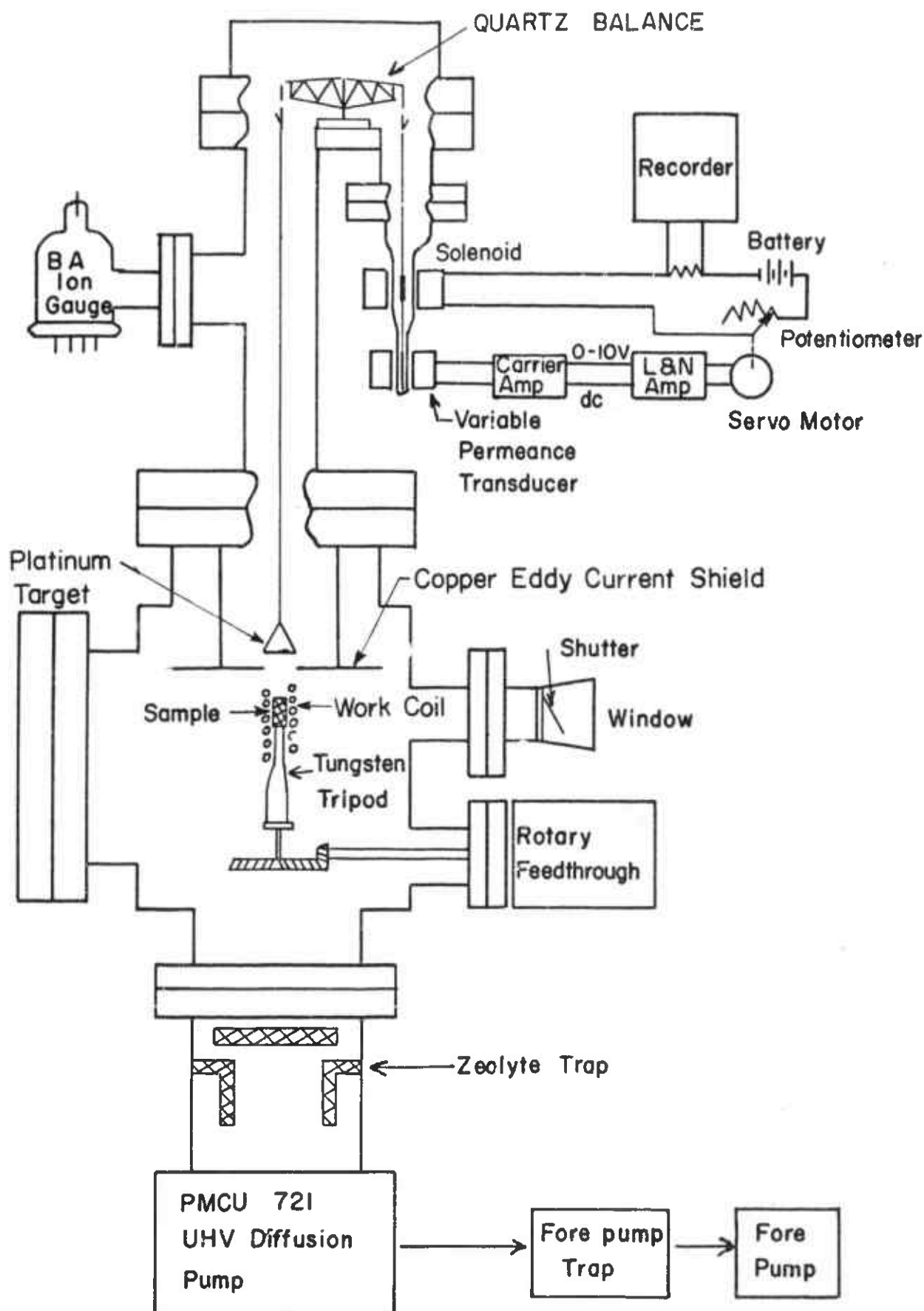
FIGURE 30   VACUUM MICROBALANCE, INDUCTION FURNACE
AND PUMPING SYSTEM

103

TO BALANCE

GLASS TARGET

VAPOR

WATER COOLED COPPER COLLIMATOR

BORON KNUDSEN CELL

BLACKBODY HOLE

WORK COIL

TUNGSTEN TRIPOD

TRIPOD BASE

ROTARY FEEDTHROUGH

BEVELED GEARS
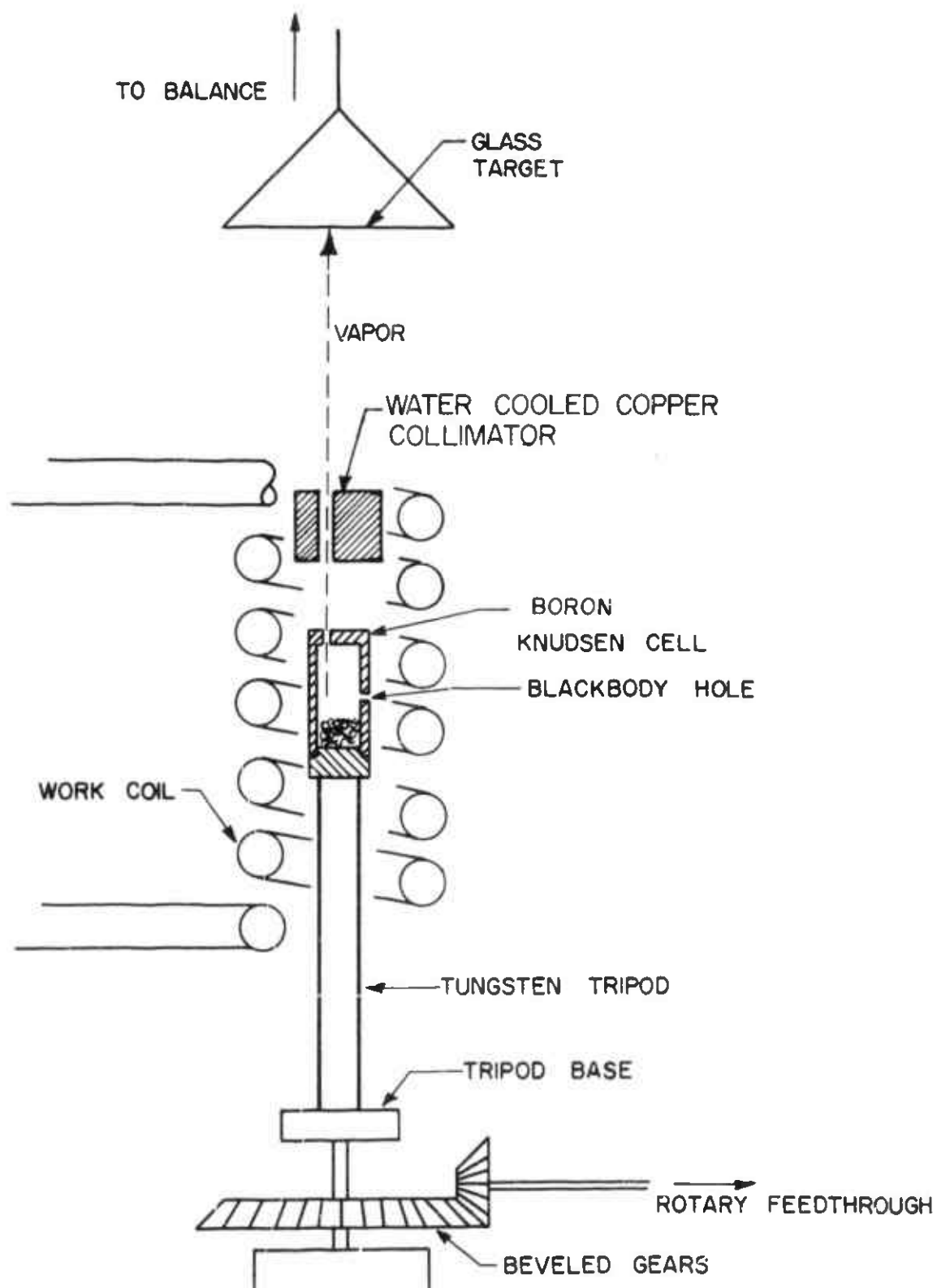
FIGURE 31   KNUDSEN CELL
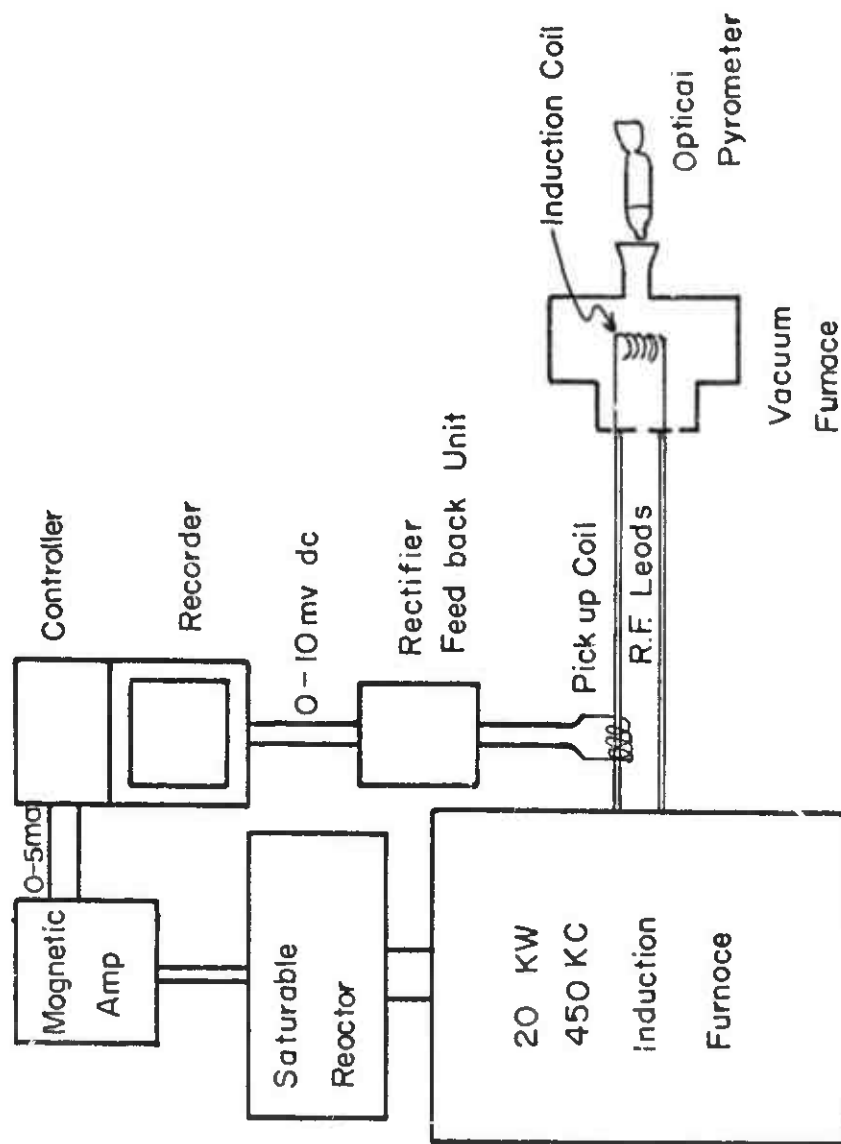
FIGURE 32   AUTOMATIC CONTROL OF INDUCTION FURNACE OUTPUT

3×10^{-10} torr assures the absence of oil vapor inside the "clean" system. A zeolite fore pump trap prevents back diffusion of mechanical pump oil. Vacuums in the system were 2×10^{-9} torr at room temperature and from 10^{-7} to 10^{-9} torr with the sample at temperature.

The vacuum induction furnace is mounted directly above the four-inch oil diffusion pump in order to achieve the maximum available pumping speed. The water cooled shell contains six flanged ports (Varian flanges) which are: 1) a 6" port for sample loading; 2) a 4" port for mounting Varian high frequency feedthroughs, consisting of a 4" copper tube brazed to a pure alumina disk containing two holes in which are sealed the copper work coil leads; 3) a 1-1/2" window protected against condensing vapor by a shutter; 4) a Bayard-Alpart ion gauge; 5) Varian rotary feedthrough; 6) 6" port on top connected to the balance chamber. Two of the ports were omitted from Figure 30 for the sake of clarity.

Figure 31 shows the sample and target in more detail. For Knudsen measurements the Knudsen cell, made of the same material as the sample, is mounted on the points of a tungsten tripod within the copper work coil. The tripod base may be rotated about its vertical axis by the Varian high vacuum rotary feedthrough and stainless beveled gears. The rotary feedthrough consists of a magnetic rod mounted on ball bearings and sealed in a tube which is attached to the vacuum system. The rod is rotated by magnets mounted outside the vacuum system.

Above the sample is a water cooled copper collimator whose 60 mil hole is aligned over the 40 mil orifice in the Knudsen cell. Above the collimator, a target of glass, platinum or aluminum sheet is suspended from the automatic-vacuum-balance. Vapor effusing from the Knudsen orifice and evaporating from the surface immediately adjacent to the orifice will pass through the collimator and strike the target. When the Knudsen cell is rotated 180°, only vapor evaporating from the surface can strike the target.

The target is surrounded by a copper eddy current shield which virtually eliminates interaction of the target with the magnetic field produced by the work coil.

From the evaporation rate of the surface and the geometry of the system, it is possible to determine how much of the vapor striking the target is from the surface adjacent to the orifice. The difference is vapor from the orifice.

Langmuir measurements are made with the collimator removed.

2. Vacuum Balance

The automatic-recording-vacuum-microbalance consists of two parts, a mechanical quartz beam balance sealed inside the vacuum system, and an electronic sensing and control apparatus located outside the system.

The balance is a quartz truss beam supported on a fulcrum of steel bearing pivots resting in sapphire cups. The pivots are welded to tungsten rod which is sealed to the quartz beam. The hangdowns at the end of each arm are quartz fibers fused directly to the beam and to quartz hooks.

The balance is held at its null position automatically by an electromagnet acting on a magnet rod suspended from one arm of the balance. The null position is detected with a variable permeance transducer which surrounds a steel rod hanging below the magnet rod. When the balance is displaced from its null a signal is generated by the transducer controller which drives a potentiometer through a servo mechanism. The potentiometer changes the current flowing in the electromagnet restoring the balance to its null. The current, which is proportional to the weight change, is recorded continuously. The electronic arrangement is essentially the same as that used by Cochran.[54]

The noise level of the balance with the sample at temperatures is ±4 micrograms.

3. Temperature Control

Figure 32 shows a schematic diagram of the temperature control instruments. The work coil is fed by a 20 kw, 450 kc Westinghouse generator equipped with saturable reactor control. In order to maintain a constant temperature, the output of the generator is held constant, using a rectifier feedback unit attached to a pickup coil on the r.f. leads. The rectified and attenuated signal is sent to a recorder controller with output amplified by a magnetic amplifier. The amplified signal drives the saturable reactor which governs the induction furnace output.

The recorded signal indicates the constancy of the generator's output. This, in effect, established a record of the temperature during a run.

Sample temperatures are found by sighting a Leeds & Northrup optical pyrometer on the blackbody hole drilled in the side of the Knudsen cell. Since the temperature of the sample is held constant, frequent temperature measurements are not necessary. Corrections are made for window adsorption by calibrating the pyrometer with the window placed between a tungsten ribbon lamp and the pyrometer.

4. Samples

The Knudsen cells and Langmuir samples are fabricated from zone refined borides and carbides prepared by George Feick of Arthur D. Little. Two pieces are spark gap machined from 1/4" to 3/8" diameter bars as shown in Figure 31 to form a Knudsen cell. The base consists of a cap which fits inside the top somewhat like a cork in a bottle. Three indentations are drilled in the base so it may be mounted on the points of the tungsten tripod. The top is a hollow cylinder fitting over the base, with a blackbody hole in the side for temperature measurement and an effusion hole near the edge in the top. The method used for obtaining effusion rates is described under subsection 1 above. The solid Langmuir cells of about 1/4" diameter and 3/8" high contained 3 small holes in the bottom for mounting and a .040 blackbody hole drilled in the side 2/3 of the diameter in depth.

Although we intended to do much of this study by using Knudsen cells prepared from sample material, various difficulties were encountered which prevented us. Several cells cracked or melted at temperature. In some cases it was not possible to achieve the temperature necessary to obtain a measurable rate of effusion with the collimated beam.

D. PROCEDURE

The Knudsen cell is partially filled with pieces of the zone-refined bar from which the cell was machined, the base is inserted, and the cell is weighed. The target is also weighed on an analytical microbalance. The cell is mounted on a tungsten tripod inside the apparatus with the target suspended above it. The same procedure is followed for Langmuir samples.

After sealing and evacuating the vacuum system to 10^{-8} torr, the sample is brought to temperature and held at temperature while recording the weight change of the target. During initial heating of the sample, the pressure may rise as high as 10^{-6} torr, but after reaching temperature the pressure soon drops to the 10^{-7} and 10^{-8} torr range.

After several experiments are carried out, the vacuum is broken and the target and sample weighed to determine the condensation efficiency of vapor on the target. Chemical analysis of the initial material and the condensate on the target is used to establish solid and vapor composition.

1. Chemical Analysis for Boron

The boride sample targets were analyzed for boron by fusing the aluminum substrate and the condensed film in potassium pyrosulfate within platinum crucibles. The melt was dissolved in water, filtered, and the filtrate analyzed in polyethylene equipment by the carminic acid method.[55] From experiments on known samples the analytical results are believed to be good to between 10 and 20%

2. X-Ray Fluorescence Analysis for Zirconium and Hafnium

All but one of the samples were analyzed by a calibrated X-ray fluorescence technique. A homogeneous area of the X-ray beam was mapped out and known amounts of zirconium and hafnium on aluminum, approxi ate $1/3 \, cm^2$ in area, were placed in the beam and counted. Portions of the target of the same area as the standards were also counted. From the intensity of the strong line for each element, less the background of the substrate material and the total target area, the amount of the metal present in the deposited film was calculated from the calibration curve.

The mean deviation of a six zirconium standards from a least squares curve was $\pm 4\%$. Zirconium was more difficult to determine in our X-ray tube because of the presence of a large, broad tungsten line from the target at the same wave length as the strong zirconium line. The 6 hafnium standards, however, deviated by $\pm 3.8\%$ from a least squares curve.

3. Mass Spectrometric Determination of Amount of Carbon as Carbon Dioxide

Two samples each of zirconium and carbon ($Zr + C$ on Pt and $Zr + C$ on Al) and of hafnium and carbon ($Hf + C$ on Pt and $Hf + C$ on Al) were oxidized and the carbon dioxide produced was analyzed on CEC's 21-610 Mass Spectrometer. A known amount of graphite was also analyzed in the same manner so that the sensitivity of carbon as carbon dioxide was obtained, and the amounts of carbon in the samples were determined.

Each sample was placed on the platinum filament ($1'' \times 1'' \times .0005''$) inside the sample bulb and oxidized in a volume of oxygen by heating the filament with a current of 40 amperes for 15 minutes. The filament temperature was about $1000^\circ C$. The amount of oxygen was determined to be in excess to the theoretical value required for complete oxidation of the sample. During the heating period, a liquid nitrogen trap was used so that the carbon dioxide produced was trapped into the side arm of the sample bulb. After heating was completed and the bulb cooled for 5 minutes, the oxygen was pumped out. A volume of argon was let into the bulb and the side arm was warmed. The carbon dioxide produced was then analyzed in the volume of argon. This use of argon rather than oxygen was necessary to prevent CO_2 production within the mass spectrometer.

Possible impurities in the supply of oxygen and argon, such as carbon dioxide and water, were removed by passing the gases through a liquid nitrogen trap before they entered the sample bulb. A constant amount of carbon dioxide was found to be present in the sample bulb as background. This level of carbon dioxide also served as a check for the completion of oxidation. With samples of Hf + C on Al and Hf + C on Pt, a second oxidation operation was found to be necessary. The uncertainty in the carbon present varied from 2 to 10%.

E. RESULTS AND DISCUSSION

1. ZrB_2

A Knudsen cell was spark gap machined from zone refined bar 81-2. This material, the complete analysis of which is given in Section III of this report, had a B/Zr ratio of 1.99 and contained 50 ppm O and 215 ppm C as principal impurities.

Langmuir measurements were made with the empty cell, depositing the vapor on an aluminum target. A comparison of the weight gain of the target, weight loss of the sample and the calculated vapor striking the target indicated that 89% of the vapor sticks. This value is considered to be within experimental error of unit condensation. These errors include vapor calculated as coming from the sides of the sample (14% of that striking), thermal gradients in the sample, etc.

Chemical analysis for boron and X-ray fluorescence determination for zirconium gave B/Zr ratio in the vapor of 1.94 ± 0.10. The vapor pressure results are given in Table 13 where the effective sample area was calculated, by dividing the sample weight loss into the target weight gain and multiplying by the total sample area. That is, a constant fraction of the vapor from the sample was assumed to condense on the target, and this fraction was found experimentally. The total evaporation rate was divided into fraction of boron and zirconium, using the ratio of 1.94 given above.

TABLE 13

EVAPORATION RATE OF ZIRCONIUM AND BORON FROM $ZrB_{1.99}$

Run No.	$T(^{\circ}K)$	Time (sec)	Total Evap. Rate $(g\text{-}cm^{-2}\text{-}sec^{-1}) \times 10^6$	p_{Zr} (atm) x 10^7	p_B (atm) x 10^7
1	2527	4320	5.91	5.69	3.81
2	2416	14,400	1.36	1.28	0.859
3	2582	2700	9.77	9.52	6.38
4	2610	1380	18.1	17.7	11.9

110

Table 14 gives the heat of vaporization of $ZrB_{1.99}$ to the gaseous elements and the heat of formation of solid ZrB_2 at $298^\circ K$, using Skinner's data for pure zirconium as recently revised in the JANAF Tables; Paule and Margrave's data for boron;[42] Margrave's free energy functions for the ZrB_2 from this report, and the JANAF free energy function for the elements. These values give a heat of formation for $ZrB_{1.99}$ of -75.6 ± 1.6 kcal/mole, in good agreement with the tentative "best" value from calorimetric studies (-76.0 kcal/mole for ZrB_2) discussed in Section II of this report.

The values found here indicate that Langmuir measurements will yield reliable data for this system. The Zr and B measurements as well as those measured here on $ZrB_{1.99}$ were all Langmuir data. The low evaporation coefficients for ZrB_2 reported by Leitnaker et al.[32] and by Lyon[34] are not compatible with the results found here.

The reaction between ZrB_2 and tungsten found by Goldstein and Trulson was confirmed in the present study. There was an obvious reaction between the tungsten fingers on which the sample was supported and ZrB_2. The amount of tungsten involved, however, was too small to significantly alter the composition of the ZrB_2 sample.

TABLE 14

HEAT OF FORMATION OF ZrB_2

$T(^\circ K)$	$-R\ln p_{Zr}$ (cal/deg)	$-R\ln p_B$ (cal/deg)	Δ fef (cal/deg)	ΔH°_{298} (kcal/mole)	$-\Delta H^\circ_{f298}$ (kcal/mole)
2527	28.58	29.37	108.30	492.8	75.1
2416	31.54	32.33	108.10	493.0	75.3
2586	27.55	28.38	107.90	496.6	79.0
2610	26.32	27.11	107.69	490.8	73.1

Avg. 75.6 ± 1.6

2. Hafnium

Five measurements were made on a Langmuir sample cut from arc melted and electron beam melted hafnium sample (see Section III). There were 468 ppm of oxygen in the sample after beam refining, while 270 ppm Zr and 150 ppm Nb were present before the refining process. As in all of the Langmuir measurements, the vapor was collected on a target, and the effective area for the experiment was found by multiplying the sample area by the weight gain of the target and dividing by the sample weight loss. The results are summarized in Tables 15 and 16.

TABLE 15

EVAPORATION OF HAFNIUM

T($^\circ$K)	Time (sec)	Evaporation Rate $(g\text{-}cm^{-2}\text{-}sec^{-1}) \times 10^7$
2200	25,200	3.08
2253	18,780	6.62
2299	10,800	9.59
2350	5700	19.1
2363	19,080	22.0

TABLE 16

HEAT OF VAPORIZATION OF HAFNIUM

T($^\circ$K)	$-R\ln p$ (cal/deg)	Δ fef (cal/deg)	ΔH°_{298} (kcal/mole)
2200	34.84	31.76	146.5
2253	33.29	31.70	146.4
2299	32.54	31.65	147.7
2350	31.15	31.60	147.5
2363	30.87	31.58	147.6
			147.1 $\pm$ 0.6

The free energy functions were taken from Schick.[41] The heat of vaporization is in very good agreement with the previously measured values given in the literature review.

Interestingly enough, the sample reacted with the supporting tungsten tripod so thoroughly that the tripod rods were fused into the cavities drilled in the sample base.

3. Hafnium Borides

The hafnium and boron pressures over boron rich HfB_2 and two-phase $HfB_2 + HfB$ have been measured by the Langmuir method. The procedure used was essentially the same as that used for ZrB_2 with one exception. The aluminum target was placed about 2 inches from the sample instead of 4 inches as had been done for ZrB_2. The total boron on the target was analyzed chemically, and the hafnium was analyzed by X-ray fluorescence.

Since the target was closer to the sample, the total target was not coated due to collimation by the work coil, nor was the coated portion as uniform as had been the case for targets at a greater distance. These factors resulted in uncertainties about the amount of hafnium present, since this calculation involves the area of the target coated by hafnium. The hafnium was therefore calculated by taking the difference between the total target weight gain and the analyzed weight of boron. This procedure was followed because the calculated hafnium exceeded the total weight gain, whereas there was quite good agreement in the study of ZrB_2 between target gain and the sum of Zr plus B ($\pm 10\%$) as determined by analysis. It was also found that the weight of the target was unaffected in a tungsten blank run at these temperatures.

a. HfB_2

The results for $HfB_{2.035}$ (bar 477-2) are given in Tables 17 and 18. The B/Hf ratio in the vapor was 3.80. The free energy functions for the solids and gases were taken from Schick's tables[41] where values for $HfB_{2.035}$ were found by multiplying ΔC_p by 3.035/3.000. The heat of vaporization of Hf was that found experimentally in this work, while that for B was Paule and Margrave's[42] Langmuir value, $\Delta H^\circ_{298} = 136.9$ kcal/g-atom. These data give a ΔH°_{f298} of -77.3 ± 2.3 kcal for HfB_2, which may be compared to Paderno's[56] value of -74.2 ± 3.7. The value found here, as expected is in reasonably good agreement with the values for the corresponding zirconium compound (see section on ZrB_2).

As in the case of zirconium with tungsten, hafnium also diffuses into tungsten. This was confirmed by an X-ray analysis of the tips of the tungsten tripod rods which had been used to support the HfB_2 sample. In addition to finding HfB_2 on the tungsten it was found that the tungsten lattice had contracted a significant amount. It was not possible to determine the exact amount due to hafnium, because of the interference of HfB_2. However, the contraction lies between 0.04 and 0.015%. Since the atomic radius of hafnium lies so close to that of tungsten this contraction indicates an appreciable reaction between HfB_2 and W.

113

It is difficult to make a direct comparison with Krupka's work, since it is believed that the use of tungsten in his study may have introduced an error in his measured pressures. Hafnium diffusion through the tungsten lid would lead to higher apparent pressures, while reaction with the tungsten susceptor walls could have decreased the apparent pressure. However, the hafnium pressure he calculates at $2500^{\circ}K$ is about twice that measured here by the Langmuir method. Since there is doubt about his experimental procedure it is not possible to cite this factor of two for the pressures as a refutation of his claim that the evaporation coefficient is 0.1. Krupka's own Langmuir measurements seem to contradict his claim of a low HfB_2 evaporation coefficient, since they agree fairly well with his Knudsen measurements. (The effects of tungsten in the Knudsen measurements are difficult to assess, however.)

The good agreement between the heat of formation of HfB_2 found here and the previously measured value indicates that the evaporation coefficient must not be very low. Only the heat of vaporization used for boron is open to question since it may not have a unit evaporation coefficient. If the lowest reported heat of vaporization of boron (excluding a dubious value of 103 kcal), 128 kcal/g-atom is used, it would mean that the evaporation coefficient could be as low as 0.4 for HfB_2. It seems more likely that both boron and HfB_2 have unit evaporation coefficients.

TABLE 17

EVAPORATION OF HAFNIUM AND BORON FROM HfB_2

Series I	$T(^{\circ}K)$	Time (sec)	Total Evap. Rate $(g\text{-}cm^{-2}\text{-}sec^{-1}) \times 10^6$	Evap. of B $(g\text{-}cm^{-2}\text{-}sec^{-1}) \times 10^7$	Evap. of Hf $(g\text{-}cm^{-2}\text{-}sec^{-1}) \times 10^6$
1	2621	780	12.7	24.0	10.3
2	2586	1800	8.24	15.6	6.68
3	2569	1800	5.10	9.64	4.14
Series II					
4	2525	2100	2.51	4.74	2.05
5	2596	1200	6.93	12.8	5.65
6	2560	2160	4.37	8.10	3.56
7	2530	1380	2.46	4.56	2.00
8	2647	1140	12.3	22.8	10.0

TABLE 18

HEAT OF FORMATION OF HfB_2

$T(^\circ K)$	$-R\ln p_B$ (cal/deg)	$-R\ln p_{Hf}$ (cal/deg)	$-\Delta fef$ (cal/deg)	ΔH°_{298} (kcal/mole)	$-\Delta H^\circ_{f298}$ (kcal/mole)
2621	27.81	27.69	106.11	499.0	72.7
2586	28.66	28.53	106.14	499.1	72.8
2569	29.63	29.52	106.18	503.6	77.3
2525	31.10	30.83	106.21	505.6	79.3
2596	29.06	29.16	106.13	504.5	78.2
2560	29.98	29.82	106.19	504.3	78.0
2530	31.15	30.98	106.21	508.2	81.9
2647	27.89	27.74	106.09	504.5	78.2

Avg. 77.3 ± 2.3

b. HfB and HfB_2

The Langmuir measurements (on sample bar 318-3) over the two-phase region are summarized in Tables 19 and 20. A boron-hafnium ratio of 2.8 was found over a solid with Hf:B equal to 1:1.75. This suggests that the congruent vaporization point at 2400 to $2600^\circ K$ is in the two-phase region at a more metal rich composition than the sample. Kaufman[59] has pointed out that the congruent composition should decrease with temperature. These data yield a heat of formation for HfB of -47.3 ± 2.9 kcal/mole in good agreement with Kirkorians[57] estimate of -48 kcal/mole. No other data are available for this compound. The free energy functions for Hf and B were taken from Schick. An estimated free energy function for HfB was calculated by using 2/3 of Schick's ΔC_p values for HfB_2,[41] together with the free energy functions. Heats of vaporization of Hf and formation of HfB_2 were taken from the present study.

TABLE 19

EVAPORATION RATES OF HAFNIUM AND BORON OVER HfB_2 + HfB

Series I	$T(^\circ K)$	Time (sec)	Total Evap. Rate $(g\text{-}cm^{-2}\text{-}sec^{-1})x10^6$	Evap. of B $(g\text{-}cm^{-2}\text{-}sec^{-1})x10^7$	Evap. of Hf $(g\text{-}cm^{-2}\text{-}sec^{-1})x10^6$
1	2497	1440	4.92	7.31	4.19
2	2454	3540	2.25	3.35	1.92
3	2404	3180	1.28	1.92	1.09
Series II					
4	2575	1380	8.44	12.1	8.89
5	2543	960	4.69	6.75	4.96
6	2519	2040	4.16	5.99	4.40

TABLE 20

HEAT OF FORMATION OF HfB

T (°K)	−Rln p_B (cal/deg)	(−Rln p_{Hf})* (cal/deg)	−fef (cal/deg)	ΔH°_{298} + (kcal/mole)	−ΔH°_{f298} (kcal/mole)
2497	30.20	29.52	36.19	165.8	48.4
2454	31.77	31.10	36.20	166.8	47.4
2404	32.91	32.24	36.22	163.2	51.0
2575	29.26	28.87	36.17	165.5	45.7
2543	30.35	29.17	36.18	169.2	45.0
2519	30.59	29.42	36.18	165.2	46.0

Avg. 47.3 ± 2.9

+ For reaction: $HfB_2 \rightarrow HfB_{(s)} + B(g)$

* The pressure of Hf is not used to calculate the heat of formation of HfB.

4. Hafnium Carbide (Tentative Results)

$HfC_{.97}$

A Langmuir cell was cut with an ultrasonic tool from an arc melted button of HfC. The analysis of this material gave an initial composition of $HfC_{.97}$. The vapor composition was nearly congruent. Unfortunately, the finished piece was of an irregular shape and did not heat uniformly in the induction coil. Two measurements were made on this sample with the results reported below. There is an uncertainty in the temperature of ±60° because of the thermal gradients.

TABLE 21

EVAPORATION OF Hf AND C FROM $HfC_{.97}$

T (°K)	Time (sec)	Evaporation Rate (g-cm^{-2}-sec^{-1}) Total x 10^6	Hf x 10^6	C x 10^7
2890	2100	8.05	6.79	12.5
2800	5940	2.16	1.82	3.37

116

TABLE 18

HEAT OF FORMATION OF HfB_2

$T(^\circ K)$	$-R\ln p_B$ (cal/deg)	$-R\ln p_{Hf}$ (cal/deg)	$-\Delta$ fef (cal/deg)	ΔH°_{298} (kcal/mole)	$-\Delta H^\circ_{f298}$ (kcal/mole)
2621	27.81	27.69	106.11	499.0	72.7
2586	28.66	28.53	106.14	499.1	72.8
2569	29.63	29.52	106.18	503.6	77.3
2525	31.10	30.83	106.21	505.6	79.3
2596	29.06	29.16	106.13	504.5	78.2
2560	29.98	29.82	106.19	504.3	78.0
2530	31.15	30.98	106.21	508.2	81.9
2647	27.89	27.74	106.09	504.5	78.2

Avg. 77.3 ± 2.3

b. HfB and HfB_2

The Langmuir measurements (on sample bar 318-3) over the two-phase region are summarized in Tables 19 and 20. A boron-hafnium ratio of 2.8 was found over a solid with Hf:B equal to 1:1.75. This suggests that the congruent vaporization point at 2400 to 2600°K is in the two-phase region at a more metal rich composition than the sample. Kaufman[59] has pointed out that the congruent composition should decrease with temperature. These data yield a heat of formation for HfB of -47.3 ± 2.9 kcal/mole in good agreement with Kirkorians[57] estimate of -48 kcal/mole. No other data are available for this compound. The free energy functions for Hf and B were taken from Schick. An estimated free energy function for HfB was calculated by using 2/3 of Schick's ΔC_p values for HfB_2,[41] together with the free energy functions. Heats of vaporization of Hf and formation of HfB_2 were taken from the present study.

TABLE 19

EVAPORATION RATES OF HAFNIUM AND BORON OVER HfB_2 + HfB

Series I	$T(^\circ K)$	Time (sec)	Total Evap. Rate (g-cm^{-2}-sec^{-1})x10^6	Evap. of B (g-cm^{-2}-sec^{-1})x10^7	Evap. of Hf (g-cm^{-2}-sec^{-1})x10^6
1	2497	1440	4.92	7.31	4.19
2	2454	3540	2.25	3.35	1.92
3	2404	3180	1.28	1.92	1.09
Series II					
4	2575	1380	8.44	12.1	8.89
5	2543	960	4.69	6.75	4.96
6	2519	2040	4.16	5.99	4.40

TABLE 20

HEAT OF FORMATION OF HfB

T($^{\circ}$K)	$-R\ln p_B$ (cal/deg)	$(-R\ln p_{Hf})$* (cal/deg)	$-\Delta$fef (cal/deg)	ΔH°_{298} + (kcal/mole)	$-\Delta H^{\circ}_{f298}$ (kcal/mole)
2497	30.20	29.52	36.19	165.8	48.4
2454	31.77	31.10	36.20	166.8	47.4
2404	32.91	32.24	36.22	163.2	51.0
2575	29.26	28.87	36.17	168.5	45.7
2543	30.35	29.17	36.18	169.2	45.0
2519	30.59	29.42	36.18	168.2	46.0

Avg. 47.3 ± 2.9

-- For reaction: $HfB_2 \rightarrow HfB_{(s)} + B(g)$

* The pressure of Hf is not used to calculate the heat of formation of HfB.

4. Hafnium Carbide (Tentative Results)

HfC$_{.97}$

A Langmuir cell was cut with an ultrasonic tool from an arc melted button of HfC. The analysis of this material gave an initial composition of HfC$_{.97}$. The vapor composition was nearly congruent. Unfortunately, the finished piece was of an irregular shape and did not heat uniformly in the induction coil. Two measurements were made on this sample with the results reported below. There is an uncertainty in the temperature of $\pm 60^{\circ}$ because of the thermal gradients.

TABLE 21

EVAPORATION OF Hf AND C FROM HfC$_{.97}$

T($^{\circ}$K)	Time (sec)	Evaporation Rate (g-cm^{-2}-sec^{-1})		
		Total x 10^6	Hf x 10^6	C x 10^7
2890	2100	8.05	6.79	12.5
2800	5940	2.16	1.82	3.37

TABLE 22

HEAT OF FORMATION OF HfC

T($^\circ$K)	p_{Hf} (atm)x10^7	p_C (atm)x10^7	$-R\ln p_{Hf}$ (cal/deg)	$-R\ln p_C$ (cal/deg)	$-\Delta fef$ (cal/deg)	ΔH°_{298} (kcal/mole)	$-\Delta H^\circ_{f298}$ (kcal/mole)
2890	6.16	4.37	28.41	29.10	70.46	367.3	55.2
2800	1.63	1.16	31.07	31.74	70.50	370.6	58.6

Avg. 56.9 ± 1.7

The heat of formation of HfC is in fair agreement with Mah's calorimetric value of -52.4 kcal/mole. Due to possible temperature errors there is an uncertainty of ± 7 kcal in the heat of formation.

Free energy functions were taken from Schick for hafnium and HfC and from Stull and Sinke[58] for carbon.

5. Zirconium Carbide Langmuir Measurements

The rate of evaporation over ZrC$_{.97}$ (bar 262-3) given in the semi-annual report were recalculated. From X-ray fluorescence analysis, a C/Zr ratio of 6.21 was found which seems to be high compared to Kaufman's prediction that the congruent composition is near the stoichiometric compound.[59] The results are in fair agreement with Pollock's Langmuir measurements, being about 3 kcal higher. The zirconium-carbon ratio, however, is much higher than his, in part, perhaps, because his initial sample is richer in zirconium.

The results are given in Tables 23 and 24.

TABLE 23

EVAPORATION OF ZrC$_{.97}$

T($^\circ$K)	Time (sec)	Total Evap. Rate (g-cm^{-2}-sec^{-1})x10^6	Evap. of Zr (g-cm^{-2}-sec^{-1})x10^7	Evap. of C (g-cm^{-2}-sec^{-1})x10^7	p_{Zr} (atm)x10^8	p_C (atm)x10^8
2717	3150	1.35	7.44	6.08	9.13	20.6
2783	1182	3.16	17.37	14.2	21.6	48.8
2859	1110	7.68	42.2	34.6	53.3	12.0
2736	2025	1.76	9.67	7.92	11.9	27.0
2824	990	4.44	24.5	20.0	30.9	69.3
2750	1800	3.21	17.6	14.4	21.8	49.3

117

TABLE 24

HEAT OF FORMATION OF ZrC$_{.98}$

$T(^\circ K)$	$-R \ln p_{Zr}$ (cal/deg)	$-R \ln p_C$ (cal/deg)	$-\Delta$fef (cal/deg)	ΔH°_{298} (kcal/mole)	$-\Delta H^\circ_{f298}$ (kcal/mole)
2717	32.21	30.60	71.82	365.8	49.0
2783	30.50	28.88	71.76	365.0	48.2
2859	28.71	27.13	71.69	364.6	47.8
2736	31.69	30.06	71.80	365.4	48.6
2824	29.79	28.18	71.68	366.3	49.5
2750	30.49	28.86	71.78	360.6	43.8
				Avg. =	47.8 ± 1.2

The results given in the latter table are based on Margrave's free energy functions for the solid from this report and Stull and Sinke's[58] values for the gases. The heat of reaction was computed for stoichiometric ZrC and the heat of formation for the reported limit of ZrC$_{.98}$.[60] The latter value differs by about 3 kcal from the combustion value of Mah and the vapor pressure measurements of Pollock[52] and of Lyon[34] using Skinner's zirconium pressures.

6. ZrC$_{.67}$

Two sets of measurements were made by the Langmuir method on this sample. It had an initial composition of ZrC$_{.67}$ well within the single-phase region.

In the first series an aluminum target was used, and the vapor showed a C/Zr ratio of 0.12. The second series, using a platinum target, gave a C/Zr ratio of 0.28. These numbers indicate that the congruent composition was being approached during the course of the experiments. The initial set of measurements gave higher pressures than the second set. This could be due to the relatively high impurity content of the sample, which contained 0.2 percent O, 0.2 percent N and 0.1 percent Ti.

The results are given in Tables 25 and 26.

118

TABLE 25

EVAPORATION OF Zr AND C FROM ZrC$_{.67}$

Series 1	T($^\circ$K)	Time (sec)	Total x 10^6	Zr x 10^6	C x 10^7
			Evaporation Rate (g-cm^{-2}-sec^{-1})		
1	2668	600	22.3	21.9	3.55
2	2652	900	11.6	11.4	1.84
3	2647	1238	9.61	9.46	1.53
Series 11					
4	2660	3900	4.17	4.02	1.48
5	2743	4500	6.37	6.14	2.27
6	2796	1200	18.1	17.4	6.44

TABLE 26

HEAT OF FORMATION OF ZrC$_{.67}$

T($^\circ$K)	P$_C$ (atm)x10^8	P$_{Zr}$ (atm)x10^7	-Rln p$_C$ (cal/deg)	-Rln p$_{Zr}$ (cal/deg)	-Δ fef (cal/deg)	ΔH°_{298} (kcal/mole)	-ΔH°_{f298} (kcal/mole)
2668	11.9	2.67	31.69	25.51	57.34	276.0	19.5
2652	6.16	1.39	32.99	26.80	57.36	280.0	23.5
2647	5.12	1.15	33.36	27.18	57.36	281.2	24.7
2660	4.97	4.89	33.41	28.88	57.35	287.1	30.6
2743	7.74	7.59	32.54	28.01	57.27	291.9	35.4
2796	22.2	21.7	30.45	25.92	57.20	287.7	31.2

Avg. of Series 11 + 32.4 ± 2.0

Series 11 measurements gave a heat of formation for ZrC$_{.67}$ in good agreement with Mah's calorimetric value of 31.2 mentioned in Section II of this report. The free energy functions for Zr and those estimated for ZrC$_{.67}$ were found using Schick's tables.[41] Carbon values are from Stull and Sinke.[58]

7. Hafnium Carbide in a Graphite Knudsen Cell

This experiment was carried out using a water cooled collimator to select the vapor effusing from the graphite orifice as described under Section 1 of the apparatus section. The collimator was so efficient and placed far enough away from the sample (1/2") that a relatively small amount of vapor reached the target. Furthermore, the half inch separation of collimator and sample resulted in the area

"seen" by the target as only 17% orifice area with the remaining 83% cell surface. Winslow and Thorn[45] have shown that the total evaporation coefficient from graphite is 0.14. Data from Hoch et al.[43] when compared to Stull and Sinke's pressures over carbon result in a total evaporation coefficient of 0.12. Since Winslow's study was specifically designed to measure evaporation coefficients, his value of 0.14 will be used. Under these conditions the relative effective area of the orifice is increased to 60% if it is assumed that the orifice has an evaporation coefficient near unity. Because of the necessity to operate at such a high temperature and high carbon pressure to get a reasonable amount of vapor deposited on the target, some problems were encountered. On a few occasions there was arcing within the apparatus, associated with the high carbon pressure. Thus it was not possible to measure the evaporation from the surface separately in order to compare it to the combined evaporation and effusion.

The neutron activation analysis of the target indicated that of 275 micrograms deposited on the target $6.0 \pm 0.5 \times 10^{-7}$ g were Hf. The hafnium pressure, assuming that hafnium comes only from the orifice, is almost six times higher than that required to give an activity consistent with the calorimetric heat of formation of HfC. If, on the other hand, one assumes that hafnium evaporates from the total surface seen by the target, then an activity for hafnium is found which yields a heat of formation of -44.7 kcal/mole.

SUMMARY

The partial pressures over the carbides and borides of zirconium and hafnium have been measured by the Langmuir method. In all but one case the calculated heat of formation of the compound was within experimental error (± 3 kcal) of the calorimetric value. The exception was HfC where the sample failed to heat uniformly. The present Langmuir boride measurements agree better with the calorimetric heats than do the Knudsen experiments in the literature. Contrary to the measurements in tungsten Knudsen cells, where evaporation coefficients between 0.025 and 0.1 for ZrB_2 and 0.1 for HfB_2 were reported, the present study indicates that the evaporation coefficient for each of these compounds is close to unity.

120

APPENDIX I

SPECTROSCOPY OF HIGH TEMPERATURE SPECIES BY MATRIX ISOLATION*

A. PROJECT SUMMARY BY O. SCHNEPP

The infrared spectra of lithium fluoride, chloride and bromide have been investigated by the matrix isolation technique. A complete scientific report on this work is included in a paper which has been prepared for publication and is included as section B of this report.

The studies conducted and described in section B allow definite conclusions to be drawn concerning the validity and applicability of the matrix isolation technique to the study of the infrared spectra of high temperature molecules in general. These conclusions will be summarized in the following paragraphs.

The systems investigated have been the subject of exhaustive mass spectrometric studies such that the composition of the vapor is well known. The principal components are monomers and dimers. It has been demonstrated that the same molecular species were trapped in the inert solid matrices and the infrared spectra of these molecular species could be studied. It can also be concluded that liquid hydrogen temperature is sufficient for the studies and the spectra obtained were the same at this temperature as they were at liquid helium temperature. It is therefore possible to state that the molecular species present in the vapor in equilibrium with the salt can be trapped in inert solids at liquid hydrogen temperatures.

It remains to be investigated if changes in the relative concentration of different molecular species such as monomers and dimers in the vapor are reflected by parallel changes in the concentrations in the trapped solid phase. Such experiments using double ovens [61] which will permit the variation of the ratio of monomer to dimer in the effusion beam over a wide range are at present under way in this laboratory but have not, as yet, progressed to a stage which would allow conclusions to be drawn.

The important problem which exists in connection with the matrix isolation technique is that of the solvent shifts. It is, today, not possible to calculate this

---

* Report on subcontracted study at Israel Institute of Technology, Haifa, Israel under the direction of Prof. O. Schnepp.

shift theoretically and our efforts to devise a physically sound extrapolation pro-
cedure have not been successful. However, it has been found that the frequency
shift between the argon and nitrogen matrices is a good indication of the size of
the argon matrix shift relative to the free molecular vibrational frequency. It
is, however, likely that for many systems solvent shifts will not be as large as
those encountered in the present work and therefore this would not present as great
a difficulty.

Future work in this area should be concerned with lower frequencies
since many important vibrational modes can be expected to be located in the farther
infrared region of the spectrum. It will also be of great importance to adapt the
technique to Raman spectroscopy so as to make possible the observation of infrared
inactive frequencies and therefore complete vibrational assignments. Such complete
observations will allow the development of the theory of the structure of and binding
in molecules of highly ionic character.

It was intended that the vibrational spectra of ZrO and HfO would be in-
vestigated by the matrix isolation technique during this report period. However
difficulties were experienced with the oven. The electron beam bombardment fur-
nace for this study was modified and is now capable of reaching temperatures above
2000 C. Work will continue on this aspect of the project during the next six months.

B. THE INFRARED SPECTRA OF THE LITHIUM HALIDE MONOMERS AND DIMERS
   IN INERT MATRICES AT LOW TEMPERATURE, BY S. SCHLICK AND
   O. SCHNEPP

1. Introduction

The molecular species produced on vaporization of alkali halides have been
the subject of a large number of investigations over the last ten years' period. The
occurrence of dimer and trimer molecules in addition to the monomers has been
established and it was found that the dimer to monomer ratio is as high as 3:1 for
some of the lithium halides. [62] Molecular beam measurements [63] and micro-
wave investigations [64] have provided accurate values for the structural constants
of many monomer molecules. The infrared spectra of the monomer alkali halides
in the gas phase have been measured [65] and in spite of the considerable line widths
encountered it has been possible to determine the vibrational constants with good
accuracy. Infrared absorptions have also been assigned to the dimer molecules of
the lithium halides, [66] however in this case the vibrational frequencies could not
be accurately determined in view of the great line widths caused by the high temper-
atures which have to be used to ensure adequate concentration in the gas phase. The
structures of the dimer molecules have been established by electron diffraction

measurements [67] and the vibrational frequencies of the lithium halide dimers have been treated theoretically on the basis of an ionic model. [68]

The matrix isolation technique has been applied to the spectroscopic investigation of lithium fluoride by Linevsky. [69] This author found that the monomer frequency undergoes very considerable shifts in rare gas and nitrogen matrices and he used an isotopic substitution technique in order to characterize monomer and dimer absorptions. [70] He found that two bands had to be assigned to the monomer on this basis and concluded that different matrix sites in argon give rise to the two bands with a separation of 120 cm^{-1}. He also found that one of the dimer frequencies he observed agreed very well with the gas phase measurements but the second band deviated considerably.

In view of the potential value of the matrix isolation technique for the spectroscopic investigation of high temperature molecules it was considered of importance to extend such studies in an effort to determine the extent of applicability of this technique. At the same time, it seemed of importance to further investigate the lithium halide dimer vibrational frequencies. In addition, further information on solvent shifts in simple systems is essential at the present stage of insight into this important problem. [71]

While the present investigation was in progress, the infrared spectra of natural lithium fluoride and chloride and of sodium fluoride in rare gas matrices were published. [72]

In the present work, the infrared spectra of natural lithium fluoride and of natural ($93\%Li^7$) and of Li^6 - lithium chloride and bromide vaporization species were studied in argon, krypton, xenon and nitrogen matrices. The solvent shifts of the monomer bands are discussed in terms of existing theories and the applicabilities of the theoretical treatments due to Buckingham [71] and Kirkwood-Bauer-Magat have been tested. The solvent shifts are also discussed in terms of specific solute-solvent interactions. Two dimer frequencies of lithium chloride and bromide have been definitely characterized and assigned.

2. Experimental Details

The sample to be investigated was prepared by simultaneous deposition of a molecular beam emerging from an effusion cell containing the salt and a stream of inert matrix gas on a cold cesium bromide window. The window was mounted in a copper holder screwed to the bottom end of a stainless steel double cryostat. Good thermal contact between the window and the holder was ensured by means of indium wire. The window was surrounded by a radiation shield attached to the same end of

the dewar bearing the window holder and a second radiation shield kept at liquid nitrogen temperature. These shields were fitted with holes to transmit the light beam and to admit the materials to be deposited. Liquid helium or liquid hydrogen served as coolants. The window temperature was measured by means of a copper-constantan thermocouple soldered into a hole drilled into the window. Wood's metal was used as soldering material. The temperatures so measured were 10°K or 21°K depending on the coolant used.

The effusion cell was made of tantalum sheet and was 16 mm long and 6 mm in diameter, with 0.125 mm wall thickness. The effusion aperture was 0.8 mm in diameter. The cell was heated by radiation from a surrounding tantalum element heated by currents in the neighborhood of 100 amperes. The temperature inside the effusion cell was measured by means of a chromel-alumel thermocouple. The temperatures used in the course of this work corresponded to a vapor pressure of 10 microns of the material to be effused. Thus closely ideal effusion conditions prevailed. The materials investigated were lithium fluoride, chloride and bromide. The natural lithium salts contain the natural abundance of $Li^7(92.6\%)$. The Li^6 - chloride was purchased from Oak Ridge National Laboratories while Li^6 - bromide was prepared by titration of the hydroxide with HBr. The concentration of Li^6 in these salts was 95.6%. The inert gas matrices used were argon, krypton, xenon and nitrogen.

It was attempted to estimate the concentration of the lithium fluoride in the inert gas matrix. The amount of matrix gas deposited could be measured by observing the appearance of interference colors on the deposition window. The deposition rate so determined was 3000Å of layer thickness per minute. A deposition rate three times less was used occasionally. The rate of flow of the lithium halides was calculated on the assumption that effusive conditions prevailed. This calculation showed that the ratio matrix to salt on the deposition window was 1000 when the effusion cell was heated to a temperature which corresponded to a vapor pressure of 1μ. No spectra were observed under these conditions. With the effusion cell at temperatures corresponding to a salt vapor pressure of 10μ as used in the experiments reported here the described calculation yields the result that the matrix to salt concentration was 100. It is, however, probable that the salt vapor beam was strongly scattered by the matrix gas with the result that the final concentration in the deposited solid film may well have been lower than that calculated by as much as a factor of 10. Evidence for such scattering under similar experimental conditions has been previously reported in the literature. [73]

The infrared spectra were recorded with a Perkin-Elmer, Model 21 double beam spectrophotometer with sodium chloride and cesium bromide prisms. Measurements could be successfully made to 37μ, but the instrument had to be purged with dried air for work at wavelengths longer than 33μ.

3. Results

a. Lithium Fluoride

Most of the results obtained here for lithium fluoride have already been described by Linevsky[69],[70] and by Snelson and Pitzer.[72] The bands observed are listed in Table 27. The bands at $842cm^{-1}$ and $837cm^{-1}$ in argon, have been assigned to the monomer, while the bands at $621-cm^{-1}$ and $545cm^{-1}$ in solid argon have been assigned to the dimer. The band at $720cm^{-1}$ in solid argon has been assigned to the monomer by Linevsky. This assignment seems problematic but no new information which might further clarify it has been obtained here. The doublet at $842cm^{-1}$ - $837cm^{-1}$ in solid argon was examined at liquid helium and liquid hydrogen temperatures and identical results were obtained. This spectral region was also examined with a fore-prism-grating instrument with spectral slit width of less than $1cm^{-1}$, but no further structure was observed. It can therefore be concluded that Linevsky's interpretation of this doublet as due to two distinct trapping sites is supported by these observations. Further multiple trapping site effects were observed for the low frequency dimer band in solid argon and for the high frequency dimer band in solid nitrogen. In the latter case the relative intensities of the two component bands were reversed at liquid helium temperature as compared to liquid hydrogen temperature. The spectrum of the natural lithium fluoride only was recorded.

b. Lithium Chloride

The experiments with lithium chloride were mostly carried out at liquid hydrogen temperature. One experiment at liquid helium temperature with argon as matrix was carried out for comparison and results identical to those obtained at the higher temperature were obtained. It was found necessary to carefully degas the effusion cell containing the salt and to keep it at 150°C for 24 hours in order to remove all traces of water. Spectra were recorded for the natural salt and for the Li^6-salt in all four matrices. The spectra for an equimolar mixture of the two isotopes were obtained in solid argon and solid krypton. The results are summarized in Tables 28 and 29 and in Figures 33 and 34. The results obtained with the natural salt agree well with those recently published.[72]

Comparison of the spectra obtained for the isotopic mixture with those of the nearly pure isotopic samples shows that no new bands appeared in the mixture in the highest energy absorption region, while new bands were observed in the other two absorption regions. In solid argon a band characteristic of the mixture only was observed at $499cm^{-1}$ while the intensity of the peak at $509cm^{-1}$ in the same
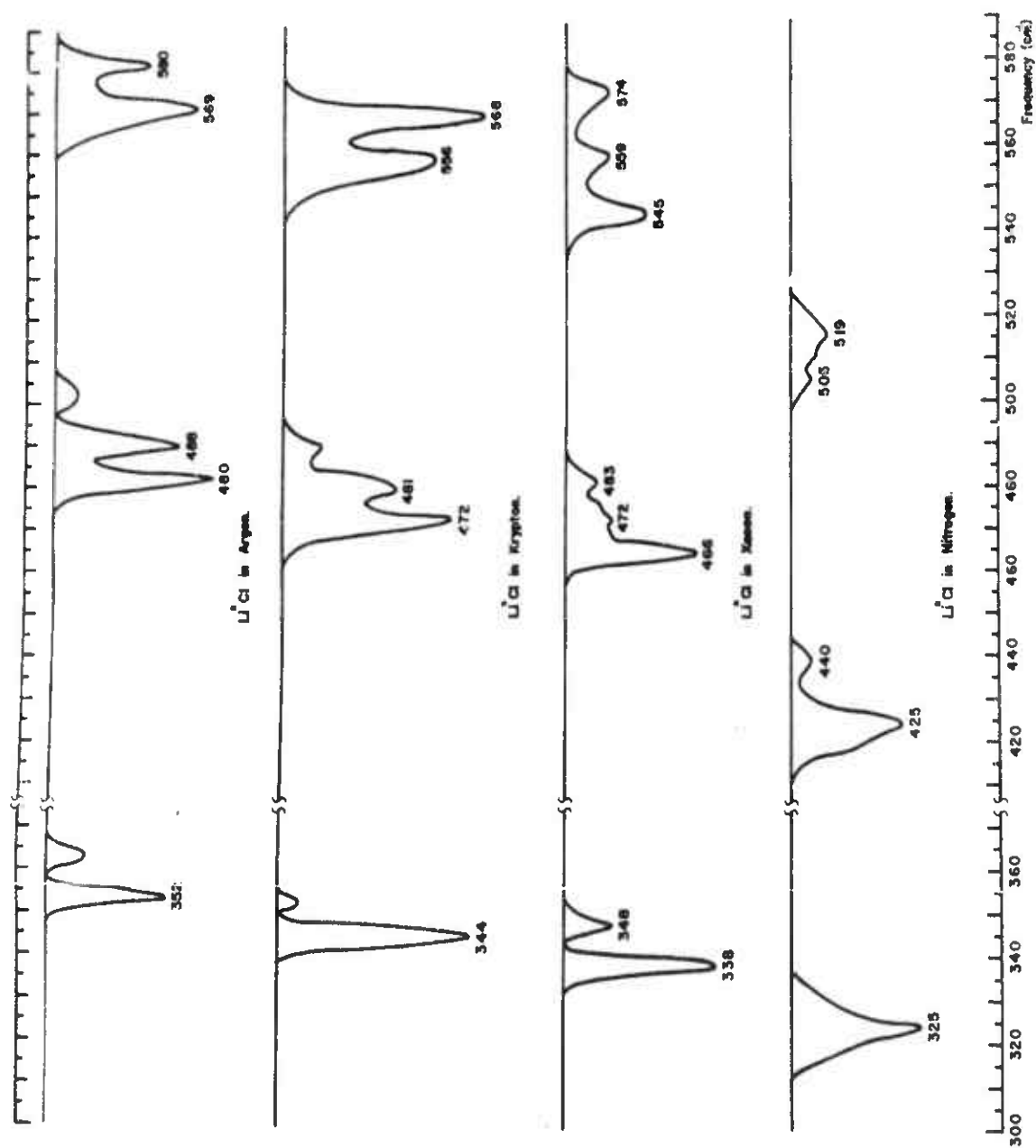
FIGURE 33   THE SPECTRA OF NATURAL LITHIUM CHLORIDE VAPORIZATION
PRODUCTS IN DIFFERENT MATRICES AT LIQUID HYDROGEN
TEMPERATURE

126

FIGURE 34   THE SPECTRA OF THE VAPORIZATION PRODUCTS OF NATURAL LITHIUM CHLORIDE, OF Li^6 - CHLORIDE AND OF AN EQUIMOLAR MIXTURE OF THE TWO IN ARGON MATRIX AT LIQUID HYDROGEN TEMPERATURE

127

experiment requires the conclusion that it represents a superposition of the Li^6-chloride band and a new mixture band. Another new band is observed at $361cm^{-1}$. The corresponding bands for the mixture in solid krypton are at $490cm^{-1}$ and $501cm^{-1}$ and at $354cm^{-1}$.

Two distinct trapping sites were observed in the highest energy absorption region. The medium energy band also consists of a doublet in all matrices while a very weak third peak at the higher energy edge of the absorption region was found to coincide with the intense band observed for the isotopic mixture. It is therefore assumed to arise from the $7\%Li^6$ isotope present in natural lithium. However, this interpretation does not fit the weak peaks at $524cm^{-1}$ and $508cm^{-1}$ observed for Li^6-chloride in solid krypton and solid xenon respectively. In these cases a third trapping site must be assumed. The same applies to the peak at $607cm^{-1}$ for the Li^6-chloride in solid xenon. The lowest energy absorption region consists of a single band in all matrices, except xenon.

c. Lithium Bromide

The measurements were all made at liquid hydrogen temperature. Careful degassing of the effusion cell was found to be essentially similar to the procedure used for lithium chloride. Spectra were recorded for the natural salt in all four matrices and for the Li^6-salt in argon and krypton. The spectra for equimolar mixture of the lithium isotopes were recorded in solid krypton only. The results are summarized in Tables 30 and 31 and in Figures 35 and 36.

Again no new bands were observed for the mixture in the highest energy absorption region while bands characteristic of the mixture were observed in the other regions. These are at $440cm^{-1}$ and $452cm^{-1}$ and at $305cm^{-1}$ in solid krypton.

Similar to the results for lithium chloride, the highest energy and the medium energy absorption regions consist of doublets which are best interpreted as arising from two trapping sites. Here again a third peak is observed in the medium energy absorption region for the natural salt in solid argon, krypton and xenon, and this peak in solid krypton is found to coincide with the intense peak characteristic of the isotopic mixture in this matrix. Also no third peak was observed for the Li^6- salt. It may therefore be concluded that the weak third peak is due to the presence of the Li^6 isotope in the natural salt. The lowest energy absorption consists of a single band in all matrices.

4. Discussion of Results

Comparison of the spectra obtained for a mixture of the isotopic species of lithium with those of pure isotopes makes possible the assignment of absorption bands to monomer or dimer molecular species. Linevsky[70] used this method to

Li⁷Br in Argon.

Li⁷Br in Krypton.

Li⁷Br in Xenon.

Li Br in Nitrogen.
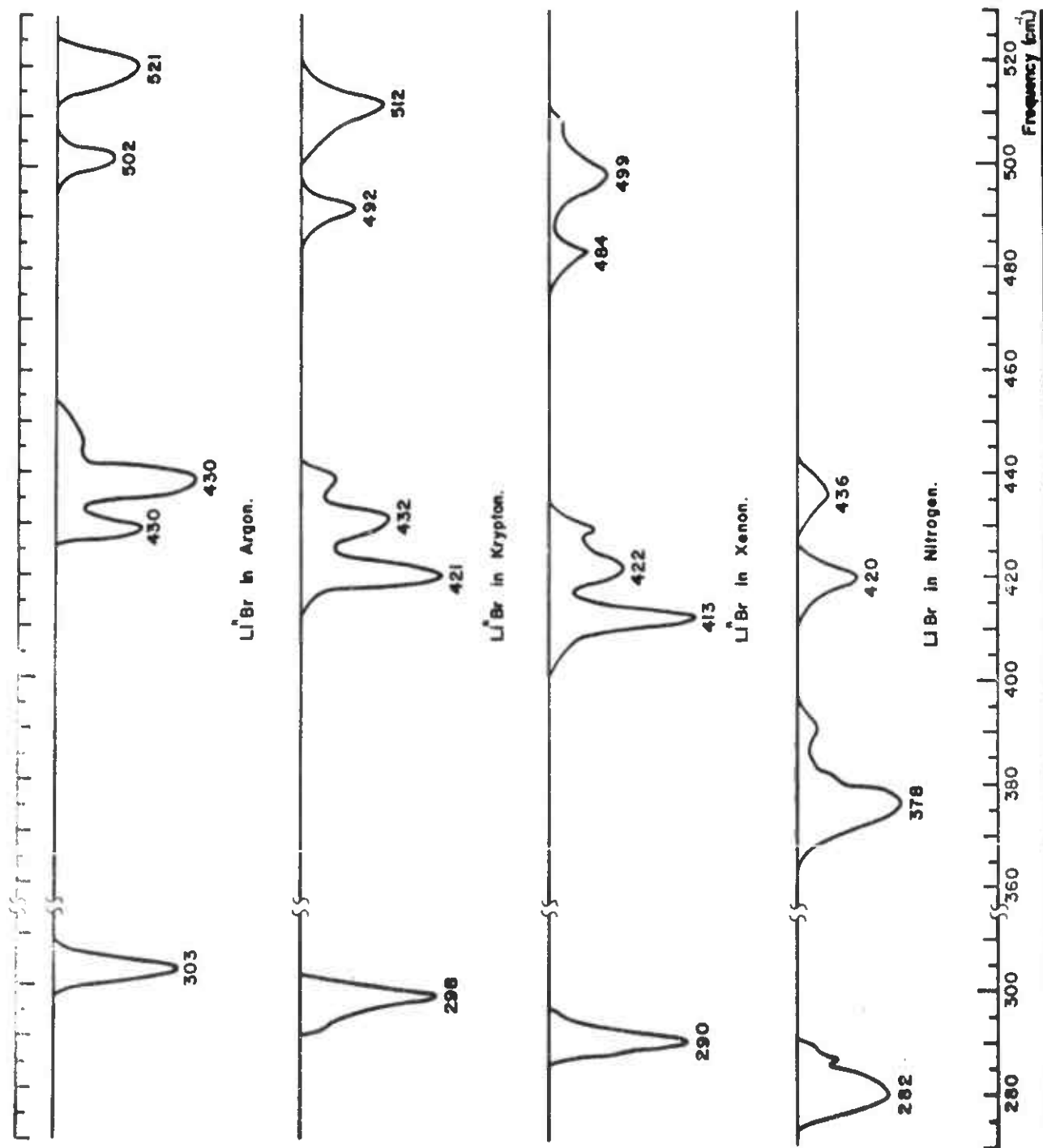
FIGURE 35   THE SPECTRA OF NATURAL BROMIDE VAPORIZATION PRODUCTS IN DIFFERENT MATRICES AT LIQUID HYDROGEN TEMPERATURE
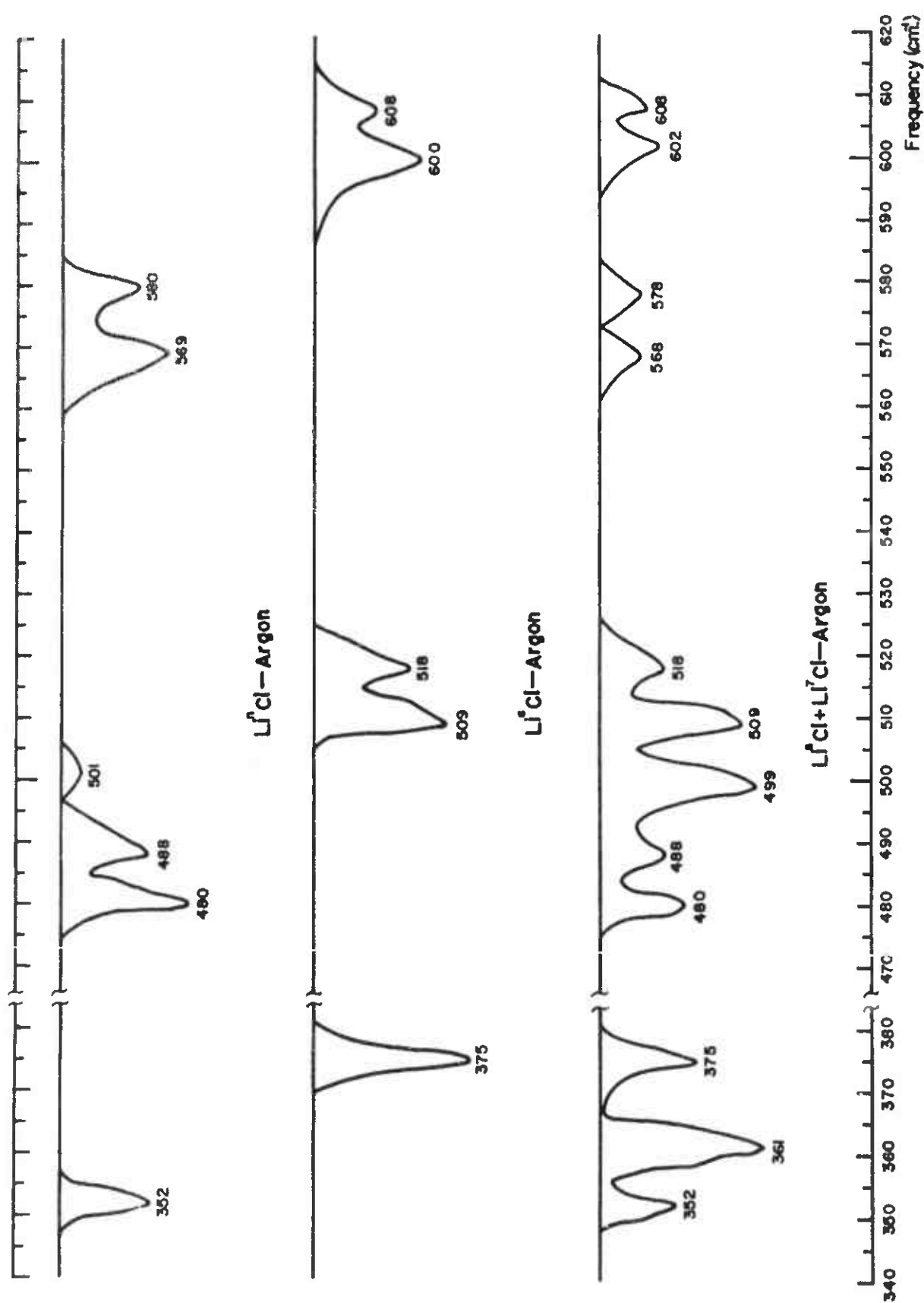
129
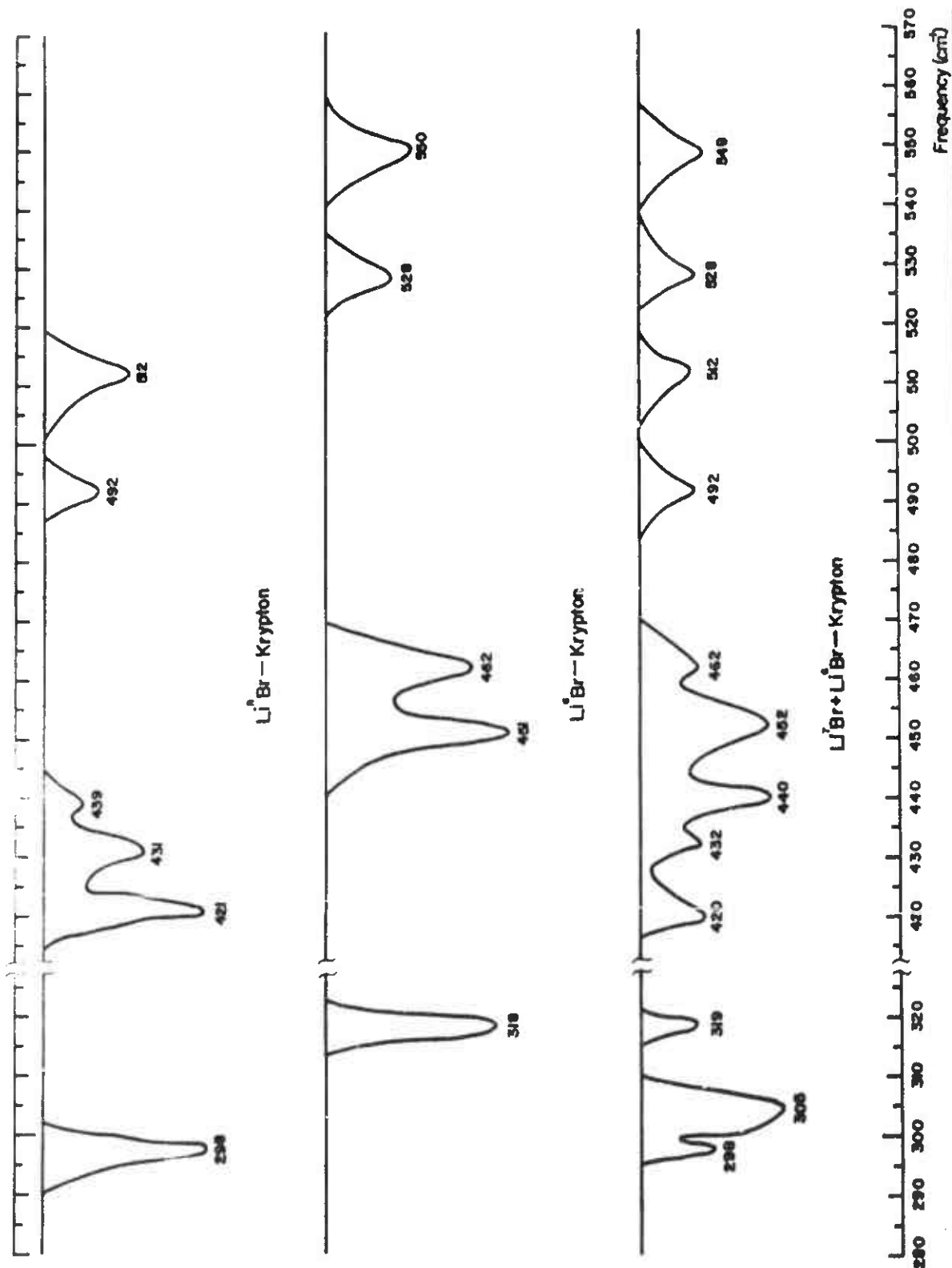
FIGURE 36   THE SPECTRA OF THE VAPORIZATION PRODUCTS OF NATURAL LITHIUM BROMIDE, OF Li^6 - BROMIDE AND OF AN EQUIMOLAR MIXTURE OF THE TWO IN KRYPTON MATRIX AT LIQUID HYDROGEN TEMPERATURE

130

assign the observed frequencies of lithium fluoride, but found that he had to assign two absorptions to the monomer on this basis ($820cm^{-1}$ - $837cm^{-1}$ and $720cm^{-1}$ in solid argon). No such difficulty was encountered in the case of lithium chloride or bromide. Clearly, no new bands were observed in the mixtures in the highest energy absorption region and therefore the bands at $580cm^{-1}$ - $569cm^{-1}$ for lithium chloride in argon and at $521cm^{-1}$ - $502cm^{-1}$ for lithium bromide in argon are unambiguously assigned to the monomer species. On the other hand, the remaining two absorption regions must be assigned to the dimer species since the spectra testify to the fact that they are due to a molecule containing two lithium atoms. In these cases the band of the mixed dimer $Li^6Li^7X_2$ was observed at a frequency inter-mediate between those of the pure isotopic molecules. The intensity ratios in the spectra of the isotopic mixtures were also approximately as predicted except in the case of the lowest energy absorption of lithium chloride in solid krypton. In this case the water vapor absorption band at 28.3μ reduces the sensitivity of the instrument and most likely caused the discrepancy in the observation.

Since the monomer frequencies for the three lithium halides investigated are known for the vapor phase, the matrix shifts or solvent shifts are readily obtained. These are summarized in Table 32. Linevsky [69] has discussed the matrix shifts for LiF and has shown that they are of an order to be expected from known molecular constants. He used for this purpose the data of Braunstein and Trischka [63] and of Vidale [79] which made it possible to calculate the dipole moments of the molecule in the ground and first excited vibrational states. For LiCl the available data are somewhat less complete. Marple and Trischka [63] give the value of $\mu^2 I$ for different vibrational levels of the molecules Li^6Cl^{35} and Li^6Cl^{37}. From these q_e can be calculated by the method of Trischka [75] and therefore the internuclear distances in the different vibrational states can be obtained provided that the internuclear distance r_e in the hypothetical vibrationless state is known. This distance has been given by Klemperer [65] on the assumption of additivity of ionic radii in accordance with the model of Rittner. [76] The values of μ^2 and of μ for the states $v=0$ and $v=1$ were evaluated and from these $\mu_1^2 - \mu_0^2$ was found to be 1.1×10^{-36} and $\mu_1 - \mu_0$ was found to be 0.1×10^{-18}. These values are the same as those used by Linevsky in his calculation of the matrix shifts for LiF. The expression used for calculating the dipole-induced dipole interaction term between the host molecule and the matrix has been given by this author. A substitutional site in an undistorted ideal host lattice is assumed in these calcu-lations. In order to apply the results of the described calculation to Li^7Cl it was assumed that the ratio of $(\mu^2 I)_v$ for the isotopic molecules is equal to the ratio of their reduced masses. This approximation can be tested in the case of the molecules Li^6F^{19} and Li^7F^{19} for which accurate data exist and the error in this case is found to be less than 0.5%. The same values for $\mu_1^2 - \mu_0^2$ and $\mu_1 - \mu_0$ are then obtained for the different isotopic species. The results obtained for the dipole-induced dipole interaction term are included in Table 32.

The dipole-induced dipole interaction term was also calculated for LiBr. Accurate spectroscopic constants have been given hy Honig et al. [64] for three isotopic species and these authors have also measured μ_0 for one of these molecules. The dipole moment was expanded in a Taylor's series in terms of the internuclear distance about the equilihrium value r_e. The derivative of the dipole moment with respect to the internuciear distance evaluated at r_e was calculated using Rittner's model and r_v or the interatomic distance in the zeroeth and first vibrational levels were taken from the data given by Honig et al. In this way the values for μ_0 and μ_1 were ohtained. Again the parameters needed for the calcuiation of the interaction were identical to those for LiF and LiC1. Thus also the calculated values of the dipole-induced dipole interaction term are identical for the three lithium halide molecuies (compare Tabie 32).

Linevsky also calculated the dipole - quadrupole interaction between LiF and nitrogen and attributed to this term the difference between the solvent shifts in the rare gases on the one hand and in nitrogen on the other. However, this interaction term vanishes for a centrosymmetric solute site since it depends on odd powers of the lattice parameters. For a lithium halide solute molecule in the nitrogen lattice we can, therefore, only expect a contribution from this term to the solvent shift in as much as the lattice is distorted. Such a contribution may be expected to be rather small. It is possible that the additional soivent shifts in solid nitrogen are to be attributed to the quadrupole - quadrupole term which arises from the change in quadrupole moment of the lithium halide molecule with the change in vibrational state. Data, which would make a priori calculation possible, are not available.

The dispersion energy contributions to the solvent shifts could not be estimated due to the lack of necessary data. It also proved impossible to obtain a reasonable and consistent set of values for parameters by wholly attrihuting to the dispersion energy the differences between the observed solvent shifts and the calculated dipole-induced dipole contributions for the rare gas matrices. This failure may be due to the relatively high inaccuracy inherent in the small differences.

The observed solvent shifts for the monomer spectra of the lithium halides exhibit several regularities. The argon solvent shift for the lowest energy transition recorded (and therefore presumably for the stablest solute site) is very nearly constant for all three Li^7 - molecules studied and amounts to about $60cm^{-1}$. The shifts increase in steps of about $10cm^{-1}$ from argon to krypton and to xenon and then another large increase is observed on going to nitrogen, such that the nitrogen solvent shift is closely twice the argon shift. The close equality of the shifts for the three molecules correlates satisfactorily with the calculated prediction for the dipole-induced dipole interaction. The energy differences between absorption bands assigned to different sites are of the order to be expected if one or two vacancies occur in the matrix lattice in the immediate neighborhood of the solute inolecule.

132

Buckingham [71] has predicted that the ratio of the solvent shift $\Delta\omega$ of a band to the band frequency in the gas ω_e is constant for isotopic species of a diatomic molecule. The result means, in fact, that the ratio of the solvent shifts for two isotopic species is the same as the ratio between the gas frequencies. It would therefore, be justified to accept the ratio of the observed solution frequencies as the true isotopic ratio. It seemed of interest to test this theoretical result for the vibrations of LiF, LiCl and LiBr in the solvents argon, krypton, xenon and nitrogen. The results are given in Table 33. The isotopic species in each case are the salts containing Li^6 and Li^7. The theoretically predicted relation is seen to be good to at least $\pm 5\%$.

The applicability of the Kirkwood-Bauer-Magat relation to the observed solvent shifts was tested. The pertinent equation is as follows:

$$\frac{\Delta\omega}{\omega} = c \frac{\epsilon - 1}{2\epsilon + 1}$$

where ϵ is the dielectric constant of the solute and c is a constant dependent on the solute only. It was found that the experimental points for argon, krypton and xenon on a plot of $\frac{\Delta\omega}{\omega}$ against $\epsilon-1/2\epsilon+1$ lie fairly close to a straight line, but the points for nitrogen lie very far off this line. It must therefore be concluded that this equation cannot be used for correlating the solvent shifts in solvents that are not closely related. This conclusion is in agreement with previous extensive investigations on this subject. [77]

As described at the beginning of this section, it has been demonstrated that the two lower energy absorption regions for both lithium chloride and lithium bromide must be assigned to the dimer molecules. The isotopic ratios derived from the measured frequencies are included in Tables 29 and 31. The lithium chloride and lithium bromide dimers have been investigated by electron diffraction[67] and have been found to be planar rhombic molecules. The vibrations of these molecules have been treated theoretically by Berkowitz [66] who has calculated their frequencies on the basis of an ionic model. We shall use his symmetry classification. Three infrared active modes are predicted of which two (b_{2u} and b_{3u}) are in-plane stretching vibrations and the third (b_{1u}) is an out-of-plane motion. The isotopic frequency ratios are easily predicted from the product rule since each frequency belongs to a different representation of the point group D_{2h} of the molecule. The theoretical ratio is 1.067 for the chloride and 1.074 for the bromide and is the same for all three infrared active vibrations. The ratios are also identical to those expected for the monomers. It is seen from Tables 29 and 31 that the measured values for the isotopic frequency ratios are in very good agreement with these theoretical values. Since we are here using the frequencies in the matrix solvents to calculate these ratios it may be concluded that a rule similar to Buckingham's rule discussed in the previous section holds for the dimer molecule frequencies.

133

The isotopic frequency ratios for the mixed Li^6-Li^7 dimers cannot be accurately calculated. This is due to the fact that these molecules are of lower symmetry than D_{2h}, namely C_{2v} and therefore in general more than one vibration belong to the same representation of this lower symmetry group. This is correct for the in-plane frequencies, but the out-of-plane vibration belonging to b_{1u} for the symmetric dimer does not mix with other modes in the lower symmetry, and therefore the frequency ratio for it can he readily calculated. It is found to be 1.035 for lithium chloride and 1.038 for lithium bromide relative to the symmetric Li^7 dimers. In Tahle 34 the frequencies of the mixed dimer chloride in solid argon and krypton and of the bromide in solid argon are listed together with their measured ratios relative to the corresponding Li^7 dimer frequencies. It cannot be concluded from these data if the observed absorptions are to he assigned to the in-plane stretching motions b_{2u} and b_{3u}, or if one of them represents the out-of-plane motion. It should be mentioned here that there exists some uncertainty as to whether the frequency of the b_{1u} mode is a normal harmonic mode [78] and therefore the frequency ratios as predicted hy the usual form of the product rule may not accurately apply.

Since the b_{1u} out-of-plane vibration remains in a symmetry class by itself also in the point group of the mixed dimer $Li^6Li^7X_2$, it is possihle to use the sum rule in order to test the possibility of assigning the observed frequencies to this mode. The sum rule for the present case has the following form:

$$\sigma\,(Li^7_2X_2) \;+\; \sigma\,(Li^6_2X_2) \;-\; 2\sigma\,(Li^6Li^7X_2) = 0$$

where

$$\sigma = \sum_k \lambda_k \;=\; 4\pi^2 c^2 \sum_k \omega_k^2$$

and the sum extends over all vihrations belonging to the same representation in the lower symmetry group, C_{2v}. The result for the observed frequencies is as follows:

1. higher frequency

    a. Li_2Cl_2 in argon: $\qquad 480^2 + 509^2 - 2 \times 499^2 = -8521$

    b. Li_2Cl_2 in krypton: $\qquad 473^2 + 501^2 - 2 \times 490^2 = -5470$

    c. Li_2Br_2 in krypton: $\qquad 421^2 + 451^2 - 2 \times 440^2 = -6558$

2. lower frequency

    a. Li_2Cl_2 in argon: $\qquad 352^2 + 375^2 - 2 \times 361^2 = 3887$

    b. Li_2Cl_2 in krypton: $\qquad 344^2 + 367^2 - 2 \times 354^2 = 2393$

    c. Li_2Br_2 in krypton: $\qquad 298^2 + 319^2 - 2 \times 305^2 = 4515$

The sum rule has been established to be accurate to one part in a thousand [79] and therefore the evidence presented here supports the assumption that the b_{1u} vibration has not been observed.

Attempts were made to evolve a well-based extrapolation procedure for determining the gas phase dimer frequencies from the observed matrix spectra. For this purpose, the quadrupole-quadrupole and quadrupole-induced dipole interaction terms were investigated, and the change in the quadrupole moment and the change in the square of this moment with vibrational level were used as parameters. These attempts were, however, abandoned, since physically reasonable and internally consistent values for these parameters could not be determined from the measurements.

It is proposed to extrapolate the observed frequencies to obtain the free molecule values by analogy to the monomer solvent shifts. To justify this completely empirical procedure for the lithium chloride and bromide dimer modes, we note that the shifts from matrix to matrix are very closely the same for the two dimer molecules, just as they are for the monomer species. These relative matrix shifts also follow a pattern similar to the monomer values, the observed frequencies moving to lower energies by small intervals from argon to krypton to xenon and then by a larger interval to nitrogen. On the basis of these similarities to the monomer matrix shifts, the free molecule dimer frequencies are estimated by adding to the argon frequency the difference between the argon and nitrogen matrix frequencies. The lower frequency peak of each group of absorption bands in each case is used. The resulting extrapolated frequencies are believed to be accurate to $\pm 20 cm^{-1}$. The resulting frequencies are as follows: Lithium Fluoride: $640 cm^{-1}$, $550 cm^{-1}$; lithium chloride: $535 cm^{-1}$, $380 cm^{-1}$; lithium bromide: $490 cm^{-1}$, $325 cm^{-1}$. These frequencies are mostly somewhat higher than the gas phase absorption maxima reported by Klemperer and Norris [66] but in view of the uncertainties involved, the agreement may be considered as fair.

In view of the fact that the out-of-plane b_{1u} mode of the dimer is expected to be of lower frequency, the observed gas phase absorptions have been assigned to the in-plane b_{2u} and b_{3u} modes. According to theoretical predictions, the possibility can, however, not be excluded that the b_{1u} mode is only of slightly lower energy than the other two infrared active vibrations. Evidence based on the "sum rule" presented here supports the conclusion that the b_{1u} vibration has not been observed in the present work. It is, therefore, concluded that here also the in-plane modes have been recorded. The normal coordinates for these modes are of the following form:

$$S_{b_{2u}} = 1/2 \ (r_1 - r_2 - r_3 + r_4)$$

$$S_{b_{3u}} = 1/2 \ (r_1 + r_2 - r_3 - r_4)$$

where r_1, r_2, r_3 and r_4 are the displacement coordinates representing elongations of the metal-halide bonds. The F-matrix elements can be written down by inspection. They are as follows:

$$F_{b_{2u}} = F_{11} - F_{12} - F_{13} + F_{14} = (F_{11} - F_{13}) - (F_{12} - F_{14})$$

$$F_{h_{3u}} = F_{11} + F_{12} - F_{13} - F_{14} = (F_{11} - F_{13}) + (F_{12} - F_{14})$$

The G-matrix elements have been given by Berkowitz. [68] It follows that the force constant combinations $F_{11} - F_{13}$ and $F_{12} - F_{14}$ can be calculated for a given assignment of the two frequencies. The results for the two possible choices when the two observed frequencies are assigned to the two in-plane vibrational modes are given in Table 35. The argon matrix frequencies were used for the calculations. The results are very similar if the frequencies estimated for the free dimer molecules are used. It may be expected that F_{13} will be small compared to F_{11} and therefore the difference $F_{11} - F_{13}$ may be accepted as an indication of the magnitude of F_{11}. On the other hand, F_{12} and F_{14} are expected to be very similar and consequently $F_{12} - F_{14}$ should be small compared to $F_{11} - F_{13}$. In view of this condition the results clearly lend strong support to the assignment of the higher frequency mode to b_{3u} (assignment B in Table 35). This order of the frequencies is in agreement with the results of the calculation of Berkowitz [68] and the conclusions of Klemperer and Norris. [66]

It has been pointed out that the doublet structure of the monomer bands of lithium chloride and bromide is attributed to the occurrence of two trapping sites. The higher energy dimer band (medium energy absorption region) has similar structure in most matrices and here again the occurrence of at least two trapping sites of the dimer molecules must be assumed. On the other hand, the different sites do not manifest themselves in the lower energy dimer band (lowest energy absorption region) where, for the most part, a single absorption peak was recorded. It must therefore be concluded that the b_{2u} vibrational frequency is less sensitive to changes in the molecular environment and therefore the energy difference between the two sites falls within the line width. The frequency shifts between different matrices are, in fact, also considerably smaller for this absorption than for the higher energy vibration. The normal vibration of symmetry h_{3u} is such that the lithium ions undergo displacements tangentially to the solvent cage while the halide ion displacements are radial to the cage. The situation is reversed for the b_{2u} vibration. It is therefore seen that radial motion of the halide ions correlates with greater effect on solute-solvent interaction. In view of the fact that the amplitude of the lithium ion is considerably greater than that of the chloride or bromide ion, the evidence is against the assumption that the repulsive contribution to the interaction determines the solvent shift. Such an argument has recently been used in an attempt to assign the vibrational frequencies on the basis of the comparative solvent shifts of the absorptions. [72]

Table 27

IR spectrum of LiF in matrices at 20°K.

A	Kr	Xe	N_2	Assignment
837	830	822	776	monomer
842				
720	717	716	697	
621	618	611	606	dimer
			599	b_{3u}
580				
538	541	533	548	dimer
545				b_{2u}

Table 28

IR spectrum of Li^{7}Cl in matrices at 20°K.

A	Kr	Xe	N_2	Assignment
580	568	574		
569	556	559		
		545	519	monomer
501	492	483	440	dimer
488	481	472		
480	473	466	425	b_{3u}
352	344	348	325	dimer
		338		b_{2u}

Table 29

IR spectrum of Li^{6}Cl in matrices at 20°K and the frequency ratios relative to Li^{7}Cl.

A	Frequency Ratio	Kr	Frequency Ratio	Xe	Frequency Ratio	N_2	Frequency Ratio	Assignment
608	1.048	601	1.058	607	1.059	557		monomer
600	1.054	593	1.066	593	1.061	539	1.073	
				582	1.068			
518	1.061	524	1.065	508	1.052			dimer
509	1.060	510	1.060	503	1.066	453	1.066	b_{3u}
		501	1.059	496	1.064			
375	1.065	367	1.068	361	1.068	345	1.062	dimer
								b_{2u}

137

Table 30

IR spectrum of Li^7Br in matrices at 20°K.

A	Kr	Xe	N_2	Assignment
521	512	499	436	monomer
502	492	484	420	
449	439	430		dimer
439	431	422	392	b_{3u}
430	421	413	373	
303	298	290	281	dimer b_{2u}

Table 31

IR spectrum of Li^6Br in matrices at 20°K and the frequency ratios relative to Li^7Br.

A	Frequency Ratio	Kr	Frequency Ratio	Assignment
561	1.077	550	1.074	monomer
540	1.076	528	1.073	
470	1.070	462	1.072	dimer
461	1.072	451	1.071	b_{3u}
327	1.079	319	1.070	dimer b_{2u}

Table 32

Calculated (incomplete) and experimental shifts for the lithium halide monomer bands.

Matrix	Calc.*	Li^7F	Li^6F**	Li^7Cl	Li^6Cl	Li^7Br	Li^6Br
A	41	48	57	53	66	40	36
		53	61	64	74	60	57
Kr	50	60	63	65	73	44	47
				77	81	64	69
Xe	48	68	73	59	67	57	
				74	81	72	
					92		
N_2	45	114		114	117	120	
				128	135	136	

*Identical for all molecules studied; dipole-induced dipole term only.
**Reference (70).

Table 33

Values of the ratio $\Delta\omega/\nu_e$ for LiF, LiCl, LiBr monomer vibrations in different matrices (A, Kr, Xe, N_2) and at different sites (1, 2).

Matrix & Sites	A	A_2	Kr_1	Kr_2	Xe_1	Xe_2	$N_{2,1}$	$N_{2,2}$
Li^6F	0.057	0.063	0.070		0.080			
Li^7F	0.052	0.057	0.063		0.074			
Li^6Cl	0.096	0.108	0.107	0.118	0.118	0.135	0.171	0.197
Li^7Cl	0.083	0.100	0.101	0.120	0.115	0.137	0.178	0.200
Li^6Br	0.060	0.094	0.078	0.114				
Li^7Br	0.062	0.096	0.078	0.114				

Table 34

IR spectra of $Li^6Li^7Cl_2$ and $Li^6Li^7Br_2$ in matrices at 20°K and the frequency ratios relative to $Li_2^7Cl_2$ and $Li_2^7Br_2$ respectively.

Molecule	A	Frequency Ratio	Kr	Frequency Ratio	Assignment
$Li^6Li^7Cl_2$	509	1.043	501	1.046	b_{3u}
	499	1.039	490	1.036	
	361	1.026	354	1.029	b_{2u}
$Li^6Li^7Br_2$			452	1.049	b_{3u}
			440	1.045	
			305	1.023	b_{2u}

Table 35

Force constants of lithium halide dimers. Two assignments are considered:

Assignment A: $\tilde{\nu} b_{2u} > \tilde{\nu} b_{3u}$;

Assignment B: $\tilde{\nu} b_{2u} < \tilde{\nu} b_{3u}$

Molecule	Assignment	$F_{b_{2u}}$ 10^5 dyne/cm	$F_{b_{3u}}$ 10^5 dyne/cm	$F_{11} - F_{13}$ 10^5 dyne/cm	$F_{12} - F_{14}$ 10^5 dyne/cm	F-monomer 10^5 dyne/cm gas	F-monomer 10^5 dyne/cm argon
Li_2F_2	A	1.35	0.77	1.06	-0.23	2.48	2.12
	B	1.01	1.02	1.02	0.00		
Li_2Cl_2	A	1.15	0.33	0.66	-0.34	1.42	1.12
	B	0.62	0.61	0.61	0.00		
Li_2Br_2	A	1.07	0.26	0.66	-0.41	1.20	0.96
	B	0.53	0.52	0.50	0.03		

APPENDIX II

HIGH TEMPERATURE PROPERTIES OF REFRACTORY ZIRCONIUM AND HAFNIUM COMPOUNDS*

A. KINETICS OF OXIDATION AND FLUORINATION REACTIONS BY A. K. KURIAKOSE AND J. L. MARGRAVE

1. Oxidation of Zirconium Diboride and Zirconium Carbide at High Temperatures[80]

Kinetic studies were made of the oxidation of zirconium diboride at 945-1256°C, and of zirconium carbide at 554-652°C and results were presented in the previous report (ASD-TDR-62-204, Part II)[15] issued in May 1963. It was found that the ZrB_2-O_2 reaction is parabolic throughout the temperature range studied whereas the ZrC-O_2 reaction is linear. In the former case a molten layer of boron oxide is formed which protects against further direct attack of oxygen on the ZrB_2, while in the latter, a rather porous film of zirconium oxide is formed which is not protective.

2. Kinetics of the Reaction of Elemental Fluorine with Zirconium Carbide and Zirconium Diboride at High Temperatures[81]

a. Introduction

Although there have been extensive studies of rates of oxidation and nitridation of metals and compounds, there have been very few studies of reaction rates with fluorine. Haendler et al.[82-85] have, however, investigated the reaction of fluorine with several metals and some of their compounds in an attempt to synthesize and characterize metallic fluorides. They observed that fluorine reacts with zirconium metal above 190° and that the fluoride coating prevents complete reaction. They also noticed that zirconium dioxide does not react with fluorine at 100°, but converts to zirconium tetrafluoride above 250°C. There have also been several other reports[86-100] on the interaction of fluorine under different conditions, with various types of materials. As for kinetic studies with metals the reaction between fluorine and copper has been worked out in some detail.[101,102]

141

The reactions between fluorine and ZrC and ZrB_2 are complicated be-cause of the variety of possible solid and gaseous products. Also, ZrF_4 sub-limes above 600°C.[103-105] Zirconium carbide is known to be decomposed by halogens and oxidizing agents,[106] in general, and hence, a rather vigorous exothermic reaction is to be expected with fluorine. However, no previous data are available on the rate of reaction of fluorine with ZrC and ZrB_2.

b. Apparatus and Experimental Procedure

The arrangement of the fluorination furnace is shown in Figure 37. The reaction chamber consisted of a nickel tube 12" long with 1" I.D. and 1/8" wall thickness. Heating was done by a Kanthal wire-wound furnace, and the tem-perature measured with a Pt. vs Pt. - 10% Ph thermocouple introduced from the bottom of the furnace tube through a 1/4" nickel tube, closed at the top end. The metal joints of the furnace tube were made gas tight with teflon gaskets.

The flow of fluorine gas was regulated by a Matheson fluorine pressure reducing valve and metered by a Fisher-Porter borosilicate glass flowmeter con-taining a sapphire float. The fluorine was mixed with purified dry helium gas, metered by another flowmeter, in various proportions to obtain the desired fluo-rine partial pressures. The unreacted fluorine from the exit was reacted with the ammonia fumes over a concentrated NH_4OH solution.

Before commencing the reaction, the nickel furnace tube was passivated by reacting it with pure fluorine at 500 - 600°C to form a protective coating of nickel fluoride. The process was carried out during a period of three days by intermittently admitting fluorine for two or three hours each time. Also, before starting any run, a mixture of fluorine and helium was passed through the already passivated furnace tube, heated at the desired temperature for nearly half an hour to one hour as required, until fluorine was detected coming out of the combustion tube in large amounts, as indicated by use of KI paper. After passivation at the required temperature, the system was evacuated and flushed with helium several times, and the sample to be fluorinated was suspended from the helical spring by means of a 0.007" nickel wire, in the atmosphere of flowing helium gas. After about 10 minutes, fluorine was admitted, along with the helium, and a timer started simultaneously. The partial pressure of fluorine was calculated from the individual flow rates of fluorine and helium at atmospheric pressure. Any re-action of the fluorine with the nickel suspension wire was neglected on the grounds that the surface area of the nickel wire exposed to the hot zone of the furnace was negligibly small compared to the relatively large area of the specimen. The change in extension of the spring was observed by means of a cathetometer and the small-est measurable weight change was 0.05 mg. Readings were taken at suitable inter-vals of time. The silica spring was protected from attack by fluorine by having a blanket of dry nitrogen in the form of a slow, steady stream sent from the top of the system. At the conclusion of the run, the fluorine was cut off and helium and nitrogen continued to flow until the exit gas was free from fluorine.

142
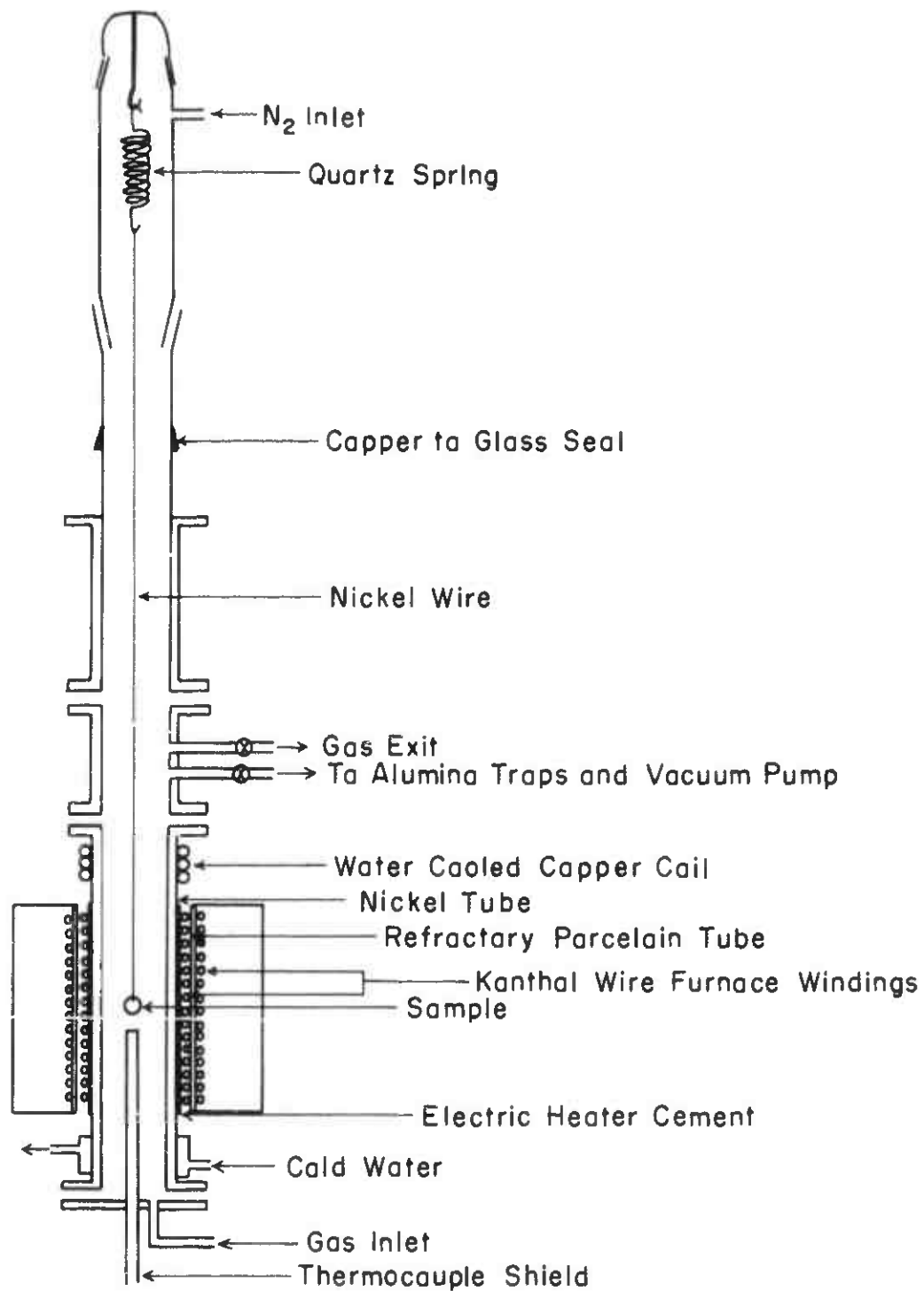
FIGURE 37   F'JORINATION FURNACE SET-UP

143

The zirconium carbide and zirconium diboride samples in the form of small discs, weighing about 0.2 to 0.4 gm., cut from electron-beam melted rods, were polished by grinding on abrasive cloth. The ZrC was 99.5%+ pure with traces of Ti, Si, B, Fe, N in the order of 0.1% and less and O, Al, Sn, Mg, Ca, Mn, Cu, Mo, Ag, Hf, and Pb in the order of 0.01 to 0.001%. The zirconium diboride was of composition $ZrB_{1.95}$ with 1.7% Hf and 200 ppm of carbon as impurities. The polished ZrB_2 had a shining mirror-like appearance while the ZrC had a shining metallic gray color. Surface areas of the specimens were determined by measuring the geometrical dimensions.

c. Results and Discussion

A preliminary examination showed that ZrC would burn in fluorine or in an atmosphere rich in fluorine, at about 250 - 300°C. On the other hand, ZrB_2 did not catch fire in pure fluorine at a pressure of 1 atm., but it broke into bits at about the same temperature. Thus, the fluorination of these materials was examined at low fluorine partial pressures where the reactions could be effectively controlled.

d. Reaction Between ZrC and Fluorine at 278 - 410°C

Initial experiments with ZrC and F_2 under a low partial pressure of F_2 (31 mm. of Hg) indicated that the reaction was rather smooth at about 300°C with a regular increase in weight. The reproducibility of the results was checked at 300°C and found to be within 20%. With the same fluorine partial pressure, the reaction was conducted at various temperatures ranging from 278 to 410°C. Above 410°C the reaction rate was too fast to measure by this technique. The weight increase per unit area of ZrC with time at the various temperatures is illustrated in Figure 38. There is no question regarding the linearity of the reaction with time. Abrupt breaks at and above 334°C indicate the crumbling away of part of the fluoride layer formed on the ZrC. Thick scales of ash-gray zirconium fluoride were observed on the surface of the ZrC after reaction. The adhesion of the scales was very poor and the material was soft and fluffy. The reacted samples had a sandwich appearance and their volumes had increased markedly because of the fluffiness of the ZrF_4 formed. The scales were apparently uniform and there were no visible cracks on them except at the edges, where the inner core was practically naked. Viewed under a microscope, the layers were made up of fine sugar-like crystals uniformly formed without any cracks. It appears that the unreacted ZrC was in direct contact with the fluorine atmosphere, in spite of the fluoride coating, and thus showed a linear rate of reaction.

It is not possible to say whether either zirconium or carbon in the system is preferentially attacked by fluorine, since the gaseous products were not analyzed. X-ray analysis of the inner core and the outer layer might show some

144
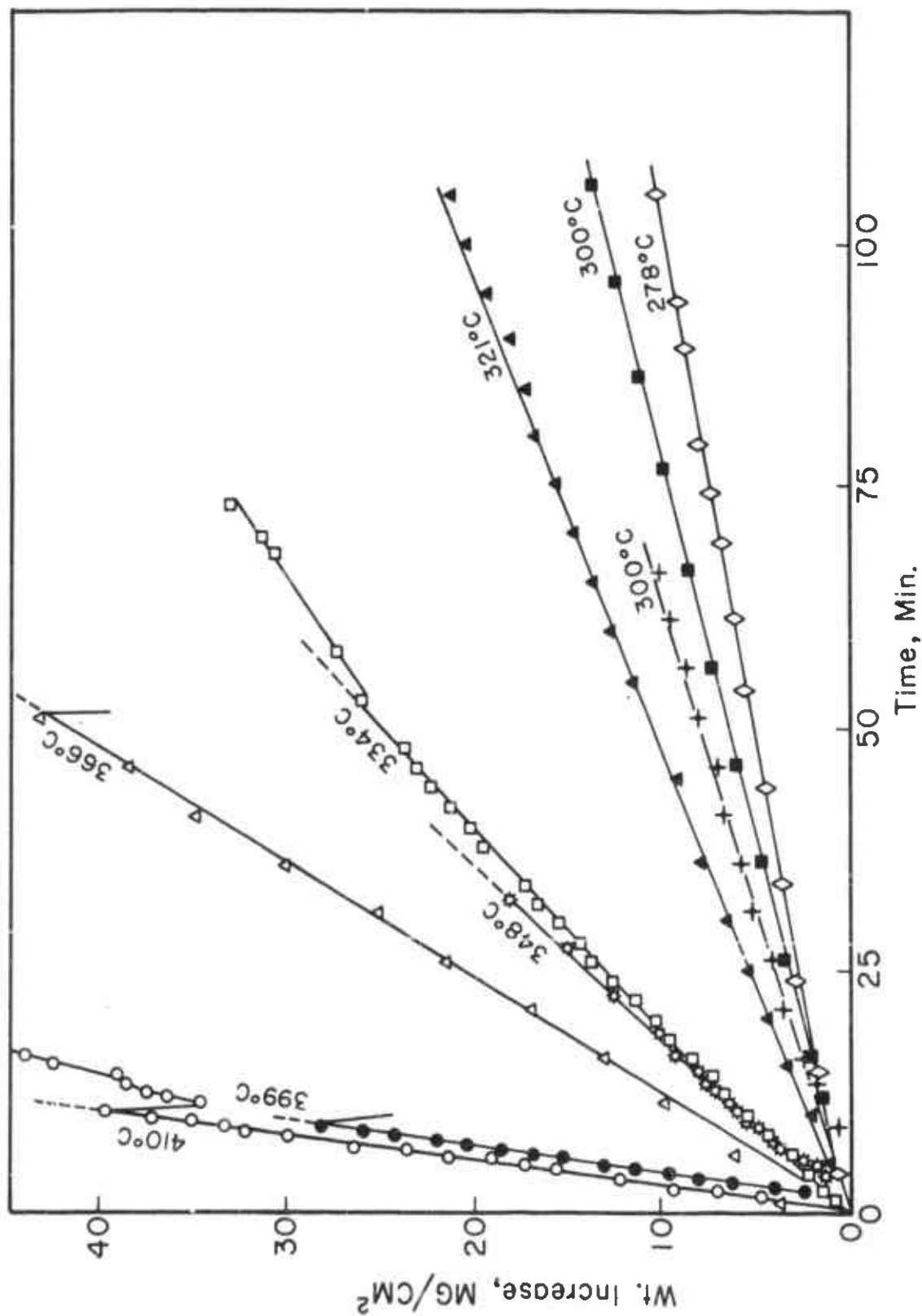
FIGURE 38   LINEAR PLOT FOR ZrC-F$_2$ REACTION. FLUORINE PARTIAL PRESSURE, 31 mm

145

evidence regarding this question; the coating gave an x-ray pattern characteristic of ZrF_4. The fact that the inner core is rough and black when once the fluoride scales are removed suggests the possibility that the Zr is reacting faster than the carbon.

From the slopes of the straight lines in Figure 38, the linear rate constants for the reactions were estimated, not taking into account the volatile products. The values obtained are displayed in Table 36. The activation energy computed by a least square method is 22.1 ± 1.6 kcal/mole.

TABLE 36

LINEAR RATE CONSTANTS FOR THE $ZrC-F_2$ REACTION
AT VARIOUS TEMPERATURES

(Fluorine Partial Pressure: 31 mm. of Hg)

Temperature ($^\circ$C)	Linear Rate Constant, k_1 $(mg/cm^2/min)$
278	0.0995
300	0.1282
300	0.1515
321	0.2010
334	0.5069
348	0.5526
366	0.8450
399	3.4545
410	3.6786

$$\Delta E_a = 22.1 \pm 1.6 \text{ kcal/mole}$$

e. Fluorination of ZrB_2 and ZrC Above 600°C

Zirconium diboride is apparently not attacked by fluorine under a low partial pressure (31 mm F_2; 709 mm helium) below 500°C. Since zirconium fluoride is very volatile above 700°C, practically no fluoride coating is formed on the boride or carbide surfaces above this temperature and hence the samples are found to lose weight during fluorination. The loss in weight can be measured and used for calculating the rates of the reactions. Figures 39 and 40 present plots of the weight loss/cm^2 of the samples with time in minutes, at 600-900° for ZrB_2 and 700-950°C for ZrC respectively, with a fluorine partial pressure of 2.7 mm of Hg (736 mm helium). The slight curvature in the lines is assumed

146
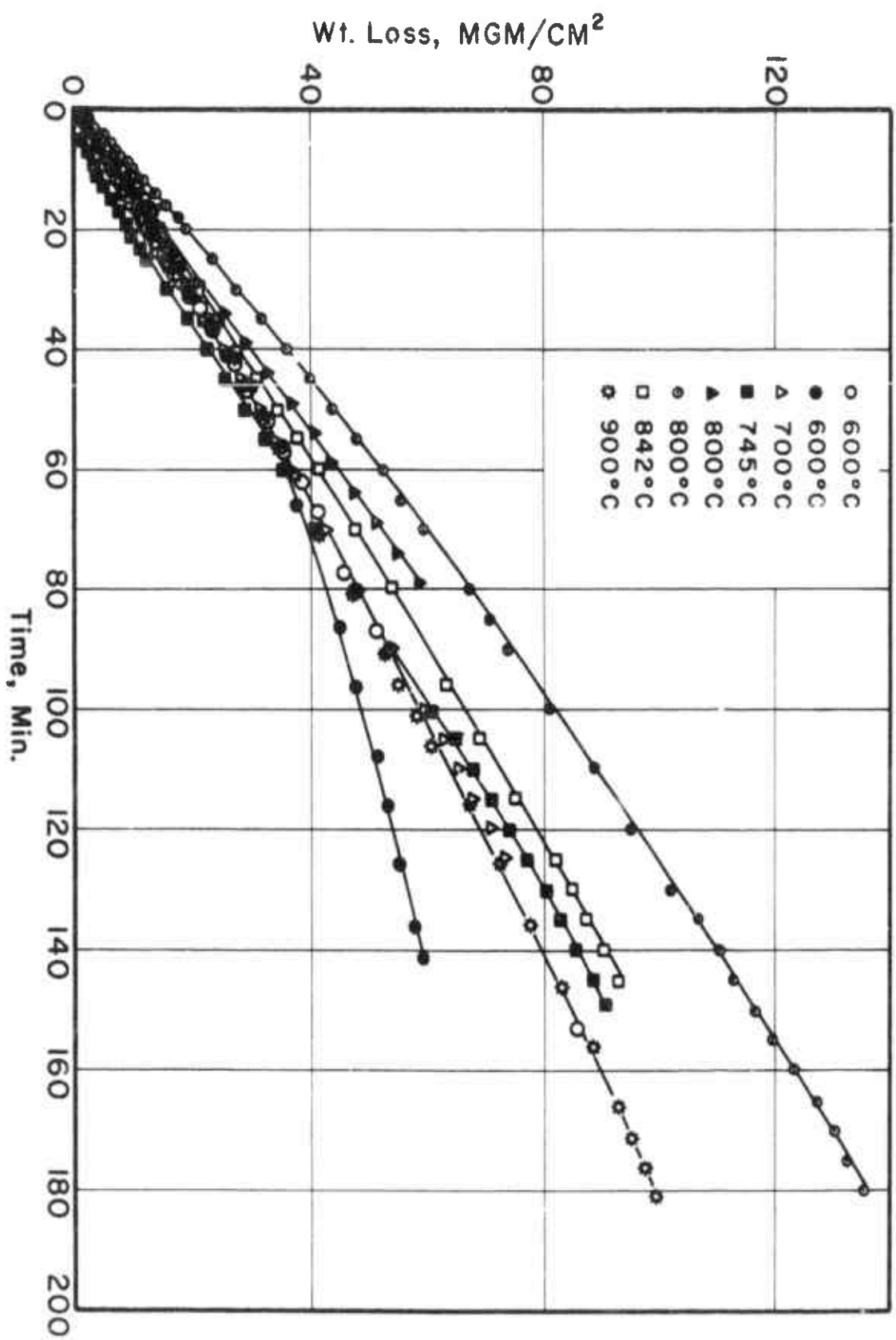
FIGURE 39)   ZrB₂-F₂ REACTION AT VARIOUS TEMPERATURES, LINEAR PLOT.
FLUORINE PARTIAL PRESSURE = 2.7 mm
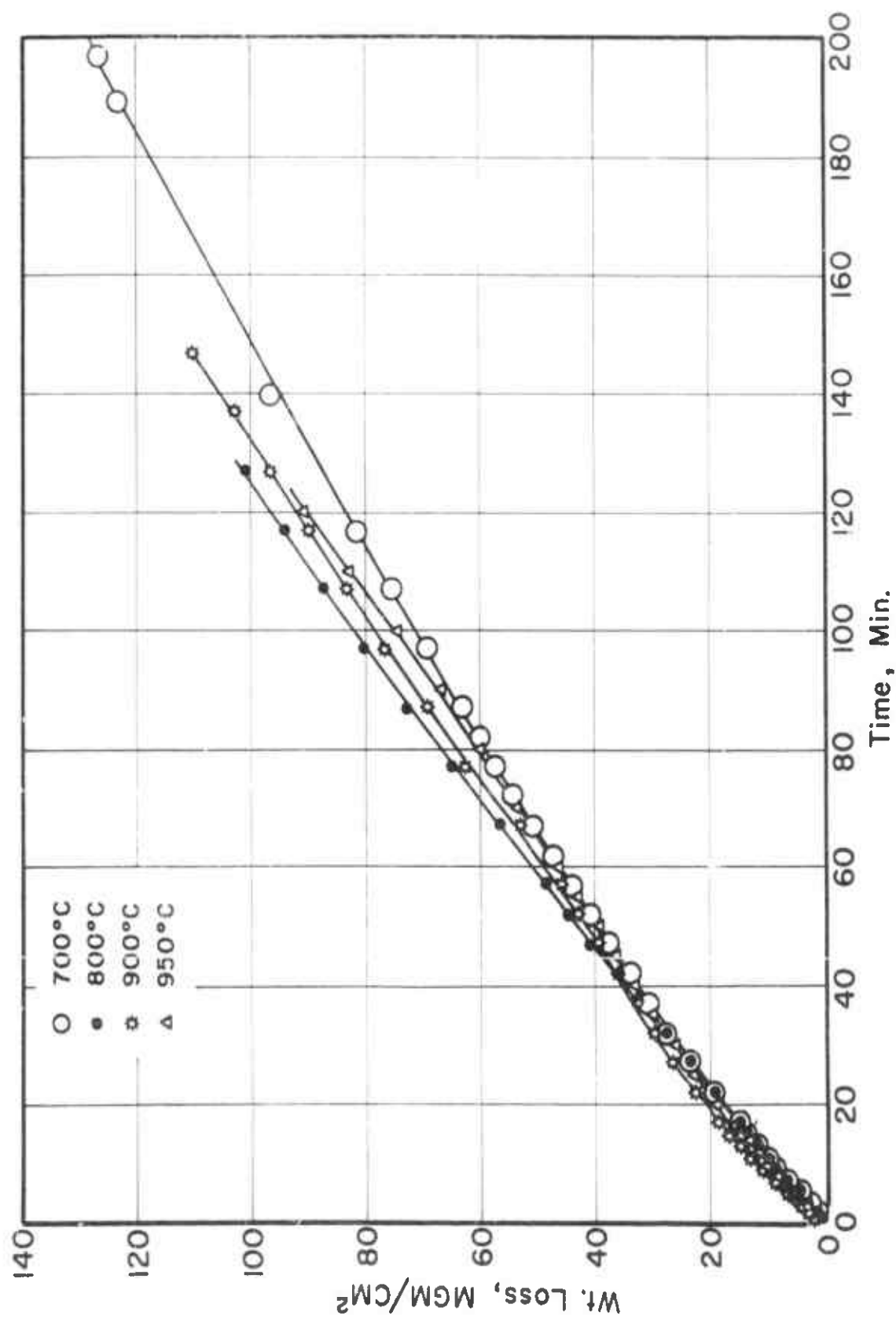
FIGURE 40   ZrC-F₂ REACTION AT 700-950°C. FLUORINE PARTIAL PRESSURE, 2.7 mm

to be due to the change in surface area of the specimens with the extent of corrosion. The rate constants for these reactions were, hence, calculated at zero-time on the basis of a linear rate law, using the equation

$$\Delta w/A = B + Ct - Dt^2 + Et^3 \tag{1}$$

where:

Δw is the weight loss; A, the initial surface area; t, the time; and B, C, D, and E are constants with C being the linear rate constant $k_{1,t=0}$.

Equation (1) was derived assuming that the length and radius of the cylindrical specimen vary linearly with time, as treated below:

The linear rate of reaction at the surface of a cylinder may be expressed by the equation:

$$\frac{d(\Delta w)}{dt} = k \ 2\pi r(r + 1) \tag{2}$$

where:

Δw represents the weight change; k, the linear rate constant; and r and l, the radius and length of the cylinder respectively.

Assuming that the cylinder is corroded at constant rate from all sides,

$$\frac{dr}{dt} = 1/2 \frac{dl}{dt} = k' \tag{3}$$

where k' is the rate constant for the change in radius and length.

Integrating (3),

$$r = r_0 - k't \tag{4}$$

$$1 = l_0 - 2 k't \tag{5}$$

where r_0 and l_0 represent the initial radius and length of the cylinder. Substituting (4) and (5) in (2)

$$\frac{d(\Delta w)}{dt} = k \ 2\pi (r_0 - k't) \ (r_0 + l_0 - 3 k't) \tag{6}$$

Integrating (6) with respect to t,

$$\Delta w = k \left[2\pi r_0 (r_0 + l_0) t - \pi k' (4r_0 + l_0) t^2 + 2\pi k'^2 t^3 \right] + B \tag{7}$$

where B is a constant.

149

Equation (7) is of the same form as (1) and

$$\frac{d(\Delta w)}{dt}_{t=0} = k \left[2\pi r_o (r_o + l_o) \right] \qquad (8)$$

and the value within the square bracket in (8) is the initial surface area of the cylinder.

The values for the zero-time rate constants w̲ c̲ la̲ ̲d with a Control Data 1604 computer and they are presented in Ta̲ ̲ an̲ ̲ ̲ The reactions of both ZrB_2 and ZrC with fluorine are not stro̲ ̲dly temperature dependent above 600°C and the activation energies calcula̲ ̲re essen̲ ̲ ̲ ero for both ZrB_2 and ZrC. The reaction rates depend on ̲he ̲rine pa̲ ̲al ̲res-sure at temperatures above 600°C and probably appear to ̲ v̲ ̲ ̲ast l̲ ̲ iy because of the rapid temperature rise produced at the surface ̲y t̲ ̲ ̲y exo-thermic fluorination process which produces more energy than the sm̲ ̲ sample can dissipate by combined radiation and conduction to the flow gas.

f. The Effect of Fluorine Partial Pressure on the Fluorination of ZrC and ZrB2

The nature of the dependence of the rate of reaction of fluorine with ZrC was investigated at two temperatures, 350° and 700° C, since the mechanism of fluorination at these two temperatures is distinctly different. For ZrB_2, the effect of fluorine partial pressure was studied only at 700°C. The rate constants for the reactions were calculated as indicated earlier, and the results are graphi-cally presented in Figures 41 and 42 for ZrC and ZrB_2 respectively. For ZrC at 350°C and for ZrB_2 at 700°C, the rate of fluorination is approximately propor-tional to the square root and for ZrC at 700°C, it is proportional to the 1.5 power of the fluorine partial pressure.

TABLE 37

LINEAR RATE CONSTANTS AT ZERO-TIME $(k_{1,t=0})$

FOR THE ZrB_2-F_2 REACTION AT 700-900°C

P_{F_2} = 2.7 mm. of Hg

Temperature (°C)	$k_{1,t=0}$ (mg. cm^2/min)
600	0.6028
600	0.7734
700	0.6354
745	0.5313
800	0.9435
800	0.6842
842	0.7265
900	0.5916

ΔE_A = 0 ± 1 kcal/mole

TABLE 38

LINEAR RATE CONSTANTS AT ZERO-TIME $(k_{1,t=0})$

FOR THE ZrC-F_2 REACTION AT 700-950°C

P_{F_2} = 2.7 mm. of Hg

Temperature (°C)	$k_{1,t=0}$ (mg/cm^2/min)
700	0.7565
800	0.8764
900	0.9058
950	0.9697

ΔE_A = 2.2 ± 0.4 kcal/mole
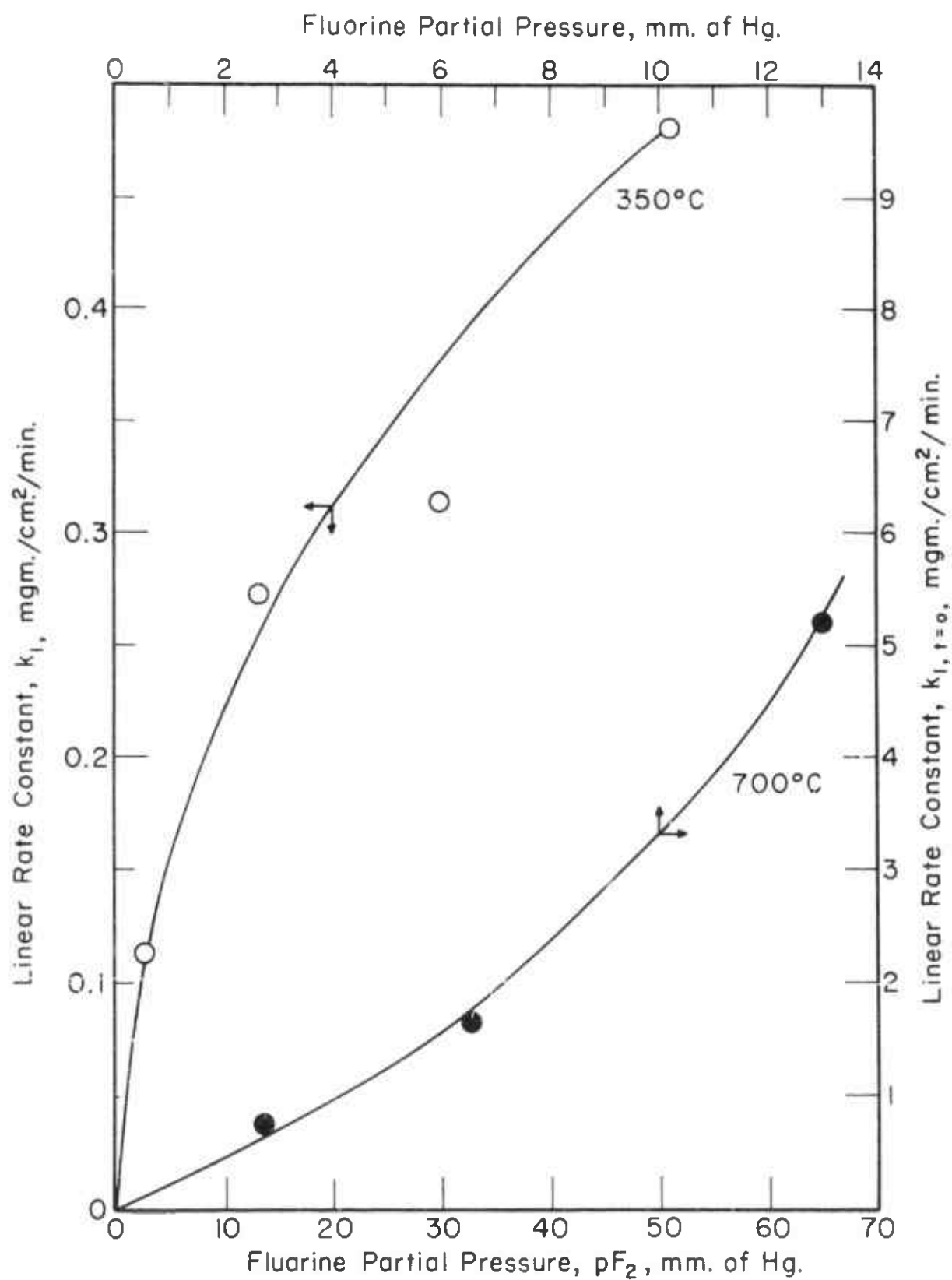
FIGURE 41   THE EFFECT OF FLUORINE PARTIAL PRESSURE
ON THE ZrC-FLUORINE REACTION

151
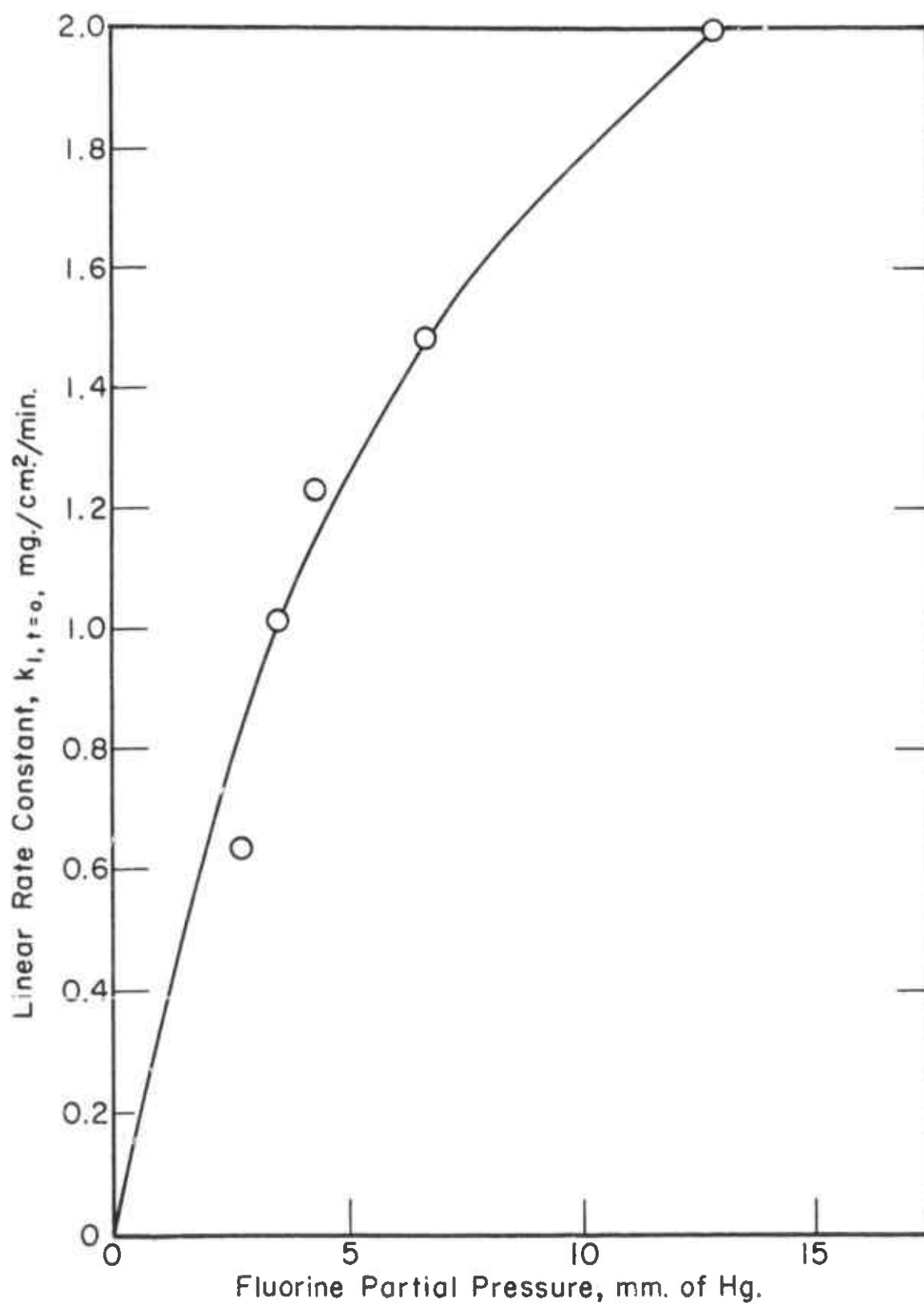
FIGURE 42   EFFECT OF F_2 PARTIAL PRESSURE ON THE
ZrB$_2$-F$_2$ REACTION: 700°C

152

3. Kinetics of the Reactions of Fluorine with Hafnium Carbide and Hafnium Diboride

a. Introduction

Because of the well-known close resemblances between zirconium and hafnium compounds, similar behaviors of HfC and ZrC and of HfB_2 and ZrB_2 with fluorine are to be expected. However, the slightly higher volatility of HfF_4 than ZrF_4 should make the Hf compounds slightly more reactive at lower temperatures.

b. Experimental

The apparatus and experimental procedure were essentially the same as for the fluorination of ZrC and ZrB_2. The HfC samples were prepared from an arc-melted piece of composition $HfC_{0.952}$ with the following impurities: 0.035% Zr; 0.031% N; 0.005% Fe; 0.003% O; 0.002% each of Ti and Si; 0.001% each of H, Cu, Mn and Mg. The HfB_2 specimens were cut from zone-refined cylindrical bars which had a composition $HfB_{2.035}$ with impurities: 0.01 to 0.1% of Zr; 0.16% of C; 0.001% each of Cr, Cu and Mg; 42 ppm of N; 30 ppm each of Ti and Fe; 26 ppm of O; and 10 ppm of Si.

Both of the sample materials were supplied by Mr. George Feick. The surfaces were polished by mechanical means and their areas were calculated from geometrical dimensions.

c. Results

Both HfC and HfB_2 were found to withstand fluorine at room temperature to a pressure of one atmosphere. The exposures at higher temperatures were done only at low fluorine partial pressures.

Fluorination of HfC - Experiments with HfC exposed to fluorine at 2.8 Torr partial pressure indicated that a detectable reaction started at about 300°C. There was formation of solid HfF_4, but the reaction rate could not be measured since the product was not adherent to the HfC surface up to 400°C The HfF_4 was collected at the bottom of the furnace and the HfC surfaces were practically clean. At 500°C, however, the product was more adhesive, but still no reproducible rate data could be obtained because of the abrupt crumbling of the product layer. From a few initial readings at this temperature, the reaction rate appeared to be linear. At 565°C the HfC began to lose weight and the reaction became smoother. The rate data from 565 - 890°C are given in Table 39. It is clear that the reaction is almost independent of temperature above 650°C and the calculated activation

TABLE 39

RATE DATA ON THE HfC-F$_2$ REACTION

Temperature (°C)	P_{F_2} (Torr)	k_1 (mg/cm^2/min)
565*	2.8	2.0606
650*	2.8	5.3602
720	2.8	6.1400
765	2.8	5.1831
800	6.7	8.2645
800	13.2	11.7140
820	52.5	49.8000
825	2.8	6.3158
890	2.8	6.0800

*Furnace temperature

energy is practically zero. At 565°C the rate is considerably lower, but it must be due to the incomplete volatilization of the HfF$_4$. The reaction rate is directly proportional to the fluorine partial pressure up to 52.5 Torr above 600°C (cf. Figure 43).

Fluorination of HfB$_2$ - Although no measurable reaction occurs between HfB$_2$ and fluorine at low fluorine pressures up to 500°C, the samples break down presumably at pre-existing cracks even at about 350°C at 13.2 Torr fluorine pressure. Small quantities of white HfF$_4$ are found within the cracks, but not on the outer surface. HfB$_2$ begins to lose weight at about 550°C but it stays together even up to 1020°C. The reaction is linear as expected and the rate constants under various conditions are recorded in Table 40. Here again, temperature has practically no effect on the reaction, but the fluorine partial pressure has a marked influence on the reaction.

As the fluorine pressure is increased, there is a proportional rise in the sample surface temperature and above 1000°C sparks begin to appear at the specimen as observed through the optical pyrometer. Shortly after the appearance of the sparks, the nickel wire burns up and the sample falls down. It has to be mentioned that although the sample surface temperatures rose above 1000°C, the actual furnace temperature was never raised above about 900°C. In Table 41 are shown the actual surface temperatures of a sample of weight about 0.7 gm and surface area about 1.3 cm^2 under various fluorine partial pressures at a
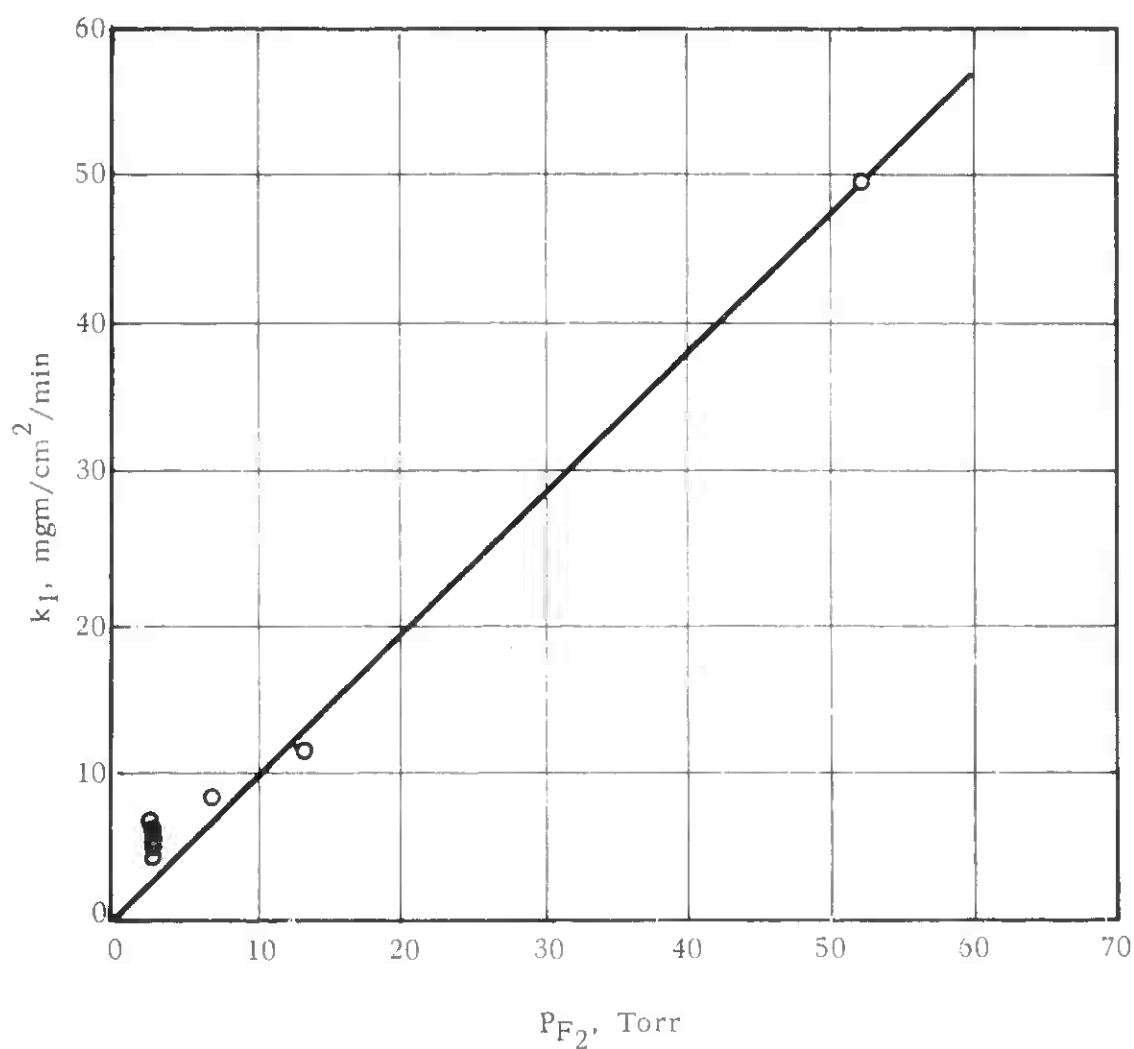
FIGURE 43   EFFECT OF FLUORINE PARTIAL PRESSURE ON THE
                 HfC-F$_2$ REACTION ABOVE 600°C

155

TABLE 40

RATE DATA ON THE HfB_2-F_2 REACTION

Temperature (°C)	P_{F_2} (Torr)	k_1 $(mg/cm^2/min)$
765	2.8	5.3125
830	2.8	5.2439
00	2.8	4.8571
975	2.8	5.1613
810	6.7	6.9231
840	6.7	6.1538
940	6.7	9.3750
1020	6.7	8.8235
610*	13.2	9.8214
835	13.2	7.9412
880	13.2	9.6154
985	13.2	11.8750
610*	30.6	13.5556
890	30.6	12.9545
950	30.6	15.7692
610*	52.5	19.4444

*Furnace temperature

156

furnace temperature of 740°C. Figure 44 is a plot of the rate constants against the square root of fluorine partial pressure. The linearity of the plot indicates that the rate of fluorination of HfB_2 varies directly as the square root of the fluorine partial pressure.

d. Discussion

As expected, the behaviors of both Zr and Hf carbides and borides toward fluorine are similar. The borides of both metals are more resistant to fluorine than the carbides. Whereas the carbides begin to react at around 300°C under low fluorine partial pressure conditions forming solid products, the borides are attacked only above the volatilization points of the metallic fluorides. Thus, a coating of the fluoride is never obtained on the ZrB_2 and HfB_2. At temperatures above 600°C all the reactions are gas diffusion controlled which is characterized by their insensitiveness of the rates to surface temperature changes.

ZrC differs from HfC in that while the former forms thick scales of ZrF_4 below 500°C, the latter does not grow any scales on it. HfB_2 crumbles in fluorine even at low fluorine partial pressure at 350 - 550°C, but the ZrB_2 stays undamaged up to 500°C under the same conditions.

The fluorination of HfC and HfB_2 is much faster than that of ZrC and ZrB_2. Even after converting the rate constants to moles, the rates for HfC and HfB_2 are found to be about four-five times faster than those for ZrC and ZrB_2.

The dependence of the reactions rates on the fluorine partial pressure is also similar for both Zr and Hf carbides and borides, except that ZrC shows a 1.5 order with respect to fluorine while the HfC shows first order.

TABLE 41

SURFACE TEMPERATURES ON HfB_2 SAMPLES WITH VARIOUS FLUORINE PARTIAL PRESSURES AT A FURNACE TEMPERATURE OF 740°C

P_{F_2} (Torr)	Surface Temperature (°C)
0	740
2.8	765
6.7	810
13.2	835
30.6	890

157
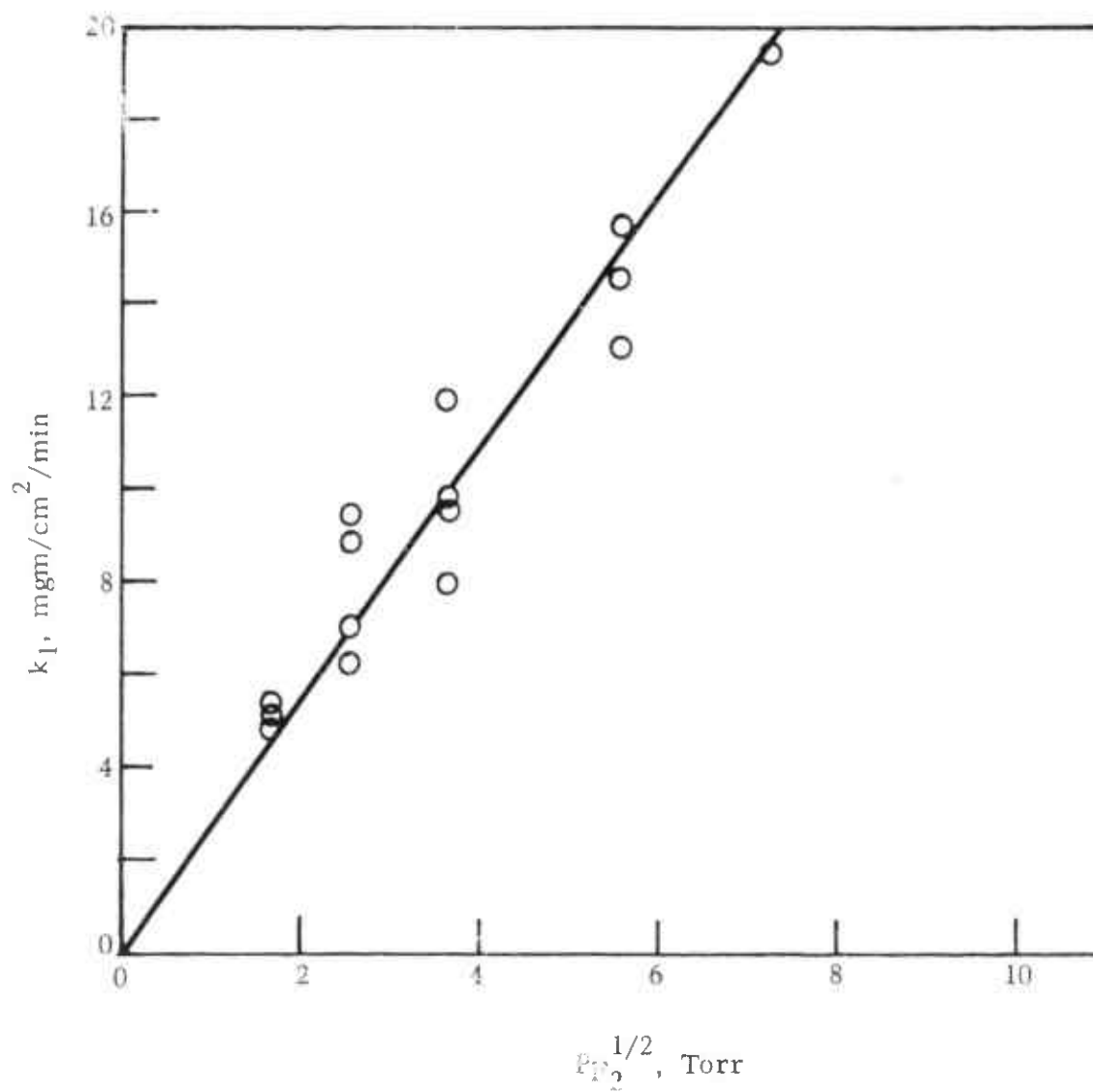
FIGURE 44   EFFECT OF FLUORINE PARTIAL PRESSURE ON THE
HfB$_2$-F$_2$ REACTION ABOVE 600°C

4. Kinetics of the Reaction of Elemental Fluorine With Silicon and Boron*

a. Introduction

Not much is known regarding the interaction of fluorine with silicon and boron except for the early observations of Molssan[107,108] that these materials burn in fluorine at or slightly above room temperature depending on their physical state, with the production of the corresponding gaseous fluorides. The amorphous forms react faster than the crystalline ones and silicon reacts more readily than boron. Although these findings are true, spontaneous ignition of these elements does not occur if the fluorine concentration is limited by reducing the partial pressure appropriately, and under such controlled conditions, the rates of their reactions can be measured by suitable means. This paper presents a study of the kinetics of the fluorination of silicon and boron at temperatures up to about 1000°C and fluorine partial pressures up to 52.5 Torr, using a thermogravimetric method in a continuous flow system.

h. Experimental

Apparatus - A detailed description of the apparatus used and experimental procedure have already been presented in Section 2 of this appendix. The fluorination reactions were carried out in a nickel combustion tube equipped with a quartz spring from which the specimens could be suspended by means of fine nickel wire. The tube was heated vertically in a resistance furnace and the temperature was measured up to 700°C with a platinum vs platinum + 10% rhodium thermocouple (shielded by a nickel tube) and above 700°C with a Micro-Optical Pyrometer by observing the specimen through a glass window attached to the bottom of the combustion tube through a kovar-glass seal. The fluorine, metered through a glass flowmeter with a sapphire float, was mixed with helium in the required proportions to obtain the desired partial pressure before admitting into the combustion tube, and all the experiments were carried out at a total pressure of one atmosphere. The fluorine flow could be controlled to as low a value as 2 ml./min. The weight loss of the specimens was calculated by observing the change in extension of the spring with a cathetometer to an accuracy of ± 0.05 mg. The quartz spring and its glass container were protected from fluorine by a slow counterflow of pure helium.

Materials - Fluorine gas of 99.8+ % purity obtained from the Allied Chemical Corporation was used after passing it through an HF trap containing NaF pellets.

---

*To be presented at the American Chemical Society Meeting, Philadelphia, Pennsylvania, April, 1964.

Polycrystalline boron in the form of rods on 12 micron diameter tungsten substrate filament was obtained from Texaco Experiment Inc. Cylindrical specimens of approximately 1 cm. in length and 0.2 cm. in diameter were made and washed with acetone and benzene and dried. By calculation from the geometrical dimensions, the boron samples had a density of 2.24 ± 0.06 g/cm^3.

The silicon samples were prepared in the forms of thin slices of approximately 1 mm. thickness cut from large crystals of silicon of purity 99.9+% supplied by E. I. du Pont de Nemours, Inc. The specimens had a surface area of about 1.5 cm^2 and a calculated density of 2.1 ± 0.1 g/cm^3.

The surface areas of both boron and silicon were computed from the measured geometrical dimensions. It should be mentioned that the boron surface was obviously rough so that the calculated value could be off by many factors, although the silicon had a smooth, shiny surface.

c. Results

As stated in the introduction, since both silicon and boron ignite spontaneously in pure fluorine around room temperature, the kinetic experiments were carried out at very low fluorine partial pressures. With silicon samples of surface area about 1.5 cm^2, no measurable reaction was observed for a period of one hour below a temperature of about 85°C, with a fluorine partial pressure of 2.8 Torr. Boron (with surface area approximately = 0.7 cm^2) was even more resistant to fluorine under the same partial pressure conditions and measurable reaction was observed only above 300°C. When the fluorine partial pressure is increased, specimens of both silicon and boron break up at around room temperature at an experimental fluorine partial pressure of about 200 Torr. The lower reactivity of boron than silicon with fluorine is in agreement with the observations of Moissan.

The Effect of Temperature - The results of the fluorination of silicon and boron are given in Tables 42 and 43, respectively. The runs, in which the reactions were very fast, were made only for short periods so that surface area changes did not become appreciable. As expected, the reactions are linear and the rate constants were calculated from a plot of the weight loss/cm^2 against time. It may be readily seen from Tables 42 and 43 that the temperature dependence of the reaction decreases appreciably above 170°C for silicon and above 396° for boron.

Figures 45 and 46 are Arrhenius plots for the reactions of silicon and boron respectively, and there is a clear change in the nature of temperature dependence between the low and high temperature regions. For silicon there are two sets of lines corresponding to fluorine partial pressures 2.8 Torr and 13.2 Torr. The solid lines are not exactly parallel to each other in the low temperature

160

TABLE 42

RATE DATA ON THE REACTION BETWEEN SILICON AND FLUORINE

Temperature (°C)	P_{F_2} (Torr)	k_1 (mg/cm^2/min)
75	13.2	0.0659
85	2.8	0.0529
85	13.2	0.1175
95	2.8	0.1005
95	13.2	0.3634
104	2.8	0.1773
120	2.8	0.3409
120	13.2	0.9867
120	30.6	2.4750
120	52.5	4.0250
150	2.8	0.7244
170	2.8	0.8442
170	6.7	1.5170
170	13.2	2.0857
170	30.6	3.7180
170	52.5	5.3186
212	13.2	1.8868
272	2.8	0.9823
272	13.2	2.5466
325	13.2	2.5026
430	13.2	2.5613
500	2.8	1.2030
500	13.2	2.1009
600	2.8	1.5151
600	13.2	3.0270
600	52.5	8.1500
692	2.8	1.8267
795	2.8	1.7241
900	2.8	2.0000

TABLE 43

RATE DATA FOR THE FLUORINATION OF BORON

Temperature (°C)	P_{F_2} (Torr)	k_1 $(mg/cm^2/min)$
300	2.8	0.0292
310	2.8	0.0630
320	2.8	0.1130
336	2.8	0.2708
336	13.2	0.8000
336	52.5	3.9000
396	2.8	0.5810
396	13.2	1.5762
396	52.5	4.9396
500	2.8	0.6449
500	13.2	1.6304
500	30.6	3.2103
500	52.5	5.2788
608	2.8	0.9746
683	2.8	0.9904
765	2.8	1.3250
870	2.8	1.2370
970	2.8	1.3889
995	2.8	1.2500
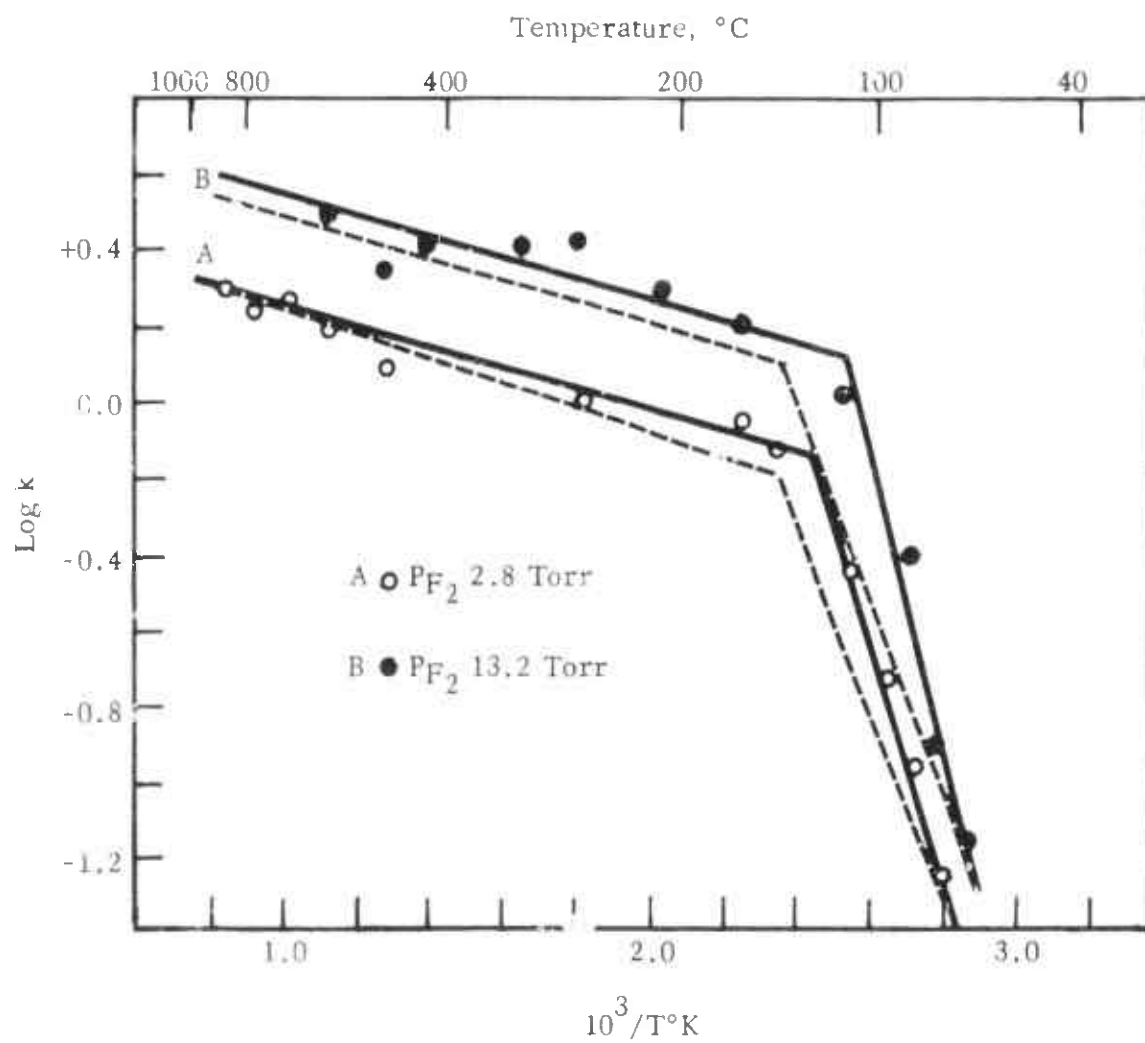
FIGURE 45   ARRHENIUS PLOT FOR THE SILICON-FLUORINE
REACTION FROM 75-900°C
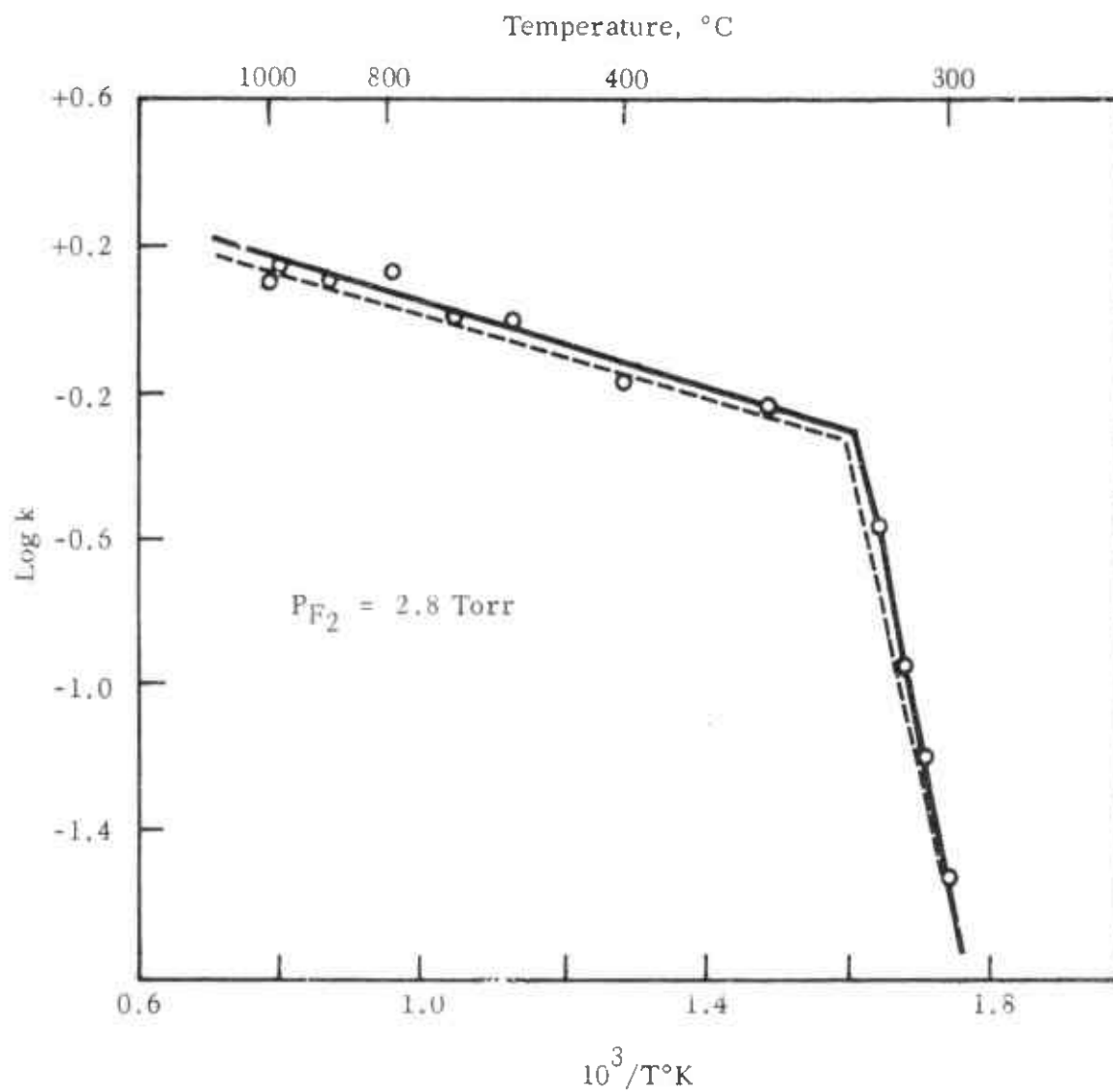
FIGURE 46   ARRHENIUS PLOT FOR THE BORON-FLUORINE
REACTION FROM 300-995°C

164

regions and the calculated activation energies are, respectively, 15.7 and 18.7 kcal/mole at 2.8 and 13.2 Torr, although the upper portions of the lines yield a value of 1.3 kcal/mole for both pressures. For boron, corresponding to the two portions of the line, the activation energies are 42.7 and 2.7 kcal/mole. On considering the values for silicon one notes an increase in activation energy with increase of fluorine partial pressure in the low temperature region. This must be attributed to the surface effects which are associated with the fluorination processes. Since temperature measurements below 700°C were made using a thermocouple, the measured values could be lower than the actual surface temperatures of the samples under the fluorination conditions. This was very clearly seen for runs above 700°C where the actual surface temperature before and during fluorination could be recorded with an optical pyrometer. Temperature rises of the order of 50 and 35°C were observed for silicon and boron, respectively, at furnace temperatures of 745 and 730°C at 2.8 Torr fluorine pressure. The reaction temperatures above 700°C given in Tables 42 and 43 are the actual sample surface temperatures while those below 700°C are the furnace temperatures.

Since all the specimens of silicon or boron used had nearly equal surface areas and masses, a rough approximation may be made that the temperature rise in each case was proportional to the rate constant, assuming specific heat and heat loss considerations remain nearly constant. Based on this assumption, the actual surface temperature rise at 85°C would be only 1.5° and that at 120° would be about 9.9°C so that the activation energy after applying the corrections (obtained from the dotted line, A, in Figure 45) would be only 12 kcal/mole instead of 15.4. Similarly applying the temperature correction for the reaction at fluorine partial pressure, 13.2 Torr, the activation energy becomes 12 kcal/mole (obtained from dotted line, B, in Figure 45) which is the same as that at 2.8 Torr. For boron, after applying similar corrections for temperature effects, the experimental activation energy of 42.7 kcal/mole comes down to 37.9 kcal/mole (corresponding to the lower portion of the dotted line in Figure 46). The greater activation energy for the boron-fluorine reaction is in keeping with the observation that silicon reacts faster and at lower temperatures.

From Figures 45 and 46 it is possible to make an estimation of the temperature at which the break in the temperature dependence occurs. For silicon, at 2.8 Torr and 13.2 Torr fluorine partial pressures, the change takes place, respectively, at 131° and 118°C experimentally. This difference vanishes when the correction for temperature rises at the sample surfaces are applied as indicated earlier and the transition temperature becomes 150 ± 5°C at both the fluorine partial pressures, corresponding to the breaks in the dotted lines A and B in Figure 45.

In the case of boron the experimental transition temperature of 344°C works out to be 352°C after the correction. Above these transition points the activation energies are very low--1.3 kcal/mole for silicon and 2.5 kcal/mole for boron. The abrupt changes in the activation energies indicate a definite change in the mechanism of fluorination between the two temperature regions.

165

The Effect of Pressure - The variation of the fluorination rates with fluorine partial pressure between 2.8 Torr and 52.5 Torr was examined at various temperatures for silicon and boron. Figures 47 and 48 illustrate the pressure dependence of the reactions at various temperatures for these elements. For silicon the reaction is fractional in order, viz., about 0.6 at 170 and 600°C, but first order at 120°C, with respect to the fluorine partial pressure while for boron it is first order at all temperatures studied.

The change in order with respect to the fluorine partial pressure from fractional to unity in the case of silicon-fluorine reaction at low temperature is probably only apparent. None of these experiments with various partial pressures at the same temperature could be done under strictly isothermal conditions because of the surface temperature changes during the reaction. This defect, however, does not seriously affect the determinations above the t .isition points where the temperature effect is very small. Therefore, the observed order of one at 120°C for the $Si-F_2$ reaction must be considered incorrect and the fractional order at higher temperatures as the true dependence of fluorine partial pressure.

d. Tentative Reaction Mechanisms

The reactions of fluorine with silicon and boron are very similar to the oxidation of carbon which has been the subject of investigation by various workers.[109-115] Temperature effects very similar to those observed in the present investigation have been reported by all these workers.

When considering the reaction between a solid and a gas to produce only gaseous products the various steps in the reaction may be assumed to be as follows:

(1) diffusion of the reacting gas to the surface of the solid across the gaseous products,

(2) adsorption of the gas at the surface which involes (a) possibly the dissociation of the gas molecules and (h) formation of an activated complex,

(3) decomposition of the activated complex to form the primary reaction products,

(4) the desorption of the product molecules, and

(5) diffusion of the product molecules away from the solid surface.

166
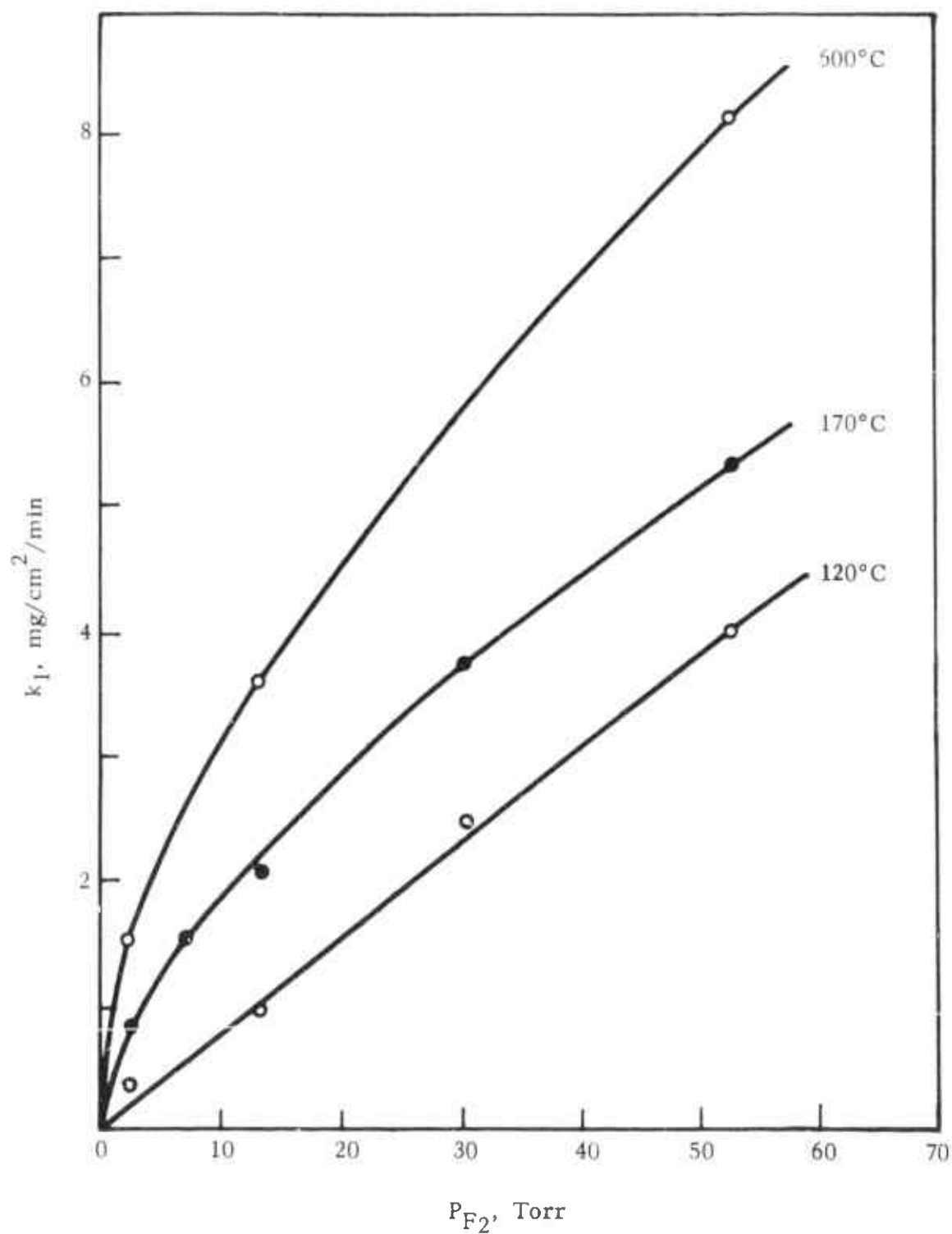
FIGURE 47   EFFECT OF FLUORINE PARTIAL PRESSURE ON THE
Si-F_2 REACTION

167
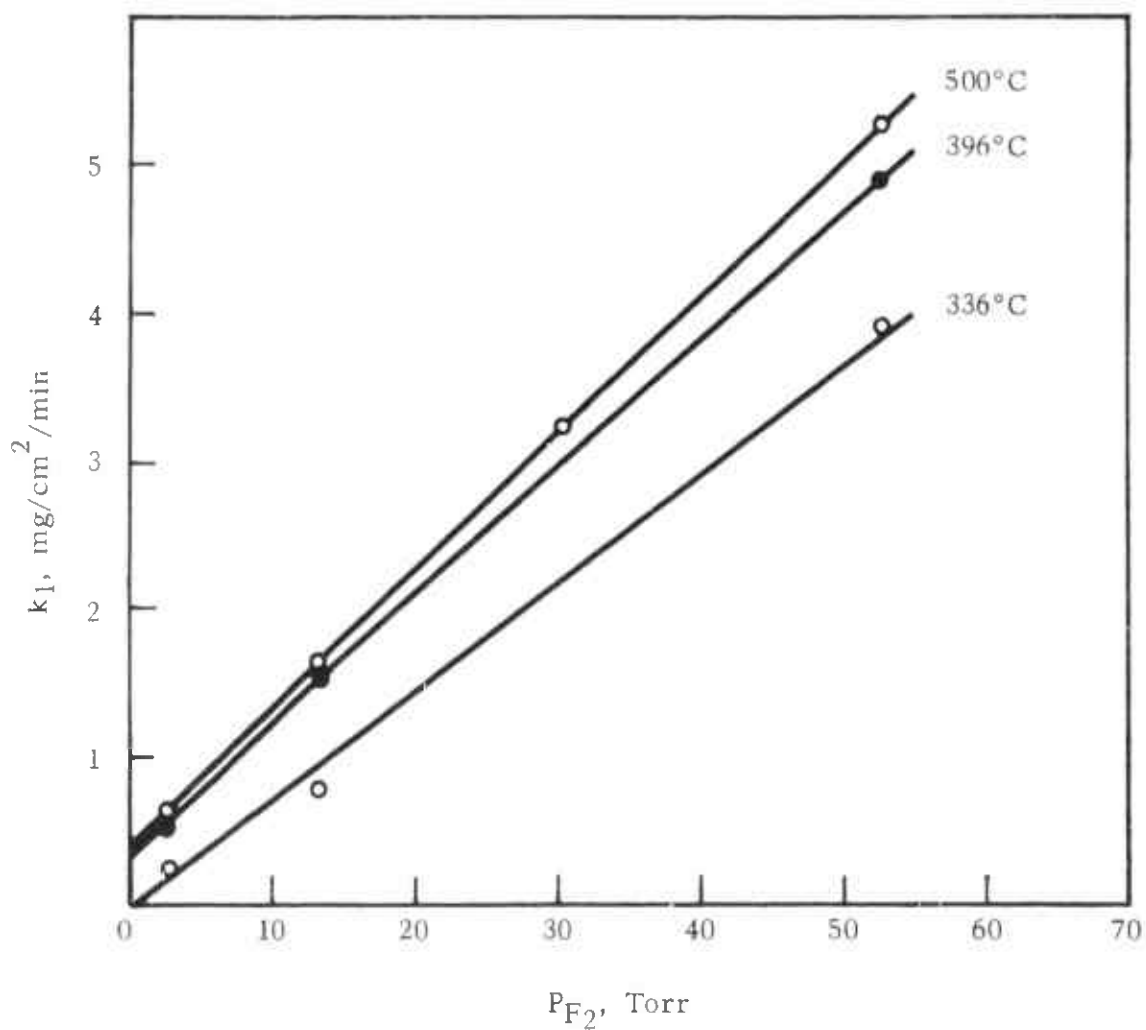
FIGURE 48   EFFECT OF FLUORINE PARTIAL PRESSURE ON THE
RATE OF BORON-FLUORINE REACTION

168

When the reaction rate is small, i.e., in the lower temperature regions, steps (1) and (5) will not be rate-determining because of the formation of only small quantities of the products as compared to the amounts of reacting gas. Under these conditions the reaction kinetics will be controlled by one or more of steps (2), (3) and (4). By consideration of the high affinity of fluorine for silicon and boron, one tends to believe that all of the adsorbed molecules should react, i.e., the activated complexes, once formed, predominantly decompose to yield the products rather than going back to elemental fluorine. This step may be assumed very fast and, hence, not involved in the rate-determining process. Since the reactions of both silicon and boron are pressure dependent, it is reasonable to assume that step (2) is rate-determining in the reactions and not step (4). Thus, the observed activation energies ($\sim$12 and $\sim$38 kcal/mole) are presumably the heats of adsorption of fluorine on silicon and boron, respectively.

The dissociation energy of fluorine, 37.7 kcal/mole,[116] is very close to the observed activation energy for the boron-fluorine reaction which suggests that the fluorine molecules are completely dissociated on the surface of boron. In the case of silicon the much lower activation energy may be assumed to indicate that the activated complex is something of the form $Si-F_2$ rather than $Si-F$. The primary products of the reactions, thus, could be BF and SiF_2.

Although the exact identity of the primary products is unknown, it is reasonable to think that these are BF (gas) and SiF_2 (gas), since there is spectroscopic evidence for the existence of BF (gas) and SiF_2 and SiF_2 polymers have been obtained at high temperatures by mass spectrometric studies,[117] spectroscopic studies,[118,119] and transpiration studies[120] with Si and SiF_4. The final products detected in the fluorination of boron and silicon are BF_3 and SiF_4 and these, we assume, are formed by the gas phase or surface reaction between BF and F_2 or SiF_2 and F_2. It has not yet been possible, however, to chill the BF and SiF_2 formed (if any) as soon as the reaction occurred at the surface. Infrared and ultraviolet spectrophotometric and mass spectrometric studies involving elemental fluorine presents various problems and, hence, it is hard to ascertain the exact nature of the primary reaction products in these fluorination reactions.

It has been shown above that the fluorination reactions of silicon below 150° and of boron below 352°C are apparently controlled by an adsorption process. This point is also indicated by the rounding off of sharp edges on the samples which are highly active centers for adsorption, during the reaction. At about the transition temperatures, the reactions have become fast enough for the products to be formed in amounts comparable to that of fluorine and, hence, diffusion of fluorine molecules through the outgoing product molecules becomes a slow process compared to the other steps of the reaction. The reactions, therefore, are now controlled only by the diffusion of fluorine through the product gas layer, for which

the energy of activation must be very low. The observed values are only 1.3 kcal for silicon and 2.5 kcal for boron. It has also been observed that a change in mechanism takes place when the rate is higher (1.2450 mg cm^{-2} min^{-1}) in the case of the reaction of silicon with fluorine partial pressure 13.2 Torr than that at 2.8 Torr (0.6166) which further indicates that diffusion processes play a significant role in determining reaction rates.

5. The Fluorination of Graphite

a. Introduction

Although amorphous forms of carbon burn in fluorine at room temperature, graphite and diamond are not attacked by fluorine at ordinary temperatures.[121] Ruff and Bretschneider[122] have found that around 420°C graphite reacts with fluorine to form a gray product which they called carbon monofluoride (C_xF_x). From 460° to 700°C the reaction is explosive and at about 700°C graphite burns in fluorine with the production of fluorocarbons, mainly CF_4. Later work by Rüdorff and Rüdorff[123-125] showed that, depending on the temperature (between 410° and 550°C) and the particle size of graphite, various compositions from $CF_{0.68}$ to $CF_{0.988}$ could be obtained and that hydrogen fluoride was a catalyst in the reaction. They[125,126] also synthesized another solid product of composition approximately C_4F in the presence of F_2 and HF at temperatures below 75°C. Our investigation was undertaken with a view to understanding more about the graphite-fluorine reaction under various conditions of temperature and pressure by measuring the rate of fluorination. Spectroscopic grade graphite was used.

b. Experimental

The apparatus and general experimental procedure have been described earlier in Section 2 of this report. The only modification was that for runs below 600°C a small aluminum or nickel cup was attached beneath the graphite samples in order to collect any falling particles from the specimen, and the sample together with the cup was suspended from the quartz spring balance. The reaction of the aluminum or nickel cup was negligibly small compared to the fluorination rate of graphite under the conditions using the cup.

The samples were cut from a single spectroscopic electrode of about 9 mm. diameter manufactured by the National Carbon Company. The circular pieces, about 2 mm. thick, were polished on abrasive cloth and finally on ordinary cloth. The surfaces were then cleaned with a blast of hot air to remove any adhering loose particles. The areas of the specimens were calculated from average micrometer readings of the diameter and the thickness.

c. Results

No measurable reaction occurred between graphite and fluorine up to about 300°C and one atmosphere fluorine pressure. Detectable reaction started at about 315°C at a low fluorine pressure of 13.2 Torr and the kinetic studies were carried out between 315° and 900°C.

The reaction rate is linear under all experimental conditions except for an initial fast spurt which we assume to be the reaction of loose graphite dust still within the pores of the graphite. The linear rate constants were calculated only after the fast reaction had subsided. After taking the necessary kinetic readings at the required fluorine partial pressure, the fluorination was completed by increasing the fluorine pressure to one atmosphere. From the weight gain data, up to about 530°C, carbon monofluoride with compositions ranging from $CF_{0.65}$ to $CF_{0.8}$ was the product with the higher fluorine content being obtained at the higher temperature. The product was collected in the attached cup and was gray in color. A small quantity of the product was obtained also at 600°C which was white in color. An infrared spectrum of the product showed a single absorption band at 1220 cm^{-1} characteristic of the carbon monofluoride polymer.[125,127]

The kinetic data on the fluorination of graphite from 315° to 900°C are presented in Table 44. The rate constants are given in terms of the amount of graphite reacted in mg/cm^2/min. Figure 49 is an Arrhenius plot of the results at a fluorine partial pressure of 13.2 Torr. Up to 530°C the points represent weight gain and above 600°C, weight loss data. From 315° to 410°C there is a rapid increase in the reaction rate with an activation energy of 42.5 ± 2 kcal/mole, while the portion between 410 and 493 is practically independent of temperature with an activation energy of only about 2 kcal/mole. There is a slight decrease in the rate at about 530°C using the weight gain data which indicates that both the monofluoride and volatile products are formed simultaneously at this temperature. Thus, there is an overlapping of two types of reactions between 530° and 650°C.

The behavior of the reaction at 570°C is particularly interesting. Up to a partial pressure of about 30.6 Torr the graphite gains weight in fluorine and above 40.5 Torr it loses weight while in the region of about 35 Torr it neither gains nor loses. The reason is that under the latter conditions the rate of formation of graphite monofluoride is equal to the rate of formation of the volatile products. Thus, the pressure coefficient for the burning of graphite in fluorine has, apparently, a higher value than for the formation of the monofluoride at and above 570°C.

Above 650°C no solid products are observed and the activation energy up to 900°C is only about 2.5 kcal/mole which shows that the reaction is controlled probably by the gas phase diffusion of fluorine to the surface. The low activation energy of 2 kcal/mole in the temperature range 410 - 493° is hard to explain because gas phase diffusion cannot be a rate determining step since the

TABLE 44

KINETIC DATA ON THE GRAPHITE-FLUORINE REACTIONS

Temp (°C)	P_{F_2} (Torr)	k_1 (mg/cm²/min of graphite)	Remarks	Temp (°C)	P_{F_2} (Torr)	k_1 (mg/cm²/min of graphite)	Remarks
315	13.2	0.00821	wt. gain	486	30.6	1.0657	wt. gain
315	52.5	0.02005	"	486	52.5	1.7223	"
315	74.7	0.02849	"	486	74.7	2.4558	"
333	13.2	0.01746	"	493	13.2	0.6558	"
333	52.5	0.04510	"	493	30.6	1.1515	"
333	74.7	0.08710	"	493	52.5	1.8287	"
360	13.2	0.1232	"	493	74.7	2.2488	"
360	13.2	0.1362	"	530	13.2	0.5326	"
360	21.2	0.2105	"	530	30.6	0.8096	"
360	30.6	0.3277	"	530	52.5	1.4472	"
360	52.5	0.4758	"	530	74.7	1.8774	"
360	52.5	0.4390	"	570	13.2	-	"
360	74.7	0.8201	"	570	30.6	-	"
396	2.8	0.2631	"	570	35.5	-	no wt. change
396	13.2	0.4511	"				
396	30.6	0.8611	"	570	52.5	-	wt. loss
396	52.5	1.1051	"	570	74.7	-	"
396	74.7	1.6577	"	600	6.5	0.3273	"
411	13.2	0.5572	"	600	6.5	0.2857	"
411	30.6	0.7104	"	600	13.2	0.6546	"
411	52.5	1.5787	"	600	30.6	1.0270	"
411	74.7	2.6718	"	600	52.5	1.9167	"
422	13.2	0.5732	"	650	6.5	0.5250	"
422	30.6	0.9317	"	650	13.2	1.0400	"
446	13.2	0.5851	"	650	30.6	2.4000	"
446	30.6	1.1493	"	650	52.5	3.6471	"
446	52.5	1.6665	"	700	6.5	0.5567	"
446	74.7	2.2669	"	700	13.2	1.0934	"
464	13.2	0.6093	"	750	6.5	0.6250	"
464	30.6	1.0811	"	750	13.2	1.1920	"
464	52.5	1.7103	"	800	6.5	0.6522	"
464	74.7	2.2390	"	800	13.2	1.3244	"
486	13.2	0.5671	"	900	6.5	0.6727	"
				900	13.2	1.5000	"
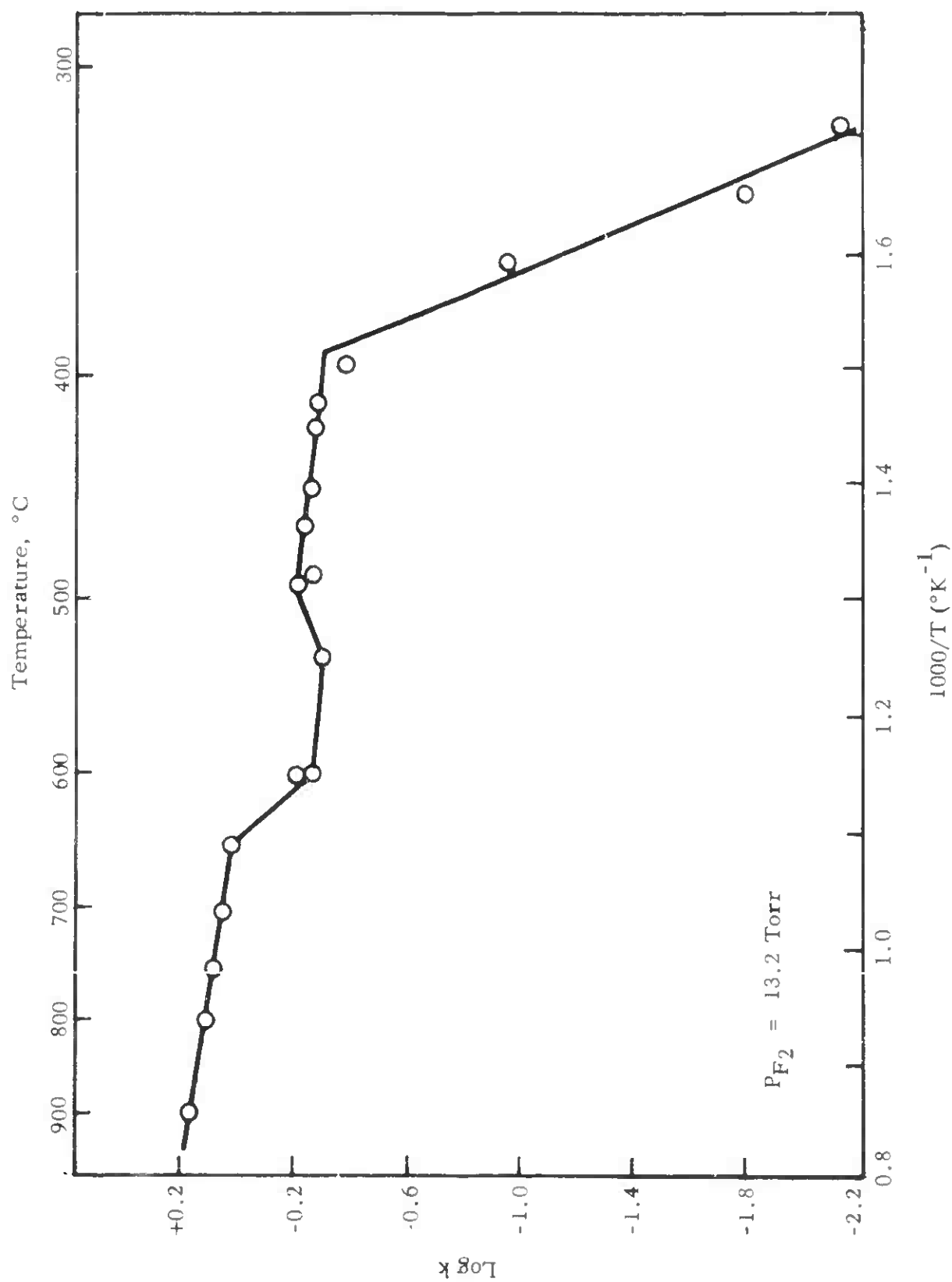
FIGURE 49   EFFECT OF TEMPERATURE ON THE GRAPHITE-FLUORINE REACTION

173

gaseous products formed are negligible. However, at and above 410°C the carbon monofluoride formed is immediately detached from the surface of the graphite substrate and this might necessitate some kind of diffusion across a barrier which could be rate controlling. Below 410°C the reaction is probably controlled by chemisorption with the relatively high activation energy of 42.5 kcal/mole. Diffusion of fluorine through the outer layers of the graphite could also be playing a part in the reaction since the specimens were initially found to expand rather than lose the product layer. At higher temperatures no such expansion was observed.

Variation of the fluorine partial pressure between 2.8 and 74.7 Torr indicated that throughout the temperature range studied the reaction rate was directly related to the pressure.

B. THERMODYNAMIC PROPERTIES OF INORGANIC SUBSTANCES

1. The High Temperature Heat Content of Zirconium Diboride by Robert H. Valentine, Thomas F. Jambois and John L. Margrave

a. Introduction

The high temperature heat content of a high-purity sample of ZrB_2 (see Section III B-1 of this report) was measured in a copper-block drop calorimeter over the range 410 - 1125°K. The results were presented in the previous report (ASD-TDR-62-204, Part II)[15] published in May 1963 and are repeated in Table 45. During this report period thermodynamic properties over the range 0 - 2000°K were derived based on experimental data up to 1200°K and on extrapolations of computer-selected fits of the experimental points to combinations of Einstein and/or Debye functions.

b. The Computational Program

A computer program has been developed for selecting combinations of Debye and/or Einstein functions to fit the experimental points and, in this way, to make possible extrapolations to high temperatures with somewhat more confidence than with the empirical Kelley equation. One of the basic problems is a choice of the proper functional representation and runs were made in which either heat contents (or heat capacities) were fitted to three equations:

$$(1) \quad Cp = D(\theta_1/T) + 2D(\theta_2/T) + aT$$

$$(2) \quad Cp = D(\theta_1/T) + 2E(\theta_2/T) + aT$$

$$(3) \quad Cp = [D(\theta_1/T) + 2D(\theta_2/T)][1 + aT] + bT$$

174

TABLE 45

EXPERIMENTAL HEAT CONTENTS OF ZrB_2

T (°K)	T_{cal} (°K)	$H_T - H_{T_{cal}}$ (cal mole^{-1})
410.46	298.60	1510
463.46	298.69	2204
553.76	298.93	3564
598.66	298.81	4288
711.06	298.89	5926
773.06	298.97	7114
450.02	297.88	1998
514.25	298.92	3017
724.16	299.44	6031
888.46	299.26	8782
986.46	299.02	10626
1123.46	299.17	12781
1125.62	299.17	13000

175

These first two equations neglect differences between Cp and Cv to a first approximation while the third represents an effort to allow for this difference by introducing the additional constant. Kaufman[128] has suggested the value $a \approx 10^{-4}$ for borides and carbides, in lieu of the necessary experimental data, by comparison with data for metals.

The low-temperature Cp-data of Westrum and Feick[9] have been fitted over the range $0 - 350°K$ with these three equations with absolute rms deviations $\approx 0.03 - 0.06$ cal deg^{-1} mole^{-1}. Results based on fits of the low temperature data only are presented in Table 46. The combination of high and low temperature data lead to the three following "best fits":

(1) $Cp + D(1550/T) + 2D(670/T) + 7.58 \times 10^{-6} T$ cal deg^{-1} mole^{-1}

which reproduces $(H_T - H_{298})$ with a rms deviation of ± 49 cal mole^{-1} over the range $0 - 1125°K$ and predicts $S^o_{298} = 8.52$ cal deg^{-1} mole^{-1}.

(2) $Cp = D(1570/T) + 2E(500/T) + 1.47 \times 10^{-5} T$ cal deg^{-1} mole^{-1}

which reproduces $(H_T - H_{298})$ with a rms deviation of ± 51 cal mole^{-1} over the range $0 - 1125°K$ and predicts $S^o_{298} = 7.94$ cal deg^{-1} mole^{-1}.

(3) $Cp = [D(360/T) + 2D(1530/T)] [1 + 10^{-4} T] + 4.85 \times 10^{-5} T$

cal deg^{-1} mole^{-1} which reproduces $(H_T - H_{298})$ with a rms deviation of ± 12 cal mole^{-1} over the range $0 - 1125°K$ and predicts $S^o_{298} = 8.89$ cal deg^{-1} mole^{-1}.

Of these three equations the first two give the best fits while the last has a form more consistent with theory and Debye θ's closer to those predicted from considerations of the elements. Also, the trend in Cp at high temperatures $(1500 - 2000°K)$ is in the direction indicated by the work of Prophet[129] over the range $1300 - 2150°K$ although his experimental data are uncertain by $\pm 10\%$. Table 47 presents thermodynamic functions based on experimental data up to $1200°K$ and on the average extrapolations of the computer-selected fits up to $2000°K$.

For comparison, high temperature heat capacities based on all the available measurements on ZrB_2 samples are tabulated in Table 48. The discrepancies clearly show the need for further studies, especially at temperatures over $1200°K$, on well-characterized samples of ZrB_2.

TABLE 46

PROPERTIES OF ZrB$_2$ DERIVED FROM LOW TEMPERATURE DATA

Equation	$C_p(298)$ (cal deg^{-1} mole^{-1}) Exptl.	Calc.	$H_{298} - H_0$ (cal mole^{-1}) Exptl.	Calc.	S^o_{298} (cal deg^{-1} mole^{-1}) Exptl.	Calc.	$C_p(2000°K)$ (cal deg^{-1} mole^{-1}) (Calc.)	$H_{2000} - H_{298}$ (cal mole^{-1}) (Calc.)
$C_p = D(500/T) + 2D(1190/T)$ $+ 9.93 \times 10^{-4}\,T$	11.53	11.51 ±0.04	1590	1594	8.59	8.68 ±0.1	19.64	30,180
$C_p = D(440/T) + 2E(860/T)$ $+ 2.43 \times 10^{-5}\,T$	11.53	11.59 ±0.06	1590	1591	8.59	8.67 ±0.1	17.74	28,510
$C_p = [D(490/T) + 2D(1200/T)]$ $[1 + 10^{-4}\,T] + 4.86 \times 10^{-5}\,T$	11.53	11.53 ±0.03	1590	1593	8.59	8.46 ±0.1	21.28	31,660

TABLE 47

SMOOTHED THERMODYNAMIC FUNCTIONS FOR ZrB$_2$*

T (°K)	H°$_T$ − H°$_{298.15}$ (cal mole^{-1})	C°$_p$ (cal deg^{-1} mole^{-1})	S$_T$ − S$_{298}$ (cal deg^{-1} mole^{-1})	$-\left(\dfrac{G^o_T - H^o_{298.15}}{T}\right)$
0	− 1590	0	− 8.59	∞
50	− 1585	0.503	− 8.45	31.83
100	− 1503	2.870	− 7.42	16.21
150	− 1296	5.410	− 5.77	11.46
200	− 964	7.840	− 3.57	9.53
250	− 518	9.919	− 1.89	8.77
298.15	0	11.53	0	8.59
300	21	11.59	0.07	8.60
350	635	12.88	1.96	8.74
400	1327	13.77	3.82	9.09
500	2754	14.70	7.00	10.08
600	4258	15.34	9.74	11.23
700	5818	15.85	12.14	12.42
800	7426	16.29	14.29	13.60
900	9075	16.69	16.23	14.74
1000	10764	17.07	18.01	15.84
1100	12489	17.43	19.65	16.89
1200	14249	17.77	21.18	17.90
1300	(16,140 ± 200)	(18.3 ± 0.6)	(21.9 ± 0.5)	(18.1 ± 0.5)
1400	(17,950 ± 300)	(18.5 ± 0.6)	(23.2 ± 0.5)	(19.0 ± 0.5)
1500	(19,770 ± 400)	(18.7 ± 0.8)	(24.4 ± 0.5)	(19.8 ± 0.6)
1600	(21,600 ± 500)	(18.9 ± 0.8)	(25.5 ± 0.5)	(20.6 ± 0.6)
1700	(23,710 ± 600)	(19.0 ± 1.0)	(26.6 ± 0.5)	(21.3 ± 0.8)
1800	(25,620 ± 700)	(19.2 ± 1.2)	(27.6 ± 0.5)	(22.0 ± 0.8)
1900	(27,540 ± 800)	(19.3 ± 1.5)	(28.5 ± 0.5)	(22.6 ± 1.0)
2000	(29,470 ± 1000)	(19.4 ± 1.5)	(29.4 ± 0.5)	(23.2 ± 1.0)

*Data from 0 − 350°K based on reference 9; from 350 − 1200°K based on this work; above 1200°K the parentheses indicate functions based on an average of the computer-selected Debye-Einstein fits and estimated confidence limits.

TABLE 48

A COMPARISON OF REPORTED HIGH TEMPERATURE HEAT CAPACITIES FOR ZrB_2

C_p in cal deg^{-1} $mole^{-1}$

T°K	Krestovnikov[130]	SRI[131]	Barnes et al.[132]	AVCO[133]	Prophet[129]	Westrum[9]	This Work
298.15	(14.41)	---	(13.1)	---	(10.55)	11.53	(11.53)
500	15.77	11.52	16.50	---	(14.06)	---	14.70
1000	17.74	19.36	19.66	---	(20.22)	---	17.07
1500	17.70	21.50	---	---	21.37	---	(18.7 ± 0.8)
2000	(15.64)	23.50	---	38.37*	22.99	---	(19.4 ± 1.5)
2500	---	25.20	---	41.76*	---	---	---

( ) Indicate extrapolated values, often beyond reliable limits of equations used.

*These excessively high results probably arise because no correction for sublimation of the sample was made.

2. The High Temperature Heat Contents of Zirconium Carbide and Tantalum Carbide by Reiji Mezaki, Thomas F. Jambois and John L. Margrave

The high temperature heat contents of powdered ZrC and TaC supplied by Carborundum Company were determined in a copper-block, drop-type calorimeter over the range 366 - 1200° and 476 - 1113°K, respectively and presented in the previous report.[15] The data were utilized, along with the low temperature results of Westrum and Feick[19] for ZrC and of Kelley[134] for TaC, to select a set of thermodynamic functions for the range 0 - 2000°K. Within ± 24 cal/mole the heat contents may be derived by integrating the functions

$$C_p (TaC) = D(300/T) + E(950/T) + 2.287 \times 10^{-3}T \text{ cal/mole}$$

and

$$C_p (ZrC) = D(550/T) + E(650/T) + 1.014 \times 10^{-3}T \text{ cal/mole}$$

over the range 0 - 1200°K.

3. Further High Temperature Studies of Zone-Melted HfB$_2$, HfC and ZrC

A powdered sample of HfB$_2$ was studied previously by Barnes et al.[132] and the results reported. Westrum and associates have completed low temperature studies of zone-melted ZrC, HfB$_2$, and HfC and the high-purity samples are now on hand for high temperature heat content studies.

Because of the shift of our laboratory to Rice University, our calorimeter was disassembled and the opportunity was taken to remodel the apparatus in the course of reassembly. The remodeled instrument will be suitable for studies up to nearly 2000°K and will utilize induction heating of the samples. No new data can be reported at this time but work is in progress and will continue until the thermodynamic properties of these materials are well established. This will form a significant part of the Ph.D. thesis to be submitted by A. Chaudhuri to the Chemistry Department at Rice University sometime early in 1965.

4. Estimation of S^o_{298} for Refractory Solids hy Thomas F. Jambois and John L. Margrave

Estimation procedures for S^o_{298} and C^o_{p298} are of great value in high temperature studies because so many refractories have not been the subject of extensive low temperature calorimetric work. For example, the only borides for

which low and high temperature data are available are ZrB_2 and HfB_2;[9,19,132,135] some nitrides which have been studied at low and high temperatures are BN, AlN, TiN, VN and ZrN and some of the carbides for which complete data are available are TiC, ZrC, VC and TaC.[136,12] Among those substances for which high temperature but no low temperature data are available are HfN, NbN, TaN, HfC, TiB_2, HfB_2, NbB_2, TaB_2, CrB_2 and MoB_2.[12,128,131-133,135,136] (Editor's note, low temperature data for HfC and HfB_2 are presented in Appendix III of this report.)

The first goal in this work was to develop a "best" fitting combination of Debye and/or Einstein functions by a machine selection process and see how well this reproduced S^o_{298} and C^o_{p298} for a series of compounds for which both low and high temperature data were available. The approximations tested were

(1) $C_p = xD(\theta/T) + aT$

(2) $C_p = xD(\theta/T) + aT^{3/2}$

(3) $C_p = xD(\theta/T) + aT \log T$

(4) $C_p = xD(\theta/T) + aT^u \quad u = 0.1, 0.2, \ldots \ldots 2.9, 3$

(5) $C_p = D(\theta_1/T) + (x-1)D(\theta_2/T) + aT$

(6) $C_p = D(\theta_1/T) + (x-1)E(\theta_2/T) + aT$

(7) $C_p = [D(\theta_1/T) + (x-1)D(\theta_2/T)][1 + aT] + bT$

where θ_1 is an empirical Debye (or Einstein) characteristic temperature, x is the number of atoms/molecule, and a and b are constants. For the first four approximations, θ and a were found by an iterative process using the rms deviation from the experimental high temperature points as a criterion for choosing the "best" theta and "best" a.

For the fifth and sixth approximations, θ_1 and θ_2 were allowed to vary from 50 - 2000°K by increments of 50°K and for each different pair of θ's a least squares fit to the heat content data was used to find a and the rms deviation was computed. Then, each 1600-entry table was searched to find the best θ's and a's.

The first six equations neglect differences between C_p and C_v to a first approximation. The seventh equation represents an effort to allow for this difference by introducing an additional constant.

181

It was found that none of the methods gave reliable values for $S_{298}-S_O$ if only data above $300 - 400°K$ were used. However, if just <u>one</u> point in the very low temperature range was added, say $H^O_{298}-H^O_{50}$, then the calculated C_ρ and entropy at $298°K$ as well as throughout the whole low temperature region, came much closer to the measured values.

In Table 49 are summarized results for refractory solids based on experimental high temperature data plus, in several cases, either an estimated value for $(H_{298}-H_{50})$ or actual low temperature data.

Ultimately one would hope that the excellent fitting of thermodynamic data over wide ranges of temperature by combinations of Debye and Einstein functions might yield θ's which were unique and related to the structure and properties of the solid. Kaufman[128] has estimated thermodynamic functions by selecting appropriate θ's based on the Lindemann formula (lattice parameters and melting points) and shown that such an approach is sometimes reliable to $\pm 10\%$ for heat capacities and entropies at high temperatures. S^O_{298}-values predicted may be in error by $20-30\%$, however.

TABLE 49

S^O_{298} FOR REFRACTORY SOLIDS

A. Diborides

	Data Used	rms Deviation	S^O_{298} (calc)** (cal deg^{-1} mole^{-1})	S^O_{298} (exptl) (cal deg^{-1} mole^{-1})	Quality*** of Fit
CrB_2	Est. 50° + HT	55	6.83 – A		
	Est. 50° + HT	55	6.36 – B	No data available	
	HT only	79	6.84 – A		
	Latimer's Rule*		(7.2)		
TiB_2	Est. 50° + HT	59	7.63 – A		FAIR
	Est. 50° + HT	59	7.15 – B	6.808	GOOD
	HT only	319	7.98 – A		POOR
	Latimer's Rule*		(6.8)		GOOD
VB_2	Latimer's Rule*		(7.1)	No data available	
MoB_2	Est. 50° + HT	102	7.66 – A		
	Est. 50° + HT	101	7.69 – B	No data available	
	HT only	214	7.9 – A		
	Latimer's Rule*		(8.9)		
ZrB_2	LT + HT	76	8.41 – A		GOOD
	LT + HT	76	8.09 – B		GOOD
	LT + HT	286	8.25 – C		FAIR
	HT only	68	8.93 – A		GOOD
	LT Cp	0.05	8.68 – A	8.586	GOOD
	LT Cp	0.08	8.67 – B		GOOD
	LT Cp	0.04	8.46 – C		GOOD
	50° + HT		8.34 – A		GOOD
			7.96 – B		FAIR
	Latimer's Rule*		(8.7)		GOOD
NbB_2	Est. 50° + HT	62	11.84 – A		BAD
	Est. 50° + HT	66	12.55 – B	8.91	BAD
	HT only	113	6.6 – A		BAD
	Latimer's Rule*		(8.8)		GOOD
WB_2	Latimer's Rule*		(10.6)	No data available	
HfB_2	Est. 50° + HT	73	9.51 – A		FAIR
	Est. 50° + HT	74	8.69 – B	10.24	POOR
	HT only	97	8.35 – A		POOR
	Latimer's Rule*		(10.4)		GOOD

183

TABLE 49 (Continued)

A. Diborides (cont.)

	Data Used	rms Deviation	S^o_{298} (calc)** (cal deg^{-1} mole^{-1})	S^o_{298} (exptl) (cal deg^{-1} mole^{-1})	Quality*** of Fit
TaB$_2$	Est. 50° + HT	87	8.98 – A		POOR
	Est. 50° + HT	86	8.70 – B	10.57	POOR
	HT only	131	8.78 – A		POOR
	Latimer's Rule*		(10.5)		GOOD

B. Monocarbides

	Data Used	rms Deviation	S^o_{298} (calc)**	S^o_{298} (exptl)	Quality of Fit
TiC	50° + HT	28	5.76 – A		GOOD
	50° + HT	27	5.59 – B		GOOD
	LT Cp	0.028	5.80 – A	5.79	GOOD
	LT Cp	0.04	5.83 – B		GOOD
	LT Cp	0.01	5.71 – C		GOOD
	Latimer's Rule*		(5.8)		GOOD
VC	50° + HT	33	7.57 – A		FAIR
	50° + HT	32	7.29 – B	6.77	FAIR
	LT Cp	0.032	6.80 – A		GOOD
	Latimer's Rule*		(6.1)		FAIR
MoC	Latimer's Rule*	(8.1)		No data available	
ZrC	LT only	1	8.05 – A		GOOD
	LT only	4	8.13 – B		GOOD
	LT only	11	7.86 – C		GOOD
	LT + HT	19	7.68 – A		GOOD
	LT + HT	18	7.80 – B	7.90	GOOD
	LT + HT	20	7.54 – C		GOOD
	Est. 50° + HT		7.2-7.5 – A		GOOD
	Est. 50° + HT		7.0-7.9 – B		GOOD
	Latimer's Rule*		(7.9)		GOOD
NbC	Latimer's Rule*		(8.0)	No data available	
WC	Latimer's Rule*		(10.2)	No data available	
HfC	Est. 50° + HT	1013	9.67 – B		POOR
	Est. 50° + HT	1013	9.82 – A	10.9	POOR
	Latimer's Rule*		(10.3)		FAIR

TABLE 49 (Continued)

B. Monocarbides (cont.)

	Data Used	rms Deviation	S^o_{298} (calc)** (cal deg^{-1} mole^{-1})	S^o_{298} (exptl) (cal deg^{-1} mole^{-1})	Quality*** of Fit
TaC	50° + HT		10.35 - A		GOOD
	50° + HT		11.39 - B		POOR
	LT + HT	23	9.25 - A		FAIR
	LT + HT	20	9.53 - B	10.1	FAIR
	LT + HT	23	8.98 - C		POOR
	LT Cp	0.05	10.23 - A		GOOD
	LT Cp	0.04	10.07 - C		GOOD
	LT Cp	0.07	10.24 - B		GOOD
	Latimer's Rule*		(10.4)		GOOD
SiC	HT only	40-60	3.34-3.39 - A	3.97 - cubic	FAIR
	Latimer's Rule*		(4.1)	3.94 - hex	GOOD

*For monocarbides the entropy contribution is taken as -4.0 for Ti, V, Cr
-4.2 for Mo, Zr, Nb
-4.5 for W, Hf, Ta

C. Mononitrides

	Data Used	rms Deviation	S^o_{298} (calc)** (cal deg^{-1} mole^{-1})	S^o_{298} (exptl) (cal deg^{-1} mole^{-1})	Quality*** of Fit
BN	50° + HT	77	2.05		POOR
	50° + HT	28	3.49 - B	3.67	GOOD
	HT only	65	1.68 - A		POOR
	Latimer's Rule*		(2.9)		FAIR
AlN	50° + HT	29	4.51 - A		GOOD
	50° + HT	29	4.62 - B		GOOD
	HT only	36	4.00 - A	4.8	FAIR
	HT only		4.30 - B		GOOD
	Latimer's Rule*		(6.0)		POOR
TiN	50° + HT	18	6.98 - A		GOOD
	50° + HT	16	7.08 - B	7.24	GOOD
	Latimer's Rule*		(7.8)		FAIR
VN	50° + HT	21	9.15 - A		GOOD
	50° + HT	20	9.13 - B	8.91	GOOD
	LT only	0.076	9.03 - A		GOOD
	Latimer's Rule*		(8.1)		FAIR

185

TABLE 49 (Continued)

C. Mononitrides (cont.)

	Data Used	rms Deviation	S^o_{298} (calc)** (cal deg^{-1} mole^{-1})	S^o_{298} (exptl) (cal deg^{-1} mole^{-1})	Quality*** of Fit
ZrN	50° + HT	25	9.82 - A		FAIR
	50° + HT	24	10.18 - B	9.288	FAIR
	HT only		8.1 - B		POOR
	Latimer's Rule*		(9.6)		GOOD
NbN	Est. 50° + HT	4	11.68 - B		POOR
	Est. 50° + HT	4	11.24 - A	10.50	FAIR
	Latimer's Rule*		(9.7)		FAIR
HfN	Est. 50° + HT	248	14.7 - A		
	Est. 50° + HT	247	16.7 - B	No data available	
	Latimer's Rule*		(11.8)		
TaN	Est. 50° + HT	37	19.19 - B		
	Est. 50° + HT	36	21.18 - A	No data available	
	Latimer's Rule*		(11.9)		
WN	Latimer's Rule*		(12.0)	No data available	

*For mononitrides, the entropy contribution for

N was taken as   -2.0 for B, Al, Ti, V, Cr
                       -2.5 for Zr, Nb, Mo
                       -3.0 for Hf, Ta and W

D. Oxides

	Data Used	rms Deviation	S^o_{298} (calc)**	S^o_{298} (exptl)	Quality*** of Fit
Li_2O	HT only	15-25	8.4 to 8.6 - A	9.06	FAIR
NbO_2	HT only	35-45	8.9 to 9.3 - A	13.03	POOR
MoO_2	HT only	300-355	7.9 to 14.3 - A	11.06	FAIR to POOR
MoO_3	HT only	71-107	11.1 to 11.9 - A	18.58	POOR
	50° + HT	58	17.00 - A		POOR
CeO_2	HT only	25-30	11.5 to 12.0 - A	14.89	POOR
	50° + HT	19	15.01 - A		GOOD

TABLE 49 (Continued)

D. Oxides (Cont.)

	Data Used	rms Deviation	S^o_{298} (calc)** (cal deg^{-1} mole^{-1})	S^o_{298} (exptl) (cal deg^{-1} mole^{-1})	Quality*** of Fit
ThO$_2$	LT + HT	8	15.01 - A		GOOD
	LT + HT	12	14.61 - B		FAIR
	LT + HT	57	15.41 - C	15.593	GOOD
	50° + HT	9	15.22 - A		GOOD
	HT only	4	17.48 - C		POOR
	HT only	4	15.68 - B		GOOD
Al$_2$O$_3$	HT only		12.5 - B	12.18	GOOD
WO$_2$	50° + HT	116	11.94 - A	12.08	GOOD

*Latimer's Rule is $S^o_{298} = S_{metal} + 2S_{boron}$ where S_{boron} = -1.5 for Cr, Ti, V
= -1.7 for Mo, Zr, Nb
= -2.25 for W, Hf, Ta

and S_{metal} was given by Latimer's original paper, J. Am. Chem. Soc. 73, 1480 (1951).

**A - Debye functions with one or two thetas and linear term in T (Equations 1 or 5 in text).
  B - Debye and Einstein function with two thetas and linear term in T (Equation 6 in text).
  C - Debye and/or Einstein functions and two thetas + C$_V$ correction term and additional linear term in T (Equation 7 in text).

***Good means that S^o_{298} (calc) is within ± 0.5 entropy units of the experimental S^o_{298}

Fair indicates a deviation in the range ± 0.5 - 1.0 e.u.

Poor indicates a deviation in the range ± 1.0 - 1.5 e.u.

Bad indicates a deviation of more than 1.5 e.u.

APPENDIX III

HEAT CAPACITY AND THERMODYNAMIC PROPERTIES FROM 5 to 350K*

A. ZIRCONIUM CARBIDE AND ZIRCONIUM DIBORIDE

Low temperature heat capacity measurements were completed on ZrC and ZrB_2 during earlier report periods. Data and experimental details were reported for ZrB_2 in Part I and for ZrC in Part II of ASD-TDR-62-204 issued in April 1962 and May 1963 respectively. Abstracts from published reports of these studies are reported herewith.

Zirconium Carbide:[19] The heat capacity of a characterized, zone-melted sample of ZrC was measured by adiabatic calorimetry from 5° to 350°K and found to be of normal sigmoid shape without transitions or thermal anomalies. At 298.15°K the measured heat capacity at constant pressure (C_p), the practical entropy (S^O), the enthalpy function ($[H^O - H_o^O]/T$), and the Gibbs function ($-[G^O - H_o^O]/T$) are 9.06, 7.96, 4.70 and 3.26 cal. (g.f.m. °K)$^{-1}$. Values of the heat capacity and entropy, adjusted to pure ZrC on the basis of the impurity content obtained by chemical analysis, are 9.13 and 7.90 cal. (g.f.m. °K)$^{-1}$.

Zirconium Diboride:[9] The heat capacity of a characterized, zone-melted sample of zirconium dihoride has been measured over the low temperature range by adiabatic calorimetry and found to be of a normal sigmoid shape without transitions or thermal anomalies. The values of the heat capacity at constant pressure (C_p), the entropy (S^O), and the Gibbs function ($-[G^O - H_o^O]/T$) are 11.53, 8.59, and 3.25 cal. (g.f.m. °K)$^{-1}$, respectively, at 298.15°K.

B. HAFNIUM CARBIDE, HAFNIUM DIBORIDE AND HAFNIUM METAL

During this report period low temperature heat capacity measurements were completed on HfB_2, HfC and Hafnium metal. Details of the experimental apparatus and techniques have been described previously in these reports.[21][15]

The preparation and purity of the samples under study is described in Section III of this report.

---

*Prepared from reports on subcontracted studies at the University of Michigan, Ann Arbor Michigan under the direction of Professor Edgar F. Westrum, Jr.

In Tables 50 and 51 are presented the experimental heat capacity data and the derived thermodynamic properties of hafnium diboride.

TABLE 50

HEAT CAPACITY OF HAFNIUM DIBORIDE
(Units: cal., g.f.m., °K)

T	C_p	T	C_p	T	C_p	T	C_p
	Series I				Series II		
5.80	0.0020	31.69	.2724	98.88	3.897	222.14	9.239
6.39	.0026	34.85	.3940	105.62	4.196	231.51	9.608
7.42	.0031	38.46	.5551	113.15	4.523	240.90	9.970
8.41	.0038	39.51	.6100	121.33	4.870	250.20	10.031
9.49	.0054	43.38	.8202	129.80	5.251	259.35	10.667
10.78	.0074	47.74	1.081	138.61	5.643	268.38	10.945
11.90	.0086	52.69	1.389	147.43	6 033	277.33	11.241
13.20	.0118	57.51	1.694	156.37	6.426	286.45	11.540
14.66	.0164	59.28	1.805	165.45	6.824	295.76	11.820
16.34	.0217	64.53	2.132	174.37	7.221	305.10	12.093
18.07	.0314	71.10	2.511	183.57	7.622	314.43	12.365
19.86	.0426	77.69	2.870	187.92	7.789	323.70	12.618
21.83	.0610	84.62	3.242	194.89	8.119	334.41	12.884
23.88	.0871	92.06	3.597	203.93	8.492	344.93	13.152
26.23	.1275	100.35	3.965	212.95	8.865		
28.90	.1886	108.86	4.337				

190

TABLE 51

THERMODYNAMIC PROPERTIES OF HAFNIUM DIBORIDE
(Units: cal., g.f.m., °K)

T	C_p	S^o	$H^o - H^o_o$	$-(G^o - H^o_o)/T$
5	0.0016	0.0006	0.002	0.0001
10	0.0055	0.0027	0.018	0.0008
15	0.0172	0.0068	0.071	0.0020
20	0.0440	0.0148	0.214	0.0041
25	0.1045	0.0303	0.567	0.0076
30	0.2196	0.0586	1.351	0.0136
35	0.3984	0.1051	2.870	0.0231
40	0.6348	0.1731	5.432	0.0373
45	0.9148	0.2637	9.291	0.0573
50	1.221	0.3758	14.623	0.0833
60	1.852	0.6541	29.98	0.1544
70	2.457	0.9856	51.56	0.2489
80	3.004	1.3500	78.92	0.3635
90	3.497	1.7327	111.46	0.4943
100	3.953	2.1250	148.73	0.6377
110	4.390	2.522	190.45	0.7909
120	4.823	2.923	236.52	0.9519
130	5.258	3.326	286.92	1.119
140	5.699	3.732	341.70	1.291
150	6.143	4.140	400.90	1.467
160	6.588	4.551	464.56	1.647
170	7.031	4.964	532.65	1.830
180	7.469	5.378	605.16	2.016
190	7.901	5.793	682.02	2.204
200	8.326	6.209	763.16	2.394
210	8.743	6.626	848.52	2.585
220	9.150	7.042	937.99	2.778
230	9.547	7.457	1031.5	2.973
240	9.932	7.872	1128.9	3.168
250	10.304	8.285	1230.1	3.365

TABLE 51 (Continued)

T	C_p	S^o	$H^o - H^o_o$	$-(G^o - H^o_o)/T$
260	10.661	8.696	1334.9	3.562
270	11.003	9.105	1443.2	3.760
280	11.331	9.511	1554.9	3.958
290	11.645	9.914	1669.8	4.156
300	11.948	10.314	1787.8	4.355
310	12.238	10.711	1908.7	4.553
320	12.516	11.104	2032.5	4.752
330	12.779	11.493	2159.0	4.950
340	13.029	11.878	2288.1	5.148
350	13.275	12.259	2419.6	5.346
273.15	11.11	9.23	1478	3.822
298.15	11.89	10.24	1766	4.318

The experimental heat capacity data for Hafnium metal is presented in Table 52. A tentative tabulation of the thermodynamic functions is presented in Table 53. Tentative tables of experimental heat capacity and derived thermodynamic functions for HfC are presented in Tables 54 and 55 respectively.

These data for the hafnium metal, HfC, and HfB_2 will be prepared in final form and submitted for publication shortly.

TABLE 52

HEAT CAPACITY OF HAFNIUM METAL
(Units: cal., g.f.m., °K)

T	C_p	T	C_p	T	C_p	T	C_p	T	C_p
Series I		Series II		Series III		Series IV		Enthalpy Run A	
108.62	5.079	5.82	0.0089	5.85	0.0089	67.00	3.895	207.97	5.863
111.40	5.117	6.74	0.0086	7.00	0.0121	73.17	4.144	217.16	5.903
117.22	5.205	7.92	0.0181	8.17	0.0211	79.93	4.395	226.25	5.934
125.15	5.359	8.70	0.0283	9.45	0.0350	87.25	4.630	235.23	5.965
133.80	5.411	9.56	0.0352	10.84	0.0546	95.14	4.811	244.12	5.998
142.71	5.496	10.84	0.0524	12.35	0.0799	103.26	4.970	252.94	6.003
152.94	5.582	12.17	0.0741	14.01	0.1238	111.41	5.110	261.68	6.032
164.49	5.661	13.47	0.1148	15.85	0.1896			269.30	6.058
175.81	5.726	14.89	0.1513	17.84	0.2825			278.03	6.093
186.93	5.778	16.46	0.2149	19.89	0.4009			286.69	6.114
197.89	5.826	17.95	0.2883	22.06	0.5469			295.93	6.136
200.73	5.837	19.65	0.3838	24.36	0.7197			305.74	6.161
211.62	5.880	21.56	0.5118	26.86	0.9313			315.48	6.175
		23.45	0.6507	29.86	1.1938			325.15	6.221
		23.88	0.6835	32.83	1.4676			333.76	6.235
		26.43	0.8915	36.54	1.807			341.34	6.245
		29.05	1.1205	41.18	2.214			348.55	6.261
		31.92	1.3812	46.23	2.625				
		35.77	1.735	51.38	3.004				
		39.98	2.108	57.07	3.371				
		43.94	2.439	63.65	3.738				
				71.27	4.074				
				79.59	4.384				
				87.56	4.640				

TABLE 53

THERMODYNAMIC FUNCTIONS OF HAFNIUM (TENTATIVE)
(Units: cal., g.f.m., °K)

T	C_p	S^o	$H^o - H_o^o$	$-(G^o - H_o^o)/T$
20	0.4080	0.1254	1.902	0.0303
40	2.114	0.9052	26.396	0.2453
60	3.538	2.052	83.93	0.653
80	4.405	3.200	164.13	1.148
100	4.918	4.242	257.78	1.664
120	5.247	5.170	359.63	2.173
140	5.474	5.997	466.98	2.661
160	5.634	6.739	578.16	3.125
180	5.746	7.409	692.01	3.565
200	5.833	8.019	807.82	3.980
220	5.911	8.579	925.27	4.373
240	5.983	9.096	1044.21	4.746
260	6.044	9.578	1164.50	5.099
280	6.095	10.028	1285.91	5.435
300	6.145	10.450	1408.31	5.755
350	6.263	11.407	1718.75	6.496
273.15	6.079	9.877	1224.22	5.322
298.15	6.140	10.412	1396.95	5.726

194

TABLE 54

HEAT CAPACITY OF HAFNIUM CARBIDE (TENTATIVE)
(Units: cal., g.f.m., °K)

T	C_p	T	C_p	T	C_p
5.09	0.0017	42.24	1.0013	194.79	6.921
6.39	0.0026	46.93	1.2998	203.96	7.146
7.16	0.0035	52.22	1.641	212.90	7.358
8.50	0.0053	57.97	2.004	221.97	7.562
9.50	0.0070	63.77	2.362	231.05	7.760
10.50	0.0093	69.85	2.701	240.11	7.947
12.09	0.0143	77.17	3.079	249.28	8.124
13.25	0.0194	85.67	3.487	258.53	8.303
14.59	0.0265	94.77	3.855	267.88	8.460
16.15	0.0343	95.28	3.874	277.07	8.619
17.89	0.0507	102.52	4.143	286.20	8.774
19.75	0.0719	111.39	4.459	295.35	8.912
21.75	0.1079	120.68	4.773	304.47	9.045
23.81	0.1501	129.96	5.074	313.47	9.173
26.36	0.2194	139.20	5.369	322.37	9.283
29.03	0.3116	148.56	5.651	331.16	9.394
31.88	0.4316	157.91	5.928	339.68	9.491
34.91	0.5792	167.14	6.189	346.90	9.582
38.29	0.7637	176.27	6.442	350.00	9.613
		185.46	6.685		

195

TABLE 55

THERMODYNAMIC FUNCTIONS OF HAFNIUM CARBIDE (TENTATIVE)
(Units: cal., g.f.m., °K)

T	C_p	S^o	$H^o - H_o^o$	$-(G^o - H_o^o)/T$
20	0.0778	0.0232	0.348	0.0059
40	0.8617	0.2647	8.196	0.0597
60	2.1334	0.8545	38.16	0.2189
80	3.214	1.6223	92.08	0.472
100	4.054	2.434	165.09	0.783
120	4.752	3.236	253.3	1.125
140	5.387	4.017	354.8	1.483
160	5.985	4.775	468.5	1.847
180	6.544	5.513	593.9	2.214
200	7.055	6.230	730.0	2.580
220	7.518	6.924	875.8	2.943
240	7.939	7.596	1030.4	3.303
260	8.325	8.247	1193.1	3.658
280	8.674	8.877	1363.2	4.009
300	8.982	9.487	1539.8	4.354
350	9.613	10.920	2005.3	5.191
273.15	8.559	8.664	1304.1	3.890
298.15	8.955	9.431	1523.2	4.322

196

APPENDIX IV

THERMODYNAMIC PROPERTIES OF
ZIRCONIUM AND HAFNIUM HALIDES*

Robert D. Freeman

Until mid-1962, most of the efforts of this group had been devoted to development of experimental techniques with which to study the disproportionation of the zirconium and hafnium subhalides. In June, 1962, support for the development of these techniques was transferred to another source of funds. The results of those developments, in particular that of the MIKER technique, are available, of course, for immediate use in these studies.

This report then summarizes work on these experimental techniques and the theoretical work on molecular flow of gases for the period February 1961 through May 1962 (items A, B, and C below). During the period June 1962 through December 1963, efforts were directed toward sample procurement and preparation and toward design of calorimetric experiments and construction of apparatus with which to obtain heats of formation of the solid subhalides (items D and E, below).

A. MOLECULAR FLOW THROUGH NON-IDEAL ORIFICES

One of the most useful techniques for obtaining thermodynamic data for vaporization and dissociation processes at high temperatures is the Knudsen effusion method for measurement of low pressures. The technique is extensively discussed in the literature (e.g., Margrave).[154] One of the difficulties with the method is that effusion orifices of finite length must be used; in contrast to the "ideal" orifice, which by definition has zero length, these non-ideal orifices have a transmission probability (or Clausing factor) different from unity. The transmission probability is defined as the probability that a molecule which enters the orifice through one end will escape through the other end. Clausing[139][140] and DeMarcus[142] have discussed in considerable detail the derivation of these transmission probabilities for cylindrical orifices.

Unfortunately, these theoretical probabilities have not been adequately confirmed by experiment; Carlson[138] has summarized the available data and has reported the results of his own work. Because of the uncertain validity of the theoretical transmission probabilities a number of workers (e.g., Searcy and

---

*Report on subcontracted study at Oklahoma State University, Stillwater, Oklahoma under the direction of Professor R. D. Freeman.

McNees, [159] have used diverging tapered, or conical orifices with a rather large (>100°) included angle, on the assumption that the transmission probability for such orifices is very nearly unity. Balson[137] has considered theoretically the transmission probability for conical orifices, but his derivations involve several approximations. Iczkowski, Margrave and Robinson[149] have recently completed a rigorous treatment of the conical orifice problem.

In the Torsion-Effusion method (Volmer), [161] and the MIKER technique (below) one needs for the effusion orifice the transmission probability and a factor which, when applied to the measured force, corrects for the non-cosine-law distribution of molecules effusing from cylindrical (Freeman and Searcy), [145] and conical orifices. A theoretical treatment of angular distribution of molecules effusing from conical orifices has not been available.

We have, concurrently with Iczkowski, Margrave, and Robinson, [149] derived the appropriate equations and computed transmission probabilities for conical and, as a special case, cylindrical orifices, and in addition have obtained angular distribution functions and the associated recoil force factors. Early work on these derivations and computations was discussed in the first annual report under this contract; the final results have been reported by Freeman[144] and in more detail by Edwards.[145] Freeman[144] has also reported current work on experimental determination of transmission probabilities and angular distributions.

B. MIKER TECHNIQUE

The Microbalance-Inverted Knudsen Effusion-Recoil (MIKER) Technique is a new one which, we have proposed, may be capable of providing reliable data for the average molecular weight of the one or more molecular species which effuse from a Knudsen cell at elevated temperature. The principal novel feature
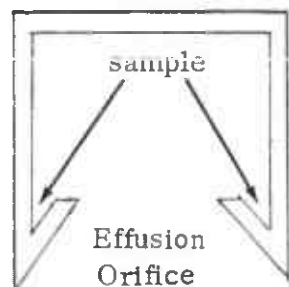
of the MIKER technique is the cell design which is depicted at left; Margrave[153] has discussed a similar technique. In operation this MIKER cell is to be suspended, in an appropriate vacuum furnace, from a recording vacuum microbalance. Effusion of vapor through the orifice will result in a recoil force acting vertically upward. At constant temperature the recoil force will be constant and the variation of weight with time will yield the rate of effusion. After the rate of effusion has been determined at a particular temperature, the power supplied to the furnace is to be suddenly reduced to zero, and the cell allowed to cool rapidly so as to minimize

sample

Effusion
Orifice

MIKER Cell

further effusion. The recoil force Φ is then to be determined from the difference δ in apparent weight of the cell when hot and when cool. If δ is expressed in grams, Φ in dynes, and g represents gravitational acceleration, $\Phi = \delta g$. Freeman and Searcy[145] have shown that the pressure P_R determined by measurement of recoil force is given by $P_R = 2\Phi/AF$, in which A is the area of orifice and F is the recoil correction factor (see Section A); for the MIKER cell $A = \pi r_m^2$, and r_m is the radius of the smaller end of the conical orifice. From the rate of effusion $\dot{w}$(g/sec), the Knudsen pressure P_K is calculated by (Knudsen, [151]) $P_K = (\dot{w}/\pi r_m^2 W) (2\pi RT/M^*)^{\frac{1}{2}}$, in which W is the transmission probability of the orifice (see Section A) and M^* is the (average) molecular weight of the effusing species. Searcy and Freeman [158] have shown that, if an assumed value M for the molecular weight of the vapor is used to calculate P_K, M^* is given by $M^* = M (P_K/P_R)^2$.

The expected advantages of this technique are:

1. Rate of effusion and recoil force are determined essentially simultaneously with the same detector, i.e., the microbalance. Errors in calibration cancel in the calculation of molecular weight of the vapor, since it is the ratio of rate of effusion to recoil force which is required.

2. Measurements of rate of effusion and of recoil force can be made rapidly and over a wide temperature range without intermittent opening of the vacuum system.

3. Cylindrical symmetry of the MIKER cell, combined with electron-impact or resistance heating, should result in minimal temperature gradients.

4. Location of the effusion orifice "within the cell" should minimize "cold orifice" problems.

5. Effusion downward minimizes difficulties with condensation on suspension wires.

The only apparent disadvantages are:

1. The recoil forces to be measured are quite small; they range approximately from 5 to 5000 microgram weight. The precise measurement, under vacuum furnace conditions, of forces in the lower decade of this range is rather difficult.

2. In the MIKER cell the probability of difficulties arising from surface diffusion along the orifice wall (Winterbottom and Hirth,[163]) and from sample creeping along a previously wetted surface inside the cell is greater than in ordinary effusion cell configurations.

3. The orifice of the MIKER cell is obviously non-ideal and correction factors for both rate of effusion and recoil force are needed (cf. Freeman and Searcy,[145] for the similar torsion-effusion problem). Theoretical correction factors are available (see Section A); these factors require experimental confirmation before they can be used with complete confidence.

The vacuum furnace, microbalance, and control circuits which have been designed and built to realize the MIKER technique have been described in ASD-TDR-63-754, Part I (Freeman,[144]); additional developments will be reported in subsequent Parts.

C. ELECTRODYNAMOMETER

The electrodynamometer (EDM) was originally conceived as a device capable of measuring with an accuracy better than ±1.0 percent and on an absolute basis (e.g., independent of calibration of a torsion wire) the momentum of a molecular beam emanating from a Knudsen cell in which the pressure might be 10^{-6} - 10^{-3} atm. If the molecular beam impinges on a target, a force is exerted which is directly related to the average momentum of the molecules in the beam; the problem then becomes one of measuring this extremely small force, or if the target is attached to a suspension wire, of a very small (0.1 - 0.0005 dyne cm) torque.

The design of the basic measuring device is based on an absolute electrodynamometer constructed a half-century ago by the National Bureau of Standards for evaluation of the absolute ampere; a precision of 10-20 ppm was obtained in the NBS work (Guthe,[147]). The EDM which we constructed is physically smaller than the NBS version by a factor of 5 and operating currents are smaller by factors of 10 to 100; the achievable precision is correspondingly decreased. In our initial design an operating precision of 0.1 percent was the goal.

The initial design and construction has been described in detail by Dawson[141]; Freeman[21][144] has described the apparatus in some detail and has reported results of various tests of the instrument. The results of the tests indicate that the electrodynamometer can measure with a precision of 0.1 - 0.2 percent and an accuracy of ± 0.2 - 0.5 percent torques near the upper end of the range (0.0005 - 0.1 dyne cm) expected for molecular beams of reasonable cross-sectional area; it appeared very unlikely that this precision and accuracy could be maintained at the middle and lower end of the range of interest.

Two types of studies were originally planned for the EDM momentum detector: (1) measurement of angular distribution of momentum in a molecular heam emerging from a non-ideal orifice, as a function of orifice parameters; and (2) measurement of beam-momentum coupled with weight-loss data for the Knudsen cell-source to give sufficient data for evaluation of the average molecular weight of effusing species. The MIKER technique discussed below appears to have more promise for studies of type (2) than does the EDM momentum detector. For measurements of type (1) use of a torque-measuring device more sensitive than the EDM appears to be needed; such devices have recently been developed (Humphrey and Johnston,[148]; Rogallo and Savage,[157]. Further, more sophisticated, and potentially more accurate, measurements of augular distribution of momentum are expected in the near future from other workers (e.g., Wahlbeck,[162]).

We therefore have concluded that further development of the EDM momentum detector is not profitable at the present time.

D. SAMPLE PROCUREMENT AND PREPARATION

Samples of $ZrCl_4$ and ZrF_4 with high purity and low hafnium content have been obtained. A sample of $ZrCl_2$, prepared by reaction of stoichiometric quantities of high-purity $ZrCl_4$ and Zr metal, but of unknown actual purity and composition, has been obtained through the generosity of Dr. Oriville Frampton, Research Division, U.S. Industrial Chemical Co., Cincinnati. A 50-g sample of high purity, low-zirconium, hafnium metal is now available from the lot prepared for this contract by Wah Chang.

Of the various methods which have been used or proposed for preparing $ZrCL_3$ and $HfCl_3$ the one which appeared to us most likely to give a high purity, stoichiometric product is reduction of the tetrahalide with atomic hydrogen (Newnham and Watts,[156]). The reaction is reported to be very specific; as an added advantage, both the reducing agent (H_2) and its oxidized form (HCl) are gases and are easily removed from the product. In the technique H_2 is passed over hot ($\sim$200°C) $ZrCL_4$(s), entrains $ZrCl_4$ (g) and carried it into the reaction zone in which a glow discharge through the H_2 (g) produces H(g); the atomic hydrogen reduces the entrained $ZrCl_4$(g) to $ZrCl_3$ which condenses on the walls of the apparatus. Power for the discharge is provided by a spark-gap-controlled oscillating circuit in which is the primary of a high voltage induction coil; the secondary of the induction coil is connected directly to the discharge electrodes.

Our initial assembly of electrical components, glass reduction line, furnaces, etc., was copied as nearly as feasible from Newnham and Watts description. Considerable difficult was encountered in achieving satisfactory operation of the discharge; modifications were made in the electrical circuit and are described below. Similarly, difficulties were encountered with the furnace

arrangement and H_2-$ZrCl_4$ flow path used by Newnham and Watts; the hydrogen reduction apparatus was rather drastically modified and is described below.

A diagram of the electrical circuit of the power supply for the high voltage discharge is given in Figure 50. The spark gap is adjustable; the silver electrodes of the gap protrude from finned, massive brass holders which dissipate the considerable thermal energy generated at the gap.

Considerable difficulty was experienced with shorting between successive layers in the secondary of the induction coil. The design which is currently in use and performing satisfactorily with no indication of electrical shorts has as the primary 16 turns of 18 gauge stranded copper wire on a Plexiglas spool 3 inches in diameter; the secondary has 1600 turns of 32 gauge copper magnet wire (with heavy Formvar insulation) in ten layers (160 turns/layer) on a 2-inch diameter Plexiglas spool which slips inside the spool for the primary. After each layer of the secondary was wound, the layer was well shellacked; then three layers of Permacel 423 Teflon adhesive tape were wrapped over the layer of wire.

The high voltage components are housed in wooden box with ample space between components. Leads from the secondary of the induction coil to the electrodes of the reduction apparatus carry insulation rated 10KV.

The new reduction apparatus is depicted in Figure 51. In the 2-1. round-bottomed flask is a liquid which boils at a temperature ($\sim 200°C$) at which appreciable amounts of $ZrCl_4(g)$ are entrained by H_2 flowing over $ZrCl_4(s)$; vapor from the boiling liquid condenses at a height in the apparatus determined by the energy input to a heating mantle which surrounds the flask, thereby providing an easily controllable method for heating the center reaction tube.

$ZrCL_4(s)$ is placed in the "pocket" in the hydrogen inlet while the apparatus (without the round-bottomed flask and the condenser) is in a dry box. The apparatus is then assembled, flow of H_2 started, and heating of liquid in the flask begun. The flow of H_2 is adjusted with a needle valve to maintain a pressure of 1 - 3 Torr in the reaction zone between the electrodes. A mechanical vacuum pump continuously removes gases from the reaction zone through an absorption train which removes $ZrCl_4(s)$ and $HCl(g)$ (the major portion of $ZrCl_4$ which escapes reduction condenses on the water-cooled finger at the top of the apparatus). When the flow of H_2 has been adjusted to produce the correct pressure in the reaction zone, the discharge is initiated by increasing the output voltage from the Variac and/or by adjusting the spark gap. Finally, energy input to the heating mantle is adjusted to position the upper condensation line of the refluxing liquid at the desired level.

This new reduction apparatus has been tested with some relatively impure $ZrCl_4$, and appears to perform satisfactorily. The main problem now appears to be achieving complete exclusion of moisture from the reaction chamber (including water absorbed on the glass tubing).
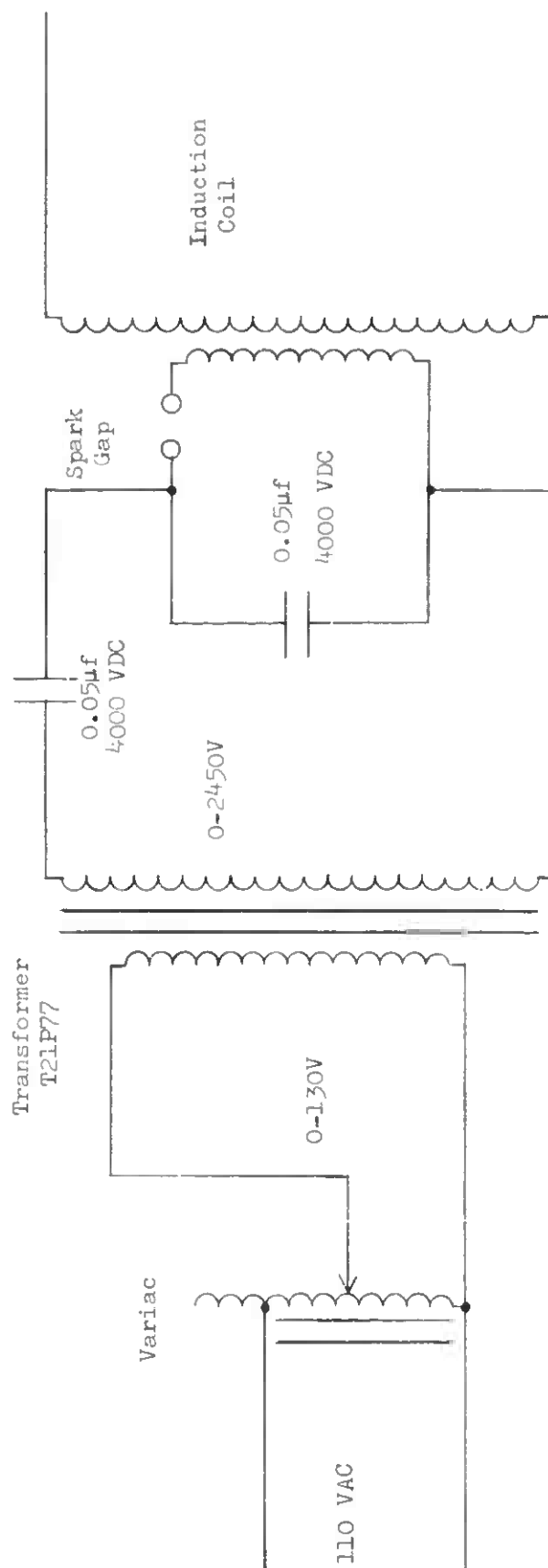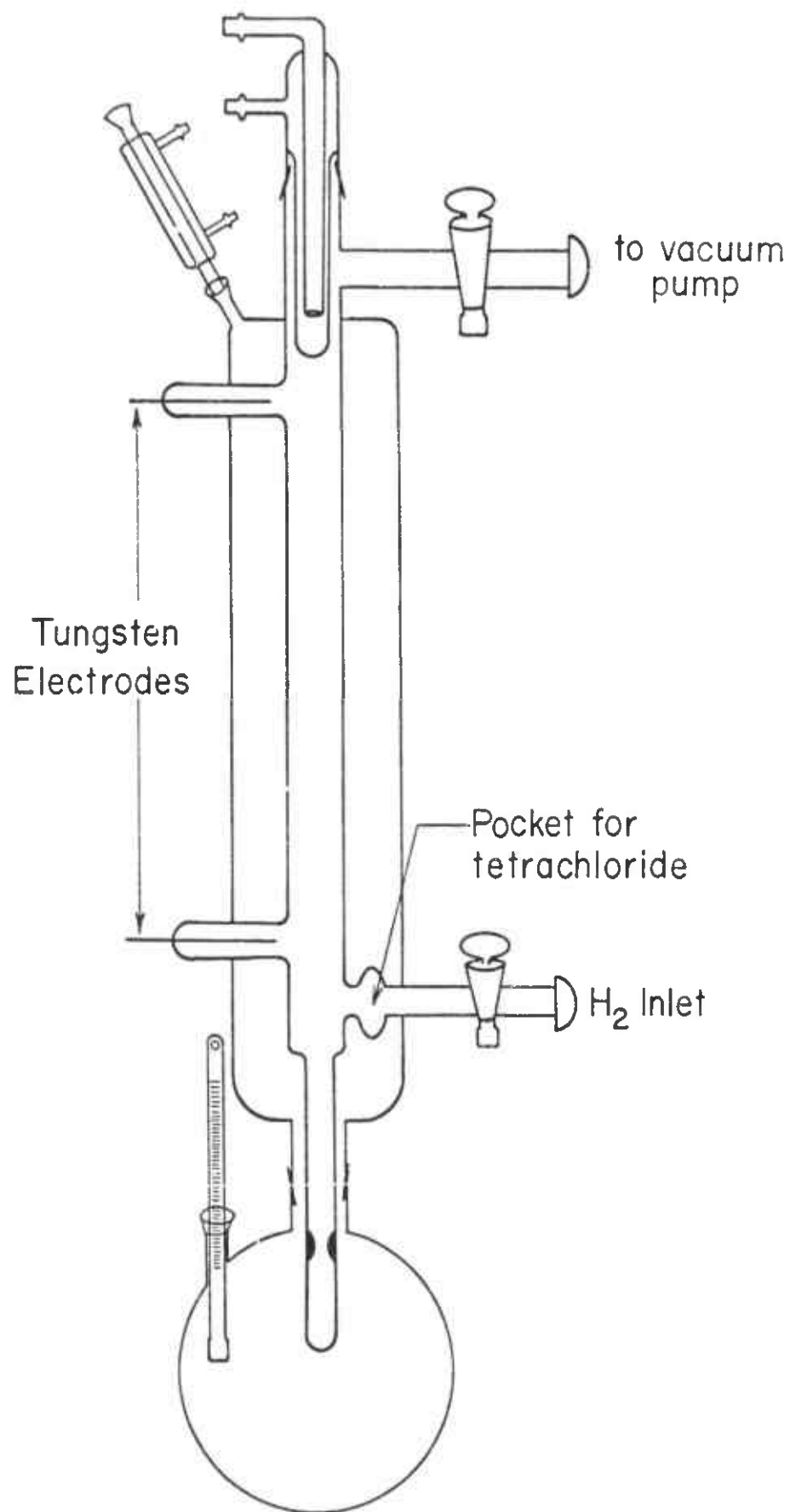
202

FIGURE 50   HIGH VOLTAGE SUPPLY FOR GLOW DISCHARGE

Tungsten
Electrodes

Pocket for
tetrachloride

to vacuum
pump

H₂ Inlet

FIGURE 51   APPARATUS FOR REDUCTION OF ZrCl₄ TO ZrCl₃
WITH ATOMIC HYDROGEN

204

E. CALORIMETRY

The studies of disproportionation of the subhalides are designed to obtain data from which to calculate heats of formation of the gaseous species; among the auxiliary data needed for the calculations are heats of formation of the solid subhalides, which are not presently available. Accordingly, we have undertaken the determination of the heats of formation at 298.15°K of the crystalline solids $ZrCl_3$, $ZrCl_2$, $HfCl_3$ and $HfCl_2$.

Because the zirconium, and presumably hafnium, subchlorides react so vigorously with water to give products with inaccurately known compositions, their heats of formation cannot be determined by the straightforward aqueous-solution calorimetry used by MacWood, et al.[152] for the titanium compounds. There appear to be two reasonable approaches. One is to construct a "chlorine bomb" calorimeter in which the energy of direct chlorination of $ZrCl_3$ and of $ZrCl_2$ to $ZrCl_4$ could be measured. The other is to find a solvent system in which the necessary enthalpies of solution can be measured.

A suitable solvent system must satisfy the following requirements: (1) $ZrCl_4$ must be readily soluble; (2) an oxidizing agent for the subchlorides and its reduced form (e.g., $FeCl_3$ - $FeCl_2$) must be readily soluble; and (3) the solvent system must be inert to the subchlorides which are very strong reducing agents, i.e., $ZrCl_3$ and $ZrCl_2$ must react with the oxidizing agent only. After review of the available information, we have concluded that N,N-dimethylformamide and/or N,N-dimethylacetamide will probably be a satisfactory medium for solution calorimetry.

Calorimetry in such a medium, with requirements for the strict exclusion of moisture, will present a number of difficulties, but these appear to be fewer in number and smaller in magnitude than those to be expected in chlorine-bomb calorimetry. Accordingly, we have proceeded with design and construction of a solution calorimeter and assembly of the necessary auxiliary equipment for calorimetric measurements. The solution/reaction calorimeter, which is depicted in Figure 52, incorporates features of calorimeters described by Gunn[146], Sunner and Wadsö[160], Keith and Mackle[150], and Meetham and Nichols[155], and two novel ones: the rocking mechanism and the capsule-breaking mechanism.

The cup (A, Figure 52) of the calorimeter vessel was machined from a solid copper bar and is 4.4 cm i.d., 7.2 cm deep, and has 0.3-cm wall thickness and a volume of approximately 100 cm³. The outer surface of the cup was grooved, 28 per inch, and then nickel-plated; into the grooves is wound (non-inductively) platinum or nickel resistance wire which serves as the thermometer; a thin-walled (0.15 cm) nickel-plated copper shield fits very tightly over the grooved surface of the cup. The inside surface of the cup and the mating surface of the flange were plated with gold (0.005-0.008 in. thick). The top (B) of the
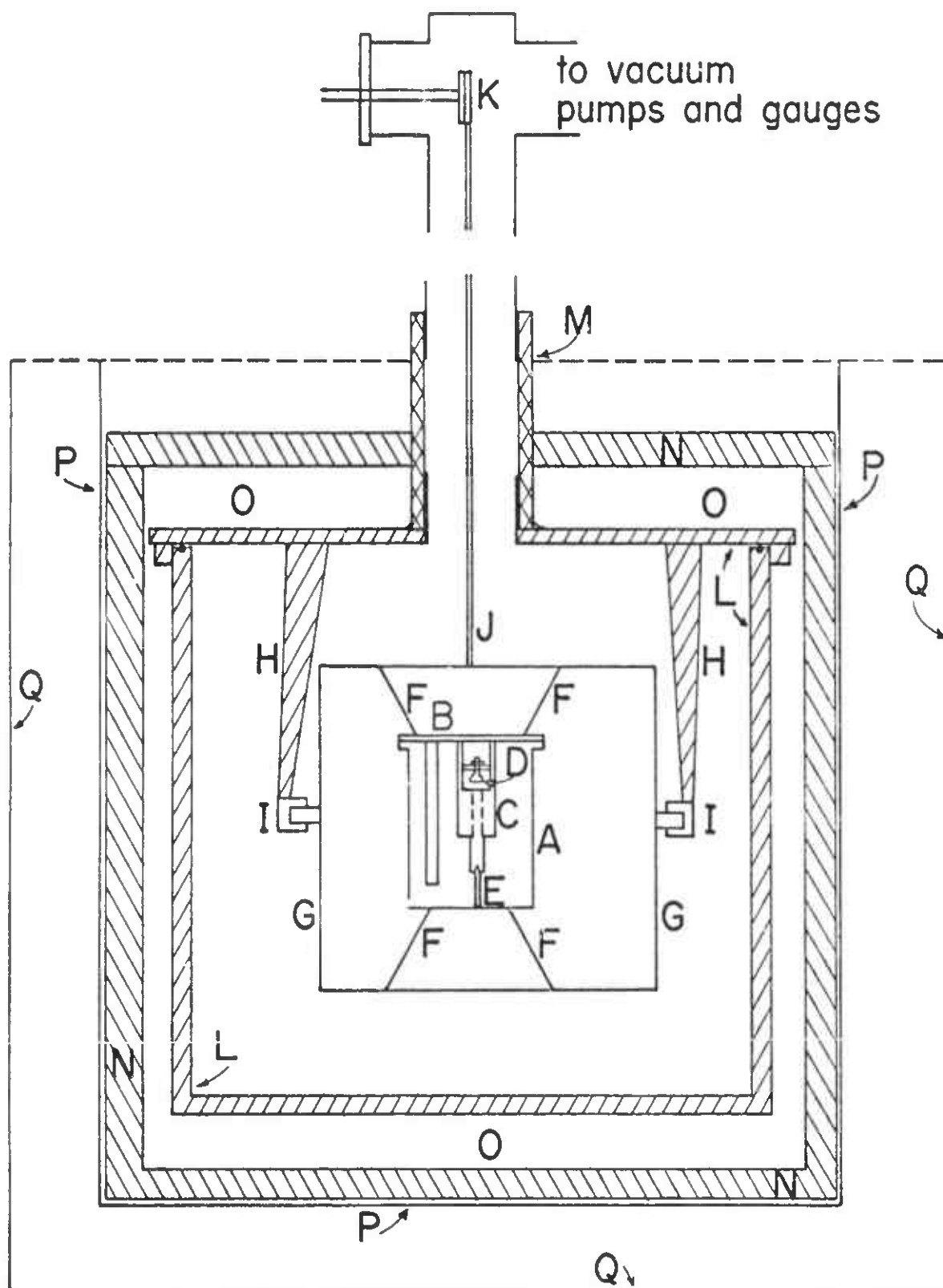
FIGURE 52　　　ROCKING ANEROID SOLUTION/REACTION CALORIMETER
WITH FLUIDLESS ISOTHERMAL JACKET

calorimeter vessel is a 0.6-cm thick copper disc with an O-ring groove to mate with the flange on the cup. A copper re-entrant well in the top contains a manganin or Evanohm heater for electrical calibration. Suspended from the top by two 0.0625-in. copper tubes, which also serve as conduits for electrical leads, is a solenoid(C) (2000 turns of No. 32, Teflon-insulated copper wire) wound on a brass form 0.150 in. i.d., 0.875 in. o.d. and 0.75 in. high; a brass cover soldered over the spool completes the isolation of the solenoid from the contents of the vessel. Immediately above the solenoid and atta_hed to the solenoid support tubes is an ampoule holder; the glass ampoule (D) is formed in a graphite mold 0.375 in. deep and 0.5 in. maximum i.d., and has a flat bottom and thin walls. Immediately below the solenoid is a plunger (E) - a 0.125-in. diameter x 0.75 in. long, gold-plated, iron rod-supported in the vertical position by a 0.5-in. long extension of the interior wall of the solenoid. When it is desired to introduce the sample, which of course is in the ampoule, into the solution in the calorimeter vessel, the solenoid is energized (approximately 1 amp) for 10 milliseconds; the plunger is accelerated by the force resulting from the gradient of the magnetic field, impinges on the thin bottom of the glass ampoule, and breaks it. All metal surfaces which might contact the contents of the vessel were gold-plated; all exterior surfaces of the vessel were nickel-plated.

The calorimeter vessel is suspended by eight nylon cords (F) in the center of a cradle (G) made of copper rod and tubing. The cradle has Plexiglas-covered brass axles which turn in Delrin AF sockets (I); the Teflon-filled Delrin AF was chosen because of its extremely low coefficient of friction. The sockets (I) are mounted in 0.25-in. thick copper bars (H) the upper ends of which are attached securely to the top of the vacuum envelope (L). The envelope is constructed from a 9.75-in. i.d. copper pipe, is 8.875 in. high and has walls 0.25 in. thick. The outside surface of the envelope is grooved for a resistance thermometer to monitor the temperature of the envelope. All metal surfaces inside the envelope and the outer surface of the envelope were nickel-plated.

The envelope is surrounded, in turn, by an air gap (O), a 0.5-in. thick aluminum jacket (N), and approximately 2 inches of insulation contained by two thin-walled metal cans (P and Q). The outer surface of the cylindrical walls of jacket (N) is doubly grooved, for a resistance heater and for a resistance thermometer; the top and bottom of the jacket are grooved for the heater only. The thermometer and heater are connected to a Hallikainen Thermotrol temperature regulator which controls the temperature of the jacket.

The envelope (L) is evacuated through a short length of thick-walled Plexiglas pipe (M), which minimizes loss of heat from the envelope and jacket, and 1.5-in. copper pipe to the upper end of which is soldered a "cross" copper fitting. Vacuum pumps are connected to one horizontal arm of the "cross" and electrical leads (not shown in Figure 52) to the calorimeter vessel enter through the upper end of the "cross." In the other horizontal arm of the "cross" is supported a pulley (K) on a shaft which is driven through a vacuum seal by an

207

adjustable-speed, slow-speed, reversible electric motor. Nylon cords (J) pass around the pulley (K) and down to the cradle (G); rotation of the pulley by the motor then also accomplishes rotation of the calorimeter vessel and cradle about axies (I) and consequent agitation of the contents of the vessel. Reversal of direction of rotation when the vessel is about 70 degrees from the vertical orientation is achieved with limit switches.

This particular design achieves the advantages of isothermal, aneroid operation which has been discussed in detail by Meetham and Nichols[155] and of fluidless operation (Keith and Mackle,[150]), requires rotation of only the calorimeter vessel and cradle rather than the entire vacuum envelope (Gunn,[146]), and provides a simple technique for breaking a sample ampoule which is inside the completely sealed reaction vessel.

The heat capacity of the assembled calorimeter vessel is about 75 cal/deg; with approximately 75 cm^3 of solution the total heat capacity becomes 150 cal/deg. The mass of sample is to be chosen to provide a heat of reaction around 100 cal, i.e., a temperature rise of 0.5 - 1.0 deg. The energy input to the solenoid (for ampoule breaking) is approximately 1 amp into 40 ohms for 0.010 sec, or about 0.1 cal, i.e., 0.1% of the heat of reaction; this solenoid input energy should be reproducible within, at worst, ±5% or 0.005 cal, i.e., ±0.005% of the heat of reaction and an appropriate correction can easily be made.

The calorimeter has been completed and is now being tested with the reaction: HCl(aq) + tris-(hydroxymethyl) aminomethane (THAM).

ELECTRON DIFFRACTION STUDIES*
by S. H. Bauer

This is a preliminary report of our results on electron diffraction work performed under Contract No. AF 33(616)-7472. At this date we have completed radial distribution analyses for $ZrCl_4$, $HfCl_4$, $HfBr_4$ and HfI_4, and preliminary results are presented in Table 56. We still have to complete the analysis of the data for the tetrachloride and tetrabromide of tellurium. So far we have established that the first four compounds are strictly tetrahedral in structure. The final radial distribution curves showed complete agreement with this model, with regard to the ratio of the two distances, the areas under the two peaks corresponding to the M-X and X-X interferences, and the absence of extraneous peaks. Some additional refinement will have to be carried out to establish the mean root square fluctuations in the interatomic distances due to the normal vibrations. These appear to be somewhat larger than we had expected. Our present theory is that we have not introduced a sufficient correction for the phase shift scattering factors. One problem remains to be solved before we can quote final values for the M-X distances in these four compounds; there is still some ambiguity of the scale factor for the apparatus we used. We hope that this can be cleared up before the final values are submitted for publication.

The structures of the tellurium compounds are clearly non-tetrahedral. We suspect that they have C_{2v} symmetry. However, a demonstration of this fact will have to await completion of the analysis of the distribution curves. Below I have outlined some of the experimental problems we have encountered in obtaining these electron diffraction data.

At the beginning of this program we had considered the matter of sample preparation to be of paramount importance and spent considerable time in attempting to purify the commercial samples by fractional sublimation in quartz tubes at elevated temperatures, under vacuum. I believe that we did achieve considerable purification; however, the subsequent handling of the samples thus prepared proved very difficult. It seems that in the removal of the vaporized sample from the quartz traps, and the introduction into the furnace-nozzle of the electron diffraction apparatus led to contamination by the atmosphere. Eventually we found that we had yet to encounter the second and more severe difficulty, the design of a proper high temperature nozzle, which could withstand the corrosive effects of these materials at the elevated temperatures. After a great deal of work in which

---

*Report on a subcontracted study at Cornell University, Ithaca, N. Y., under the direction of Professor S. H. Bauer.

TABLE 56

SUMMARY OF ELECTRON DIFFRACTION DATA

T_d Symmetry demonstrated for: $ZrCl_4$, $HfCl_4$, $HfBr_4$, HfI_4

Values of interatomic distances: PRELIMINARY

	$(M-X)_1$	$(M-X)_2$	Area ratio (M-X)	Area ratio (X-X)
$ZrCl_4$	2.38	2.33 ± .02	2020/2285	970/892
$HfCl_4$	2.44	2.39 ± .03	3800/4029	900/873
$HfBr_4$	2.52 ± .03		7600/8022	3486/3585
HfI_4	2.75 ± .03		10,318/11,101	7460/7507

$(M-X)_1$:   deduced directly from RD curves

$(M-X)_2$:   reduced value, 2% scale factor (nozzle and Au foil not coincident)

Area ratio: exp/theoretical areas, under RD peaks

Peak widths: analysis incomplete
        allowance must be made for phase shift factor

we constructed a variety of sample holders with high temperature valves, we found our efforts fruitless. We returned to the simplest nozzle design, which consisted of a small crucible surmounted by a conical nozzle, the temperature of which could be rapidly controlled. No valve was inserted. The amount of gas which was injected into the electron diffraction apparatus is merely controlled by the temperature of the crucible. Crucible materials were stainless steel and inconel.

When a commercially available sample was placed in the apparatus and raised up to a temperature of about 140° there was an initial large gas evolution. These observations check the preliminary mass spectrometer measurements made by Professor Porter on $ZrCl_4$ and $HfCl_4$. He found that on initial heating there was a large amount of HCl and Cl_2 generated. After this flush gas evolution the vapor pressure settled down to a lower value. We didn't take electron diffraction photographs during this initial heating, but only after subsequent cooling and reheating. Then higher temperatures had to be reached before any significant amount of material was ejected from the nozzle. It is true that some of the salt by that time may have been converted to the oxy-halide, but since that has a much lower vapor pressure than the pure halide (even though its presence does lower the activity of the condensed tetrahalide) it would not affect electron diffraction photographs.

Two or three runs were made with each compound. When we compared the photographs for the second and third runs, we found that they were identical. This we take as a demonstration that at the second stage there was sufficient purification by sublimation of the more volatile impurities, such that we had the desired material. In preparation for a run, the entire electron diffraction apparatus was filled with dry nitrogen and maintained at a slight over-pressure. The nozzle was removed and was loaded with the material directly supplied by the manufacturer or the Bureau of Mines. Operating entirely under a blanket of dry nitrogen this loading operation was carried out as rapidly as possible. The nozzle section was then reinserted into the apparatus and the pumping was immediately initiated. After attainment of pressure 10^{-5} mm. of Hg, the crucible was heated slowly. The heating rate was adjusted so that about a half hour was required for the sample to reach 100°C. The sample was then raised rapidly to 150°C. at which there was a large gas evolution. The crucibles were heated by radiation. After the initial large gas evolution, a sample was cooled down to 100° and pumping was continued. The temperature was raised to about 200°C. to obtain electron diffraction photographs. In all cases the second and third set of photographs obtained were identical. The estimated minimum impurity detectable through the R.D. curves is 5 to 10%. The absence of extraneous peaks in the radial distribution curve, and the occurrence of peaks only at the distances required for tetrahedral symmetry is a good indication of the purity of the sample.

211

REFERENCE CITATIONS

1. G. D. Kneip, J. O. Betterton and J. O. Scarbrough, Phys. Rev., 130, 1687 (1963).

2. O. H. Kriege, The Analysis of Refractory Carbides, Borides, Nitrides and Selicides, Los Alamos Scientific Laboratory Report LA-2306, March 1959.

3. P. L. Pauson, J. McLean, W. J. Cielland, Nature, 197, 1200 (1963).

4. WADD Technical Report 60-143, Part III.

5. F. H. Brown, Jr., Progress Report. No. 20-252, Jet Propulsion Laboratory, Pasadena, California, February 25, 1955.

6. G. A. Meyerson, G. V. Samsonov, R. B. Kotelnikov, M. S. Voyonova, 1. P. Yerterjera and S. D. Krasnenkova, Akad. Nauk. SSSR Zh. Neorgancheskoy Khimii, from Konferenskiya Po Khimii Bora I Yego Soyedineii 1955, 577 (1960).

7. A. K. Kuriakose and J. L. Margrave in L. A. McClaine, Thermodynamic and Kinetic Studies for a Refractory Materials Program, ASD-TDR-62-204, Part II, Contract No. AF 33(616)-7472, May 1963, p. 98.

8. Ym. B. Paderno, T. I. Serebryakova and G. V. Samsonov, Tsvetnye Metally (1959) 11, pp. 48-50, D.S.1. Trans. No. 614.

9. E. F. Westrum, Jr., and G. Feick, J. Chem. Eng. Data 8, 193 (1963).

10. J. Berkowitz-Mattuck,"High Temperature Oxidation, I. Copper"(accepted for publication by J. Electrochem. Soc.).

11. J. Berkowitz-Mattuck, Kinetics of Oxidation of Refractory Metals and Alloys at 1000°-2000°C, ASD-TDR-62-203, Part II, Contract No. AF 33(616)6154, March 1963.

12. JANAF Tables of Thermodynamic Data.

13. Paul Blackburn, Oxidation of Tungsten and Tungsten Base Alloys, WADD-TR-59-575, Part II (1960).

14. O. Kubaschewski and B. E. Hopkins, Oxidation of Metals and Alloys, Academic Press, New York (1963).

15. L. A. McClaine, Thermodynamic and Kinetic Studies for a Refractory Materials Program, ASD-TDR-62-204, Part II, May 1963.

16. P. Kofstadt and D. J. Ruzicka, J. Electrochem. Soc. 110, 181 (1963).

17. R. W. Bartlett (University of Utah, 1961) Dissertation Abstr. 22 (11), 3973 (1961-62).

18. W. Watt, G. H. Cockett, and A. R. Hall, Metaux 28, 222 (1963).

19. E. F. Westrum, Jr., and G. Feick. J. Chem. Eng. Data 8, 176 (1963).

20. L. A. McClaine, Thermodynamic and Kinetic Studies for a Refractory Materials Program, 4th Semiannual Progress Report (August 1963), Contract No. AF 33(616)-7472.

21. ASD-TDR-62-204 Part I, Thermodynamic and Kinetic Studies for a Refractory Materials Program, (April 1962) Contract No. AF 33(616)-7472, Arthur D. Little, Inc., Cambridge, Mass.

22. W. D. Kingery and G. E. Meiling, J. Appl. Phys. 33, 556 (1961).

23. W. D. Kingery, J. Pappis, M. E. Doty and D. C. Hill, J. Am. Cer. Soc. 42, 393 (1959).

24. E. Mollwo, Z. Physik 138, 478 (1954).

25. D. G. Thomas and J. J. Lander, J. Chem. Phys. 25, 1136 (1956).

26. F. H. Kroger and H. J. Vink, Solid State Physics, Vol. 3, p. 307, Academic Press (1956).

27. G. Brouwer, Phillips Res. Reports, 9, 366 (1954).

28. Seymour Aronson, J. Electrochem. Soc., 108, 312 (1961).

29. D. L. Douglass, pp. 223-255 in Corrosion of Reactor Materials, International Atomic Energy Agency, Vienna (1962).

30. J. Belle, A. B. Auskern, W. A. Bostrom and F. S. Sasko in Reactivity of Solids, J. H. DeBoer, editor, Elsevier Publishing Co. (1961)

31. I. Langmuir, Phys. Rev. 2, 329 (1913).

32. J. M. Leitnaker, M. G. Bowman and P. W. Gilles, J. Chem. Phys. 36, 350 (1962); and J. M. Leitnaker, Los Alamos Sci. Lab. Rept. LA-2402 (April 1960).

33. H. W. Goldstein and O. C. Trulson, Union Carbide Corp. Quart. Prog. Rept. by Lowrie et al., Contract DA-30-069-ORD-2787 (31 December 1962), p. III-28.

34. T. F. Lyon, Technical Report No. WADD TR-60-646, Part III (to be published) and T. F. Lyon, personal conversation, March 1964.

35. E. G. Wolf and C. B. Alcock, Trans. British Ceram. Soc. 61, 667 (1962).

36. J. M. Leitnaker, private communication.

37. S. Dushman, D. Dennison and N. B. Reynolds, Phys. Rev. 29, 903 (1927).

38. O. C. Trulson, personal conversation, March 1964.

39. G. B. Skinner, J. W. Edwards and H. L. Johnston, J. Am. Chem. Soc. 73, 174 (1951).

40. O. C. Trulson and H. W. Goldstein, Union Carbide Corp., Quarterly Rept. by Lowrie et al., Contract DA-30-069-ORD-2787 (31 March 1962), p. III-14.

41. H. L. Schick, D. F. Anthrop, R. E. Dreikorn, R. C. Feber, P. L. Hanst, M. B. Panish, and C. H. Ward, AVCO Corp. Quarterly Progress Rept. Contract AF 33(657)-8223, Task No. 73603 (15 December 1962).

42. R. C. Paule and J. L. Margrave, J. Phys. Chem. 67, 1368 (1963).

43. M. Hoch, P. E. Blackburn, D. P. Dingledy, and H. L. Johnston, J. Phys. Chem. 59, 97 (1955).

44. W. A. Chupka and M. G. Inghram, J. Phys. Chem. 59, 100 (1955).

45. R. J. Thorn and G. H. Winslow, J. Chem. Phys. 26, 186 (1957).

46. P. E. Blackburn, "Vapor Pressures Over the Two-Phase System $TaC-Ta_2C$," presented at the Electrochem. Soc. Meeting, Los Angeles, May 1962.

47. M. B. Panish and L. Reif, J. Chem. Phys. 38, 253 (1963).

48. T. F. Lyon, private communication of Schick (see ref. 41 and ref. 34).

215

49. O. C. Trulson and H. W. Goldstein, Union Carbide Corp., Quarterly Progress Rept. by Lowrle, et al., Contract DA-30-069-ORD-2787 (30 Sept. 1963), p. III-48.

50. M. C. Krupka, Los Alamos Sci. Lab. Rept. LA-2611 (April 1960).

51. J. A. Coffman, G. M. Kihler, et al. (General Electric Company, Cincinnati, Ohio), Progress Reports under Contract AF 33(616)-6841.

52. B. D. Pollock (Atomics International, Canoga Park, California), J. Phys. Chem. 65, 731 (1961).

53. Dr. K. K. Kelley, personal communication.

54. C. N. Cochran, Rev. Sci. Instr. 29, 1135 (1958).

55. ASTM Methods - Chemical Analysis of Metals 1960, p. 459.

56. Y. Paderno et al., Tsvetnye Metally 11, 48 (1959).

57. O. H. Kirkorian, University of California Laboratory Report UCRL-2888 (1955).

58. D. R. Stull and G. C. Sinke, Thermodynamic Properties of the Elements, No. 18 of the Advances in Chemistry Series, American Chemical Society (1956).

59. L. Kaufman, MANLABS, ASD-TR-61-445, Part III, Contract AF 33(657)-9826, p. 26.

60. Pitzer and Brewer, revision of Lewis and Randall, Thermodynamics, McGraw-Hill, New York (1961).

61. J. Berkowitz, H. A. Tasman and W. A. Chupka, J. Chem. Phys., 36, 2170 (1962).

62. L. Friedman, J. Chem. Phys., 23, (1955), 477.

    R. C. Miller and P. Kusch, J. Chem. Phys., 25 (1956), 860.

    J. Berkowltz and W. A. Chupka, J. Chem. Phys., 29 (1958), 653.

    J. Berkowitz and W. A. Chupka, J. Chem. Phys., 36 (1962), 2170.

63. D. T. F. Marple and J. W. Trischka, Phys. Rev., 103 (1956), 597.

    J. C. Schwartz and J. W. Trischka, Phys. Rev., 88 (1952), 1085.

    A. Braunstein and J. W. Trischka, Phys. Rev., 98 (1955), 1092.

64. A. Honig, M. Mandel, M. L. Stitch and C. H. Towhes, Phys. Rev., 96 (1954), 629.

    D. R. Lide, unpublished.

65. W. Klemperer, W. G. Norris, A. Buchler, and A. G. Emslie, J. Chem. Phys., 33 (1960), 1534.

66. W. Klemperer and W. G. Norris, J. Chem. Phys., 34 (1961), 1071.

67. S. H. Bauer, I. Tadashi and R. F. Porter, J. Chem. Phys., 33 (1960), 685.

    P. A. Akishin and N. G. Rambidi, Z. Physik. Chem. 213 (1960), 111.

68. J. Berkowitz, J. Chem. Phys., 29 (1958), 1386.

    Ibid,   32 (1960), 1522.

69. M. J. Linevsky, J. Chem. Phys., 34 (1961), 587.

70. M. J. Linevsky, J. Chem. Phys., 38 (1963), 658.

71. A. D. Buckingham, Proc. Roy. Soc. (London), A248 (1958), 169.

72. A. Snelson and K. S. Pitzer, J. Phys. Chem., 67 (1963), 882.

73. L. L. Ames, D. White and D. E. Mann, J. Chem. Phys., 38 (1963), 910.

74. G. Vidale, J. Phys. Chem., 64 (1960), 314.

75. J. W. Trischka, Phys. Rev., 76 (1949), 1365.

76. E. S. Rittner, J. Chem. Phys., 19 (1951), 1030.

77. A. M. Benson and H. G. Drickamer, J. Chem. Phys., 27 (1957), 1164.

78. R. P. Bell, Proc. Roy. Soc. (London), A183 (1945), 328.

79. J. C. Decius and E. B. Wilson, Jr., J. Chem. Phys. 19 (1951), 1409.

80. A. K. Kuriakose and J. L. Margrave, to be published, J. Electrochem. Soc. (1964).

81. A. K. Kuriakose and J. L. Margrave, J. Phys. Chem. 68, 290 (1964).

82. H. M. Haendler and W. J. Bernard, J. Am. Chem. Soc. 73, 5218 (1951).

83. H. M. Haendler, W. L. Patterson, Jr., and W. J. Bernard, J. Am. Chem. Soc. 74, 3167 (1952).

84. H. M. Haendler, S. F. Bertram, R. S. Becker, W. J. Bernard, and S. W. Bukata, J. Am. Chem. Soc. 76, 2177 (1954).

85. H. M. Haendler, L. H. Towler, E. F. Bennett, and W. L. Patterson, Jr., J. Am. Chem. Soc. 76, 2178 (1954).

86. R. M. Gunzik and C. E. Feider, NACA-TN-3333, Lewis Flight Propulsion Lab., Sept. 1954.

87. L. Stein and R. C. Vogel, ANL-5441, Argonne National Lah., May 1955.

88. H. G. Price, Jr., and H. W. Douglass, NACA-RM-E57 G18, Lewis Flight Propu'sion Lab., November 1956.

89. J. Fischer and R. K. Steunenberg, J. Am. Chem. Soc. 79, 1876 (1957).

90. M. J. Steindler and R. C. Vogel, ANL-5662, Argonne National Lab., Jan. 1957.

91. Stephen Lawroski, W. A. Rodger, R. C. Vogel and V. H. Munnecke, Summary Report, Chemical Engineering Division, ANL-5924, Argonne National Lab., March 1959.

92. G. L. Ericson, W. K. Boyd and P. D. Miller, NP-6729, Battelle Memorial Inst. April 1958.

93. Stephen Lawroskl, W. A. Rodger, R. C. Vogel and V. H. Munnecke, Summary Report, Chemical Engineering Division, ANL-5959, Argonne National Lab., Dec. 1958.

94. E. L. White and F. W. Fink, Proceedings of the Propellant Thermo-dynamics and Handling Conference, pp. 161-181, Special Report 12, Engineering Experimental Station, The Ohio State University (1959).

95. C. F. Hale, E. J. Barber, H. A. Bernhardt and K. E. Rapp, AECD-4292, Oak Ridge Gaseous Diffusion Plant, July 1959.

218

96. C. F. Hale, E. J. Barber, H. A. Bernhardt and K. E. Rapp, K-1459, Oak Ridge Gaseous Diffusion Plant, Sept. 1960.

97. F. W. Fink, TID-5935, Batelle Memorial Inst., May 1960.

98. R. B. Jackson, Final Report NP-8845, Allied Chemical Corporation, General Chemical Division, New York 1960.

99. F. W. Fink, TID-13206, Battelle Memorial Institute, June 1961.

100. A. P. Litman, and A. E. Goldman, ORNL-2832, Oak Ridge National Lab., June 1961.

101. P. M. O'Donnell and A. E. Spakowski, NASA Technical Note D-768, April 1961.

102. F. E. Brown, J. M. Crabtree, and J. F. Duncan, J. Inorg. and Nucl. Chem. $\underline{1}$, 202 (1955).

103. K. A. Sense, M. J. Snyder, and J. W. Klegg, Rept. AECD-BMI 3708 (1953).

104. K. A. Sense, M. J. Snyder, and R. B. Filbert, J. Phys. Chem. $\underline{58}$, 995 (1954).

105. K. A. Sense, R. E. Bowman, R. W. Stone, M. J. Snyder, and R. B. Filbert, Rept. BMI 1064 (1956).

106. P. Schwarzkopf and R. Kieffer, in Refractory Hard Metals, p. 95, Macmilian Company, New York, 1953.

107. H. Moissan, Compte Rendus $\underline{139}$, 711 (1904).

108. H. Moissan. Ann. Chim. Phys. (6), $\underline{24}$, 237 (1891).

109. C. M. Tu, H. Davis and M. C. Hottel, Ind. Eng. Chem. $\underline{26}$, 749 (1934).

110. G. Blyholder and H. Eyring, J. Phys. Chem. $\underline{61}$, 682 (1957).

111. G. Blyholder and H. Eyring, J. Phys. Chem. $\underline{63}$, 1004 (1959).

112. E. A. Gulbransen, K. F. Andrew and F. A. Brassart, J. Electrochem. Soc. $\underline{110}$, 476 (1963).

113. E. A. Gulbransen and K. F. Andrew, Ind. Eng. Chem. $\underline{44}$, 1034 (1952).

114.   J. M. Kuchta, A. Kant and G. H. Damon. Ind. Eng. Chem. <u>44</u>, 1559 (1952).

115.   M. Levy, Ind. Eng. Chem., Product Research and Development <u>1</u>, 19 (1962).

116.   J. G. Stamper and R. F. Barrow, Trans. Farad. Soc. <u>79</u>, 1320 (1957).

117.   G. D. Blue, J. W. Green, T. C. Ehlert and J. L. Margrave, ASTM Conference on Mass Spectrometry, San Francisco, California, May 23, 1963, p. 344.

118.   R. Onaka, J. Chem. Phys. <u>27</u>, 374 (1957).

119.   M. Chretien, Helv. Physic. Acta. <u>23</u>, 259 (1950).

120.   A. S. Kana'an and J. L. Margrave, to be published, J. Inorg. Chem. (1964)

121.   H. Moissan, Compte Rendus <u>110</u>, 276 (1890); Ann. Chim. Phys. (6) <u>24</u>, 242 (1891).

122.   O. Ruff and O. Bretschneider, Z. Anorg. Allgem. Chemie <u>217</u>, 1 (1934).

123.   W. Rudorff and G. Rudorff, Z. Anorg. Chem. <u>253</u>, 281 (1947).

124.   W. Rudorff and G. Rudorff, Chem. Ber. <u>80</u>, 413 (1947).

125.   W. Rudorff, in <u>Advances in Inorganic and Radiochemistry,</u> Vol. I, p. 230, Academic Press, Inc., New York (1959).

126.   W. Rudorff and G. Rudorff, Chem. Ber. <u>80</u>, 417 (1947).

127.   W. Rudorff and K. Brodersen, Z. Naturforsch. <u>12B</u>, 595 (1957).

128.   L. Kaufman,   <u>Investigation of Boride Compounds for Very High Temperature Applications,</u>   Progress Reports to Aeronautical Systems Division, Wright-Patterson Air Force Base, Contract No. AF 33(657)-8635, October 1962, and April 1963 and December 1963.

129.   H. Prophet, Unpublished work cited in the JANAF Tables, edited by D. R. Stull, Dow Chemical Company, Midland, Michigan.

130.   A. N. Krestovnikov et al., Izvest. Vysshikh Ucheb. Zavedenii, Razvedoch Tsvetnoya Met., No. <u>1</u>, 73-75 (1958); also Chem. Abstr. <u>53</u>, 19552C (1959).

131. D. Neel, C. Pears and S. Oglesby, Southern Research Institute Report
      No. ASD-TDR-62-765 to Wright Air Development Division, August 1962.

132. D. W. Barnes, R. Mezaki, E. W. Tilleux and J. L. Margrave, Proc.
      International Symposium on Thermodynamics of Nuclear Materials,
      paper SM-26/48, Vienna, Austria, May 21, 1962, p. 775.

133. R. Barriault et al., Thermodynamics of Refractory Compounds, AVCO
      Reports to Wright-Patterson Air Force Base under Contract No. AF 33(616)-
      7327, ASO-TR-61-260, Vol. I, pp. 350, 378-80 (1961), and Vol. II (1962).

134. K. K. Kelley, J. Am. Chem. Soc. 62, 818 (1940).

135. R. H. Valentine, T. F. Jambois and J. L. Margrave, to be published,
      J. Chem. Engr. Data, 1964, and reference therein.

136. K. K. Kelley, U. S. Bureau of Mines, Bulletin 584 (1960).

137. E. W. Balson (1961). J. Phys. Chem. 65, 1151.

138. K. D. Carlson (1960). Argonne National Laboratory Report ANL-6156;
      also PhD. Thesis, University of Kansas.

139. P. Clausing (1929). Physica 9, 65.

140. P. Clausing (1932). Ann. Physik 12, 961.

141. J. P. Dawson (1959). M.S. Thesis, Oklahoma State University.

142. W. C. DeMarcus (1957). Oak Ridge Gaseous Diffusion Plant Report
      K-1302, parts 1-6.

143. J. G. Edwards (1964). PhD. Thesis, Oklahoma State University.

144. R. D. Freeman (1963). ASD-TDR-63-754, Part I, submitted by Oklahoma
      State University to Aeronautical Systems Division, W-PAFB, Ohio, under
      Contract AF 33(657)-8767.

145. R. D. Freeman and A. W. Searcy (1954). J. Chem. Phys. 22, 762.

146. S. R. Gunn (1958). Rev. Sci. Instr. 29, 377.

147. K. E. Guthe (1906). Bull. N.B.S. 2, 33.

148. F. B. Humphrey and A. R. Johnston (1963). Rev. Sci. Instr. 34, 348.

149. R. P. Iczkowski, J. L. Margrave and S. M. Robinson (1963). J. Phys. Chem. 67, 229.

150. W. A. Keith and H. Mackle (1958). Trans. Faraday Soc. 54, 353.

151. M. Knudsen (1909). Ann. Physik (4) 28, 999.

152. G. E. MacWood, et al. (1955) Technical Reports No. 1, 2 and 3, Project NRO37-024, Office of Naval Research, Washington (Ohio State University, Dept. of Chemistry).

153. J. L. Margrave (1957). J. Chem. Phys. 27, 1412.

154. J. L. Margrave (1959). In Physico-Chemical Measurements at High Temperatures (J. O'M. Bockris, et al., ed.) Butterworths, London.

155. A. R. Meetham, and J. A. Nichols (1960). Proc. Roy. Soc. A256, 384.

156. I. E. Newnham and J. A. Watts (1960). J. Am. Chem. Soc. 82, 2113.

157. V. L. Rogallo, and H. F. Savage (1963). Rev. Sci. Instr. 34, 988.

158. A. W. Searcy and R. D. Freeman (1954). J. Am. Chem. 76, 5229.

159. A. W. Searcy and R. A. McNees (1953) J. Am. Chem. Soc. 75, 1578.

160. S. Sunner and I. Wadsö (1959). Acta Chem. Scand. 13, 97.

161. M. Volmer (1931). Z. Physik. Chem. Bodenstein Festband, 863.

162. P. G. Wahlbeck (1962). Private communication.

163. W. L. Winterbottom and J. P. Hirth (1962). J. Chem. Phys. 37 784.

164. A. D. Mah and B. J. Boyle, JACS 77 6512 (1955).

165. Dr. Elliott Greenberg. Personal communication.

166. L. A. McClaine, Thermodynamic and Kinetic Studies for a Refractory Materials Program, Third Semi-annual Progress Report (August 1962), Contract AF 33(616)-7472.